

**e-ISSN : 2320-0847**  
**p-ISSN : 2320-0936**



# **American Journal of Engineering Research (AJER)**

**Volume 5 Issue 3– March 2016**

**[www.ajer.org](http://www.ajer.org)**

**[ajer.research@gmail.com](mailto:ajer.research@gmail.com)**

## Editorial Board

### American Journal of Engineering Research (AJER)

**Dr. Moinuddin Sarker,**

Qualification :PhD, MCIC, FICER,  
MInstP, MRSC (P), VP of R & D  
Affiliation : Head of Science / Technology  
Team, Corporate Officer (CO)  
Natural State Research, Inc.  
37 Brown House Road (2nd Floor)  
Stamford, CT-06902, USA.

**Dr. June II A. Kiblasan**

Qualification : Phd  
Specialization: Management, applied  
sciences  
Country: PHILIPPINES

**Dr. Jonathan Okeke  
Chimakonam**

Qualification: PHD  
Affiliation: University of Calabar  
Specialization: Logic, Philosophy of  
Maths and African Science,  
Country: Nigeria

**Dr. Narendra Kumar Sharma**

Qualification: PHD  
Affiliation: Defence Institute of Physiology  
and Allied Science, DRDO  
Specialization: Proteomics, Molecular  
biology, hypoxia  
Country: India

**Dr. ABDUL KAREEM**

Qualification: MBBS, DMRD, FCIP, FAGE  
Affiliation: UNIVERSITI SAINS Malaysia  
Country: Malaysia

**Prof. Dr. Shafique Ahmed Arain**

Qualification: Postdoc fellow, Phd  
Affiliation: Shah Abdul Latif University  
Khairpur (Mirs),  
Specialization: Polymer science  
Country: Pakistan

**Dr. Sukhmander Singh**

Qualification: Phd  
Affiliation: Indian Institute Of  
Technology, Delhi  
Specialization : PLASMA PHYSICS  
Country: India

**Dr. Alcides Chaux**

Qualification: MD  
Affiliation: Norte University, Paraguay,  
South America  
Specialization: Genitourinary Tumors  
Country: Paraguay, South America

**Dr. Nwachukwu Eugene Nnamdi**

Qualification: Phd  
Affiliation: Michael Okpara University of  
Agriculture, Umudike, Nigeria  
Specialization: Animal Genetics and  
Breeding  
Country: Nigeria

**Dr. Md. Nazrul Islam Mondal**

Qualification: Phd  
Affiliation: Rajshahi University,  
Bangladesh  
Specialization: Health and Epidemiology  
Country: Bangladesh

S.No.	Manuscript Title	Page No.
<b>01.</b>	Design and Development of SMS Based Generator Start/Stop System KESHINRO K. K   BALOGUN W. A    OYETOLA J. B   OMOGOYE S. O	01-06
<b>02.</b>	Design and Development of SMS Prepaid Energy Meter IKESHINRO K. K.    AKINLEYE A. O.   SALAMI S. O.   SARUMI A. J.	07-11
<b>03.</b>	A Novel Convergence Approach for an Adaptive Equalizers Sayed Shoaib Anwar    Dr. D. Elizabeth Rani    Dr. S.G.Kahalekar    Dr.Syed Abdul Sattar	12-21
<b>04.</b>	Prospects of Implementing E-Learning Systems based on Learning Objects and XML in Nigeria's Educational Sector ARTHUR U. UME	22-28
<b>05.</b>	Analysis of Geostatistical and Deterministic Techniques in the Spatial Variation of Groundwater Depth in the North-western part of Bangladesh Ibrahim Hassan   I. M. Lawal    A. Mohammed   S. Abubakar	29-34
<b>06.</b>	Fin pitch to effect efficiency of evaporator and HVAC Dr. Mohammad Arsalan Khan    Mohd Danish	35-38
<b>07.</b>	An application of Auto-regressive (AR) model in predicting Aero-elastic Effects of Lekki Cable Stayed Bridge Hassan Abba Musa    Dr. A. Mohammed	39-50
<b>08.</b>	Radiological Assessment of Sediment of Zobe Dam Dutsinma, Katsina State, Northern Nigerian. Najib M. U.   Zakari Y. I.    Sadiq U.   Bello I. A.   Ibrahim G. G.   Umar S. A.    Sanda Y.S.    Abdu N.M.	51-58
<b>09.</b>	Evaluation & Optimization of Software Engineering Ashiqur Rahman    Asaduzzaman Noman    Atik Ahmed Sourav   Shakh Md. Alimuzjaman Alim	59-63
<b>10.</b>	Assessment of Physicochemical Parameters and Heavy Metals in Gombe Abattoir Wastewater Nasiru A    Osakwe C.E    Lawal I.M    Chinade A.U.	64-69

## CONTENTS

<b>11.</b>	A Brief History of Virtual Pheromones in Engineering applications Ioan Susnea	70-76
<b>12.</b>	Cost Efficient Design Approach for Reversible Programmable Logic Arrays Md. RiazurRahman	77-85
<b>13.</b>	Development of Evaluation Models for Estimation of Economic Values of Natural Gas Fractionation in the Niger Delta Udie, A. C.    Nwakaudu, S. M	86-95
<b>14.</b>	Study the effect of cryogenic cooling on orthogonal machining Process Arvind Kaushal   Ajay Vardhan    A.C.Tiwari   S.K.Saluja	96-104
<b>15.</b>	Variation of stresses at different nodal points in a isotropic beam using ANSYS Shabbir Ahmed Osmani	105-110
<b>16.</b>	Is there a way to provide mobility in a spatial direction within the virtual environment provided by Google Cardboard Virtual Reality System? Gourav Acharya	111-120
<b>17.</b>	Development of Visually Impaired Guided System Using GPS, Sensors and Wireless Detection Emmanuel Kobina Payne   Dennis Joe Harmah	121-126
<b>18.</b>	Numerical Investigation of inlet distortion on the flowfield within the NASA rotor67 HengMing Zhang   XiuQuan Huang    Xiang Zhang   QingZhen Yang	127-131
<b>19.</b>	Investigation into Unsteady Blade Row Interaction Effects of a Two-Stage Counter-Rotating Lift-Fan by Harmonic Balance Method Xiang Zhang   XiuQuan Huang   HengMing Zhang   YuChun Chen	132-139
<b>20.</b>	View of Flood Disaster Management in Indonesia and the Key Solutions Ratih Indri Hapsari    Mohammad Zenurianto	140-151
<b>21.</b>	Thermal Comfort Temperature Range for Industry Workers in a Factory in Malaysia A.Z.A. SAIFULLAH    Y.H.YAU   B.T. CHEW	152-156

## CONTENTS

<b>22.</b>	Krill Oil Quantification in CS/TPP Nanoparticles Using Novel One Step Fourier Transform Infrared Spectroscopy JunaidHaider   Hamid Majeed   Hafiz RizwanSharif   Muhammad Shamoona   HaroonJamshaidQazi   Ali Haider   JianguoMa  Fang Zhong	157-164
<b>23.</b>	Over Coming of Errors in Tmr System Utilizing Scanchain Methods PARAMESHAPPA.G    MADHUKAR.G.N.MALIGERA    Dr. D. JAYADEVAPPA	165-170
<b>24.</b>	Marine Offshore Accidents in Nigeria, Causes and Necessary Preventive Measures Oyinkepreye L. Bebetidoh    Robert Poku	171-183
<b>25.</b>	Mapping and Assessment of Soil Loss in Berrechid Plain Using a Gis And the Universal Soil Loss Equation (Usle) M. Aboulouafa    H. Taouil    S.Ibn Ahmed	184-190
<b>26.</b>	A brief review of biomedical sensors and robotics sensors Yanli Luo    Qiaoying Zhou    Wenbin Luo	191-194
<b>27.</b>	Bluetooth Based Android Controlled Robot Rowjatul Zannat Eshita    Tanwy Barua    Arzon Barua    Anik Mahamood Dip	195-199

## Design and Development of SMS Based Generator Start/Stop System

KESHINRO K. K<sup>1.</sup>, BALOGUN W. A<sup>2.</sup>, OYETOLA J. B<sup>3.</sup>, OMOGOYE S. O<sup>4</sup>

<sup>1,2</sup>Department of Computer Engineering, Lagos State Polytechnic Ikorodu, Lagos State, Nigeria

<sup>3,4</sup>Department of Elect/Elect, Lagos State Polytechnic Ikorodu, Lagos State, Nigeria

**ABSTRACT :** This paper offers an integrated SMS alert and remote control system for a generator. This unit can be integrated into any diesel generator. The Generator can be Started or Stopped by sending an SMS to the generator from anywhere in the world. Used in conjunction with the alert, the generator can be turn on and off even if the owner is not at home or the office when the lights go out. The SMS unit is mounted inside the generator housing (space permitting) and runs off the generators battery. When the generator is in automatic mode it will start-up when the power fails and in doing so sends an SMS to operators predetermined phone number. The methodology used was the principle of serial communication with embedded system. Sim900 was used as the GSM module and 8051 microcontroller was program, the simulation of the schematics diagram was done using Proteus 8.4 software. The microcontroller code was done using keil compiler and the hex file was transfer to proteus software for simulation.

The unique SMS Alert and command system allows users to quickly and easily control their Generator worldwide, with the knowledge that problems can be sorted out quickly and efficiently. In addition to that, the security system allows for safe and secure use without interference.

**Keywords:** Generator, 8051, Microcontroller, KEIL, SMS, SIM900

### I. Introduction

This Paper is a very good example of embedded system as all its operations are controlled by intelligent software inside the microcontroller. The aim of this paper is to control i.e. to ON/OFF of generator, the electrical or electronic appliances connected to this system from anywhere in the world. For this purpose user can use any type of Mobile. This way it overcomes the limited range of infrared and radio remote controls[5]. Using the convenience of SMS, this paper lets you remotely control equipment by sending plain text messages, such as "abcdn1", "abcdnaf3", "abcdf57n142"— all of which can be pre-programmed into the controller and easily remembered later. It can control up to eight external devices Short Message Service (SMS) is defined as a text-based service. That enables up to 160 characters to be sent from one mobile phone to another. In a similar vein to email, messages are stored and forwarded at an SMS centre, allowing messages to be retrieved later if you are not immediately available to receive them. Unlike voice calls, SMS messages travel over the mobile network's low-speed control channel[7].

"Texting", as its also known, is a fast and convenient way of communicating. In fact, SMS has taken on a life of its own, spawning a whole new shorthand language that's rapidly Many industries have been quick to make use of this technology, with millions of handsets currently in use. As new models with "must have" features hit the market, older models become virtually worthless and if not recycled, end up in landfill[8].

### II. Review of Related Works

Amit sachen et al have discussed the user can send commands in the form of SMS messages to read the remote electrical parameters. This system also can automatically send the real time electrical parameters periodically (based on time settings) in the form of SMS. This system can be designed to send SMS alerts whenever the Circuit Breaker trips or whenever the Voltage or Current exceeds the predefined limits. This project makes use of an onboard computer which is commonly termed as microcontroller [1].

Mallikarjun et al proposed this system is a specially designed computer system that is completely encapsulated by the device it controls. The embedded system has specific requirements and performs pre-defined tasks. The diesel generator is used when electricity is not readily available, or when power failures occur due to natural disasters such as typhoons or floods, or during other unexpected crises. Generally, the diesel generator operates

in analog. The analog type controller cannot be processed precisely due to the distortions and noises coming from the data. In order to increase data accuracy, the controller needs to be digitalized [2]

Vimalraj et al have described a distribution transformers have a long service life if they are operated under good and rated conditions. However, their life is significantly reduced if they are overloaded, resulting in unexpected failures and loss of supply to a large number of customers thus effecting system reliability. This system provides flexible control of load parameters accurately and also provides effective means for rectification of faults if any abnormality occurs in power lines using SMS through GSM network [3].

Andriy Palamar et al proposed the system the Cellular phone containing SIM (Subscriber's Identifying Module) card has a specific number through which communication takes place. The mode of communication is wireless and mechanism works on the GSM (Global System for Mobile communication) technology. Here, the communication is made bi- directional where the user transmits and also receives instructions to and from the system in the form of SMS [4].

### III. Methodology

The method used for the design and implementation are as follows

#### a. Power supply stage

Step 1: Connect one of the ac section of the bridge rectifier to the ac output of the transformer

Step 2: Connect the other terminal of the ac output of the bridge rectifier to the ac output of the transformer

Step 3: Connect the ac input of the transformer to 220v ac power source

Step 4: Connect the positive terminal of the bridge rectifier to the positive terminal of c1

Step 5: Connect the negative terminal of the bridge rectifier to the negative terminal of c1

Step 6: Connect the positive of c1 to the input of 7812

Step 7: Connect the negative of c1 to the ground of 7812

Step 8: Connect the output of 7812 to the input of 7805 and bias with the positive of c2 to prevent the capacitor from heating and to allow a stable voltage

Step 9: Connect the ground of 7805 to the ground of 7812

Step 10: Measure your output voltage

Step 11: The 12v output voltage will be measured from the 7812 and the 5v output will be measure from 7805

#### b. Programming of the gsm module

The programming of the gsm module was done using the ATCommand Instruction.

Table 1: ATCOMMAND Instruction

Command	Description
AT	Check if serial interface and GSM modem is working.
ATE0	Turn echo off, less traffic on serial line.
AT+CNMI	Display of new incoming SMS.
AT+CPMS	Selection of SMS memory.
AT+CMGF	SMS string format, how they are compressed.
AT+CMGR	Read new message from a given memory location.
AT+CMGS	Send message to a given recipient.
AT+CMGD	Delete message.

Source: Developed with Labview Software([www.labview.com](http://www.labview.com))

**c. Programming of the microcontroller**

The following steps were implemented

Step 1: The component used are 33pf capacitor, at89s52, 11.0592mhz crystal, 10uf 16v, 10k resistor, reset button

Step 2: Mount a 40pin ic socket onto the veroboard

Step 3: Connect 11.0592mhz crystal across pin18 and pin19

Step 4: Connect the 33pf across the crystal

Step 5: Connect the reset button

Step 6: Download keil on the internet and install it

Step 7: Program the sms based generator start/stop using embedded c

Step 8: Compile the program, testrun, debug and generate hex file

Step 9: Load the hex file into the chip with the help of burner

ORG 00H

```

MOV R0,#10
MOV R1,#10
MOV R2,#10
MOV R3,#10
MOV TMOD,#01H
MOV TCON,#00H
MOV TL0,#F4H
MOV TH0,#FFH
SETB TR0
;#####;
;      START OF MAIN PROGRAM      ;
;#####;
L1:  JNB TF0,L1
      CPL P1.0
      CLR TF0
      MOV TL0,#F4H
      MOV TH0,#FFH
      DJNZ R0,L1
      CPL P1.1
      MOV R0,#10
      DJNZ R1,L1
      CPL P1.2
      MOV R1,#10
      DJNZ R2,L1
      CPL P1.3
      MOV R2,#10
      DJNZ R3,L1
      CPL P1.4
      MOV R3,#10
      SJMP L1
;#####;
;      END OF MAIN PROGRAM      ;
;#####;

```

END

**d. Connection of the generator to the embedded device**

The device can be used with any type of generator . it was used with both key starter and the one that are not using key. Some other condition was also observed based on demand. The output of the device was connected to H-BRIGE before connecting to a generator.

**e. Relay Driver Section**

The relay driver used for this paper is uln2003. It can withstand high current/voltage. Connect pin28 of the ic socket to pin1 of the ic. The output of the ic was taken at pin16. Pin16 was connected to the relay as indicated in the diagram in fig 1

f. Complete Circuit Diagram

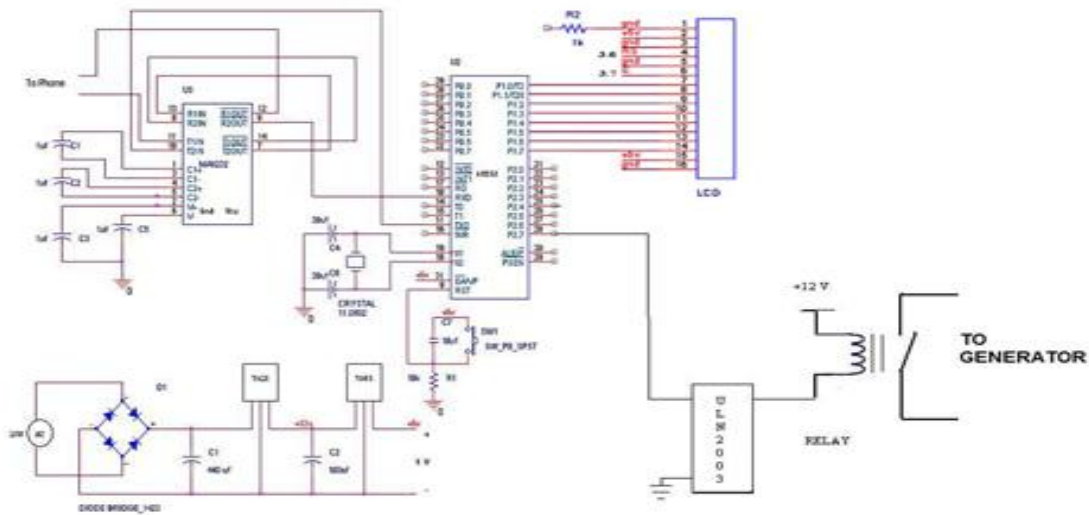
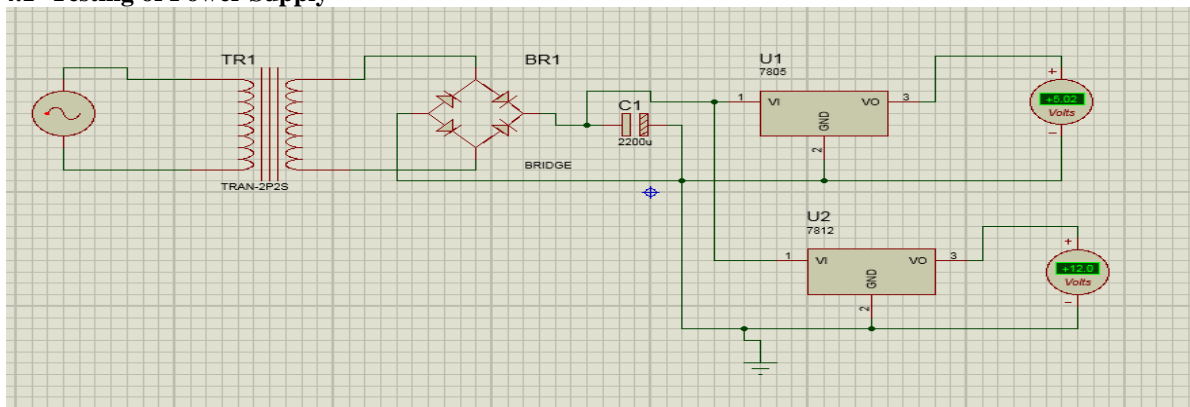


Fig 1: Developed Circuit Diagram of SMS based Generator  
 Source: designed with Proteus Software (www.proteus.com)

GSM (SMS) Controlled DC Motor is automatic control system which capable of receiving a set of command instructions in the form of Short message service and performs the necessary actions like Start , Stop and speed control. I will be using a dedicated modem/mobile at the receiver module i.e. with the robot it self and send the commands using SMS service as per the required actions. The mobile unit which is dedicated at the motor driver is interfaced with an intellectual device called Micro controller so that it takes the responsibility of reading the received commands in the form of SMS from the mobile unit and perform the corresponding predefined tasks such as motor start, stop, motor direction and speed control at different levels etc.

IV. Test and Result

4.1 Testing of Power Supply



4.2 Testing of the Generator Unit

The Generator can be Started or Stopped by sending an SMS to the generator from anywhere in the world. Used in conjunction with the alert you can decide when to turn on and off your generator even if you're not at home or the office when the lights go out. The SMS unit was mounted inside the generator housing (space permitting) and runs off the generators battery. When the generator is in automatic mode it will start-up when the power fails and in doing so sends an SMS to UP TO 5 predetermined phone numbers. An SMS can then be sent back to the generator using a predetermined "code" and command. The code allows to safe guard the generator from malicious SMS have to turn it on and off. If the generator has a problem when running it will again send an SMS to up to 5 users notifying them of the problem encountered. When the generator is shuts down the user is also notified, allowing them to confirm that the generator has successfully shutdown. The unique SMS Alert and command system allows users to quickly and easily control their Generator worldwide, with the knowledge that problems can be sorted out quickly and efficiently. In addition to that, the security system allows for safe and secure use without interference

### 4.3 Testing of the Load with Generator

System is controlled by SMS commands: start, stop, status, timer on, timer off.

- i. Requesting "status" it returns: Load in Amps (which tells me that the pump is working fine), running time, and whether timer is currently activated or not.
- ii. The generator starts up connected to a small load, about 0.4A for a ceiling fan, but is disconnected from the pump. The startup sequence is:

Step 1: Give start signal to generator

Step 2: Check current sensor to see if output is more than 0.4A, if not shut down generator and send error message that generator failed to start

Step 3: Wait for 2minutes

Step 4: Close pump relay

Step 5: Check current sensor to make sure the pump came on, if not shut down generator and send error message.

Step 6: The shutdown sequence is in reverse and also uses the current sensor to make sure everything is off as it should be.

## V. CONCLUSION AND RECOMMENDATION

### 5.1 Conclusion

There are so many industries which need 24 hours power. So they develop their own mini power plants. If there are any faults in main system at that time we make manual operation to run mini power plant generator. Due to this there is so much time consume. Here, if we provide this system so there are no needs of manual operation and we get constant power in very short time. We can get the feedback from generator, whenever the fuel level goes below the normal level. The same thing is applicable for any change in temperature of the system. Also if any parameter goes below the preset limit, also a feedback message is there from the circuit and also generator stop to working. This procedure is applicable in any kind of fault also

### 5.2 Recommendation

We are interfacing the circuit with GSM module so that generator can be operated from remote place. In this system if we send sms (START), the generator starts working and if we send sms (STOP), the generator stops working. Also, we can get the feedback from generator, whenever the fuel level goes below the normal level. The same thing is applicable for any change in temperature of the system. To achieve this, testing will need to be carried out to create a useful system. The report consists of a background into the area of 8051 microcontroller and mobile communication, how they are interfaced to each other and AT (Attention) commands set used in communication. The microcontroller pulls the SMS received by phone, decodes it, and recognizes the Mobile no. The switches on the relays attached to its port to control the appliances. After successful operation, controller sends back the acknowledgement to the user's mobile through SMS. Future work can focus on fault diagnosis of the generator using embedded system and developed a NEURO FUZZY expert system

## REFERENCE

- [1] A. Sachan, "Microcontroller based Substation Monitoring and Control System with Gsm Modem" IOSR Journal of Electrical and Electronics Engineering, vol. 1, no. 6, (2012).
- [2] M. Sarsamba "The Load Monitoring and Protection on Electricity Power lines using GSM Network", International Journal of Advanced Research in Computer Science and Software Engineering, vol. 3, no. 9, (2013).
- [3] S.Vimalraj, R.B. Gausalya, "GSM Based Controlled Switching Circuit between Supply Mains and Captive Power Plant", International Journal of Computational Engineering Research, vol, 03, no. 4, (2013).
- [4] A. Palamar "Control System for a Diesel Generator and UPS Based Microgrid", Scientific Journal of Riga Technical University Power and Electrical Engineering, vol. 27, (2010).
- [5] GSM Multiple Access Scheme, <http://www.eecg.toronto.edu/~nazizi/gsm/ma/> William Stallings Data and Computer Communications 7th Edition: Chapter 9 Spread Spectrum, <http://juliet.stfx.ca/~lyang/csci-465/lectures/09-SpreadSpectrum-new.ppt>
- [6] ETS 300 608. Digital Cellular Telecommunication System (Phase 2); Specification of the Subscriber Identity Module-Mobile Equipment (SIM-ME) Interface. European Telecommunications Standards Institute., May 1998.
- [7] ETR 100. European Digital Cellular Telecommunication System (Phase 2); Abbreviations and Acronyms. European Telecommunications Standards Institute., April 1995.

- [8] Jörg Eberspächer and Hans-Jörg Vögel. GSM switching, services and Protocols. John Wiley and Sons, 1999.
- [9] Klaus Vedder GSM: Security, Services, and SIM. State of the art in Applied Cryptography. Course on Computer Security and Industrial Cryptography. Leuven, Belgium, June 3-6, 1997.
- [10] J. Wu and A. H. Aghvami, "A new adaptive equalizer with channel estimator for mobile radio communications," IEEE Transactions on Vehicular Technology,
- [11] A. Clark and R. Harun, "Assessment of kalman-filter channel estimators for an HF radio link," IEE Proceedings, vol. 133, pp. 513-521, Oct 1986.
- [12] ETS 300 502. European Digital Cellular Telecommunication System (Phase 2); Teleservices Supported by a GSM Public Land Mobile Network (PLMN). European Telecommunications Standards Institute. September 1994.

## Design and Development of SMS Prepaid Energy Meter

<sup>1</sup>KESHINRO K. K., <sup>2</sup>AKINLEYE A. O., <sup>3</sup>SALAMI S. O., <sup>4</sup>SARUMI A. J.

<sup>1,4</sup>Department of Computer Engineering, Lagos State Polytechnic Ikorodu, Lagos State, Nigeria

**ABSTRACT:** This paper presents a prepaid energy meter to facilitate energy consumption measurement and to know consumer's maximum demand. The prepaid energy meter concept is shown by Proteus 8 software simulation. The major components are AVR microcontroller, Voltage and Current transformer, LCD, Relay and a load. Electricity has become one of the basic requirements for people and widely used for domestic, industrial and agricultural purposes.

The energy billing system used nowadays are labour and time consuming. Errors are inevitable at every stage of billing, some are human errors while noting down the meter readings, errors while processing the paid bills and the due bills. There is no proper way to know the consumer's maximum demand, usage details. This paper demonstrates the use of prepaid energy meter system. If we use this system it will be beneficial for the consumer to manage power. It is easy to operate and cost effective. Another advantage of the prepaid system is that the human errors in taking meter readings and processing bills can be reduced to a large extent.

**Keywords:** Billing, Voltage, Current, LCD, AVR, Microcontroller

### I. Introduction

Electricity meters operate by continuously measuring the instantaneous voltage (volts) and current (amperes). The product of which gives the instantaneous electrical power (watts) which is then integrated against time to give energy used. A Prepaid Energy Meter enables power utilities to collect electricity bills from the consumers prior to its consumption. The prepaid meter is also attributed with prepaid recharging ability and information exchange with the utilities pertaining to customer's consumption details.. Literature has witnessed quite an amount of work in this area (Nwaoko, 2006; Omijeh, 2012)

In recent years, Nigerian power sector has been facing a serious problem of lean revenue collection with respect to energy supplied due to energy thefts and network losses. It is observed that one of the faulty subsystems is the metering and meter-reading system, which has to improve, if revenue collection is to be increased (Nwaoko, 2006).

Electric energy meters is the direct billing interface between utility grid and consumers and it undergone several advancements in the last decade. The trend of the time has always been in favor of that technology which finally become cost effective as well as an elegant one. Traditional meter reading is done by the human operator, this require a more number of labor operator and long working hour to achieve the complete area data reading and billing. The major drawback of traditional billing system is power and energy theft. In postpaid system, there is no control use of electricity from the consumer's side, and there is a lot of wastage of power in the consumer's side due to lack of planning of electrical consumption in an efficient way This drawback is reduced by using a prepaid energy meter which is based on the concept "Pay first and then use it" (Schwendtner, 1996; Jawarkar, 2008). Due to the increase in the development of residential and commercial buildings, the meter reading task increases which requires more number of human operators. In order to achieve efficient meter reading, reduce billing error and operation cost, automatic meter reading system play an important role.

These drawbacks of the present prevailing metering systems are motivations into this work. They include:

- i) Inaccurate calculation of voltage, current and power by the energy meter.
- ii) Inability of query request about the working condition of the energy meter from distant locations.
- iii) Consumers have to form long queues to buy credit for their Energy Meters.
- iv) Those who do not use the prepaid meter have to wait for several days for them to be re- connected whenever there is disconnection.
- v) Some of the prepaid payment points are very far from the consumers.

## II. Review of Related Works

(Zhang, et al, 1998) utilized a DSP-based meter to measure the electricity consumption of multiple users in a residential area. A Personal Computer (PC) at the control centre was used to send commands to a remote meter, which in turn transmitted data back, using the power Line Communication (PLC) technique. The major problem with this system is that it cannot detect tampering by consumers.

(Koay et al, 2003) in their work, designed and implemented a Bluetooth energy meter where several meters are in close proximity, communicated wirelessly with a Master PC. Distance coverage is a major set-back for this kind of system because the Bluetooth technology works effectively at close range.

In their paper, (Scaradozzi, 2003) viewed home- automation systems as Multiple Agent Systems (MAS). Home automation system was proposed where by home appliances and devices are controlled and maintained for home management. It is only a home management system and does not measure the amount of energy consumed by users.

(Hong et al, 2005) in their paper, proposed the use of Automatic Meter Reading (AMR) using wireless networks. Some commercial AMR products use the internet for data transmission.

(Stanescu et al, 2006) present a design and implementation of SMS -based control for monitoring systems. The paper has three modules involving sensing unit for monitoring the complex applications. The SMS is used for status reporting such as power failure. Issues on billing system for electricity board usage were not considered.

(Malik et al,2009) in their paper, mainly focused on the controlling of home appliances remotely and providing security when the user is away from the place using an SMS- based wireless Home Appliance Control.

## III. Methodology

The following algorithm were used for the implementation

### 3.1 Algorithm for Energy Metering system at consumer's end

1. Start
2. Initialize the display and RTC.
3. Display date and time.
4. Check GSM Connection and set to Text Mode.
5. If GSM disconnected, display that on LCD and turn LED OFF, otherwise turn ON.
6. Receive User number and set it for communication.
7. Decide whether the number of units in Microcontroller is sufficient or not. If the balance is insufficient then disconnect the load from supply and send message to user number notifying of balance recharge otherwise connect to the load to supply.
8. Count the number of pulses initiated from inbuilt ADC when the load consumes power.
9. Measure time with the help of timer1.
10. Calculate power,  $P = 3000 \times X$  using this equation, where X denotes the frequency of pulses that is produced by the microcontroller.
11. Calculate energy
12. Store energy and power reading into the EEPROM of ATmega32 Microcontroller for future use.
13. Check for updates from GSM for rate updates according to real time.

### 3.2 Development of the Software

For the software part we use an algorithm and is given below

- i) The controller continuously scans the ports which receive inputs from maximum demand section and optical section.
- ii) If the optical pickup receives a pulse then the counter increments and display the unit consumed in LCD. Then count is compared to display the warning for recharging.
- iii) When the total unit finishes, after that the tripping relay is activated to disconnect the power.
- iv) If the maximum demand section gives a pulse then it activates the tripping mechanism.

Continuously the controller rechecks the maximum demand section and regains the power when load is reduced

### 3.3 Algorithm used for the implementation

- Step 1. Initialize display
- Step 2. Check balance (B) stored in EEPROM. If B=0, go to Step13.
- Step 3. Count no. Of pulse initiated from IC AD7751 with the help of counter and time by timer.
- Step 4. Calculate power (P) and Energy (E) units.
- Step 5. Perform  $B=B-E$  and stored B in EEPROM.
- Step 6. If B=50, go to step11, otherwise go to step2.
- Step 7. If SMS received check the no. From which SMS came.
- Step 8. If SMS coming from unknown number go to step12.

Step 9. If SMS from known number with valid command, form B=B+R and stored B in EEPROM, where R= recharge amount.

Step 10. Sent SMS to Customer “Recharge Successful” and go to step12.

Step 11. Sent SMS to customer “Keep Sufficient balance to avail uninterrupted service”.

Step 12. Delete SMS. Go to step2.

Step 13. Stop relay. Sent SMS to customer”Power off due to zero balance”.

**3.4 DESIGN OF A VOLTAGE SENSING DEVICE.**

The voltage sensor is needed to measure voltage and the phase angle of the voltage across the load accurately, and is expected to behave linearly in some specific voltage range. The voltage sensor module was designed to be connected to the main power on the input side and to the Energy Meter IC on the output side

**3.5 DESIGN OF A CURRENT SENSING DEVICE**

The current sensor is needed to monitor the current flow by measuring and reporting the actual current usage and the current phase angle to the microcontroller. It is also needed to operate accurately and linearly in order to obtain the accurate usage and consequently the accurate power usage. It is expected to be able to hold the maximum current of 10 Amperes. The current sensor was designed to connect directly to the load on the input side and to the Energy Meter IC on the output side. The input to the entity is the value of the voltage drop across a shunt resistor and the output to the meter IC is the voltage that is proportional to the input voltage. The ratio of the input and output voltage would depend on the model of the current transformer used in the circuit

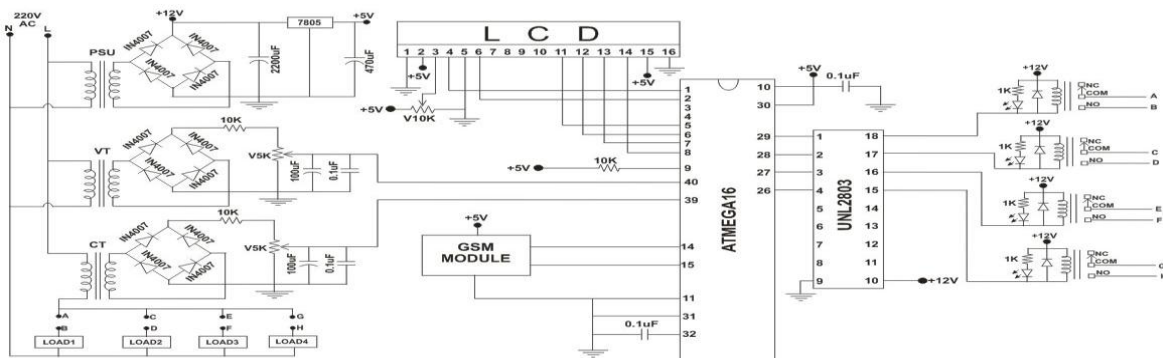


Figure 1: Complete Circuit Diagram of the SMS Prepaid Energy Meter  
Source: designed and impleneted with Labview ([www.labview.com](http://www.labview.com))

**IV. Result and Discussion**

**4.1 CALCULATION AND RESULT**

Energy is the total power delivered or consumed over a time interval,

That is Energy = Power x Time

Power = voltage x current x power factor

The Energy Meter was tested with one Electric bulb of 220 volt was used as a load with 0.4A current. The supply voltage was between 210 V and 230 V. Energy measurement process is described step by step. Table 1 test result of Energy measurement by proposed prepaid Energy meter. Here power =60 watt

Table 1: Energy Output

Time (Sec)	Measiured Energy Value (kw)	Intelligent EnergyValue(kw)
0	0	0
10	120	125
20	235	245
30	350	355
40	495	485
50	6000	6000
60	7100	7200
70	8500	8400
80	8700	8650
90	9000	8970
100	9800	9824

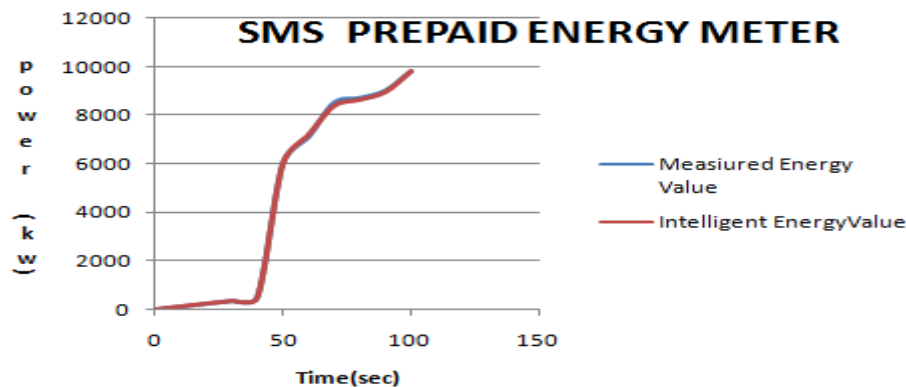


Figure 2: Power output Analysis

From Figure 2 above, the blue symbol (expected energy) is the measured value, the system calculate the energy consumption automatically by using current sensor to get the current readings and voltage sensor to get the voltage readings. The result was then store in log over certain period of time to get the energy consumption. The brown symbol is the intelligence. It can be proved that the intelligence shows slight variation with the manual system

## V. CONCLUSION AND RECOMMENDATION

### 5.1 Conclusion

This proposed simple and economic digital prepaid energy meter controlled by GSM based communication can cover rural area as well as urban areas. This is an effort about improving the present conventional electromechanical meters through the fusion of analog and digital circuits which have aim of collecting bills for consumption of power thus improved the revenue collection for scheduled supply. This is beneficial for Nigeria like developing country which having huge population for improving economic through power utility.

### 5.2 Recommendation

The distribution company is unable to keep track of the changing maximum demand for domestic consumers. The consumer is facing problems like receiving due bills for bills that have already been paid as well as poor reliability of electricity supply and quality even if bills are paid regularly. The remedy for all these problems is to keep track of the consumers load on a timely basis, which will help assure accurate billing, track maximum demand, and detect online theft. These are all the features to be taken into account for designing an efficient energy billing system. The present paper incorporates these features to address the problems faced by both the consumers and the distribution companies.

## Reference

- [1]. Amit, J. and Mohnish, B. (2011). A prepaid meter using mobile communication. *International Journal of Engineering, Science and Technology*-Vol. 3( No. 3), pp. 160- 166.
- [2]. Farhangi, H. (2010).The path of the smart grid. *Power and Energy Magazine, IEEE*. Vol. 8,pp 58.
- [3]. Hong. L. and Ning.L. (2004). Design and Implementation of Remote Intelligent Management System for City Energy Resources base on Wireless Network. *Study of Computer Application Vol 12* pp 237-239.
- [4]. Kistler R., , Knauth S., and Klapporth, A. *EnerBee* (2008).– *Example of an Advanced Metering Infrastructure based on ZigBee*. Munich, Germany : s.n.,. pp. 1-11.
- [5]. Koay .B.S, Cheah.S.S, Sng .Y.H,Chong. P.H.J, Shun.P,Tong.Y.C (2003) . Design and implementation of a Blue tooth energy meter. *proceedings of the Joint 4th International Conference on Information, Communication and Signal Processing and the 4th Pacific Rim Conference on Multimedia* .3: 1474-1477.
- [6]. Long Z.X., Yuan F.M and Qingdao, Y.N. (2010) Impact of smart metering on energy efficiency. *International Conference on Machine Learning and Cybernetics(ICMLC)*. pp. 3213 - 3218 .
- [7]. Maheswari, C; Jejanthi, R (2009). Implementation of Energy Management Structure for street Lighting System. *A Journal of Modern Applied Science* 5:6-10.
- [8]. Malik S.H ., Aihab. K, and Erum .S (2009). SMS Based Wireless Home Appliance Control System (HACS) for Automating Appliances and Security. *Issue in informing Science and Information Technology* 6:887-894.
- [9]. Nwaoko K.J. (2006).*Electrical Energy Accounting methods*, Lagos: Impressed publishers pp30-40
- [10]. Rodney, H. G., Lee, C.H. and Mok V. H. (2007), Automatic power meter Reading System Using GSM IEEE 8<sup>th</sup> International power engineering conference.
- [11]. Scaradozzi, D. and Conte, G. (2003). Viewing home automat ion systems as multiple agents systems. *RoboCUP2003*, Padova, Italy. Retrieved from [http://www.robosiri.it/ROBOCUP\\_2003/ROBOCUPSITOSIRI/articles/pdf/Conte.pdf](http://www.robosiri.it/ROBOCUP_2003/ROBOCUPSITOSIRI/articles/pdf/Conte.pdf)
- [12]. Shang L.W. 2009, Development of a smart power meter for AMI based on ZigBee communication . Taipei : IEEE, 2-5 Nov. *International Conference on Power Electronics and Drive Systems*. pp. 661 – 665

- [13] Shwehdi.M.H. and Jackson.C (1996). A microprocessor based digital wattmeter system design. *proceedings of the 31st Intersociety Conference on Energy Conversion Engineering* 31 pp 1840-1845.
- [14] Stanescu, D., Ciubotaru-Petrescu, B., Chiciudean, D., Cioarga, R.. (2006). Wireless Solutions for Telemetry in Civil Equipment and Infrastructure Monitoring. *3rd Romanian-Hungarian Joint Symposium on Applied Computational Intelligence (SACI)* . Retrieved from <http://www.bmf.hu/conferences/saci2006/Ciubotaru.pdf>
- [15] Sharma.S and Shoeb.S. (2011)- Design and Implementation of wireless automatic meter reading system . *International Journal of Engineering Science and Technology (IJEST)*- Vol. 3, No. 3, March 2011, pp. 2329-2334.
- [16] Zhang.J, Oghanna and Bai.C.L (1998). DSP based electricity meter with remote reading. *proceedings of the 4th International Conference on Signal Processing 2* :1581-1584

## A Novel Convergence Approach for an Adaptive Equalizers

Sayed Shoaib Anwar<sup>1</sup>, Dr. D. Elizabeth Rani<sup>2</sup>, Dr. S.G.Kahalekar<sup>3</sup>, Dr.Syed Abdul Sattar<sup>4</sup>

<sup>1</sup>Assistant Professor, MGM's College of Engineering, Nanded.431605 (M.S), India.

<sup>2</sup>Professor & Head, Gandhi Institute of Technology, Vishakhapatnam, 530045 (A.P),India.

<sup>3</sup>Professor,SGGSI of Engg. & Tech., Nanded,431606 (M.S),India.

<sup>4</sup>Dean, Royal Institute of Technology & Science, RR District, 501503 (T.S), India.

**ABSTRACT :** Linear equalizers were derived either on the deterministic Zero Forcing (ZF) approach for equalizers of ZF type or on the stochastic Minimum Mean Square Error (MMSE) approach for equalizers of the MMSE type. We present a new formulation of the equalizer problem based on a Weighted Least Squares (WLS) approach. Here, we show that it is possible and in our opinion even simpler to derive the classical results in a purely deterministic setup, interpreting both equalizer types as Least Squares solutions. This, in turn, allows the introduction of a simple linear reference model for equalizers, which supports the exact derivation of a family of iterative and recursive algorithms with optimize behavior. Due to this reference approach the adaptive equalizer problem can equivalently be treated as an adaptive system identification problem for which very precise Statements are possible with respect to convergence, optimization and  $l_2$ -stability.

**Keywords:** Zero Forcing (ZF), Minimum Mean Square Error (MMSE), Least Squares (LS), WeightedLeastSquare (WLS) and SingleInput SingleOutput (SISO).

### I. INTRODUCTION

Linear equalizers were designed either on the deterministic ZF approach for equalizers of ZF type or on the stochastic MMSE approach for equalizers of the MMSE type. We proposed a new formulation of the equalizer problem based on a weighted least squares (LS) approach. This deterministic concept is very much in line with Lucky so original formulation [11], leaving out all signal and noise properties (up to the noisevariance) but at the same time offers new insight into the equalizer solutions, as they share common LS or thogonality properties. This novel LS approach allows very general formulation to cover a multitude of equalizer problems, including different channel models, multiple antennas as well as multiple users [1].

In practice, the equalizer problem is not yet solved once the solution is known, as it typically involves a matrix inversion, a mathematical operation that is highly complexandchallenginginlow-costfixed-pointdevices.Adaptivealgorithmsarethus commonly used to approximate the results. Suchadaptive algorithmsforequalization purposescomeintwoforms, aniterative (alsooff-lineorbatch process) approach as well asarecursiveapproach (alsoon-lineordata-drivenprocess) that readjusts its estimates oneachnewdata elementthat isbeingobserved. Both approaches have their benefits and drawbacks. Ifchannlestimation isperformedinapreviousstep (forvarious reasons), then the iterative algorithm based onthe channelimpulseresponsemaybe most effective.Onthe other hand, itisnot required tocompute firstthe channelimpulseresponseifonlythe equalizer solution isofinterest. In particularintime-variantscenarios, onemay not have the chance to continuously estimate thechannelandthen compute equalizersolutionsiteratively andtherefore, arecursive solution that isableto track changes, may betheonlyhopeforgood results[2],[3].

However, such adaptive algorithms require a deep understanding of their properties as selecting their free parameter, the step-size, turns out to be crucial. While forward cascades adaptive filter designers were highly satisfied when they able to prove convergence in the mean-square sense, more and more situations now become known, in which this approach has proved to be insufficient, since, despite the convergence in them enquire sense, the worst case sequences exist that cause the algorithm to diverge. This observation has started with Feintuchs adaptive IIR algorithm and the class of adaptive filters with a line are filter in the error path [4],[5]but has recently found in other adaptive filters[6],[7],as well as in adaptive equalizers[8]. A robust algorithm design, on the other hand, is much more suited to solving the equalization problem as it can guarantee the adaptive algorithm will not diverge in any case. In this contribution we show how to design robust, adaptive filters for linear equalizers [9],[10].

**II. Formulation For Transmission Model**

Throughout this paper, we adopt that the separable transmit signal elements  $s_k$  have unit energy  $E[|s_k|^2] = 1$ , and the noise variance at the receiver is given by  $E[|v_k|^2] = N_0$ . We are considering several similar but distinct transmission schemes:

**2.1 Single User (SU) Transmission for Frequency Selective SISO Channels**

The following SU transmission defines frequency selective (also called time dispersive) single-input single-output (SISO) scenarios:

$$r_k = H s_k + v_k \tag{1}$$

Here, the vector  $s_k = [s_k, s_{k-1}, \dots, s_{k-S+1}]^T$  consists of the current and  $S - 1$  past symbols according to the span  $L < S$  of the channel  $H$ , which is typically the Toeplitz form as describe in (2). The received vector is defined as  $r_k = [r_k, r_{k-1}, \dots, r_{k-R+1}]^T$ . Let the transmission be disturbed by additive noise  $v_k$  being of the same dimension as  $r_k$ .

$$\begin{bmatrix} r_k \\ r_{k-1} \\ \vdots \\ r_{k-R+1} \end{bmatrix} = \begin{bmatrix} h_0 & h_1 & \dots & h_{L-1} & & \\ & \ddots & \ddots & & \ddots & \\ & & h_0 & h_1 & \dots & h_{L-1} \end{bmatrix} \begin{bmatrix} s_k \\ s_{k-1} \\ \vdots \\ s_{k-S+1} \end{bmatrix} + \begin{bmatrix} v_k \\ v_{k-1} \\ \vdots \\ v_{k-R+1} \end{bmatrix} \tag{2}$$

Note that for a toeplitz form channel  $H$  we have  $R < S$ . A linear equalizer applies an FIR filter  $f$  on the received signal  $r_k$  so that  $f^H r_k$  is an estimate of  $s_{k-\tau} = e_\tau^T s_k$  for the delayed version of  $s_k$ . A unit vector  $e_\tau = [0, \dots, 0, 1, 0, \dots, 0]^T$  with a single one at position  $\tau$  facilitates the description.

**2.2 Single User (SU) Transmission for Frequency Selective MIMO Channels**

The transmissions follow the same form as described in equation (5), although with a different meaning as we transmit over  $N_T$  antennas and receive by  $N_R$ . Such multiple input multiple- outputs systems are generally referred to as MIMO systems. The transmit vector  $s_k = [s_{1k}, s_{2k}, \dots, s_{N_T k}]^T$  is of dimension  $1 \times N_T$ , the channel matrix  $H$ , and thus the receive vector and the additive noise vector are of dimension  $1 \times N_R$ . Here,  $N_T$  is the number of transmit antennas. As in the previous case, we assume each entry of the transmit vector to have unit power. Unlike the earlier situation, however, we have to distinguish  $N_R > N_T$  (under determined LS solution) and  $N_R < N_T$  (over determined LS solution). For  $N_R = N_T$  both solutions coincide. In order to detect the various entries of the transmit vector  $s_k$ , we again employ a unit vector  $e_t : e_t^T s_k = s_{tk}$ . Note however that in contrast to the previous channel model, a set of  $N_T$  different vectors  $e_t, t = 1, 2, \dots, N_T$  will be employed in order to select all  $N_T$  transmitted symbols while in the frequency selective SISO case a single vector  $e_\tau$  is sufficient. Early works on linear MIMO equalization can be found in [15] and [16]. Note that precoding matrices are often applied in particular in modern cellular systems such as HSDPA and LTE. In this case the concatenation of the precoding matrix and the wireless channel has to be considered as a new compound channel. Such precoding matrices can also have an impact on the dimension of the transmit vector  $s_k$  as in many cases fewer symbols than rank are transmitted at each time instant  $k$ . A particular form of this is given when the precoding matrix shrinks to a vector, in which case we talk about beamforming where only one symbol stream is transmitted.

**2.3 Maximizing SIR and SINR**

To understand the vast amount of research and information available on this subject, one has to ask the question “What is the purpose of an equalizer?” While Lucky’s original work focused on the SU scenario, attempting a minimax approach to combat intersymbol interference (ISI), today we typically view the equalizer in terms of signal-to-interference ratio (SIR) or signal-to-interference and noise ratio (SINR). If a signal, say  $s_k$ , is transmitted through a frequency selective channel, a mixture of ISI, additive noise and signals from other users multiuser interference (MUI) is received. If signals are transmitted by multiple antennas, then additional

so-called spatial ISI (SP-ISI) is introduced. The ratio of the received signal power  $P_s$  and all disturbance terms before an equalizer indicated by the index ‘be’) is easily described as

$$SINR_{be} = \frac{P_s}{P_{ISI} + P_{SP-ISI} + P_{MUI} + N_0} \tag{3}$$

The task of the equalizer is to improve the situation, i.e., to increase this ratio. A linear filter applied to the observed signal can for example result in an increased  $P'_s > P_s$ , utilizing useful parts of  $P_{ISI}$  and  $P_{SP-ISI}$ , while the remaining and/or  $P'_{SP-ISI} < P_{SP-ISI}$  and/or  $P'_{MUI} < P_{MUI}$  is decreased. Unfortunately, the noise power  $N_0$  as well as its power spectral density is in general also changed when an equalizer filter is applied. At best it can be considered possible to achieve the post equalization SINR (the index ‘ae’ denotes after equalization)

$$SINR_{ae} \leq \frac{P_s + P_{ISI} + P_{SP-ISI}}{N_0} \tag{4}$$

Where the equalizer manages to treat the ISI and SP-ISI as useful signal whilst at the same time eliminating the MUI (for example by successive interference cancellation). The ratio of  $SINR_{be}$  to the eventually achieved  $SINR_{ae}$  is considered as the equalizer gain. The purpose of this paper is to develop a unified view of the SINR and SNR relation to the MMSE and ZF equalizer, which permits the introduction of a simple linear reference model as well as its application in an adaptive system identification framework.

### III. A Reference Model for An Adaptive Equalizers

While classical literature views the equalizer problem as minimizing a mean square error, we show in the following section that this is in fact not required and a purely deterministic approach based on a least squares modeling is possible. This approach in turn leads to the novel interpretation of the adaptive equalizer problem in terms of a classic system identification problem. For such problems, however, a much stronger  $l_2$ -stability and robustness has been derived in the past to ensure convergence of the adaptive algorithms under worst case conditions. In order to apply such robust techniques, we first have to show the equivalent system identification approach for equalizers. We start with the ZF equalizer and then continue with its MMSE counterpart [8].

#### 3.1 Zero Forcing (ZF) Equalizer

A solution to the ZF equalizer problem is equivalently given by the following LS formulation:

$$\begin{aligned} f_{\tau,t,m}^{ZF} &= \mathbf{arg\,min} \, \| \mathbf{H}^H f - \mathbf{e}_{\tau,t,m} \|_2^2 \\ &= \mathbf{arg\,min} \, \| \mathbf{H}^H [ f - (\mathbf{H}\mathbf{H}^H)^{-1} \mathbf{H} \mathbf{e}_{\tau,t,m} ] \|_2^2 \end{aligned} \tag{5}$$

With  $\mathbf{e}_{\tau,t,m}$  indicating a unit vector with a single one entry at Position  $\tau$ , for transmit antenna  $t$  of user  $m$ , thus  $\mathbf{e}_{\tau,t,m}^T \mathbf{s}_k = s_{k-\tau,t,m}$ , the transmit signal at antenna  $t$  of user  $m$  that will be decoded at delay lag  $\tau$ . Note that this form of derivation requires no signal or noise information, focusing instead only on properties of linear time-invariant systems of finite length (FIR); it thus entirely ignores the presence of noise. This is identical to Lucky’s original formulations [14], where system properties were the focus and the particular case of  $N_T = 1, M = 1$  was considered. If  $R N_R < S N_T M$  (for example, in Lucky’s SISO frequency selective scenario, we have  $R < S$ ) the solution to this problem is obviously given by

$$f_{\tau,t,m}^{ZF,o} = (\mathbf{H}\mathbf{H}^H)^{-1} \mathbf{H} \mathbf{e}_{\tau,t,m} \tag{6}$$

Commonly known as the ZF solution. Note that this is a so-called overdetermined LS solution as we have more equations than entries in  $f_{\tau,t,m}^{ZF}$ . When  $R N_R > S N_T M$  an alternative so-called underdetermined LS solution exists, as long as  $rank(\mathbf{H}) = S N_T M$

$$f_{\tau,t,m}^{ZF,o} = \mathbf{H}(\mathbf{H}\mathbf{H}^H)^{-1} \mathbf{e}_{\tau,t,m} \tag{7}$$

And requires independent consideration as will be provided further on in this section.

Let us first consider the overdetermined case of (7). As ISI does not vanish for finite length vectors, we propose the following reference model for ZF equalizers

$$\mathbf{e}_{\tau,t,m} = \mathbf{H}^H f_{\tau,t,m}^{ZF,o} + \mathbf{v}_{\tau,t,m}^{ZF,o} \tag{8}$$

With the modeling error vector

$$v_{\tau,t,m}^{ZF,o} = (I - H^H (HH^H)^{-1} H) e_{\tau,t,m} \tag{9}$$

The term  $v_{\tau,t,m}^{ZF,o}$  models ISI, SP-ISI, and MUI. The larger the equalizer length  $R_{N_R}$ , the smaller the ISI, e.g., measured in  $\|v_{\tau,t,m}^{ZF,o}\|_2^2$ . The cursor position  $\tau$  also influences the result.

### 3.2 Minimum Mean Square Error (MMSE) Equalizer

MMSE solutions are typically derived on the basis of signal and noise statistics [21], e.g., by

$$f_{\tau,t,m}^{MMSE} = \text{argmin}_f [ \|f^H r_k - s_{k-\tau,t,m}\|^2 ] \tag{10}$$

However, the linear MMSE solution can alternatively be defined by

$$f_{\tau,t,m}^{MMSE} = \text{argmin}_f (\|H^H f - e_{\tau,t,m}\|_2^2 + N_0 \|f\|_2^2) \tag{11}$$

$$= \text{argmin}_f \| (HH^H + N_0 I)^{-1} [f - (HH^H + N_0 I)^{-1} H e_{\tau,t,m}] \|_2^2 + MMSE$$

With an additional term, according to the additive noise variance  $N_0$ . We consider here white noise; alternative forms with colored noise, as originating, for example from fractionally spaced equalizers, is straightforward; one only has to replace  $N_0 I$  with  $R_{vv}$ , the autocorrelation matrix of the noise.

This formulation of the equation (11) has now revealed that the MMSE problem equivalently can be written as a weighted LS problem with the

$$MMSE = e_{\tau,t,m}^T [I - H^H (HH^H + N_0 I)^{-1} H] e_{\tau,t,m} \tag{12}$$

Defines the minimum mean square error. As the term is independent of  $f$ , it can thus be dropped when minimizing equation (11). The well-known MMSE solution is now obviously

$$f_{\tau,t,m}^{MMSE} = (HH^H + N_0 I)^{-1} H e_{\tau,t,m} \tag{13}$$

Similarly to the ZF equalizer, an over determined solution for  $R_{N_R} < S_{N_T M}$  also exists here.

$$f_{\tau,t,m}^{MMSE,o} = H (HH^H + N_0 I)^{-1} e_{\tau,t,m} \tag{14}$$

Under white noise both solutions are in fact identical  $f_{\tau,t,m}^{MMSE,o} = f_{\tau,t,m}^{MMSE}$ , which is very different to the ZF equalizer. Correspondingly, to thereference model for ZF equalizers in equation (8), we can now alsodefine a reference model for MMSE equalizers

$$e_{\tau,t,m} = H^H f_{\tau,t,m}^{MMSE} + v_{\tau,t,m}^{MMSE} \tag{15}$$

With the modeling error

$$v_{\tau,t,m}^{MMSE} = (I - H^H (HH^H + N_0 I)^{-1} H) e_{\tau,t,m} \tag{16}$$

Note, however, that unlike in the case of the ZF solution the modeling error is not orthogonal to the MMSE solution, i.e.,  $v_{\tau,t,m}^{MMSE H^H} f_{\tau,t,m}^{MMSE}$  is not equal to zero. MMSE equalizers are typically designed on the basis of observations rather than system parameters. Multiplying the signal vector with  $e_{\tau,t,m}$  we obtain

$$e_{\tau,t,m}^T s_k = s_{k-\tau,t,m} = f_{\tau,t,m}^{MMSE H} H s_k + v_{\tau,t,m}^{MMSE H} s_k \tag{17}$$

How does a received signal look after such MMSE-equalization? We apply on the observation vector and obtain

$$f_{\tau,t,m}^{MMSE,H} r_k = s_{k-\tau} - v_{\tau,t,m}^{MMSE,H} s_k + f_{\tau,t,m}^{MMSE,H} v_k \tag{18}$$

$$= s_{k-\tau} + \tilde{v}_{k,t,m}^{MMSE}$$

From classic equalizer theory it is well known that the remaining ISI energy of the ZF equalizer is smaller than that of the MMSE parts. The weighted LS solution  $f_{\tau,t,m}^{MMSE}$  of equation (17), applied to the observation vector  $r_k$ , defines a linear reference model in which the desired output signal is  $s_{k-\tau}$ , originating from a transmitted signal over antenna  $t$  of user  $m$ , corrupted by additive compound noise  $\tilde{v}_{k,t,m}^{MMSE}$ . The compound noise is defined by  $f_{\tau,t,m}^{MMSE,H} v_k$  as well as by the modeling noise  $v_{\tau,t,m}^{MMSE,H} s_k$ , defined by the modeling error vector  $v_{\tau,t,m}^{MMSE,H}$  in equation (16)

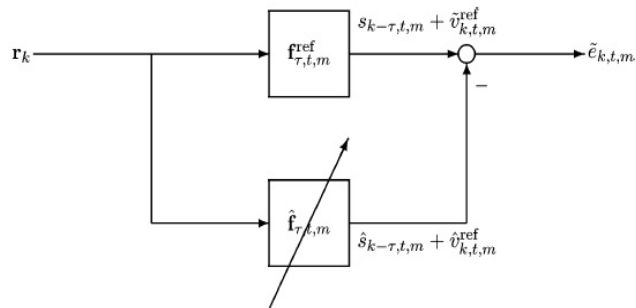


Fig 1: Adaptive Equalization as System Identification problem.

In conclusion, the adaptive equalizer problem has thus taken on the form of an identification problem as depicted in Fig 1. The linear system with impulse  $f_{\tau,t,m}^{ref}$  response is estimated as  $\hat{f}_{\tau,t,m}$  by an adaptive equalizer algorithm. Here, ‘ref’ stands for either MMSE or ZF. The outcome of the reference system is disturbed by the compound noise  $\tilde{v}_{k,t,m}^{ref}$  (see equation (18)) and constructs a noisy reference symbol  $s_{k-\tau,t,m}$ . The adaptive filter with its output  $\hat{s}_{k-\tau,t,m} + \hat{v}_{k,t,m}^{ref}$  tries to resemble  $s_{k-\tau,t,m} + \tilde{v}_{k,t,m}^{ref}$ . The distorted error signal  $\tilde{e}_{k,t,m}$  is applied to the adaptive filter in order to adjust the equalizer solution.

#### IV. An Iterative Algorithms for An Adaptive Equalizers

Equalizer solutions requiring matrix inverses are highly complex and numerically challenging, in particular when the matrix size is 50 or over. An iterative algorithm, as referred to here, is one that possesses all data and attempts to achieve an optimal solution. In the literature such algorithms are also referred to at times as off-line or batch algorithms since they require no new data during their operation. In this contribution we show convergence conditions for numerous known and novel algorithms, but do not deal with the question of when to stop the iterations [1].

##### 4.1 An Iterative Zero Forcing Equalizer (IZF)

Let Starting with an initial value  $f_0$  (which can be the zero vector), we arrive at the ZF iterative algorithm for  $x = H$

$$\hat{f}_l = \hat{f}_{l-1} + \mu H(e_\tau - H^H \hat{f}_{l-1}), \quad l = 1, 2, 3, \dots \tag{19}$$

With the reference model in equation (8) we can introduce the parameter error vector  $\bar{f}_l = f_\tau^{ZF} - \hat{f}_l$  and obtain we recognize that the noise condition is satisfied, as property  $H v_\tau^{ZF} = 0$  for  $\bar{v} = v_\tau^{ZF}$ . Convergence conditions for the step-size  $\mu$  are now also readily derived, being dependent on the largest Eigen value of  $HH^H$ .

$$0 < \mu < \frac{2}{\max \lambda(HH^H)} \tag{20}$$

As computing the largest eigenvalue may be a computationally expensive task, simpler bounds are of interest, even though they may be conservative.

1. A classic conservative bound is given by

$$0 < \mu < \frac{2}{\text{Trace}(HH^H)} \tag{21}$$

And can be computed with low complexity once the matrix  $H$  is known.

2. For a Single User in a frequency selective SISO channel, the channel  $H$  is defined by a single Toeplitz matrix, the largest eigenvalue of which can also be bounded by  $\max_\Omega |H(e^{j\Omega})|$ , with  $H(e^{j\Omega})$  denoting the Fourier transform of the channel impulse response. The corresponding condition for the step-size reads now

$$0 < \mu < \frac{2}{\max_\Omega |H(e^{j\Omega})|^2} \tag{22}$$

Such a step-size may be more conservative than the condition in equation (20) but it is also more practical to find.

In the simulation examples presented the bound so obtained is very close to the theoretical value in equation (20).

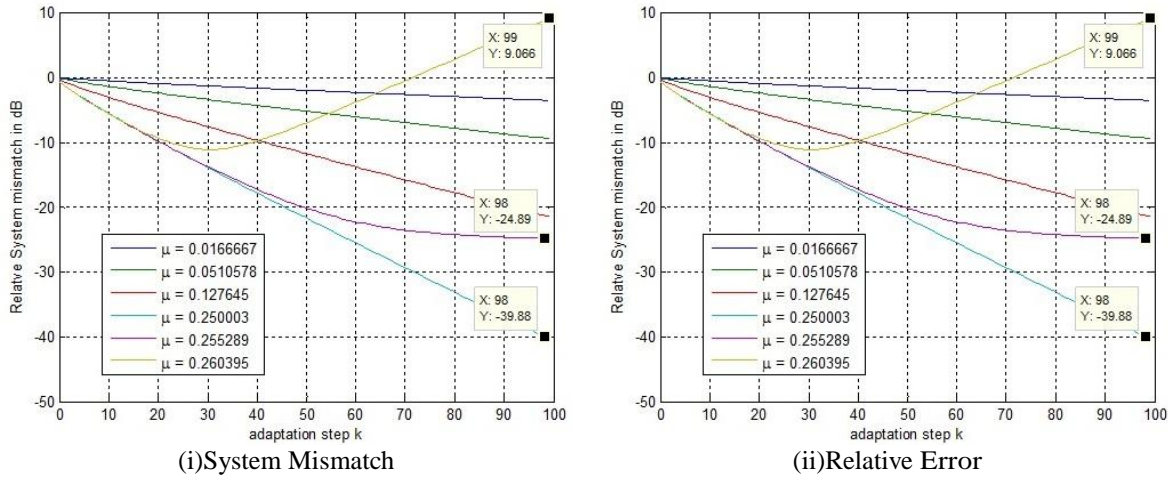


Fig.2:Iterative Zero Forcing Equalizer

Depending upon different step size conditions we have calculated Relative System mismatch and Error. Here as the number of iterations increases error decreases means we are converging towards desired values of filter weights.

4.2 An Iterative Fast Convergent An Zero Forcing Equalizer (IF-ZFE)

As the convergence of the previous equalizer algorithm (Iterative ZF Algorithm) is dependent on the channel matrix  $H$ , the algorithm exhibits much slower convergence for some channels than for others, even for optimal step-sizes. The analysis of the algorithm shows that the optimal matrix  $B$  that ensures fastest convergence is given by  $B = [HH^H J^{-1}]$ , which is exactly the inverse whose computation we are attempting to avoid with the iterative approach. If, however, some a priori knowledge is present on the channel class (e.g., Pedestrian or Vehicular A), then we can precompute the mean value over an ensemble of channels from a specific class, for example

$$E[HH^H J^{-1}] = R_{HH}^{-1} \tag{23}$$

In this case, the algorithm updates read

$$\hat{f}_l = \hat{f}_{l-1} + \mu R_{HH}^{-1} H(e_\tau - H^H \hat{f}_{l-1}); l = 1, 2, \dots \tag{24}$$

Convergence condition for this algorithm will be

$$0 < \mu < \frac{2}{\max \lambda(HH^H)} \tag{25}$$

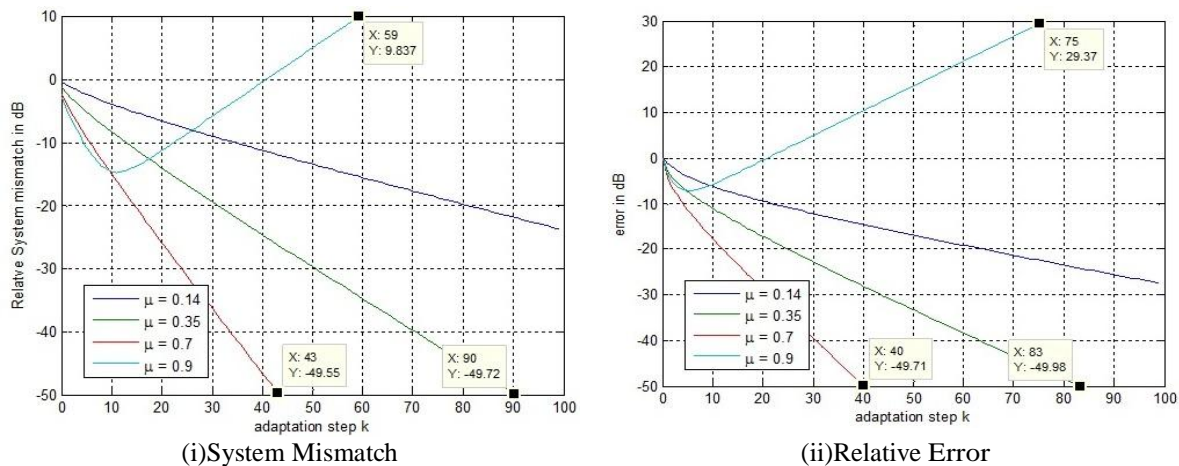


Fig.3:Fast Convergent of An Iterative Zero Forcing Equalizer

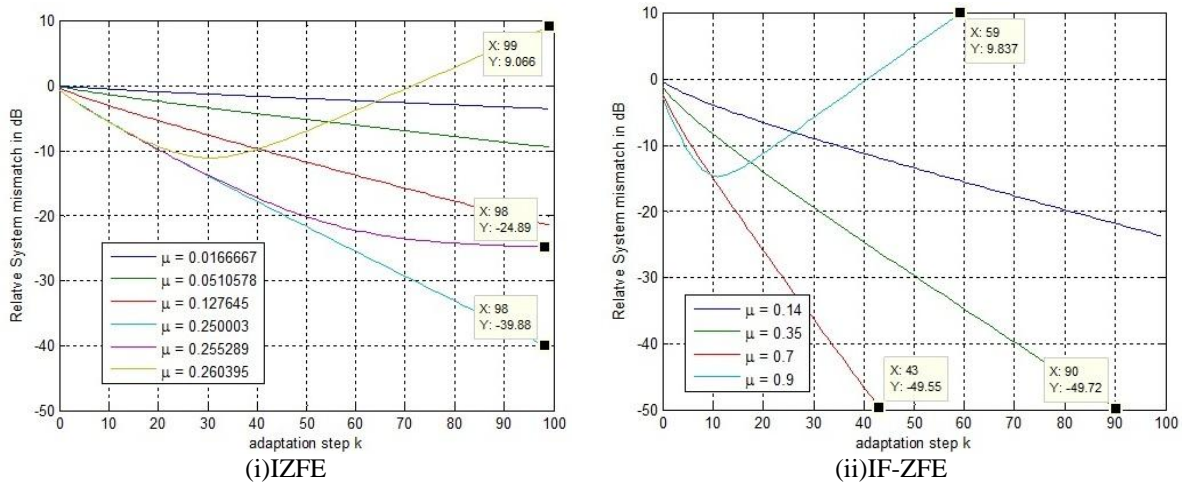


Fig.4: System Mismatch Comparison of IZFE v/s IF-ZFE

The convergence speed of above Zero Forcing Equalizer depends upon the channel, for some channels it is slowly convergent and for others it is fast convergent. For IF-ZFE, We can observe from results that this algorithm is fast convergent as compared to an IZFE algorithm as it reaches the desired value in very few iterations.

4.3 An Iterative Minimum Mean Square Error Equalizer (IM<sup>2</sup>SE<sup>2</sup>)

Let's start with our MMSE reference model equation (15), we consider the following update equation

$$\hat{f}_k = \hat{f}_{k-1} + \mu X(H e_\tau - (HH^H + N_o I) \hat{f}_{k-1}) \tag{26}$$

We can thus reformulate equation (26) into

$$\hat{f}_k = \hat{f}_{k-1} - \mu X(HH^H + N_o I) \hat{f}_{k-1} \tag{27}$$

If we select  $X = I$ , we can identify  $B = HH^H + N_o I$  and we find as a condition for convergence that

$$0 < \mu < \frac{2}{\max \lambda(HH^H + N_o I)} \tag{28}$$

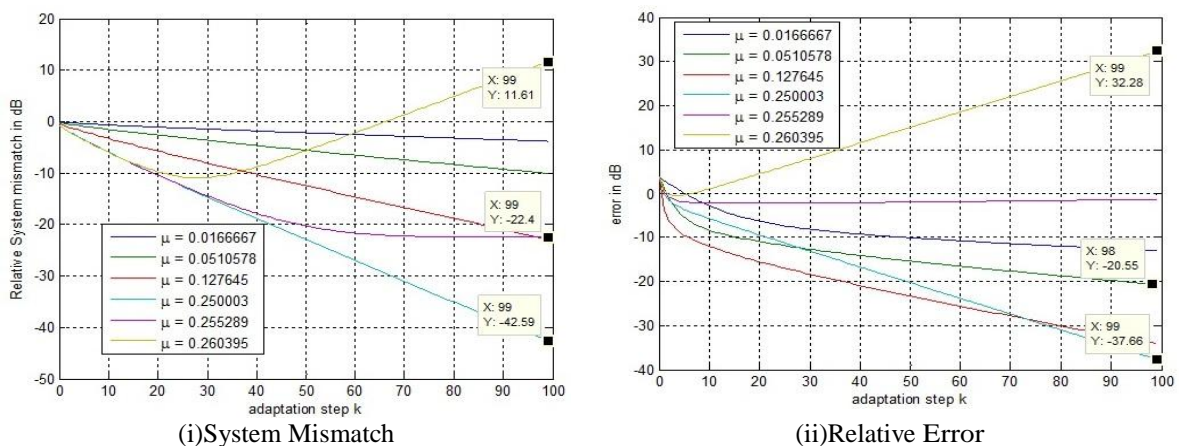


Fig.5: Iterative Minimum Mean Square Error Equalizer

The an IZF Equalizer does not consider channel noise, it cannot deal with noisy channel, and to deal this problem we designed MMSE Equalizer which considers channel noise in its algorithm for calculating the step size and Equalizer solution. Here also depending upon different step size conditions we have calculated Relative System mismatch and Error. Here as the number of iterations increases error decreases means we are converging towards desired values of filter weights.

4.4 An Iterative Fast Convergent Minimum Mean Square Error Equalizer (IF-M<sup>2</sup>SE<sup>2</sup>)

As the convergence of the previous equalizer algorithm (Iterative MMSE Algorithm) is dependent on the channel matrix H, the algorithm exhibits much slower convergence for some channels than for others, even for optimal step-sizes. The analysis of the algorithm shows that the optimal matrix B that ensures fastest convergence is given by  $B = [HH^H]^{-1}$ , which is exactly the inverse whose computation we are attempting to avoid with the iterative approach. If, however, some a priori knowledge is present on the channel class (e.g., Pedestrian B or Vehicular A), then we can precompute the mean value over an ensemble of channels from a specific class, a speedup algorithm is possible with

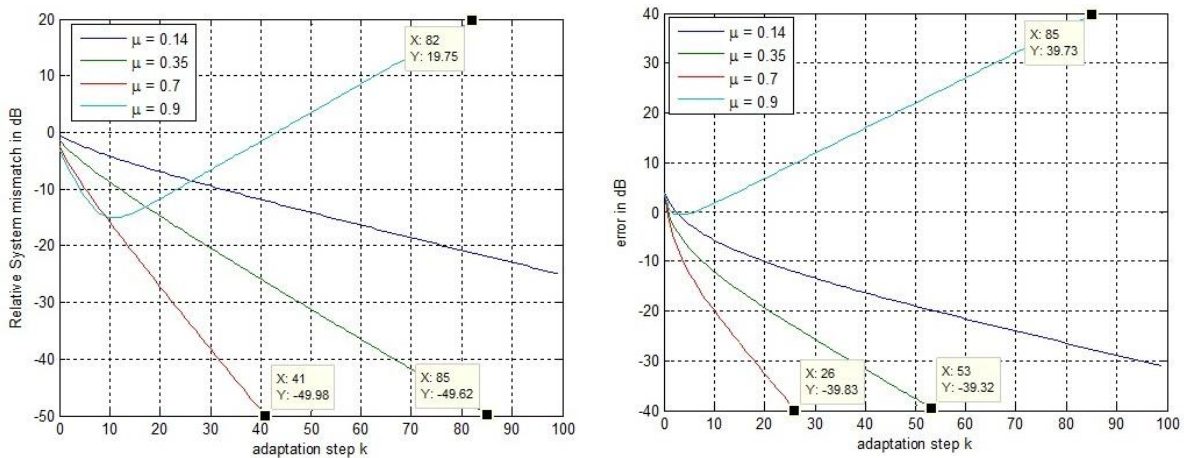
$$X = (R_{HH} + N_o I)^{-1} \tag{29}$$

In this case our Fast Convergent MMSE Algorithm will become

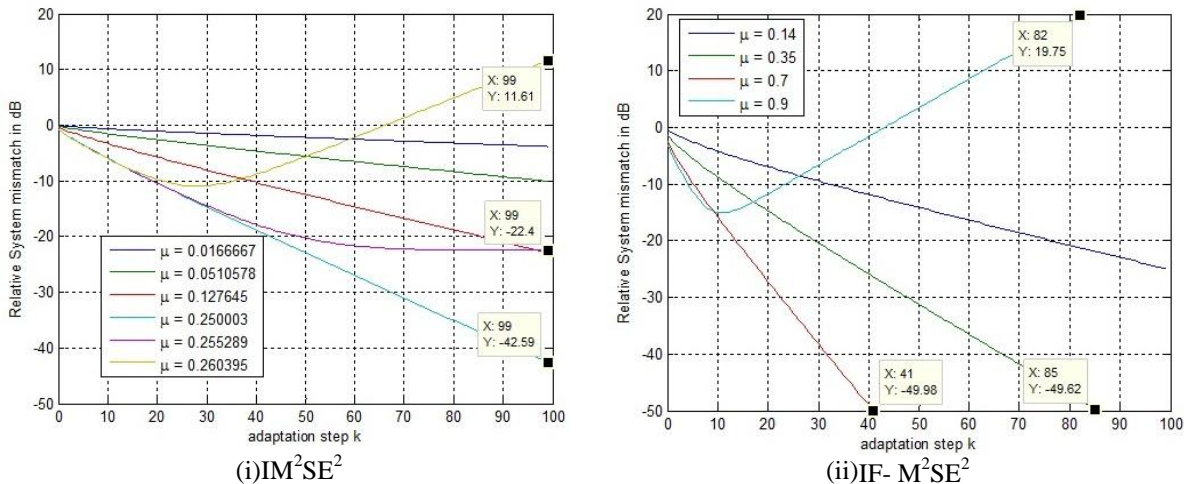
$$\hat{f}_k = \hat{f}_{k-1} + \mu(R_{HH} + N_o I)^{-1}(He_{\tau} - (HH^H + N_o I)\hat{f}_{k-1}) \tag{30}$$

The Convergence condition for this algorithm will be

$$0 < \mu < \frac{2}{\max \lambda(HH^H + N_o I)} \tag{31}$$



(i)System Mismatch (ii)Relative Error  
Fig.6:Fast Convergent An Iterative Minimum Mean Square Error Equalizer



(i)IM<sup>2</sup>SE<sup>2</sup> (ii)IF- M<sup>2</sup>SE<sup>2</sup>  
Figure7:SystemMismatch Comparison ofIM<sup>2</sup>SE<sup>2</sup> v/s IF- M<sup>2</sup>SE<sup>2</sup>

The convergence speed of above IM<sup>2</sup>SE<sup>2</sup> depends on the channel, for some channels it is slowly convergent and for others it is fast convergent. For IF- M<sup>2</sup>SE<sup>2</sup>, We can observe from results that this algorithm is fast convergent as compared to aIM<sup>2</sup>SE<sup>2</sup> algorithm as it reaches the desired value in very few iterations. We have also compared IZF with IM<sup>2</sup>SE<sup>2</sup>, which is shown in the results. From the results, we can observe that the relative Error of IM<sup>2</sup>SE<sup>2</sup> is less as compared to IZF, because IZF Equalizer can't deal with noisy channels this problem we have overcome using IM<sup>2</sup>SE<sup>2</sup> Equalizer which reduces ISI as well as noise power.

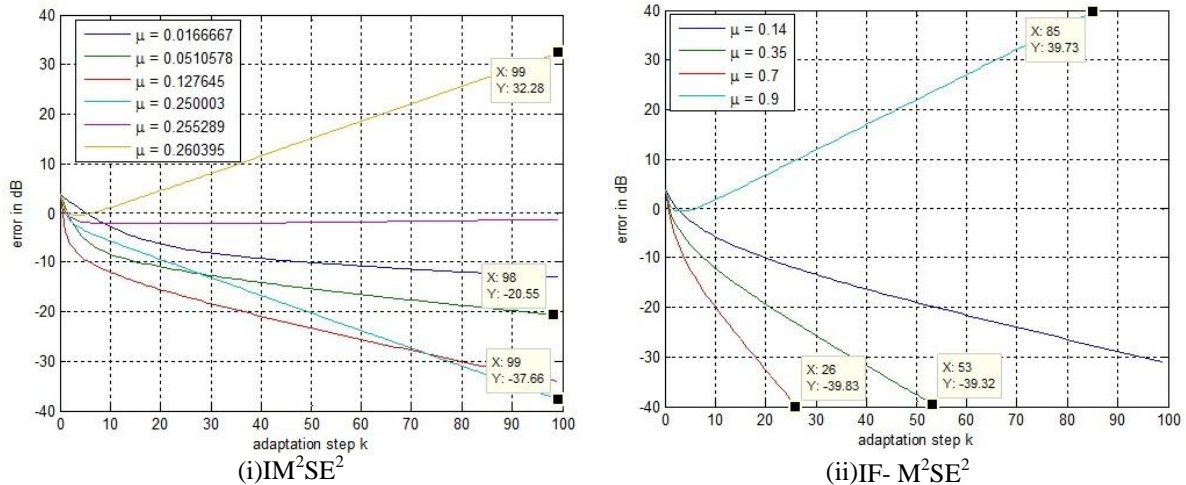


Figure8:Relative Error Comparison of  $IM^2SE^2$  v/s  $IF- M^2SE^2$

As compared to an  $IM^2SE^2$  algorithm as it reaches the desired value in very little iteration. We have also compared an IZF with a  $IM^2SE^2$ , which is shown in the results. From the results, we can observe that the relative Error of a  $IM^2SE^2$  is less as compared to an IZF, because an IZF Equalizer can't deal with noisy channels this problem we have overcome using  $IM^2SE^2$  Equalizer which reduces ISI as well as noise power.

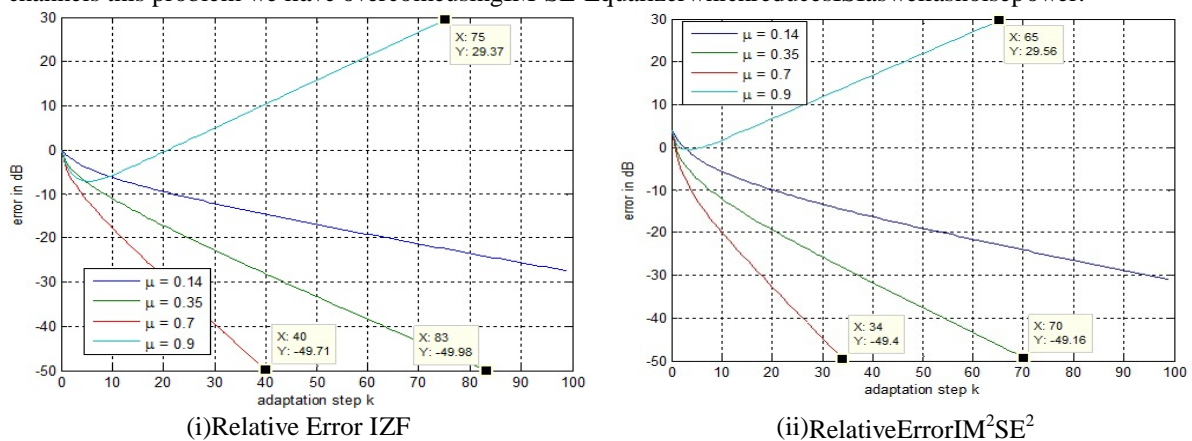


Fig.9:Relative Error Comparison of IZF and  $IM^2SE^2$  Equalizers

In order to perform out theoretical findings, we present selected Matlab examples, we consider a set of seven channels impulse response of finite length [8] with the length of the channel to be  $M = 50$  for which even the first four impulse responses have decayed considerably. If we run an iterative receiver (also of 50 taps), the result for  $h_k^{(i)}$  is depicted on the left-hand side (LHS) of Figures, with  $f_0$  denoting the ZF solution and  $\hat{f}_k$  denoting its estimate. Based on the convergence condition in equation (20) it is possible to compute the exact step-size bound (0.255), given the channel matrix  $H$ . Also shown in the figure are the conservative bound in equation (20), which is the smallest step-size (0.017) in the figure, resulting in the slowest convergence speed and equation (21), which is just a fraction smaller (0.25 vs. 0.255) than the step-size bound. The average inverse autocorrelation  $R_{HH}^{-1}$  is computed over all seven channels, and applied in the algorithm's updates. This results in a considerable speed-up in the iterations as proposed and is depicted on the right-hand side (RHS) of Figures.

### V. Conclusion

Due to an LS approach it is now possible to derive the classical equalizer types with an alternative formulation, and LS formulation for IZF and a weighted LS formulation for  $IM^2SE^2$  equalizers. This in turn resulted in a linear reference model for both. Based on such a linear reference model, it is possible to derive iterative forms of equalizers that are robust. Conditions for their robustness were presented, and in particular ranges for their only free parameter, the step-size, were presented to guarantee robust learning. We have also compared IZF and  $IM^2SE^2$  and  $IF- M^2SE^2$  Equalizers, it is found that  $IF- M^2SE^2$  Equalizer performs better as compared to IZF and  $IM^2SE^2$  Equalizer. Simulation example validates our findings.

## References

- [1] Markus Rupp. "Robust design of adaptive equalizers" *Signal Processing, IEEE Transactionson*, 60(4):1612–1626, 2012.
- [2] Paul L Feintuch. "Anadaptive recursive LMSfilter". *Proceedings of the IEEE*, 64(11):1622–1624, 1976.
- [3] C Richard Johnson Jr, Michael G Larimore, PL Feintuch, and N.J.Bershad."Comments onandadditions toanadaptive recursiveLMSfilter". *Proceedings oftheIEEE*, 65(9):1399–1402, 1977.
- [4] Markus Rupp and Ali H Sayed."On the stability andconvergenceofFeintuch'salgorithmforadaptiveIRfiltering".In*Acoustics, Speech,and SignalProcessing, 1995.ICASSP-95, 1995InternationalConferenceon*, volume2,pages1388–1391, 1995.
- [5] Markus Ruppand AliHSayed. "Atime-domain feedbackanalysisoffiltered- erroradaptive gradientalgorithms". *Signal Processing, IEEE Transactionson*, 44(6):1428–1439, 1996.
- [6] Robert Dallinger and Markus Rupp."A strict stability limit for adaptive gradient type algorithms" In *Signals, Systems and Computers, 2009 Conference Record of the Forty-Third Asilomar Conference on*, 1370–1374.IEEE, 2009.
- [7] Markus Rupp."Pseudo affineprojection algorithmsrevisited: robustness andstability analysis" *SignalProcessing, IEEE Transactionson*, 59(5):2017–2023, 2011.
- [8] MarkusRupp. "Convergencepropertiesofadaptiveequalizationalgorithms" *Signal Processing, IEEE Transactionson*, (6): 2562 – 2574, 2011.
- [9] AliHSayed andMarkusRupp. "Error-energy bounds for adaptive gradient algorithms" *Signal Processing, IEEE Transactions*, 44(8):1982–1989,1996.
- [10] A.H.Sayed andMRupp. "Robustness issuesin adaptive f i l t e r s " *The DSPHandbook*.
- [11] RWLucky. "Automatic equalization for digital communication" *Bell System Technical Journal*, 44(4):547–588,1965.
- [12] Dominique Godard."Self-recovering equalization and carrier tracking in two-dimensional data communication systems" *IEEE Transactions on*, 28(11):1867–1875,1980.
- [13] Simon S Haykin. *Adaptive filter theory*. Pearson Education India, 2007.
- [14] Bjorn A Bjerke and John G Proakis. "Equalizationanddecodingformultiple- input multiple-outputwirelesschannels". *EURASIP Journal onAppliedSignal Processing*, 2002(1):249–266, 2002.
- [20] Shahid U H Qureshi. "Adaptive equalization". *Proceedings of the IEEE*, 73(9):1349–1387,1985.
- [21] John G Proakis. *Intersymbol Interference inDigitalCommunication Systems*". WileyOnlineLibrary, 2001.



**Sayed Shoaib Anwar**, was born on 15<sup>th</sup> June 1982 in Nanded, Maharashtra, India. He received his bachelor of Engineering from Dr. B.A.M. University, in 2005. He completed his Master degree in 2007 from S.G.S.I.E&T. He started his doctoral studies in the area Multicarrier Communication. He is having the research interest in the field of wireless communication, Multicarrier Communication and OFDM system. He Published more than 14 papers in different journals and conferences. [sayed\\_shoaib@mgmcen.ac.in](mailto:sayed_shoaib@mgmcen.ac.in)



Dr. D. Elizabeth Rani, She is recently working as Professor & Head in Electronics and Instrumentation Engineering department, GIT-GITAM, Visakhapatnam, India. She received her bachelor of Engineering in 1982, Master degree in 1984 from and Doctorate in the field of Communication in 2003. Her area of specialization is Signal processing. She published more than 20 research papers in different Journals and conferences. [kvelizabeth@gitam.edu](mailto:kvelizabeth@gitam.edu)



**Dr. S.G. Kahalekar**, he worked as a Professor, SGGSI of Engg. & Tech, Nanded. He received his bachelor of Engineering in 1975. He completed his Master degree in 1977 from IIT, Kharagpur. He completed his Doctorate in the field of Biomedical in 2008. He has more than 40 years of experience in research field. He received different awards in research field. [sgkahalekar@yahoo.com](mailto:sgkahalekar@yahoo.com)



**Dr. Syed Abdul Sattar**, he is currently working as Dean, Royal Institute of Technology & Science, he is having the qualification B.Tech. (ECE), M.Tech. (DSCE), Ph.D.(ECE), Ph.D. (CS), his area of research is Electronic Communications and Computer Engineering. He has more than 25 years of experience in research. He published more than 150 research papers in different journals and conferences. [syedabdulsattar1965@gmail.com](mailto:syedabdulsattar1965@gmail.com)

## Prospects of Implementing E-Learning Systems based on Learning Objects and XML in Nigeria's Educational Sector.

ARTHUR U. UME (PhD)

*International Development Consultant & Solutions Expert, School of Computing and Information Technology,  
Baze University- Abuja, Nigeria*

**ABSTRACT:** *This paper started with highlighting the forms of e-learning and pointing out the key difference between Synchronous and Asynchronous e-learning. It described the popular e-learning systems that gained ground and recognition in Higher Institutions in countries like Nigeria, and went on to point out the need for resident application developers and computer interaction designers to study the existing conventional e-learning systems out there with the aim of finding possible ways to extend/improve the interactivity, accessibility and compatibility of such disparate systems through the use of XML (Extensible Markup Language) and learning objects such as Avatars and Embodied Conversational Agents (ECAs).*

**KEYWORDS:** *E-learning, e-learning systems, Synchronous e-learning, asynchronous e-learning, XML, Learning objects, Avatars, Embodied Conversational Agents (ECAs), Artificial Intelligence (AI), Virtual characters, Anthropomorphism.*

### I. INTRODUCTION

E-learning is not a new phenomenon in promoting education in the developed parts of the world. Presently, with the tremendous boom in Information technology in Nigeria many educational institutions are increasingly using e-learning capabilities to promote distance education (DE) and lifelong learning. Much literature abound regarding e-learning and e-learning management systems.

According to Abbaszadi et al., (2010) with accelerating developments in educational technologies in Nigeria, distance learning is becoming more convenient than it was some decades; Abbaszadi et al., also state that e-learning offers great opportunity to those individuals who have little time to spare because of their jobs, to earn their living while studying.

E-learning according to Timothy O.A et al (2008), is the use of electronic technology to deliver education and training applications, monitor learner's performance and report learner's progress. Hedge and Hayward (2004), also defined e-learning as an innovative approach for delivering electronically mediated, well-designed, learner-centered and interactive learning environments to anyone, anyplace, anytime by utilizing the internet and digital technologies in concern with instructional design principles. In other words, e-learning involves the use of the computer or any other electronic device (mobile, handheld or wearables) to acquire knowledge through the internet or through offline electronic data storage (CD-ROM, flash drives etc.). It should be noted that the online aspect involves the use of browsers. Thus, e-learning is all about learning with the use of ICTs.

Islam (1997) writes that the convergence of the internet and learning, or Internet enabled learning is called e-learning. The applications and process of e-learning include computer-based learning, web-based learning, virtual classroom and digital collaboration where contents is delivered via the internet, intranet/extranet, audio and or video tapes, satellite TV and CD-ROM.

Higher educational institutions are increasingly moving towards the use of the Internet as a blended capability for delivery of courses, both on campus and at a distance (Ally, 2004, Kim & Bonk, 2006). The Internet provides significantly different and interesting possibilities for computer-mediated communication and learning from other forms of educational technologies (Weller, 2002, p. 34). There are, therefore, ways in which e-learning environments may be utilized based upon pedagogical needs. The development of instructionally effective online learning environments that meet the pedagogical needs require the application of appropriate instructional design principles. The literature suggests that there are gaps between the bodies of knowledge relating to learning theories, instructional design principles and student learning in higher education, (Siragusa & Dixon, 2005a).

In a recent PhD study (Siragusa, 2005) developed a theoretical framework and research methodology aimed at putting forward instructional design principles that effectively promote the use of online learning to meet the varying pedagogical needs in higher education.

(Ozkul, 2003), records that the use of internet brought lots of opportunities to different fields and especially to Instructional Technologies. This author went further to note that based on these new technologies, learning environments are able to provide a wide range of educational alternatives for learners. Distance learning he says is one of these alternatives which became attractive where students and instructors are physically in different locations and time. By using distance learning tools, education can be more flexible with respect to place and time constraints. Thus, students can access information anytime and anyplace, such as either in libraries or during lectures.

(Dutta et al., 2011) Broadly speaking, e-learning is the delivery of educational content through electronic media, including Internet, intranet, extranet, satellite broadcast, audio and video tapes, interactive TV, interactive CDs and computer-based system. However, the strength of recent e-learning systems lies in the emergence of Web 2.0 tools which according to Awodele et al. (2009) is a concept that has developed some new initiatives in education identified as e-learning 2.0. Web 2.0 tools have influenced e-learning systems in terms of pedagogy and delivery as a result of a high degree of user involvement and social networking (Anderson, 2007). The Web has therefore been established as a major platform for applications in learning.

According to Friesen, N. (2009), e-learning is an educational system for providing learning through electronic technologies especially the Internet. This researcher writes that e-learning brings a community of learners together and unrestricted by the time and place where students are able to discuss with other fellows and teachers via online and gather different types of knowledge from the different discussion forums. Holmberg, B. (2005). Also writing about e-learning noted that e-learning is a relatively new phenomenon and can be defined as delivering education to students who are not physically present; rather than being in lecture halls in person, students and teachers can communicate with each other using the Internet.

Concerning the design and implementation of e-learning systems, according to Observatory on Borderless Higher Education (2002), some higher educational institutions continue to develop in-house systems or buy into open source alternatives, but it is being reported that an ever-larger majority is purchasing licenses for proprietary platforms. In another study that supports the results of Observatory on Borderless Higher Education. (Paulsen 2003) shows that, usually many institutions find it quite easy to start with a commercial-of-the-Shelf Learning Management Systems (LMS), but they face many problems such as; Linguistic, assessment tools, suitability to target groups and pricing. It is therefore no wonder that, open source LMS is having a great impact on the future of the LMS market with its cost effectiveness and advanced features. Due to the advantages of distance learning, schools and companies are increasingly adopting these new learning technologies and increasing their investments in it. However, along with the advantages that accompany these innovations, installation and support costs appear to be big disadvantages compared to a traditional learning environment. There is also the problem of incompatibilities of platforms if modules of the e-learning systems do not come from the same software developer or vendor. This is actually the case with many Nigerian universities that implemented massive and robust e-learning systems, and are presently stuck with its perceived "incompatibilities" with surround instructional technologies.

It is worth noting that in order for different e-learning systems to communicate and interoperate with each other, it is important to have a common language among the systems. Nowadays, the common language adopted by most learning organizations is the Extensible Markup Language (XML), since XML can facilitate significant features in the e-Learning framework, such as personalization, interoperability, reusability and flexibility [XML 2000]. The XML was actually originally developed to facilitate the description and exchange of data with the aim to enhance interoperability on the Web by the World Wide Web Consortium.

Regarding the mode communication of e-learning systems, Andersen A., Hristov, E. & Karimi, H. (2008), noted that e-learning could be either synchronous or asynchronous or both.

## II. SYNCHRONOUS E-LEARNING

This is when teachers and students communicate in real time by using webcams and microphones for instance. The communication is done live and thus it leaves some room for interaction in the form of students asking questions and getting answers to their questions shortly after. It is interesting to note that since synchronous e-learning is done in real time, it requires a relatively fast Internet connection, something that was not available ten years ago.

Examples of synchronous online technology types include videoconferencing, webcasts, interactive learning models, and telephone conferences (Er et al., 2009; eLearners.com, 2012). The advantages of synchronous e-learning include the following: instructional pacing, improved student engagement, synchronous real-time collaboration.

### **ASYNCHRONOUS E-LEARNING**

Asynchronous e-learning on the other hand is when students can download or stream pre-recorded materials (lectures or written documents for instance). Asynchronous e-learning has its limitations when it comes to interaction between teacher and student

However, it possess a great advantage in that it offers students more flexibility as students can download lectures and watch them at any point they wish.

For synchronous as well as asynchronous e-learning, the platform that is generally used is an intranet—where lectures and documents can be uploaded and made accessible for everyone within the intranet. However, due to technological development in recent years, new platforms for online learning have been made available.

Regarding the design, creation and development of e-learning systems, Hall (2003) wrote that all Learning Management Systems (LMS) are built in a way to “manage the log-in of registered users, manage course catalogs, record data from learners, and provide reports to management.”

### **III. STATEMENT OF PROBLEM**

Just like in the other parts of the world, with the current penetration of ICTs in Nigeria, e-learning educational technology is becoming more prevalent in the country. Consequently gradually teaching and learning is no longer being restricted just to face – to – face instruction by teachers in traditional classroom enclosures. In the formal educational institutions, the combination of e-learning technology and face - to –face teaching and learning is continuing to increase accessibility, flexibility and choices for student – instructor interactivity. This is causing a leap in instructional productivity. Traditional instructional activities such as information presentation, managing course materials, collection, tracking and evaluation of students’ work are all now being complemented using e-learning systems.

Nevertheless, there is still need to design e-learning systems in such a way to increase compatibility, accessibility, and interactivity between instructors and the students. The incorporation of Avatars and ECAs (Embodied Conversational Agents) in the design of e-learning systems would further enhance the effectiveness in delivering instructional contents to remote areas, where distance learning is expected or anticipated and few teachers are on ground to provide face-to-face teaching. This possibility and penetration can as well be extended to improve the teeming informal education sector in developing countries like Nigeria.

### **IV. OBJECTIVES OF PAPER**

The key objectives of this paper are:

- i. To discuss the forms of e-learning systems.
- ii. To spur Information Technology designers and developers to improve and extend e-learning systems’ compatibility use of XML and learning objects such as Avatars and Embodied Conversational Agents (ECAs).
- iii. To discuss the limitation of outright purchase and installation of off-the-shelf disparate e-learning systems.

### **V. THE CONVENTIONAL E-LEARNING MANAGEMENT SYSTEMS**

In an educational context, e-learning platforms are also known as Learning Management Systems (LMSs) which are Internet based software. The Learning Management Systems allow instructors to manage materials distribution, assignments, communications and other aspects of instructions for their courses Abu, S.B. (2009). Today, LMSs have become an integral component of the educational systems in most universities and interest is increasing in hybrid approaches that blend in class and online activities as stated by Pishva, D. et al. A LMS is not intended to replace the traditional classroom setting, but its main role is to supplement the traditional lecture with course content that can be accessed from campus or the Internet Landry, B. Griffeth, R. & Hartman, S. (2006).

The most popular LMS are out there in most Universities in countries like Nigeria are the following: Modular Object-Oriented Dynamic Learning Environment (MOODLE), Online Learning and Training (OLAT), Claroline, eFront, Blackboard, Share Point LMS Faxen, T. (2011).

- **THE MODULAR OBJECT-ORIENTED DYNAMIC LEARNING ENVIRONMENT (MOODLE)**

The Moodle is an Open Source Learning Management System, which is known as one of the most widespread and famous Learning Management Systems. Moodle has been translated to 30 languages and found in 1026 sites from 75 countries over the world (Itmazi&Megías, 2005). Moodle gives the educators the best tools to manage and promote learning (Raadt, 2013; Jin, 2012). However, some of the disadvantages and missing features are as follows, Working Offline: Occasionally, students download their course contents and they access the content on a CD-ROM to work offline. In this regard, the course placeholder automatically returns to the location in their course where they were working the last time they logged off. A big issue with Moodle is the fact that it is not fully developed to cope with big projects. While it may be useful for colleges or universities of small to medium size, the system might not work efficiently with larger schools or serve as a great way to conduct all classes in a city. In addition to the lack of complete development, Moodle users frequently complain about the troubles they experience with customizations.

- **THE ONLINE LEARNING AND TRAINING (OLAT)**

OLAT (Online Learning and Training) is an Open Source LMS (Learning Management System) tailored to the needs of Universities and Higher Education institutions. The development of OLAT was driven by the University of Zurich where it is presently extensively used. There are approximately 70,000 users and nearly 50 institutions in Switzerland using OLAT (with up to 5,000 courses and millions of resources), and the numbers keep on growing. OLAT is available in several languages and can provide diverse functionality for all e-learning needs in web-based learning and training

- **CLAROLINE**

Claroline is a collaborative e-Learning and eWorking platform (Learning Management System) released under the GPL Open Source license. Created in 2000 at the Catholic University of Louvain (UCL), Claroline is the second most commonly used online learning application in Europe. It is easy to use, owing in part to its lesser functional depth in comparison to Moodle

- **eFRONT**

The core of eFront is distributed as an open-source project and custom software solution for your training needs. eFront is designed to assist with the creation of online learning communities while offering various opportunities for collaboration and interaction through an icon-based user interface. eFront comes in a number of editions, from an open-source edition to the latest eFrontPro edition.

- **SHAREPOINT LMS**

The SharePoint LMS is an award-winning learning management system for the internal SharePoint platform. SharePoint LMS lets instructors intuitively combine new and existing training elements, documentation, materials, media, communication channels, and learning methods to deliver a media-rich training experience learners find valuable, and enables the following Webinars, Blended classroom training, Instructor-led and self-study workflows, Embedded procedures, manuals, and other compliance documents.

- **ILIAS**

This is a Learning Management System (LMS), developed at the University of Cologne/Germany.

ILIAS is a web-based Open Source Learning Management System. ILIAS has been translated to at least 16 languages and found in 115 sites from 18 countries over the world (ILIAS, 2013; Itmazi&Megías, 2005). It was developed using PHP, MySQL and the Apache to work mainly under UNIX/Linux.

## **VI. IMPROVING E-LEARNING MANagements SYSTEMS BY LEVERAGING XML, VIRTUAL CHARACTERS AND LEARNING OBJECTS**

- **XML (EXTENSIBLE MARKUP LANGUAGE) IN E-LEARNING**

Regarding the adoption of XML and learning objects, (Gerber 2001), reports that the great potential of using XML has been predicted by many developers and technology-driven companies. He said that in fact, several learning organizations, including a group newly formed by IEEE, are trying to develop e-Learning standards using XML. XML allows developers to create structured exchangeable learning content which can be manipulated in different ways to achieve educational deliverables among disparate systems. XML tags provide flexibility to create customizable, interoperable and transferable learning content. XML thus is used as data descriptor to make integration between components that render e-learning content easier.

It is worth noting that XML was originally developed to facilitate the description and exchange of data on the Web by the World Wide Web Consortium. It is a means of representing information according to its internal structure. Such a structure makes the information in the XML files meaningful and machine-readable, and therefore achieves interoperability and reusability of information. The great potential of using XML has been predicted by many developers and technology-driven companies. In fact, several learning organizations, including a group newly formed by IEEE, are trying to develop e-Learning standards using XML.

When XML is used to store unstructured or semi-structured data, for which the traditional relational database is not suitable, it gives application designers and developers the ability to manipulate the information easily and quickly. With XML, course developers may put semi-structured information, such as the course content or course structure, into a discrete relational field, and then work with this information as with structured blocks of data, not as with a string of bytes. Therefore, for e-Learning, XML provides a flexible approach to represent and track the content and the structure of a course, and to keep such information separate from the software used for delivery and presentation. Moreover, content stored using XML can be independent of any course, and is in a form ideally suited to re-use in any number of different courseware and other learning-related products. For example, learning content in XML may be transformed into printable PDF to form a part of a book, or into HTML to provide online education.

#### - **ARTIFICIAL INTELLIGENCE, VIRTUAL CHARACTERS AND AVATARS IN E-LEARNING**

Artificial intelligence (AI) which is an increasingly growing subfield of Computer Science aims at using computers to imitate and simulate human intelligence. AI can be used to make it possible for e-learning systems to use intelligent methods for analysis, evaluation and assessment of user knowledge and skills as well as process control, supervision and optimization. Using AI concept and techniques, new forms of intelligent software can be created to allow the computer to act as an intelligent learner or tutor. Thus, presently, there is an emerging broader perspective among system designers and developers on the various aspects of e-learning which can be extended and augmented with AI technologies; for example, wherever it may not be possible or desirable to incorporate real people or wherever it is possible to complement real teachers, especially in inaccessible remote regions. When incorporated, the ability to hold meaningful dialogues and interaction sessions with humans is a useful characteristic of AIs. This can be utilized while implementing e-learning systems.

Of late, interaction designers are trying to use human-like "virtual characters" on interaction screens to improve interaction in the form of characters in videogames, teaching companions, wizards, newsreaders. It should be noted that a virtual character may be used to provide a persona that is welcoming, and has personality that makes the user feel involved with them. Computer interaction designers classify virtual characters in terms of the degree of the anthropomorphism they possess and exhibit. Based on the degree of anthropomorphism which virtual characters possess and exhibit the types of virtual characters which are presently in use by interaction designers are the following:

- Synthetic characters
- Animated agents
- Emotional agents
- ECAs (Embodied conversational agents)
- Avatars

These are all software agents driven by AI to improve human computer interaction (HCI); these software agents when programmed with the capacity for emotional expression and embedded as extensions can improve the interactivity of e-learning systems.

For example, ECAs are human-centered, personalized and at the same time more engaging speech-based interactive systems. ECAs employ real human gestures, mimics and speech to communicate with the human user. During the last decade research groups as well as a number of commercial software developers have started to deploy embodied conversational characters in the user interface interaction ...especially in application systems where a close emulation of multimodal human-human computer communication is needed. The ECAs may be designed and programmed to actually carry on face-to-face communication that enables pragmatic communication acts such as conversational "turn-taking", synchronous facial expression of emotions. Research has indicated that the use of ECAs results in improved recall of the information presented to the learner.

In computing, an avatar is the graphical representation of the user or the user's alter ego or character. It may take either a three-dimensional form, as in games or virtual worlds, or a two-dimensional form as an icon in Internet forums and other online communities. Increasingly avatars are being introduced in e-learning. Speaking Avatars are now increasingly serving roles in delivering online learning in "human" like manner, so that learning has

become widely accessible, interesting, engaging, and memorable. In many instances they are used to give remote learners a campus-like feel, and also enable effective learning for people living with disability. According to the Stanford study, Interactive avatars are increasingly being perceived as real social actors.

Gitika Nagra(2015) writes that Avatars when incorporated and embedded into e-learning systems can enhance the quality of learner engagement by grabbing and retaining his/her attention. This designer and author went on to say that “Avatars go a long way in motivating people in the online learning environment. However, if we want to use avatars/characters effectively in e-Learning courses, we must clearly understand what avatars are, why they are useful and how they can be used in e-Learning”.

He concludes by saying that Avatars are powerful learning agents that can transform a boring subject into an interesting one. He maintains that they can be effectively used to guide and motivate learners throughout a course. Because Avatars help learners comprehend the subject-matter of online learning courses effectively, in that they facilitate efficient learner interaction. They serve the same function in a course as an anchor does in a live event, and can be used to personalize learning; form a relationship with learners; retain the knowledge gained; and make learning fun and interesting.

## VII. CONCLUSION

This write-up makes a call to improve effectiveness of learning and interaction between students and instructors in Nigeria’s Educational sector. It advocates using XML and programmable software agents to do so; the paper provides basis that spur further discussions among software application developers and designers for a possible incorporation of software agents as learning objects (such as ECAs, Avatars) to complement, enhance and improve the interactivity/effectiveness of the disparate e-Learning systems already out there in use by many institutions of learning in the country. Such enhanced e-learning system will surely improve e-learning and interaction between learners and instructors, and allow improved accessibility to instructional resources even from spatially remote inaccessible locations by diverse learners.

However, it should be noted that several key problems still remain unsolved for developing e-Learning content based on learning objects and XML. Firstly, the exact definition of what a learning object actually is... still remains unclear. Several different definitions exist, and most of them are so broad that they may lose any useful meaning. Secondly, many designers report that though it may be possible to find the appropriate learning objects by their metadata, it is still not clear whether it is possible for computer agents to integrate these learning objects in an appropriate way to form a higher level of course unit that makes instructional sense. Thirdly, there are many e-Learning specifications in XML available now, however each of them has their own emphasis, and none of them provides a complete solution for developing an e-Learning system. Therefore, most online instructional systems are still developed in proprietary ways without adopting the existing specifications. Finally, although XML was introduced several years ago, it is still far from being mature. Many technologies associated with it are still under development or change frequently; so, learning specifications based on XML have to change accordingly. All of these issues make the use of XML in developing a reusable e-Learning system difficult to implement.

## REFERENCES

- [1] **Abu, S.B. (2009).** Learning Management System and Its Relationship with Knowledge Management. 4th International Conference on Intelligent Computing and Information Systems, Cairo, 19-22 March 2009, 3-5.
- [2] **Ajadi, O. et al., (2008)** Turkish Journal: E-learning and distance Education in Nigeria. The Turkish online journal of educational technology 7(4), 2008, pp. 61-70.
- [3] **Ally, M. (2004).** Foundations of educational theory for online learning. In T. Anderson & F. Elloumi (Eds.), Theory and practice of online learning. Athabasca, Canada: Creative Commons: Athabasca University.
- [4] **Andersen A., Hristov, E. and Karimi, H. (2008).** Second Life: New Opportunity for Higher Educational Institutions. Bachelor Thesis within Business Administration, Jönköping International Business School, Jönköping University, Jönköping, 17.
- [5] **Berteau P. (2009).** Measuring student’s attitude towards e-learning: A case study. Proceedings of the 5th standing conference on e-learning and software for development held in Bucharest from 09-10 April 2009 Bucharest Romania 1-8.
- [6] **Bosak (1997) Bosak, J: XML, Java, and the future of the Web, 1997.** <http://www.ibiblio.org/pub/sun-info/standards/xml/why/xmlapps.htm> (Retrieved on Dec 5, 2015).
- [7] **Douglas, S. (1993).** Digital Soup: The ABCs of Distance Learning. EDUCOM Review, 28, 22-30.
- [8] **Gitika Nagra (2015).** What, Why, and How to Use Avatars in E-learning Courses?, <http://blog.commlabindia.com/elearning-design/how-to-use-avatars-in-elearning-courses>; (Retrieved on Dec 30, 2015).
- [9] **Gustafson, D.A. (2002).** Theory and Problems Software Engineering. The McGraw-Hill Companies, New York, 14-20. [24] Greer, D. (2010) Software Engineering. Queens University Belfast, Belfast.
- [10] **Hall, B. (2003).** New Technology Definitions, retrieved August 5, 2015 from <http://www.brandonhall.com/public/glossary/index.htm>.
- [11] **Hedge, N. and Hayward, L. (2004).** Redefining roles. University e-learning contributing to Life-long learning in a networked world. E-Learning, 1:128-145 <http://www.nationmaster.com/country/ni/Internet>.
- [12] **Hedge, N. and Hayward, L. (2004).** Redefining roles. University e-learning contributing to Life-long learning in a networked world. E-Learning, 1:128 – 145 <http://www.nationmaster.com/country/ni/Internet>.
- [13] **Holmberg, B. (2005).** The Evolution, Principles and Practices of Distance Education. Open Learning, 21, 273-277.

- [14] **Islam, M.T (1997)**. Educational Technology for 21st century. Observer magazine, Dhaka, May 9, 1997, pp. 3 – 4.
- [15] **Karadag, E. and Caliskan, N. (2009)**. Interaction and Communication in the Process of Education and Shared Common Area in the Classroom. College Student Journal, **43**, 123-128.
- [16] **Landry, B., Griffeth, R. and Hartman, S. (2006)**. Measuring Student Perceptions of Blackboard Using the Technology Acceptance Model. Decision Sciences Journal of Innovative Education, **4**, 87-99. <http://dx.doi.org/10.1111/j.1540-4609.2006.00103.x>.
- [17] **Miller, R. L. (1990)**. Learning Benefits of Interactive Technologies, Multimedia and Videodisc Monitor, February.
- [18] **Miller, S. M., & Miller, K. L. (2000)**. Theoretical and practical considerations in the design of web-based instruction. In B. Abbey (Ed.), Instructional and cognitive impacts of Web-based education (pp. 156-177). Hershey, USA: Idea Group Publishing.
- [19] **Nyiri, J.C. (1997)**. Open and Distance Learning in an Historical Perspective. European Journal of Education, **32**, 347- 357.
- [20] **Olaniyi S. (2006)**. E-learning technology: The Nigeria experience. Shape the change XX111 FIG Congress Munich Germany October 8-13. 1-11.
- [21] **Paulsen, M. F. (2002)**. Online Education Systems in Scandinavian and Australian Universities: A Comparative Study. The International Review of Research in Open and Distance Learning, Volume 3 (2), 152-167.
- [22] **Peters, O. (2001)**. Learning and Teaching in Distance Education—Analyses and Interpretations from an International Perspective. 2nd Edition, London, 4-25.
- [23] **Pishva, D., Nishantha, G.G.D. and Dang, H.A. (2010)**. A Survey on How Blackboard is Assisting Educational Institutions around the World and the Future
- [24] **Reeves, T., & Reeves, P. (1997)**. Effective dimensions of interactive learning on the World Wide Web. In B. H. Khan (Ed.), Web-based instruction (pp. 59-66). Englewood Cliffs, N.J.: Educational Technologies Publications.
- [25] **Siragusa, L., & Dixon, K. C. (2005a)**. Closing the gap between pedagogical theory and online instructional design: a bridge too far? In G. Chiazzese, M. Allegra, A. Chifari & S. Ottaviano (Eds.), Methods and Technologies for Learning. Southampton: WIT Press.
- [26] **Watabe, K., Hamalainen, M. and Whinston, A.B. (1995)**. An Internet Based Collaborative Distance Learning System: Codiless. Computers & Education, **24**, 141-155. [http://dx.doi.org/10.1016/0360-1315\(95\)00013-C](http://dx.doi.org/10.1016/0360-1315(95)00013-C).

## Analysis of Geostatistical and Deterministic Techniques in the Spatial Variation of Groundwater Depth in the North-western part of Bangladesh

Ibrahim Hassan<sup>1</sup>, I. M. Lawal<sup>2</sup>, A. Mohammed<sup>3</sup>, S. Abubakar<sup>4</sup>  
<sup>1,2,3,4</sup>(Civil Engineering Department, Abubakar Tafawa Balewa University Bauchi, Nigeria)

**ABSTRACT:** Various geostatistical and deterministic techniques were used to analyse the spatial variations of groundwater depths. Two different geostatistical methods of ordinary kriging and co-kriging with four semi-variogram models, spherical, exponential, circular, Gaussian, and four deterministic methods which are inverse distance weighted (IDW), global polynomial interpolation (GPI), local Polynomial Interpolation (LPI), radial basis function (RBF) were used for the estimation of groundwater depths. The study area is in the three North-western districts of Bangladesh. Groundwater depth data were recorded from 132 observation wells in the study area over a period of 6 years (2004 to 2009) was considered for the analysis. The spatial interpolation of groundwater depths was then performed using the best-fit model which is geostatistical model selected by comparing the observed RMSE values predicted by the geostatistical and deterministic models and the empirical semi-variogram models. Out of the four semi-variogram models, spherical semi-variogram with co-kriging model was considered as the best fitted model for the study area. Result of sensitivity analysis conducted on the input parameters shows that inputs have a strong influence on groundwater levels and the statistical indicators of RMSE and ME suggest that the Co-kriging work best with percolation in predicting the average groundwater table of the study area.

**Keywords** -Groundwater level prediction, spatial interpolation, Semi-variograms, Ordinary Kriging, Co-kriging and GIS.

### I. INTRODUCTION

Geostatistical and deterministic techniques play an important role in sustainable management of groundwater systems. These methods provide a set of statistical tools for analysing the spatial variability and interpolation as well as predicting the model input parameters at regular spots from their measurements at random locations (Kitanidis, 1997). Geostatistics is a collection of techniques for solving estimation problems involving spatial variables, which provides a mixture of tools including interpolation, integration and differentiation of hydro-geologic parameters to make the prediction surface and other derived characteristics from measurements at known positions (Journel and Huijbregts, 1978). The semi-variogram used to describe the structure of spatial variability, which plays a key role in the analysis of geostatistical data using the kriging and co-kriging methods.

In the past, a number of studies have been carried out on the comparison of interpolations methods on groundwater table elevation in different regions. Geostatistical analysis was performed on water table elevation of some 70 wells in Kansas by Christakos (2000). Kumar and Ahmed (2003) monitored the groundwater level during 12 months of the year and used kriging method to estimate groundwater level for unmeasured points and wells for each month. Another study by Reghunath et al. (2005) revealed that geostatistical methods are efficient instruments for water resources management and can effectively be used to gain the long term drifts of the groundwater. Stahl et al. (2006) used regression-based and weighted-average approaches for daily maximum and minimum temperatures over British Columbia, Canada. Benavides et al. (2007) compared ordinary kriging, ordinary kriging with external drift, and universal kriging and regression models for mapping air temperature in northern Spain. Zhang and Srinivasan (2009) incorporated nearest neighborhood, inverse distance weighted, simple kriging, ordinary kriging, simple kriging with local means, and kriging with external drift for mapping precipitation over Luohe River, China. Eldrandaly and Abu-Zaid (2011) compared six GIS interpolation

methods for estimating air temperature in western parts of Saudi Arabia. Bostan et al. (2012) compared multiple linear regression, ordinary kriging, regression kriging, universal kriging and geographically weighted regression for mapping average annual precipitation over Turkey. Mutua and Kuria (2013) compared inverse distance method, global polynomial interpolation and kriging and cokriging for rainfall estimation in Nyando river basin, Kenya. Delbari et al. (2013) compared univariate (inverse distance weighing and ordinary kriging) and multivariate (linear regression, ordinary cokriging, simple kriging with varying local mean and kriging with an external drift) interpolation methods for mapping monthly and annual rainfall over Golistan province, Iran. The above studies emphasized that the application of single interpolation method may produce unrealistic results. Therefore, it is better to choose the best model by comparing different methods.

The major objectives of this study are to compare various deterministic and geostatistical interpolation methods available in ArcGIS 9.3 for mapping and analysis of spatial variations of groundwater depths, to find the best fit of semi-variogram model viz; spherical, exponential, circular and Gaussian models, with kriging and co-kriging of geostatistical technique to develop spatial predictions of groundwater depths, and to consider all variables which have significant effect on the groundwater-based irrigation in the North-western region of Bangladesh.

## II. DESCRIPTION OF THE STUDY AREA

The subject area of this research comprises three North-western districts of Bangladesh namely, Rajshahi, Naogaon and Nawabganj which are geographically placed at a latitude ranging from  $24^{\circ}08'N$  to  $25^{\circ}13'N$  and a longitude ranging from  $88^{\circ}01'E$  to  $89^{\circ}10'E$ , which encompasses an area of  $7587 \text{ km}^2$ . The placements of these regions, as considerably as the positioning of water-wells used for picking up the groundwater data are presented in Figure 1 (a) and (b).

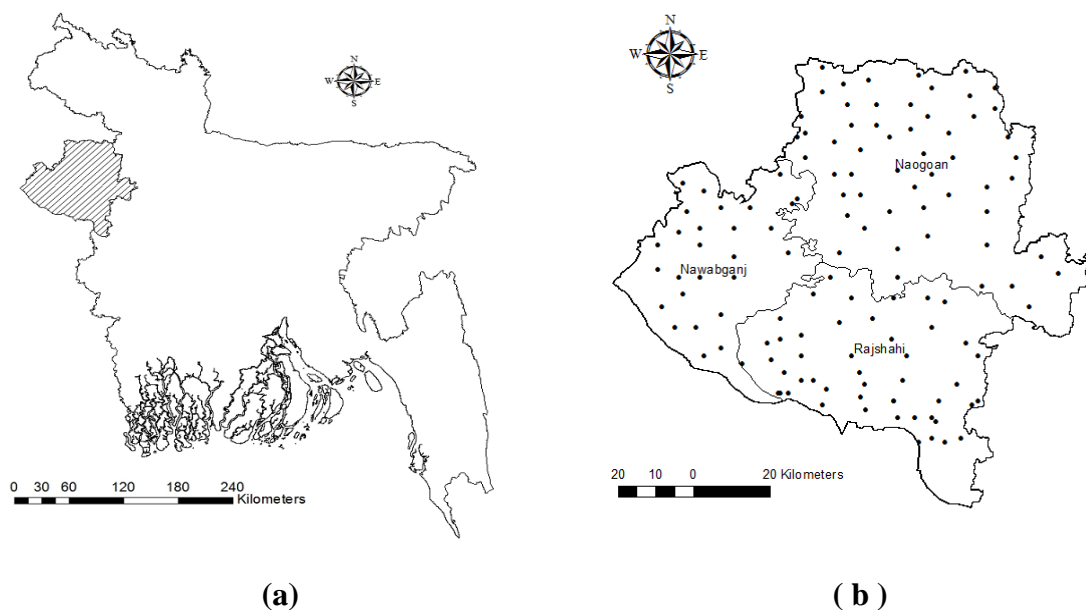


**Figure 1;**(a) Location of study area in Bangladesh; (b) location of groundwater sampling points used for the study

The topography of the study area contains mainly of a flat earth with an average height of 25 m above the mean sea level and comprise of a mild surface gradient towards southeast. The surface geology in the major part of the area comprises of uplifted terraces of Pleistocene sediments called Barind Tracts. Barind tract is an uplifted land formed over the Madhupur Clay (an older alluvium of Pleistocene age). Barind Tract sediments can be grounded at depths ranging between 150–200 m and more in the areas with concentration of alluvial. Hydro-geological surveys have been carried out in the area (Jahan et al., 1994; Ahmed and Burgess, 1995; Shwets et al., 1995; Jahan and Ahmed, 1997; Begum et al., 1997; Haque et al., 2000; Azad and Bashar, 2000; Rahman and Shahid, 2004; Islam and Kanungoe, 2005; Faisal et al., 2005; Asaduzzaman and Rushton, 2006). These studies show that upper aquifers in the region are unconfined or semi-confined in nature. The thickness of the exploitable aquifer ranges from 10 to 40 m. Jahan et al. (1994) worked out the specific output of the aquifer in the area vary from 8 to 32% with a general decreasing trend from north towards central portion.

Climatically, the study area belongs to dry, humid zone with annual average rainfall, which varies between 1400 to 1650 mm, among which about 83% of the rainfall occur in monsoon (June to October). Rainfall in the region varies widely from year to year.

### III. DATA AND METHODOLOGY

The criteria used for selecting sites for this study were the availability and continuity of long-term daily water table data at individual sites. Based on these criteria, data from 132 different observation wells across 25 different Upazillas were selected for the simulation of water table fluctuations for 2004-2009 periods by using Geostatistical and Deterministic techniques. Before developing the models, the groundwater level data were checked for the presence of spatial trends and found suitable for geostatistical modelling due to lack of spatial trends. Then, four deterministic models, viz; inverse distance weighted (IDW), global polynomial interpolation (GPI), local polynomial interpolation (LPI), radial basis function (RBF) and the two geostatistical models viz; kriging and co-kriging with their four semi-variogram models, viz., spherical, exponential, circular and Gaussian models were developed. Finally, the best-fit model for the groundwater depths was selected based on goodness-of-fit criteria. The best-fit geostatistical model thus obtained was used to generate spatial maps of groundwater depths by using ArcGIS9.3 software. The goodness-of-fit criteria used in this study are root mean square error (RMSE), the coefficient of determination ( $R^2$ ) and mean error (ME) for evaluating the performance of the models.

#### 3.1 Deterministic methods

The deterministic methods available in ArcMap 9.3 are inverse distance weighted (IDW), global polynomial interpolation (GPI), local Polynomial Interpolation (LPI), radial basis function (RBF). They employ the use of mathematical functions based on the degree of similarity or smoothing. Deterministic interpolation techniques can be either exact or inexact interpolators. Exact interpolators include Inverse Distance Weighted Interpolation and Radial Basis Functions which are used to generate a surface that passes through the control points. Inexact interpolators which are Global and Local Polynomial are used to predict a value at a point or location that differs from its known value (Johnston et al., 2003; Eldrandaly and Abu-Zaid, 2011). All the deterministic methods available in ArcMap 9.3 are used in this study.

#### 3.2 Geostatistical methods

Geostatistical processes use both mathematical and statistical functions based on the spatial autocorrelation of the data. The techniques of Geostatistical interpolation create surfaces incorporating the statistical properties of the measured data by developing not only prediction surfaces, but also error or uncertainty surfaces, which turns over the analysis as an indication of how good the predictions are. There are many geostatistical methods under Kriging. The different kriging methods available in the Geostatistical Analysis for spatial interpolation are Ordinary, Simple, Universal, Probability, Indicator, and Disjunctive Kriging (Johnston et al., 2003; Eldrandaly and Abu-Zaid, 2011). In this study ordinary, simple, universal and disjunctive kriging were used. Detail theories about geostatistical models can be found in (Isaaks and Srivastava, 1989; Johnston et al., 2003; Webster and Oliver, 2008).

##### 3.2.1 Semi-variogram

The semi-variogram is a geostatistical function which describes the spatial variability of the values of a variable. It relates the semi-variance with the spatial separation, providing a concise and unbiased description of the scale and the pattern of spatial variability (Curran, 1988). There are many types of semi-variograms viz; circular, exponential, Gaussian, whole effect, J-Bessel K-Bessel, penta-spherical, rational quadratic, spherical, stable, tetra-spherical, etc. In this study, four popular semi-variogram models namely, Circular, Exponential, Gaussian and Spherical models were compared and the best fit model was proposed based on least observed error after simulation.

### IV. RESULTS AND DISCUSSION

#### 4.1 Comparison of Deterministic models

In the interpolation of the four deterministic models, viz; inverse distance weighted (IDW), global polynomial interpolation (GPI), local polynomial Interpolation (LPI), radial basis function (RBF), the selection of power value and neighbourhood search is important for the proper interpolation. In this study, power values between 1 and 3 were used and the smooth function was used for neighbourhood search to produce smoother surfaces by assigning smoothing factor values. The accuracy of interpolations was assessed by considering the lowest root mean square error (RMSE). The RMSE values were found to vary with the power and neighbourhood search parameters. The radial basis function (RBF) model gave the best deterministic model with the lowest RMSE value of 2.154 while the global polynomial interpolation (GPI) gave the poorest result with the highest RMSE value of 2.930.

**4.2 Comparison of Geostatistical models**

Ordinary kriging and co-kriging methods of interpolation were used to interpolate the average water table using Circular, Spherical, and Exponential and Gaussian semi-variograms. The goodness-of-fit statistics results are shown in Table 1, and the residual analysis results are shown in figure 2. The performance of the semi-variogram models showed that spherical semi-variogram with co-kriging yielded the lowest RMSE value of 2.105 and circular semi-variogram with co-kriging yielded the highest error of 2.491, respectively.

**Table 1;** Results of Semi-variograms Models

Model	Kriging	Co-Kriging
Semi-Variogram	RMSE	RMSE
Circular	2.186	2.491
Spherical	2.222	2.105
Exponential	2.252	2.145
Gaussian	2.222	2.141

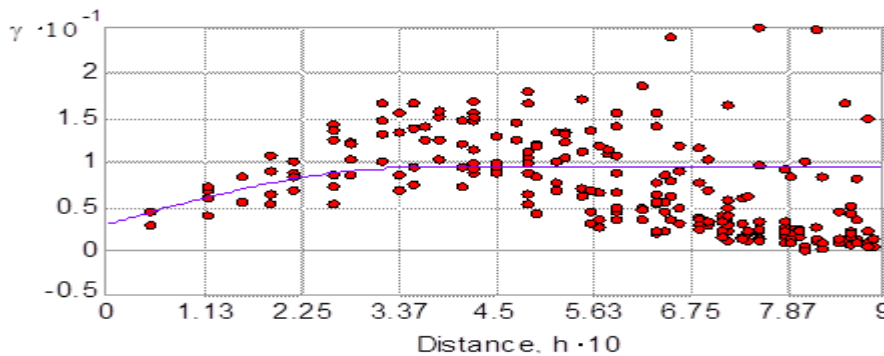


**Figure 2:** Fitted semi-variogram of Spherical model for groundwater depths with co-kriging

The overall performance of co-kriging was outstanding with Spherical, Exponential and Gaussian semi-variogram which gave lowest error in all the cases. In case of kriging, circular semi-variogram gave lowest error while Spherical, Exponential and Gaussian semi-variograms gave approximately the same error.

**4.3 Comparison of Geostatistical and Deterministic models**

Finally, the best model from deterministic and geostatistical methods are compared to find the most suitable spatial interpolation method for the region. The results obtained are shown in Table 2. Co-kriging with Circular semi-variogram gave lowest error among all geostatistical methods, while the radius basis function gave best results among the deterministic methods. Overall, the performance of geostatistical methods was superior compared to deterministic method. Performance of co-kriging was found to be the best among all the methods.

**Table 2:** Comparison of the Results of deterministic and geostatistical methods

Models	RMSE	Mean Error
IDW	2.180	0.036
GPI	2.930	0.031
LPI	2.251	-0.314
RBF	2.154	0.022
Kriging	2.186	-0.051
Co-kriging	2.105	0.010

### 4.4 Results of Sensitivity analysis

On investigating the influence of the input parameters on the average groundwater table using the best interpolation methods with the best semi-variogram model, results of the sensitivity analysis as depicted in table 3; below indicates that all the inputs have a strong influence on groundwater levels in the study area. Looking at the general performance of the input variables, it can be seen that percolation has the highest influence on the average water table while the geology of the area has the lowest influence on the average water table. Assessment of the general results; it was deduced that the statistical indicators suggests that Co-kriging with percolation is inferior for interpolating the average water table in the study area.

Input Parameters	Ordinary Co-Kriging	
	RMSE	AIC
R, P, G	2.45	4.21
R, MC, G	2.37	4.27
R, A, G	2.34	4.30
P, A	2.13	4.49
R, P, MC	2.44	4.22
R, MC, A	2.26	4.37
R, P, A	2.35	4.29
P, MC, A	2.04	4.57
R	2.49	0.18
P	2.11	0.51
MC	2.10	0.52
A	2.16	0.46
G	2.49	0.17

Where;

R = Rainfall, P = Percolation, MC = Soil moisture content, A = Altitude, and G = Geology of the area.

### 4.4 Spatial Variation of Groundwater Depth in the Study Area

The contour map of 6-year (2004-2009) average groundwater depth was generated by co-kriging technique (Spherical geostatistical model) which reveals that the mean pre-monsoon groundwater depth in the area generally varies from 2.4 to 15.72 m belowground surface (m bgs) with a major portion of the area having 2.4 to 7.05m bgs depth (Figure 3).

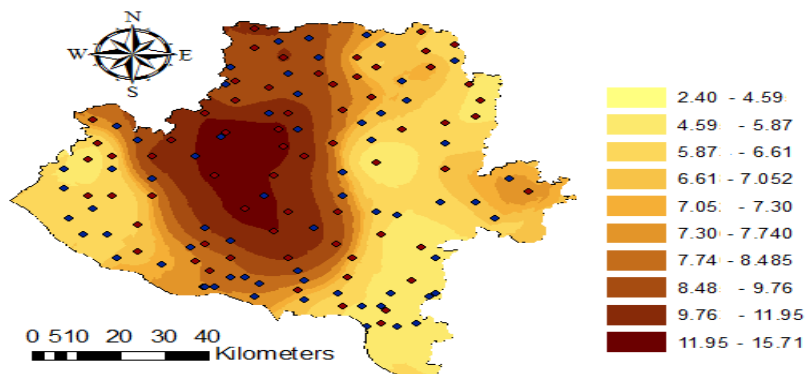


Figure 3: Maps of average Groundwater level of the study area obtained by ordinary co-kriging methods with Spherical semi-variogram

## V. CONCLUSION

In this paper, the spatial analysis of groundwater depth was performed using geostatistical and deterministic models of GIS. The analysis of results indicated that geostatistic models are more suitable for spatial interpolation than the deterministic models and that the geostatistical model can reveal stochastic structure of groundwater level variations in the study area. The co-kriging model with spherical semi-variogram was found to be the best-fit geostatistical model for the study area, which were used for developing contour maps for spatial analysis to show a significant groundwater fluctuation in the study area. On investigating the influence of the input parameters on the average groundwater table using the best interpolation methods with the best semi-variogram model, statistical indicators also indicates that co-kriging works best with percolation. The results obtained suggest the usefulness of applying geostatistic techniques in investigating the spatial variations of groundwater depths in the study area.

## REFERENCES

- [1] Kitanidis P. K. (1997), Introduction to Geostatistics: Application to hydrogeology. University Press, Cambridge, UK.
- [2] Journel A. G and Huijbregts C. J (1978), Mining Geostatistics, Academic Press, New York.
- [3] G Christakos (2000), *Modern Spatiotemporal Geostatistics*, Oxford University Press, New York, USA.
- [4] Kumar, D., & Ahmed, S. (2003). Seasonal behaviour of spatial variability of groundwater level in a granitic aquifer in monsoon climate. *Current Science*, 84(2), 188-196.
- [5] Reghunath R., Murthy T. R. S & Raghavan B R (2005), Time series analysis to monitor and assess water resources: A moving average approach. *Environmental Monitoring and Assessment*, 109, 65-72.
- [6] Stahl, K., Moore, R. D., Floyer, J. A., Asplin, M. G., & McKendry, I. G. (2006). Comparison of approaches for spatial interpolation of daily air temperature in a large region with complex topography and highly variable station density. *Agricultural and Forest Meteorology*, 139(3-4), 224-236.
- [7] Benavides, R., Montes, F., Rubio, A., & Osoro, K. (2007). Geostatistical modelling of air temperature in a mountainous region of Northern Spain. *Agricultural and Forest Meteorology*, 146(3-4), 173-188.
- [8] Zhang, X. S., & Srinivasan, R. (2009). GIS-Based Spatial Precipitation Estimation: A Comparison of Geostatistical Approaches (1). *Journal of the American Water Resources Association*, 45(4), 894-906.
- [9] Eldrandaly, K., & Abu-Zaid, M. (2011). Comparison of Six GIS-Based Spatial Interpolation Methods for Estimating Air Temperature in Western Saudi Arabia. *Journal of Environmental Informatics*, 18(1), 38-45.
- [10] Bostan, P. A., Heuvelink, G. B. M., & Akyurek, S. Z. (2012). Comparison of regression and kriging techniques for mapping the average annual precipitation of Turkey. *International Journal of Applied Earth Observation and Geoinformation*, 19(1), 115-126.
- [11] Mutua, F., & Kuria, D. (2013). A comparison of spatial rainfall estimation techniques: a case study of nyando river basin kenya 2013. vol. 14. 2013
- [12] Delbari, M., Afrasiab, P., & Jahani, S. (2013). Spatial interpolation of monthly and annual rainfall in northeast of Iran. *Meteorology and Atmospheric Physics*, 122(1-2), 103-113.
- [13] Jahan CS, Mazumder QH, Ghose SK, Asaduzzaman M (1994) Specific yield evaluation: Barind area, Bangladesh. *Journal of Geological Society of India* 44:283-290.
- [14] Ahmed K, Burgess W (1995) Bils and the Barind Aquifer, Bangladesh. In: Brown AG (ed) *Geomorphology and Groundwater*, Wiley, New York.
- [15] Shwets V. M, Danilov V. V, Jahan C. S (1995) Seasonal effect on regional groundwater flow: Barind area, Bangladesh. In: *Groundwater Management, Proceedings of International Symposium held in San Antonio, Texas, 14-16 August, 1995*.
- [16] Jahan CS, Ahmed M (1997) Flow of groundwater in the Barind area, Bangladesh: Implication of structural framework. *Journal of the Geological Society of India* 50:743-752.
- [17] Begum S. F, Bashir K, Hossain M. S (1997) An evaluation of hydraulic parameters of the aquifer and wells of the western part of the Barind area, Bangladesh. *Bangladesh Geoscience Journal* 3:49-64.
- [18] Haque MN, Keramat M, Rahman AMA (2000) Delineation of groundwater potential zones in the western Barind Tract of Bangladesh. *Journal of the Bangladesh National Geographical Association* 21-26:13-20.
- [19] Azad MAS, Bashir K (2000) Groundwater Zonation of Nawabganj Sadar Thana and its Relation to Groundwater Chemistry. *Bangladesh Journal of Geology* 19:57-71.
- [20] Rahman M. M, Shahid S (2004) Modeling Groundwater Flow for the Delineation of Wellhead Protection Area around a Water-well at Nachole of Bangladesh. *Journal of Spatial Hydrology*: 4(1).
- [21] Islam M. M, Kanungoe P (2005) Natural recharge to sustainable yield from the Barind aquifer: A tool in preparing effective management plan of groundwater resources. *Water Science and Technology* 52:251-258.
- [22] Faisal IM, Parveen S, Kabir MR (2005) Sustainable Development through Groundwater Management: A Case Study on the Barind Tract. *Water Resources Development* 21:425-435
- [23] Johnston, K. VerHoef, J.M., Krivoruchko, K., & Lucas, N. (2003) *ArcGIS 9: Using ArcGIS Geostatistical Analyst*: Esri Press.
- [24] Eldrandaly, K., & Abu-Zaid, M. (2011). Comparison of Six GIS-Based Spatial Interpolation Methods for Estimating Air Temperature in Western Saudi Arabia. *Journal of Environmental Informatics*, 18(1), 38-45.
- [25] Isaaks, E. H., & Srivastava, R. M. (1989). *Applied geostatistics*. New York: Oxford University Press.
- [26] Webster, R., & Oliver, M. A. (2008). *Geostatistics for Environmental Scientists* (pp. 309-315): John Wiley & Sons, Ltd
- [27] Curran, P. J. (1988). The semivariogram in remote sensing: An introduction. *Remote Sensing of Environment*, 24(3), 493-507.

## Fin pitch to effect efficiency of evaporator and HVAC

Dr. Mohammad Arsalan Khan<sup>1</sup>, Mohd Danish<sup>2</sup>

<sup>1</sup>(Aligarh Muslim University, Department of Civil Engineering, Z. H. College of Engineering & Technology, Aligarh Muslim University, Aligarh, Uttar Pradesh, India. Pin code – 202002.

<sup>2</sup>(Al-Falah School of Engg. & Tech., MaharshiDayanand University, Haryana, 124001)

**ABSTRACT:** Efficiency of a heat exchanger, such as a multi-flow heat exchanger (evaporator), is critical to any air-conditioning system. A large amount of experimental work has already been performed for the enhancement of air-side heat transfer. However, there is a further need to investigate flow profiles and the related heat transfer characteristics for complex geometries of a heat exchanger. In this direction, tests at two levels are conducted to verify the effect(s) and measure the variation(s) for further conclusion: a component level test (evaporator level) for cooling capacity and pressure drop; and a system level test on a plastic case of HVAC unit that includes evaporator, heater, blower motor, fan and the dampers. The findings indicate that an economic heat transfer enhancement can be achieved by fluctuating the fin density.

**Keywords:** Fin pitch, evaporator, HVAC,

### I. INTRODUCTION

All air conditioning systems contain at least two Heat Exchangers, usually called Condenser and the Evaporator. In either case, Condenser or Evaporator, the refrigerant flows into the heat exchanger and transfer heat, either gaining or releasing as a cooling medium. The Heat Exchangers are critical parts in a complete A/C System, and use lightweight aluminum materials to improve on heat transfer.

Studies have been done on different type of evaporator used in commercial and as well as industrial refrigeration applications. These are air-cooling evaporators which transfer heat from refrigerant-to-air using tubes to carry refrigerant with fins profiles onto the tube exterior [1]. Individual tubes of the heat exchanger are arranged in multiple rows of parallel circuits to achieve increased thermal performance [2]. Refrigerant evaporates inside the tubes as it absorbs heat from air flowing over the outside surface across finned tubes.

Traditional heat exchanger devices such as plate type, plate fin type and tubular type operate on the principle of temperature difference between two mediums and can realize efficient sensible heat transfer from one fluid to another [3, 4]. With the development of design of heat exchanger and making some changes without heavily affecting the cost, the heat transfer enhancement can be achieved. One such type of Multi flow heat exchanger (evaporator) is our target. A large number of experimental works has already been performed for this enhancement of air-side heat transfer; however, the flow profiles and the related heat transfer characteristics in the complex geometries are still needed to be verified. There are several geometric and the flow variables that affect the heat transfer coefficient and friction factor for a fin-tube type multi flow evaporator [5, 6]. Without consideration of the tube layout and fin shape, the geometry specific variables can be: fin height, fin spacing, fin thickness, tube diameter, tube pitch and the number of rows. In addition, the flow variables can be: air velocity, density, viscosity, thermal conductivity and the specific heat. Our target is to check the behavior in terms of cooling capacity, pressure drop, air flow and power consumption by changing the fin spacing of evaporator in auto air conditioning system. Fin spacing are also referred to as “fin pitch”. The density of fins, when applied to an evaporator, may have a dramatic effect on evaporator and the resulting capacity loss; this is largely due to blockage of airflow. Although, increased fin density (decreased fin spacing) may be desirable because it increases the surface area available for heat transfer, the reduced spacing between fins will result in a decrease of the open area available for air flux to flow. Earlier studies [7] have shown that the heat transfer coefficient near the fin base, having closer fin spacing, is smaller than achieved with the greater fin spacing; it is because usually, the smaller gap fin spacing creates thicker boundary layers. In addition, the stagnation zone formation at the root of the fin and the tube surface is swept by a non-turbulent flow; and therefore, it is excluded from taking part in active heat transfer. Thus, the allowable extent of reducing the fin spacing will depend on the velocity and turbulence of the flow within the inter fin spaces.

**II. EXPERIMENTAL METHODS**

In this paper, evaporator (heat exchanger) is being targeted to determine and compare the cooling capacity, pressure drop, air flow and the power consumption with two different fin pitches in auto air conditioning system. Following testes are conducted to verify the effect and measure the variation for further conclusion:

- Component Level Test (Evaporator Level) for evaluating Cooling Capacity and Pressure Drop
- System Level Test (a plastic case of HVAC unit that includes evaporator, heater, blower motor, fan and the dampers) for recording Air Flow and Power Consumption

One such multi flow type, RS (Revolutionary Slim) evaporator (Fig. 1.) is picked keeping all design parameters, including the frontal area, unchanged.



Fig. 1. Revolutionary Slim evaporator: length x breath x core-thickness as (191 x 172.5 x 38) mm

The model is run for two different fin pitches 2.6 mm and 3 mm; the data is collected and analyzed to indicate any change in heat transfer. It is also noted that the air-side cross-sectional area decreases with distance from the air flow inlet, accelerating the air as it flows across the tubes; thereby, improving the air-side local heat transfer coefficient.

**III. RESULTS**

The results are compiled for cooling capacity and pressure drop obtained though component level test, and for airflow and power consumption through system level test as follows.

**3.1 Component (evaporator) level test results for cooling capacity and pressure drop**

The test is conducted with different air flow values to measure cooling capacity. The range of air flow values considered are at 275, 325, 375 and 425 CMH.

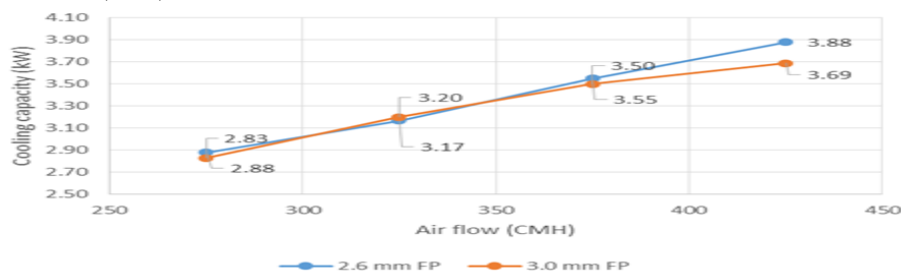


Fig. 2. Air flow verses cooling capacity

The test is conducted to measure pressure drop for the same range of air flow values as while evaluating for cooling capacity.

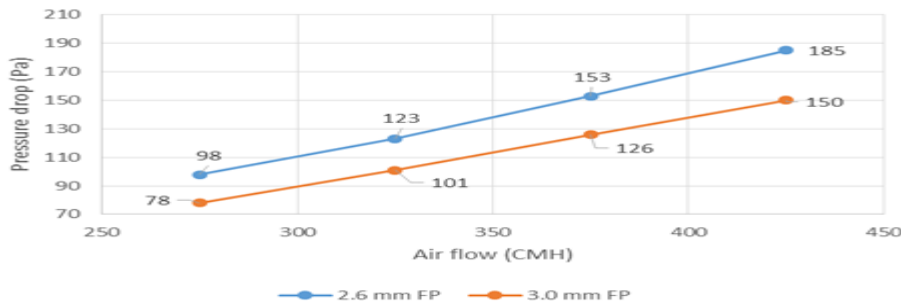


Fig. 3. Air flow verses pressure drop

With increase in air flow, the cooling capacity and pressure drop are also increasing, and the pattern is non-parallel for the two fin pitches. The variation in cooling capacity started with almost coinciding values at air flow of 275 CMH, however, differences started to emerge for higher values of air flow. The values for pressure drop for 2.6 mm FP have consistently shown higher values compared to the fin pitch of 3 mm.

**3.2 System level test results for airflow and power consumption**

A system level consists of plastic case of HVAC unit that includes evaporator, heater, blower motor, fan and the dampers. The test is conducted at different voltage values of 8.0, 10.0, 12.0 and 13.5 V. The conditions for HVAC air inlet temperature is maintained at 27°C, RH of 50%, and condenser air inlet temperature at 35°C.

Variation of air flow and effect on power consumption with varying voltage are respectively plotted in Fig. 4. and Fig. 5.

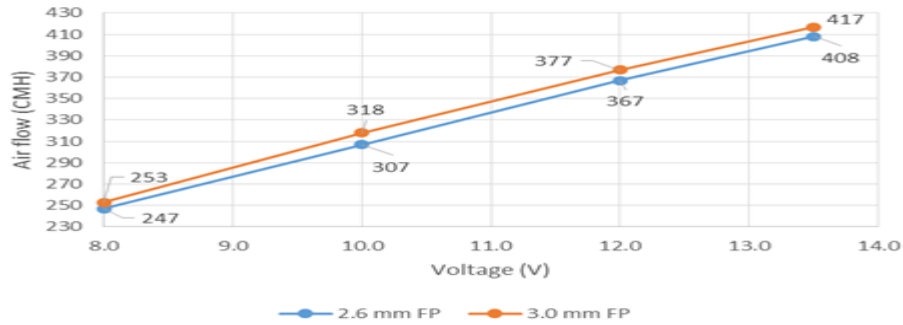


Fig. 4. Voltage verses air flow

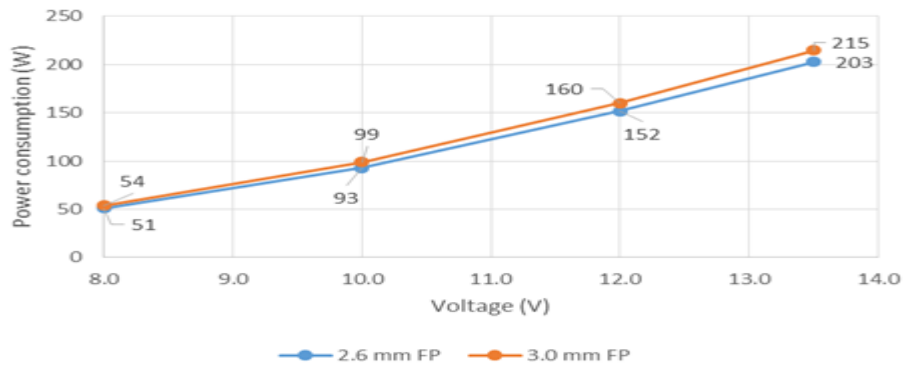
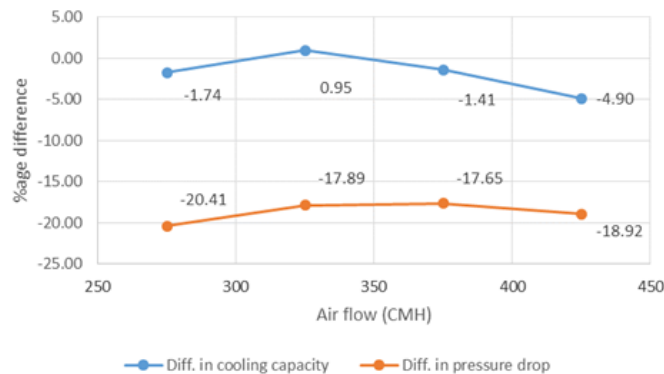
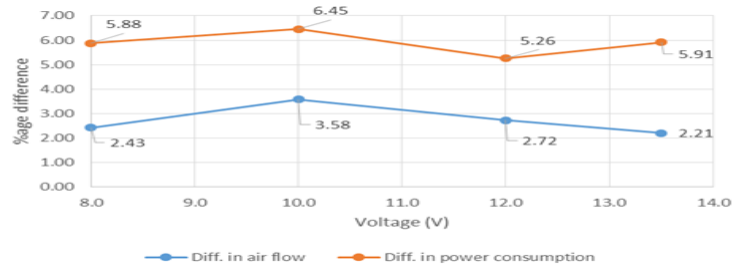


Fig. 5. Voltage verses power consumption

In Fig. 5., it is noteworthy that the power consumption is increasing with the increase in voltage; and it is at a relatively higher rate for 3 mm FP. The plots are not parallel and so the differences are plotted in Fig. 6. to establish percentage variations with the changing parameters. The percentage differences are measured relative to 3 mm fin pitch.



(a)



(b)

Fig. 6. Percentage difference for factors, (a) Air flow, (b) Voltage

In Fig. 6a. for cooling capacity, the percentage difference decreases at different values of air flow than 325 CMH. Similar pattern is seen with pressure drop in Fig. 6a. It is now clear from Fig. 6b that the percentage variation of air flow is non-consistent for the fin pitches tested. Therefore, the following conclusions are drawn.

#### IV. CONCLUSION

In this paper, evaporator (heat exchanger) is being targeted to determine and compare the cooling capacity, pressure drop, air flow and the power consumption with two different Fin Pitches in auto air conditioning system. Following test has been conducted to verify the effect and measure the variation for further conclusion

- Component Level Test (Evaporator Level) for Cooling Capacity and Pressure Drop
- System Level Test (a plastic case of HVAC unit that includes evaporator, heater, blower motor, fan and the dampers) for Air Flow and Power Consumption A complete understanding of the fin spacing effect and its relation to heat transfer and pressure drop behavior of evaporator is needed. Therefore, the effect of the fin spacing was investigated with two different Fin pitch 2.6 mm and 3 mm keeping all design parameters same. It resulted that the air-side cross sectional area decreases with the distance from the air flow inlet, accelerating the air as it flows across the tubes and, therefore, improving the airside local heat transfer coefficient.

Experiments are performed on Revolutionary Slim evaporator in auto air conditioning system. While keeping other geometric parameters fixed, observations are made for fin pitches (fin spacing) of 2.6 mm and 3 mm; a total of 32 variations are made. Air-flow varied from 275 CMH to 425 CMH with an interval of 50 CMH, to find its effects on cooling capacity and pressure drop. The percentage difference in cooling capacities are noted to vary from 0.95% to -4.90%. While a maximum percentage drop in pressure is noted, at an air flow of 275 CMH, to be -20.41% for increase in fin pitch by 0.4 mm from 2.6 mm. Effects on air flow and power consumption are observed for a range of variation in voltage at 8.0 V, 10.0 V, 12.0 V and 13.5 V. For this range, with the increase in fin pitch, a maximum increase in air flow is by 11 CMH from 307 CMH at 10.0 V; and the power consumption is increased by 6.45%, which is maximum

#### V. ACKNOWLEDGEMENTS

This paper is part of second author's dissertation submitted in partial fulfillment of requirement for the award of the degree of Master of Technology in Mechanical Engineering at MaharshiDayanand University, India. The experimental facilities, opinions and data analysis were arranged and conducted under the partial guidance of first author who was then working at Loughborough University, UK.

#### REFERENCES

- [1] P. Date and V. W. Khond, Heat transfer enhancement in fin and tube heat exchanger - a review, ARPN Journal of Engineering and Applied Sciences. 8(3), 2013, 241-245.
- [2] M. S. Mon, Numerical investigation of air-side heat transfer and pressure drop in circular finned-tube heat exchangers, Doctoral Thesis, Technischen Universität Bergakademie Freiberg, Germany, 2003.
- [3] T. D. Foust, J. E. O'Brien and M. S. Sohal, Numerical and Experimental Methods for Heat Transfer Enhancement for Finned-Tube Heat Exchangers with Oval Tubes, ASME National Heat Transfer Conference, Anaheim, June 2001, paper no. NHTC01-12363.
- [4] J. E. O'Brien and M. S. Sohal, Local Heat Transfer for Finned-Tube Heat Exchangers using Oval Tubes, Proceedings on ASME National Heat Transfer Conference, Pittsburgh, August 2000, paper no. NHTC2000-12093.
- [5] J. R. Barbosa Jr., G. A. Dubiela, P. J. Waltrich, Experimental, Theoretical and Numerical Analysis of Air-Side Heat Transfer and Fluid Flow in Tube-Fin Heat Exchangers, Internal Report, Federal University of Santa Catarina, Florianopolis-SC, Brazil (in Portuguese), 2006.
- [6] J. R. Barbosa Jr., C. Melo and C. J. L. Hermes, A Study of the Air-Side Heat Transfer and Pressure Drop Characteristics of Tube-Fin 'No-Frost' Evaporators, Proc. 12th Int. Refrigeration and Air Conditioning Conference at Purdue, West Lafayette-IN, USA, 2008, Paper 2310.
- [7] A. Joardar and A.M. Jacobi, Heat transfer enhancement by winglet-type vortex generator arrays in compact plain-fin-and-tube heat exchangers, International journal of refrigeration, 31(1), 87-97, 2008.

## An application of Auto-regressive (AR) model in predicting Aero-elastic Effects of Lekki Cable Stayed Bridge

Hassan Abba Musa<sup>1</sup>, Dr. A. Mohammed<sup>2</sup>

<sup>1</sup>Civil Engineering Department, Sharda University, Knowledge Park III, Greater Noida, UP – Delhi, India.

<sup>2</sup>Department of Civil Engineering, Abubakar Tafawa Balewa University (ATBU) Bauchi, Bauchi, Nigeria.

**ABSTRACT:** In current practice, the predictive analysis of stochastic problems encompasses a variety of statistical techniques from modeling, machine, and data mining that analyse current and historical facts to make predictions about future. Therefore, this research uses an AR Model whose codes are incorporated in the MATLAB software to predict possible aero-elastic effects of Lekki Bridge based on its existing parametric data and the conditions around the bridge. It was seen that, the fluctuating components of the wind velocity as displayed by the fluctuant curve will result in the vibration of the structure, even strengthening the resonance effect of the structure. Therefore, it suggested that, the natural frequency of the bridge should be set aside far from system frequency considering direct parametric excitation of pedestrian or vehicular traffic speed.

**Key Words:** Predictive Analytics, Stochastic, AR Model, MATLAB, Aero-elastic Effects, Lekki Bridge, Fluctuant curve.

### I. INTRODUCTION

Cable structures are encountering a growing success in modern Engineering due to technical, economic and aesthetic reasons, which justify their actual competitiveness for covering free spans in an increasingly wide length range. The structural and architectural design of suspended and cable-stayed bridges, in particular, has been fine tuned over the last few decades to conjugate efficient geometric shapes, optimal material usage, and appreciable visual pleasantness. Focusing on the structural view points, the virtuous synergy among the load-bearing capacity of beams (or arches) and the force transferring ability of cables has been optimally exploited in a variety of collaboration schemes (Fig. 1.1a). Nonetheless, this optimization trend often ends up over-stressing the inherent properties of slenderness and flexibility of cable supported bridges and footbridges. Such structural features, combined with low damping capacities and associated with rising performance demands due – among other things – to the increase of live loads, thus make these structures particularly vulnerable to dangerous dynamic phenomena, including for instance the aero-elastic instabilities due to wind actions, or the dynamic bifurcations due to the direct or parametric excitation of pedestrian or vehicular traffic.

The non-negligible influence of the cable vibrations on the free and forced full-bridge dynamics is a key-issue, well recognized since the early nineties of the past century [1]. Consequently, a variety of continuous and discrete formulations have been proposed to overcome the inherent shortcomings of traditional models, coarsely describing the cables as tendon elements with Ernst equivalent elastic modulus [2, 3]. The matter tends to become determinant in the newest structural realizations, considering that the modern design trend is to prevent the risk of stress localization in the suspension system (main cables, arch, towers) by increasing the total number of suspending cables. In this respect, several numerical and experimental studies confirm that cable-supported bridges typically possess a dense spectrum of natural frequencies, in which internal resonant conditions among global modes, dominated by the flexural and or torsional dynamics of the deck (Fig. 1.1b), and local modes, dominated instead of the lateral dynamics of one or more cables (Fig. 1.1c), are practically unavoidable [4].

In this challenging scenario, it may be worth devoting some theoretical research efforts to develop structural models able to well balance the competing requirements of synthesis and representativeness, with expected positive spill overs in a variety of engineering applications, including vibration controls and health monitoring systems.

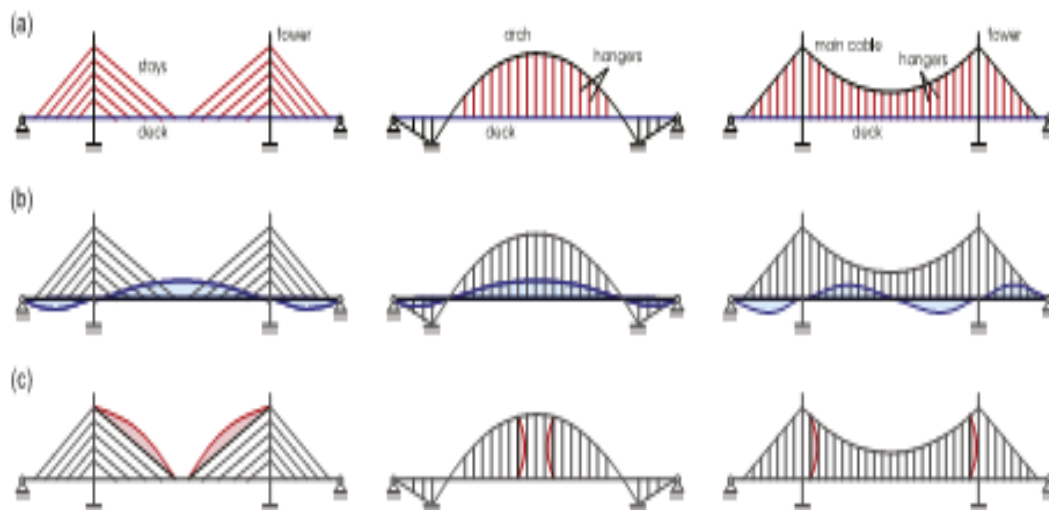


Figure 1.1: Cable-stayed bridge (left), Through-arch bridge (centre), suspended bridge (right); qualitative examples of (a) cable-beam collaboration schemes, (b) deck vibration shape in global modes, (c) cable vibration shapes in local modes (Marco et al, 2014).

In comparison with the current state-of-the-art, the present work will discuss the most common phenomena related to wind effects bridge of Lekki cable-stayed bridges, Lagos; thereby underlining the prominent roles of the dynamics of the structures.

## II. BACKGROUND OF THE RESEARCH

When designing flexible structures for wind, dynamic wind loads are of primary interest to structural Engineers. Wind loads are induced on a structure because of a complex interaction between wind and structure. The interaction of wind flow with structures can be classified under aerodynamic and aero-elastic effects (Scanlan 1981, Simiu and Scanlan 1996) [5]. The **Aerodynamic Effect** refers to the fluctuating nature of the wind and its interaction with the structure. The discipline of **Aero-elasticity** refers to the phenomenon wherein aerodynamic forces and structural motions interact significantly. Aero-elastic instability occurs if the body that is immersed in the fluid flow deflects under some force and the initial deflection causes succeeding deflections that are divergent in character. Aero-elastic instabilities also involve aerodynamic forces that are generated due to the motion of the structure. These forces that act upon a body as a consequence of its motion and cause aero-elastic instability are termed as **self-excited forces**. The self-excited wind loads will either transfer energy from wind to the structural motion or help in dissipating the kinetic energy of the structure. Above a certain wind speed, the energy increment exceeds the energy dissipation from wind such that the kinetic energy of the structure keeps increasing which makes the structure dynamically unstable. This critical wind speed at which the structure becomes unstable is called **Flutter Speed**.

### 2.1 FLUTTER INSTABILITY

Since the flutter induced failure of the Tacoma Narrows Bridge in 1940, understanding of the physical mechanisms at work in Civil Engineering structures has advanced tremendously. Flutter is an aero-elastic self-excited oscillation of a structural system. The structural system by means of its deflections and their time derivatives taps off energy from the wind flow across the body. If the system is given an initial deflection, its motion will either decay or diverge according to whether the energy of motion extracted from the wind is less than or exceeds the energy dissipated by the system through mechanical damping. The theoretical dividing line between the decaying and divergence (i.e. sustained sinusoidal oscillation) was identified as the **Critical Flutter Condition**.

Flutter phenomenon can be broadly classified into two categories, namely, single-degree-of-freedom flutter or damping driven flutter example like torsional flutter of bluff bodies (bluff-sectioned) bridges, and coupled-flutter or stiffness driven flutter example like multi-mode flutter of structures airplane (wings and streamlined) bridges. Flutter analysis of a structure can be performed either in frequency domain or in time domain.

#### 2.1.1 FREQUENCY-DOMAIN FLUTTER ANALYSIS

The frequency-domain flutter analysis approach has been widely used for estimating flutter speed of structures. The frequency-domain analysis using flutter derivative formulation for the aero-elastic forces was researched extensively by Sarkar, Jones, and Scanlan (1994), Jones et al. (1995), Matsumoto et al. (1997), Scanlan (1997), Gu, Zhang, and Xiang (2000), Zhu et al. (2002) and numerous others. Mode-by-mode flutter analysis was done by Ge and Tanaka (2000), Jones and Scanlan (2001) [5]. The frequency domain

method uses flutter derivatives which are functions of reduced frequency. These aero-elastic parameters can be experimentally obtained from wind-tunnel testing of section models.

### 2.1.2 TIME-DOMAIN FLUTTER ANALYSIS

For frequency domain flutter analysis technique, the resulting equations of motion involve reduced frequency dependent coefficients. Thus, the analysis requires iterative search for the critical flutter wind speed. Moreover, material and geometric nonlinearities in the structural system cannot be incorporated into the frequency domain flutter analysis. Also, the design of vibration suppression systems is hindered due to the reduced frequency dependence. Time domain flutter analysis, that uses frequency independent state-space equations to represent the equations of motion, is gaining popularity in recent times because:

- Flutter analysis does not require iterative calculations while solving the complex eigenvalue problem to determine the frequencies, damping ratios, and mode shapes at different velocities,
- Structural and aerodynamic nonlinearities can be incorporated in the analysis.
- The time domain formulation can be used to design vibration control systems for suppressing flutter phenomenon that are more efficient.

## III. METHODOLOGY

### 3.1 AUTO-REGRESSIVE (AR) MODEL

Fluctuating wind loads, which mostly relate to the shape and height of the structure, are (multi points) random loads and one of the main dominating excitations of large structures in civil engineering. In any study of buffeting and flutter analysis of structures, the wind velocity is indispensably considered, but an accurate wind velocity model usually requires expensive cost through a full ruler observation or a wind tunnel experiment. Therefore, it is significant to study the wind effects simulation by numerical simulation methods.

The AR model was applied mostly to forecast the time history series in wind engineering, because of its many benefits: simple algorithm and rapid calculation; besides, it can consider not only the space dependent characteristic, but also the time dependent characteristic of the **wind history**, and also those advantages can be simplistic to implement by **computer programming like Matlab**. Though the Autoregressive Moving Average (ARMA) is superior to the AR model, the parameter estimation for the ARMA model is much more difficult than the AR model. Hence, this work will concern with the issues of the AR model while using it to simulate the natural wind velocity processes.



Figure 3.1: Lekki cable stayed bridge (Julious Berger Plc, 2013)

Therefore, this paper attempts to present the corresponding solving methods whose computing programs are implemented in MATLAB Code based on the case study of Lekki link cable stayed bridge, and the method used in deducing AR model by matrix form in simulating the wind velocity of the spatial 3-D fields are all referred to the **Appendix A and Appendix B** respectively.

**3.2 SIMULATION OF RANDOM WIND VELOCITY FIELD ON CABLE STAYED BRIDGES BASED ON AUTO-REGRESSIVE (AR) MODEL**

The fluctuating wind velocity is a random time series in essence. The basic formula of the wind velocities  $u(t)$  at  $M$  spatial points, idealized as stationary Gaussian multivariate stochastic processes, it can be expressed as [6, 7, and 8]:

$$[u(t)] = \sum_{k=1}^p [\psi_k][u(t - k\Delta t)] + [N(t)] \dots (3.1)$$

Where  $[N(t)] = [N^1(t), \dots, N^M(t)]^T$ ,  $[N^i(t)]^T$  is the  $i^{th}$  normally distributed stochastic process with zero mean and unit variance,  $i = 1, \dots, p$  is the rank of AR model, and  $\Delta t$  is the time step of the series. The process of the simulation can be realized as follows.

**3.2.1 CALCULATION OF COEFFICIENT MATRIX  $[\psi_k]$**

After multiplying the two sides of Eq. 3.1 by  $[u(t - j\Delta t)]$  and calculating the expectation, we can get the following formula:

$$E\{[u(t)][u(t - j\Delta t)]\} = E\{\sum_{k=1}^p [\psi_k][u(t - k\Delta t)][u(t - j\Delta t)]\} + E\{[N(t)][u(t - j\Delta t)]\} \dots (3.2)$$

Since the covariance between stochastic process  $u(t)$  and  $u(t - j\Delta t)$  can be expressed as  $R_u(j\Delta t) = E\{[u(t) - E[u(t)]] [u(t - j\Delta t) - E[u(t - j\Delta t)]]\} = E[u(t)(u(t - j\Delta t))]$ , and the stochastic process  $N(t)$  is independent to stochastic wind velocity  $u(t)$ , then the relationship between the covariance  $R_u(j\Delta t)$  and regressive coefficient  $[\psi_k]$  can be written as:

$$R_u(j\Delta t) = \sum_{k=1}^p [\psi_k][R_u(j - k)\Delta t] \dots (3.3)$$

In which  $j = 1, 2 \dots P$ . after transpose, Eq. (3.3) can be rewritten in the matrix form:

$$[R] = [\bar{R}][\Psi] \dots (3.4)$$

Where

$$[R]_{pM \times pM} = [R_u(j\Delta t), \dots, R_u(p\Delta t)]^T$$

$$[\Psi]_{pM \times pM} = [\psi_1^T, \dots, \psi_p^T]^T$$

$$[\bar{R}]_{pM \times pM} = \begin{bmatrix} R_u(0) & R_u(\Delta t) & \dots & R_u[(P-2)\Delta t] & R_u[(P-1)\Delta t] \\ R_u(\Delta t) & R_u(\Delta t) & \dots & R_u[(P-3)\Delta t] & R_u[(P-2)\Delta t] \\ \vdots & \vdots & \ddots & \vdots & \vdots \\ R_u[(P-2)\Delta t] & R_u[(P-3)\Delta t] & \dots & R_u(0) & R_u(\Delta t) \\ R_u[(P-1)\Delta t] & R_u[(P-2)\Delta t] & \dots & R_u(\Delta t) & R_u(0) \end{bmatrix} \dots (3.5)$$

In which

$$[R_u(j\Delta t)] = \begin{bmatrix} R_u^{11}(j\Delta t) & \dots & R_u^{1N}(j\Delta t) \\ \vdots & \ddots & \vdots \\ R_u^{M1}(j\Delta t) & \dots & R_u^{MM}(j\Delta t) \end{bmatrix}, [\psi_j] = \begin{bmatrix} \psi_j^{11} & \dots & \psi_j^{1M} \\ \vdots & \ddots & \vdots \\ \psi_j^{M1} & \dots & \psi_j^{MM} \end{bmatrix} \dots (3.6)$$

According to random vibration theory, the relationship between the **power spectral density** and the **correlation function** accords with the Wiener-Khinchin theorem [9]:

$$R_u^{ik}(j\Delta t) = \int_0^\infty S_u^{ik}(f) \cos(2\pi \cdot f \cdot j\Delta t) df \dots (3.7)$$

Where  $f$  is the frequency,  $S_u^{ik}(f)$  is the auto-power spectral density if  $i = k$ , the cross-power spectral density if  $i \neq k$ ,  $k = 1, 2, \dots, M$ ,  $j = 1, \dots, p$ . The study of this term may be simplified by assuming that the imaginary component of the cross-spectrum is negligible for the purposes of the study that is to be carried out:

$$S_{ij}(f) = \sqrt{S_{ii}(f) \cdot S_{jj}(f) \cdot \text{coh}_{ij}(f)} \dots (3.8)$$

Where  $\text{coh}_{ij}(f)$  represents the coherence function of longitudinal fluctuations at points  $i$  and  $j$  of the plane orthogonal to the mean wind direction. As described, the three-dimension expression of the coherence function is:

$$\text{coh}_{ij}(f) = \exp \left[ \frac{-2f \sqrt{C_x^2(x_i - x_j)^2 + C_y^2(y_i - y_j)^2 + C_z^2(z_i - z_j)^2}}{\bar{U}(z_i) + \bar{U}(z_j)} \right] \dots (3.9)$$

Where,  $C_x$ ,  $C_y$ , and  $C_z$  are the appropriate decay coefficients. For the purpose of this present study, the following values were adopted  $C_x = 8$  (longitude direction),  $C_y = 16$  (transverse direction), and  $C_z = 10$  (vertical direction).

**3.2.2 CALCULATION OF THE NORMALLY DISTRIBUTED RANDOM PROCESSES  $N(t)$**

The normally distributed random processes  $N(t)$  can be obtained from:

$$[N(t)] = [L][n(t)] \dots (3.10)$$

Where  $[n(t)] = [n_1(t), n_2(t), \dots, n_m(t)]^T$ ,  $n_i(t)$  is the  $i^{th}$  independent normally distributed random process with zero mean and unit variance, in which  $i = 1, 2, \dots, M$ ;  $[L]$  is from the Cholesky decomposition of  $[R_N] = [L][L]^T$ , in which  $[R_N]$  is calculated from the following equation obtained by multiplying two sides of Eq. (3.1) with  $[u(t)] = [u^1(t), \dots, u^M(t)]^T$

$$[R_N] = [R_u(0)] - \sum_{k=1}^p [\psi_k][R_u(k\Delta t)] \dots\dots (3.11)$$

3.2.3 CALCULATION OF THE FLUCTUATING WIND VELOCITY

Using the results of Eq. 3.2 and Eq. 3.8, with the presumption of  $u^i(t) = 0$ , while  $t < 0$ , Eq. 3.1 can be dispersed and rewritten as:

$$\begin{bmatrix} u^1(h\Delta t) \\ \vdots \\ u^M(h\Delta t) \end{bmatrix} = \sum_{k=1}^p [\psi_k] \begin{bmatrix} u^1(h-k)\Delta t \\ \vdots \\ u^M(h-k)\Delta t \end{bmatrix} + \begin{bmatrix} N^1(h\Delta t) \\ \vdots \\ N^M(h\Delta t) \end{bmatrix} \dots\dots (3.12)$$

$h = 0, 1, 2 \dots$  and  $k = 1, \dots, p$  in which  $\Delta t$  is the time step.

3.2.4 CALCULATION OF THE FINAL WIND VELOCITY

The final wind velocity can be generated by:

$$U(t) = \bar{U} + u(t) \dots\dots (3.13)$$

Where,  $\bar{U}$  is the mean component of wind velocity.

3.5.5 SELECTION OF THE AR MODEL RANK

Iwatani point out that the low rank of the AR model can meet the requirement in general engineering with the permitted error [6]. But, for large and complex structures, it is not credible to solve the rank of AR model based on the empirical analysis only. However, much work has already been done and many experimental results have been given. Ref [10, 11, and 12] proposed a new method to select the AR model order by translating the n-variate AR model equations into **state-spaceform**. Different from those former works ref [15] developed a new method of resolving the rank of AR model based on the principle of the AIC (Akaike Information Criterion). The AIC can be expressed as:

$$AIC(p) = \ln \sigma_a^2 + 2p/N \dots\dots (3.14)$$

Where  $N$  is the sample time length,  $\sigma_a^2$  is the variance.

With the increasing rank of the AR model initially, the value of the variance  $\sigma_a^2$  and  $AIC(p)$  decrease. However, the value of  $AIC(p)$  will increase with the rising rank. Hence,  $P_0$  is taken as the best rank of the AR model if it is determined by the formula for a special rank,  $m$ .

$$AIC(P_0) = \sum_{1 \leq p \leq m} \min AIC(p) \dots\dots (3.15)$$

It is a huge job to calculate the variance  $\sigma_a^2$  for a multidimensional sequence. In this study, it is proposed that the variance  $\sigma_a^2$  can be replaced by the absolute of the maximum eigenvalue of the matrix  $[R_N]$ .

3.2.6 IMPLEMENTATION OF THE AR MODEL

There are two important points in the implementations of the AR model based on the MATLAB programming: (Fig 3.2).

3.2.6.1 SOLVING THE ILL-POSED EQ. 3.4 RESULTING FROM THE INCREASING DEGREES OF FREEDOM OF THE STRUCTURE

Eq. 3.4 can be solved by a general iterative method for a structure with a few degree freedoms. However, the large dimension of the coefficient matrix  $[R]$ , which results from a large number of degrees of freedom, will make the Eq. 3.4 an ill conditioned equation. Therefore the complicated method with better accuracy is needed for resolving the problem. Here, over relaxation iteration [13] is used to calculate the large sparse matrix equation. The iteration formula of the algorithm is:

$$\psi_{ij}^{k+1} = (1 - \omega)\psi_{ij}^k + \frac{\omega}{r_{ij}} [r_{ij} - \sum_{l=1}^{i-1} r_{lj} \cdot \psi_{lj}^{k+1} - \sum_{l=i+1}^{pM} r_{il} \psi_{lj}^k] \dots\dots (3.16)$$

Where  $\omega$  is the relaxation factor which controls the convergent rate of the iteration algorithm,  $i = 1, 2, \dots, M$ . With the condition of positive definite matrix  $[R]$ , the formula would be convergent with  $1 < \omega < 2$ . It is suggested that the relaxation factor value should be within the range of 1.0 ~ 1.05 in this study.

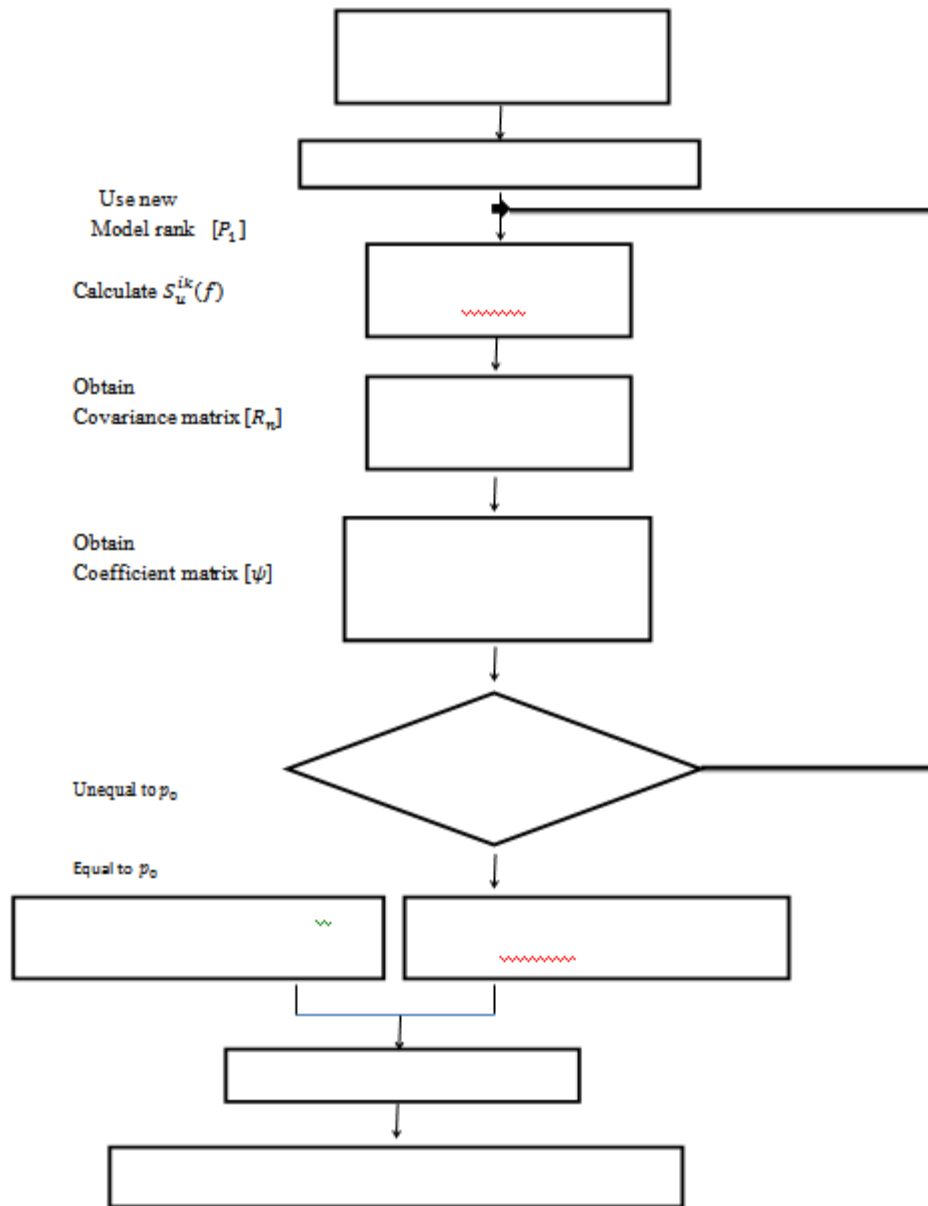


Figure 3.2: Flow chart of implementing wind velocity by AR model in Matlab

3.2.6.2 SOLVING THE NUMERICAL INTEGRAL EQUATION 3.7 WHICH CONTAINS OSCILLATING FUNCTION

The integral function of Eq. 3.7 contains the oscillating function  $\cos(2\pi \cdot f \cdot j\Delta t)$ . With the growth of the variable  $2\pi \cdot f \cdot j\Delta t$ , the integral function will have more points of zero value on x-axis coordinate. Then a general numerical interpolation can not meet the requirement of accuracy, and neither can the compound integral method. In this study, the Gauss-Lobatto formula improved from the Gauss formula is used to solve the integral of oscillation function. The formula can be expressed as [15]:

$$R_u = A_1 f(a) + A_n f(b) + \sum_{k=2}^{n-1} A_k f(x_k) + K_n f^{2n-2}(\xi) \dots (3.17)$$

Where,  $a$  &  $b$  are the ends points of each range  $A_1, \dots, A_n, K_n$  are  $n + 1$  parameters.

3.3 LEKKI CABLE BRIDGE WIND FIELD EVALUATIONS

Using those methods mentioned above, one can simulate the wind velocity at four-space points as shown in Fig 3.3. The parameters used in the simulation are: the roughness length,  $z_0 = 40\text{m}$ , the standard mean component of the wind velocity,  $\bar{v} = 28 \text{ m/s}^2$ , the discrete time  $\Delta t = 0.1 \text{ s}$ . The results of the simulation are shown in Figs. 4.2.

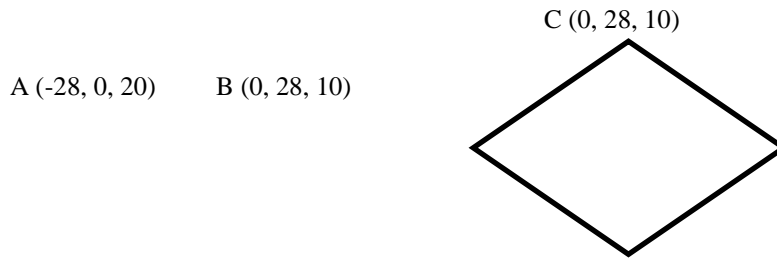


Figure 3.3: Four-space points (unit: m)

IV. RESULT

4.1LEKKI CABLE BRIDGE WIND VELOCITY SIMULATION USING AR MODEL

The results below were based on typical average weather of Ikeja Lagos (bridge location), for the historical records from 2007 – 2012 where earlier records are either unavailable or unreliable. Ikeja has a tropical savannah climate and covered by forests (35%), oceans and seas (20%), marshes (18%), croplands (12%), and grassland (7%).

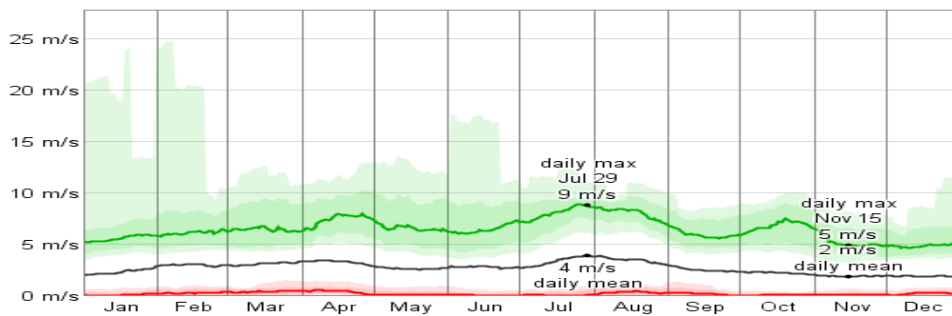
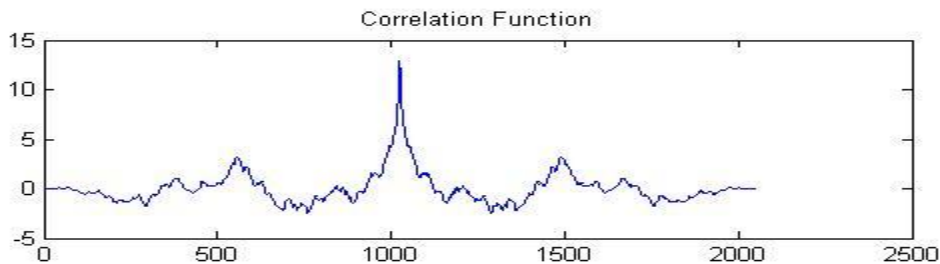
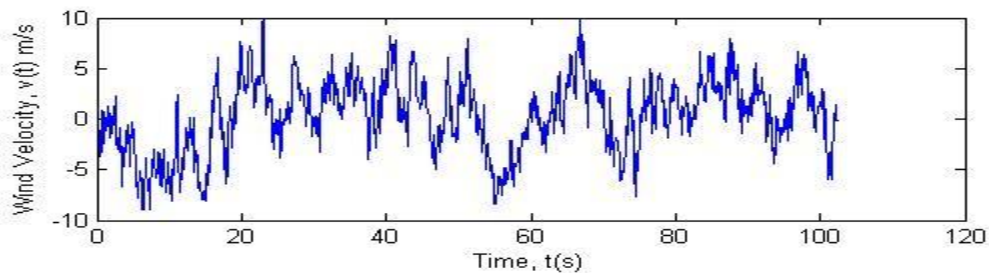


Figure 4.1: Ikeja average wind speed (Weatherspark.com)

Wind over the course of the year typical wind speeds vary from 0 m/s to 9 m/s (calm to fresh breeze), rarely exceeding 25 m/s (storm). The highest average wind speed of 4 m/s (gentle breeze) occurs around July, at which time the average daily maximum is 9 m/s (fresh breeze), and the lowest average wind speed of 2 m/s (light breeze) occurs around November, at which time the average daily maximum wind speed is 5 m/s (gentle breeze).



Node A

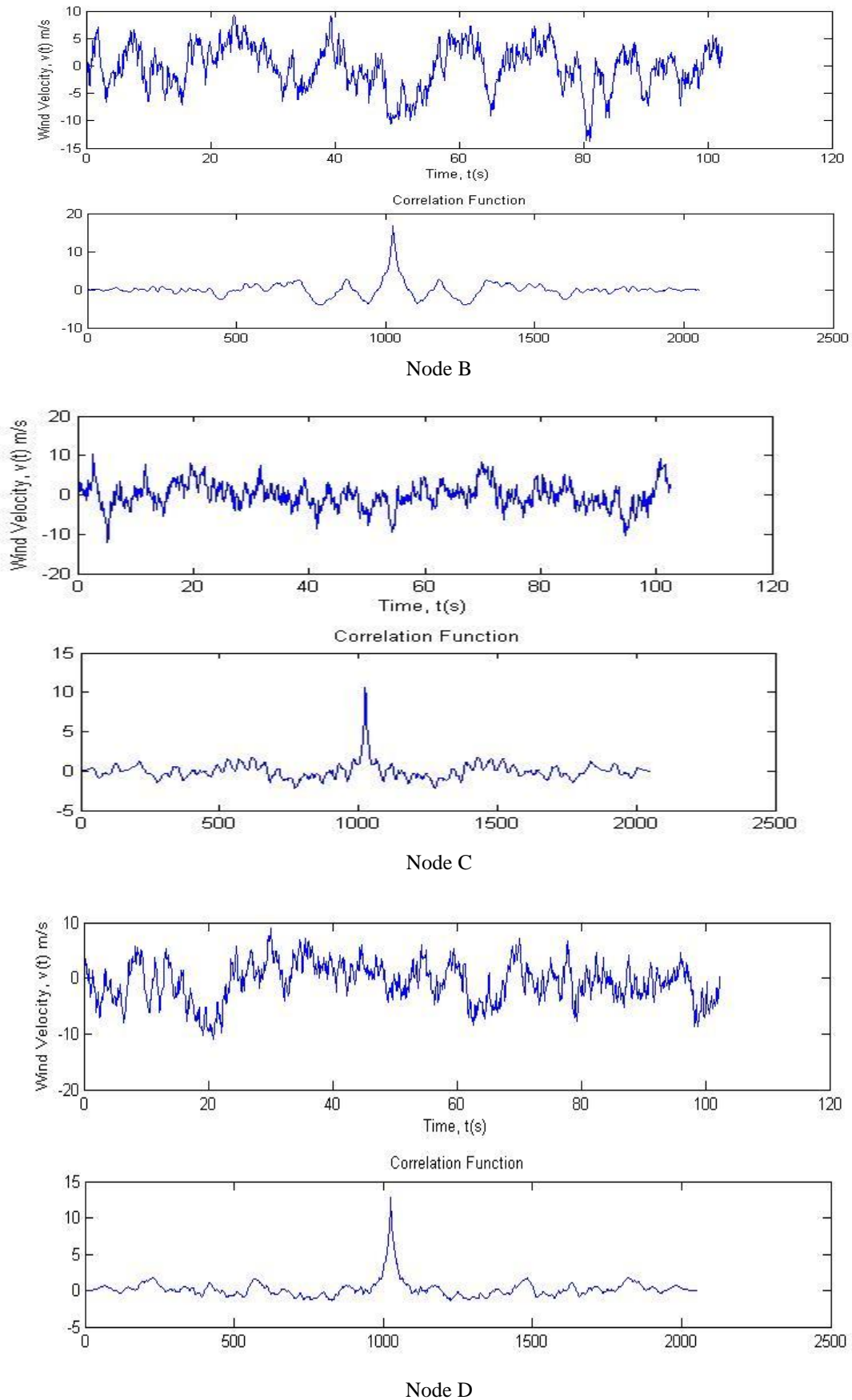


Figure 4.2: Wind velocity and correlation function simulated using AR Model.

#### 4.2 DISCUSSION

Fig. 4.2 shows the fluctuating components of wind velocities at the four-space points, with the rank of the AR model  $P = 4$ . The wind velocity curves also illuminate that the wind velocity (10 to  $-15\text{m/s}^2$ ) is a random process accompanying the varieties of time.

It further represents the type of random process; and describes certain time-varying processes in nature condition of the bridge.

#### V. CONCLUSION

From the results obtained in Fig. 4.2 above, the fluctuating components of the wind velocity which displays as (10 to  $-15\text{m/s}^2$ ) by the fluctuant curve will result in the vibration of the structure, even strengthens the resonance effect of the structure. The autoregressive model specified that the output variable depends linearly on its own previous values and on a stochastic term.

#### VI. ACKNOWLEDGMENT

I would like to acknowledge Dr. Prashant Mukherjee, Dr. A. Mohammed, and Shashi Kant for their invaluable suggestions and inputs toward this research.

#### REFERENCES

- [1] Marco L., Vincenzo G., A Parametric multi body section model for model interactions of cable supported bridges, Journal of Sound and Vibration 333 (2014) 4579–4596.
- [2] A.M. Abdel-Ghaffar, M.A. Khalifa, Importance of cable vibration in dynamics of cable-stayed bridges, Journal of Engineering Mechanics 117 (11) (1991) 2571–2589.
- [3] P. Warnitchai, Y. Fujino, T. Susumpow, A non-linear dynamic model for cables and its application to a cable-structure system, Journal of Sound and Vibration 187 (4) (1995) 695–712.
- [4] S.H. Cheng, D.T. Lau, Modeling of cable vibration effects of cable-stayed bridges, Earthquake Engineering and Engineering Vibration 1 (1) (2002) 74–85.
- [5] R.H. Scanlan, The action of flexible bridges under wind, II: Buffeting theory, Journal of Sound and Vibration, Volume 60, Issue 2, 22 September 1978, Pages 201-211.
- [6] Iwatani, Y. 1982, Journal of Wind Engineering, 11, 5-14, Simulation of multidimensional wind fluctuations having any arbitrary power spectra and cross spectra.
- [7] Iannuzzi, A. and Spinelli, P. 1987, Journal of Structural Engineering, ASCE, 113(10), 2382-2398, Artificial wind generation and structural response.
- [8] Li, Y-Q and Dong, S-L. 2001, Spatial Structure, 7(3), 3-11, Random wind load simulation and computer program for large-span spatial structures (In Chinese).
- [9] Strube, H.W. 1985, Signal Process, 8(1), 53-74, A generalization of correlation functions and the Wiener-Khinchin theorem.
- [10] Schlindwein, F. S. and Evans, D. H. 1990, Ultrasound Med. Biol. 16(1), 81-91, selection of the order of autoregressive models for spectral analysis of Doppler Ultrasound signals.
- [11] Akaike, H. 1974, IEEE Trans. Automatic Control, 19, 716-723, A new look at the statistical model identification.
- [12] Pappas, S. S., Leros, A. K., and Katsikas S. K. 2006, Digital Signal Processing, 16, 782-795, Joint order and parameter estimation of multivariate autoregressive models using multi-model partitioning theory.
- [13] Martinsm M. M., Trigo, M. E., and Santos. M. M. 1996, Linear Algebra. Appl., 232, 131-147, an error bound for the SSOR and USSOR methods.
- [14] Gander, W. and Gautschi, W. 2000, Numerical Mathematics, 40, 84,101, Adaptive quadrature revisited.
- [15] Weicheng Gao and Yanlei Yu, Journal of Wind and Structure, vol. 11, No.3 (2008), pp. 241-256, Wind velocity simulation of spatial three-dimensional fields based on autoregressive model.

#### APPENDIX A

##### EXTERNAL FILE (COOR.TXT)

```
Coordinate data
Number of Coordinates N=3
```

```
x-data
-28 0 20
```

```
z-data
15 24 56
```

#### APPENDIX B

##### MATLAB SCRIPTS

```
clc
clear all
```

```

tic
P=4;
v10=36;
n=0.01:0.01:10;
xn=1200*n./v10;
k=0.00215;
ti=0.1;
s1=4*k*v10^2*xn.^2./n./(1+xn.^2).^ (4/3);
syms plf;
fr = fopen('coor.txt', 'rt');
N = fscanf(fr, '%s %s\n%s %s %s N=%d\n', 1);
fgetl(fr);
for i=1:N
    x(i)= fscanf(fr,'%f',[1,1]);
end
fgetl(fr);
fgetl(fr);
fgetl(fr);
for i=1:N
    z(i)=fscanf(fr,'%f',[1,1]);
    v(i)=(z(i)/10)^0.16*v10;
end

A=zeros(P*N);

for p=1:P

    R=zeros(N);
    for i=1:N
    for j=i:N

H=inline(' (4*k*v10^2*(1200*f/v10).^2)./f./(1+(1200*f/v10).^2).^ (4/3) .* (exp(
-2*f*sqrt(8^2*dx.^2+10^2*dz.^2)/vt) ) .* cos(2*pi*f*(p-
1)*ti)', 'f', 'k', 'dx', 'dz', 'ti', 'v10', 'vt', 'p');
        vt=(v(i)+v(j));
        dx=x(i)-x(j);
        dz=z(i)-z(j);
        R(i,j)=quadl(H,0.01,10,0.001,0,k,dx,dz,ti,v10,vt,p);
        R(j,i)=R(i,j);

    end
    end

for l=1:P-p+1
    A(((l-1)*N+1):(l*N), ((l+p-1-1)*N+1):((l+p-1)*N))=R;
end

end

for i=1:P*N
for j=1:i
    A(i,j)=A(j,i);
end
end
R=zeros(N);
for i=1:N
for j=i:N

H=inline(' (4*k*v10^2*(1200*f/v10).^2)./f./(1+(1200*f/v10).^2).^ (4/3) .* (exp(

```

```

-
2*f*sqrt(8^2*dx.^2+10^2*dz.^2)/vt)).*cos(2*pi*f*P*ti)', 'f', 'k', 'dx', 'dz', 't
i', 'v10', 'vt', 'P');
    vt=(v(i)+v(j));
    dx=x(i)-x(j);
    dz=z(i)-z(j);
    R(i,j)=quadl(H,0.01,10,0.001,0,k,dx,dz,ti,v10,vt,P);
    R(j,i)=R(i,j);
end
end
B=A(1:N,(N+1):(N*P));
B=[B,R];
B=B';
X=A\B;
R0=A(1:N,1:N);
RN=R0;
for i=1:P
    RN=RN-(X(((i-1)*N+1):(i*N),1:N))'*B(((i-1)*N+1):(i*N),1:N);
end
L=chol(RN);
L=L';
a=zeros(N,1024);
for i=1:N
    a(i,:)=normrnd(0,1,1,1024);
end

V(1:N,1)=L*a(:,1);
for i=2:p
    V(1:N,i)=L*a(:,i);
for j=1:i-1
    V(1:N,i)=(X(((j-1)*N+1):(j*N),:))'*V(1:N,(i-j))+V(1:N,i);
end
end

for i=(P+1):1024
    V(1:N,i)=L*a(:,i);
for j=1:P
    V(1:N,i)=(X(((j-1)*N+1):(j*N),:))'*V(1:N,(i-j))+V(1:N,i);
end
end
toc

V1=V(1,:);
t=(1:1024)*ti;
figure
subplot(2,1,1);
plot(t,V1,'b-');
xlabel('Time, t(s)');
ylabel('Wind Velocity, v(t) m/s');

[power,freq]=psd(V1,1024,10,boxcar(1024),0,'mean');
power=power*2/10;
subplot(2,1,2);
loglog(freq,power,'r-',n,s1,'g-');

maxlags=1024;
cx = xcorr(V1(1,:),V1(1,:),maxlags,'biased');
plot(cx)
fid=fopen('windv.dat','wt');

```

```
for i=1:1:1024
for j=1:1:N-1
    fprintf(fid, '%e \t',V(j,i));
end
    fprintf(fid, '%e \n',V(N,i));
end
fclose(fr);
fclose(fid);
```

## Radiological Assessment of Sediment of Zobe Dam Dutsinma, Katsina State, Northern Nigerian.

<sup>1\*</sup>Najib M. U., <sup>2</sup>Zakari Y. I., <sup>2</sup>Sadiq U., <sup>3</sup>Bello I. A., <sup>4</sup>Ibrahim G. G. <sup>5</sup>Umar S. A., <sup>6</sup>Sanda Y.S., and <sup>1</sup>Abdu N.M.

<sup>1</sup>Nigerian Nuclear Regulatory Authority, North-West Zonal Office, Katsina, Nigeria

<sup>2</sup>Department of Physics, Ahmadu Bello University, Zaria, Nigeria

<sup>3</sup>Kabba College of Agriculture, Ahmadu Bello University Zaria, Nigeria

<sup>4</sup>Department of Physics, Federal College of Education (Technical), Potiskum, Yobe, Nigeria

<sup>5</sup>Department of Physics, Bauchi State University, Gadau, Nigeria

<sup>6</sup>Physics Option, S.L.T. Department, Nuhu Bamalli Polytechnic, Zaria, Nigeria

**ABSTRACT:** A radioactivity measurement was carried out in sediments of Zobe Dam. Samples of sediments from Zobe Dam were collected, prepared and analyzed using NaI(Tl) gamma ray spectrometer for the activity concentrations of the primordial <sup>226</sup>Ra, <sup>232</sup>Th and <sup>40</sup>K. The results obtained show average activity concentrations of 49.67±3.07 (35.89-75.75), 127.29±4.42 (47.21-112.91) and 443.43±9.51 (338.88-638.40) in Bq/kg for <sup>226</sup>Ra, <sup>232</sup>Th and <sup>40</sup>K respectively. To assess the radiological hazard of Dam sediments, the radiological hazard indices such as absorbed dose rate, annual effective dose equivalent (AEDE), hazard indices ( $H_{ex}$  and  $H_{in}$ ) were calculated and found to be comparable with the world average values. The mean absorbed dose rate obtained is 124.52 nGy/h, and is higher than the world average of 55 nGy/h. The measured average annual effective dose rate 0.152mSv/y is lower than the world average value of 1 mSv/y [7]. The measured average values of external and internal hazard index is 0.717 and 0.851 and are lower than unity set by [6], which indicate that the sediments in all the sampling sites can be used for safety construction of buildings.

**Key words:** sediments, hazard index, dose rate and annual effective dose rate.

### I. INTRODUCTION

All life on earth is exposed to radiation from natural sources including cosmic radiation; external radiation from natural radionuclides present in soils, rocks and building materials; and internal radiation due to potassium-40 and inhaled radionuclides, particular radon decay products. Natural radiation exposure varies regionally as the compositions of soils and rocks change, and increases with altitude as cosmic radiation intensity increases.

When rocks are disintegrated through natural processes, radionuclides are seep to the soil and are carried to the rivers by rain and flows [15]. Soil radionuclide activity concentration is one of the main determinants of the natural background radiation. The knowledge of the distribution of these radionuclides in soil, water, sediment, rock and building materials plays an important role in the protection, measurement, geoscientific research and guidelines for the use and management of these materials [14].

Due to gravitational settling and other depositional phenomena, the highest proportion of the radioactive materials is mainly found in the sediment compartment of the aquatic ecosystem [12]. Thus river sediment is considered as a durable and reliable register of the river pollution by radionuclides [1]. Knowledge of natural radioactivity present in aquatic sediments enables one to assess any possible radiological hazard to mankind, by the uses of such materials especially in building and construction material [13].

### II. MATERIALS AND METHODS

#### 2.1 The Study Area

The Zobe Dam is located between latitude 12° 20' 34.62" N to 12° 23' 27.48" N and between longitude 7° 27' 57.12" E to 7° 34' 47.68" E, in Dutsinma Local Government Area of Katsina State.

The reservoir formed by the Dam cover 4500 hectares of rocky land and during the rainy season stores 177 million cubic metres of water which is released downstream for irrigation and town water supplies.

The Zobe Dam has only two tributaries; these include river Karaduwa and river Gada in which river Gada drains to river Karaduwa.

The Dam is constructed in river Karaduwa and the Dam over Karaduwa is about 2.7 kilometres long and flowing north westward to the Sokoto river Basin. Along the river course, there are no large cities, no mining sites, no nuclear enterprises such as chemical and phosphate industries. Farmers' lives in the area generally rear animals, raise crops and some vegetables. Therefore, agrochemical such as fertilizers and pesticides, herbicides are the main contaminant of the Dam reservoir. Fishing is another major activity in the area.

## 2.2 Sample Collection Procedures

Sediments were collected from Garhi A, Garhi B, Makera and Tabobi. Garhi A, Garhi B, Makera are the areas where farming, domestic/live stocks activities and fishing are very high. While Tabobi is the control area in which the activities mentioned are very less. The sample collection method was achieved as described below.

## 2.3 Sample Collection and Preparation

Bottom sediments were collected from the 15 different locations. Four (4) samples each were collected in an area where farming, domestic/livestock activities and fishing is very high and three (3) from the control area where farming, domestic/livestock activities and fishing is very less. The sediment samples were collected in period of low water levels during the dry season so that undisturbed sediments could be taken [9]. The sediment were put into different polyethylene labeled bags and transported to the laboratory. The point of collection of each sample were given a unique code and noted with its GPS coordinate taken with a handheld GPS device.

Sample preparation and analysis was done at the Center for Energy Research and Training (CERT) Ahmadu Bello University, Zaria, Kaduna State. The collected samples were kept opened to dry at an ambient temperature in the laboratory in a clean environment in order to avoid contaminations. The dried samples were grounded into a fine powder with the use of a table ceramic mortar and pestle and then a pulverizer. The process was followed by packaging into radon impermeable cylindrical plastic containers of height 7cm by 6cm in diameter. This satisfied the selected optimal sample container height [5] i.e the detector geometry. Each container would accommodate approximately 300g of sample. A 3-stage sealing system was made for each of the packaging to prevent Ra-222 from escape. This include, smearing of the inner rims of each container lid with Vaseline, filling the lid assembly gap with candle wax to block the gaps between lid and container and tight-seal lid container with a masking adhesive tape. The prepared samples were then stored for period of 30 days to allow radon and its short-lived progenies to reach secular radioactive equilibrium prior to gamma spectroscopy measurements.

## III. Gamma Ray Spectroscopy Instrumentation and Analysis

The gamma-ray spectrometry set-up is made up of a 7.62 cm by 7.62 cm NaI (TI) detector housed in a 6 cm thick lead shield (to assist in the reduction of the background radiation) and lined with cadmium and copper sheets [3]. The samples were placed on the detector surface and each counted for about 29,000 seconds in reproducible sample detector geometry. The configuration and geometry was maintained throughout the analysis, as previously characterized based on well established protocol of the laboratory (at the Centre for Energy Research and Training, Zaria).

With reference to Ibeanu [5], there are two renowned ways of achieving spectra analysis for the energy discrimination needed for qualitative and quantitative analysis of the radionuclides; the integral and the differential spectrometry. The integral spectrometry approach involves the recording of whole spectrum from a predetermined low position that covers the energy peak of interest. The differential spectrometry involves acquisition of information on the energy peaks with an energy window set at about the peak.

In this particular work, differential spectrometry is employed in three channels and this was achieved by using a computer based Multichannel Analyser (MCA) MAESTRO Programme from ORTEC for data acquisition and analysis of gamma spectra. The 1764 keV Gamma-line of  $^{214}\text{Bi}$  for  $^{238}\text{U}$  was used in the assessment of the activity concentration of  $^{226}\text{Ra}$ , while 2614.5 keV Gamma-line of  $^{208}\text{Tl}$  was used for  $^{232}\text{Th}$ . The single 1460 keV Gamma-line of  $^{40}\text{K}$  was used in its content evaluation.

All the obtained raw data were converted to conventional units using calibration factors to determine the activity concentrations of  $^{40}\text{K}$ ,  $^{226}\text{Ra}$  and  $^{232}\text{Th}$  respectively. In order to determine the specific activity concentrations in the samples, the IAEA mixed standard consisting of  $^{40}\text{K}$ ,  $^{226}\text{Ra}$  and  $^{232}\text{Th}$  of the same dimension as the samples were subjected to the same experimental procedures. After the subtraction of background counts, conversion of the count per second to activity concentration in Bq/kg was performed using the conversion factors which are different for each nuclide such that for  $^{40}\text{K}$ ,  $^{226}\text{Ra}$  and  $^{232}\text{Th}$  as 6.431, 8.632 and 8.768, respectively.

## 3.1 Activity Concentration of the Sediments

The activity concentrations in the sediment samples were obtained using the equation (1.0) [8].

$$C(\text{Bqkg}^{-1}) = kC_n \dots\dots\dots (1.0)$$

where  $k = \frac{1}{\epsilon P_{\gamma} M_s}$ , C is the activity concentration of the radionuclide in the sample given in Bq/kg,  $C_n$  is the count rate under the corresponding peak,  $\epsilon$  is the detector efficiency at the specific  $\gamma$ - ray energy,  $P_{\gamma}$  is the absolute transition probability of the specific  $\gamma$ -ray, and  $M_s$  is the mass of the sample (kg). The below detection limit (BDL) of a measuring system describes its operating capability without the influence of the samples. The BDL given in  $Bqkg^{-1}$  which is required to estimate the minimum detectable activity in samples was obtained using equation (2.0), [8]

$$DL(Bqkg^{-1}) = 4.65 \frac{\sqrt{C_b}}{t_b} k \dots\dots\dots (2.0)$$

where  $C_b$  is the net background count in the corresponding peak,  $t_b$  is the background counting time (s) and k is the factor that converts count per second (cps) to activity concentration ( $Bqkg^{-1}$ ) as given in equation (1.0).

All the obtained raw data were converted to conventional units using conversion factors of  $8.632 \times 10^{-4}$ ,  $8.768 \times 10^{-4}$  and  $6.431 \times 10^{-4}$  for  $^{40}K$ ,  $^{226}Ra$  and  $^{232}Th$  respectively to determine their activity concentrations [3]. With the counting time of 29,000 seconds for each sample, the environment  $\gamma$ -ray background of the laboratory site was determined using an empty container under identical measured conditions. This then gave the below detectable limit (BDL) limits to be  $310.99 Bqkg^{-1}$  for  $^{40}K$ ,  $16.21 Bqkg^{-1}$  for  $^{226}Ra$  and  $123.16 Bqkg^{-1}$  for  $^{232}Th$  respectively. This was subtracted from the measured  $\gamma$ -ray spectrum of each sample.

**3.2 Absorbed dose rate from measured activity concentration for sediments**

Radiation emitted by a radioactive substance is absorbed by any material it encounters. [16] has given the dose conversion factors for converting the activity concentrations of  $^{226}Ra$ ,  $^{232}Th$  and  $^{40}K$  into dose ( $nGyh^{-1}$  per  $Bqkg^{-1}$ ) as 0.427, 0.662 and 0.043, respectively. Using these factors, the total absorbed dose rate in air is calculated as given in the Equation (3.0) [16].

$$D = (0.427C_{Ra} + 0.662C_{Th} + 0.043C_K) nGyh^{-1} \dots\dots\dots (3.0)$$

where  $C_{Ra}$ ,  $C_{Th}$  and  $C_K$  are the activity concentrations ( $Bqkg^{-1}$ ) of radium, thorium and potassium, respectively in the samples.

**3.3 Annual effective dose from sediment**

The estimation of the annual effective dose rates, depended on conversion coefficient from absorbed dose to effective dose as  $0.7 SvGy^{-1}$  and outdoor occupancy factor of 0.2 as proposed by [16]. The effective dose rate in units of  $mSvGy^{-1}$  was calculated by the following formula in equation (4.0)

$$\text{Effective dose rate (mSvGy}^{-1}) = D (nGyh^{-1}) \times 870h \times 0.2 \times 0.7 SvGy^{-1} \times 10^{-6} \dots\dots (4.0)$$

**3.4 External hazard index ( $H_{ex}$ )**

Radiation exposure due to  $^{226}Ra$ ,  $^{232}Th$  and  $^{40}K$  may be external. This hazard, defined in terms of external hazard index or indoor radiation hazard index and denoted by  $H_{ex}$ , can be calculated using the equation (5.0) [2]:

$$H_{ex} = \frac{C_{Ra}}{370} + \frac{C_{Th}}{259} + \frac{C_K}{4810} \dots\dots\dots (5.0)$$

where  $C_{Ra}$ ,  $C_{Th}$  and  $C_K$  are the activity concentrations ( $Bqkg^{-1}$ ) of radium, thorium and potassium, respectively as obtained in the analyzed samples. The value of this index should be less than  $1 mSvy^{-1}$  in order for the radiation to be considered acceptable to the public.

**3.5 Internal hazard index ( $H_{in}$ )**

The internal hazard index ( $H_{in}$ ) gives the internal exposure to carcinogenic radon and is given by equation (6.0), [2]:

$$H_{in} = \frac{C_{Ra}}{185} + \frac{C_{Th}}{259} + \frac{C_K}{4810} \dots\dots\dots (6.0)$$

The value of this index should be less than  $1 mSvy^{-1}$  in order for the radiation hazard to have negligible hazardous effects to the respiratory organs of the public [2].

**IV. RESULTS AND DISCUSSION**

**4.1 Activity Concentration in Sediments**

The activity concentrations of the three primordial radionuclides  $^{226}Ra$ ,  $^{232}Th$  and  $^{40}K$  were measured and an average of  $49.67 \pm 3.07 Bqkg^{-1}$ ,  $127.29 \pm 4.42 Bqkg^{-1}$  and  $443.43 \pm 9.51 Bqkg^{-1}$  respectively were obtained. The minimum activities for  $^{226}Ra$ ,  $^{232}Th$  and  $^{40}K$  were found to be  $41.51 Bqkg^{-1}$ ,  $62.49 Bqkg^{-1}$  and  $316.18 Bqkg^{-1}$  while the maximum values were  $57.91 Bqkg^{-1}$ ,  $291.9 Bqkg^{-1}$  and  $516.29 Bqkg^{-1}$  respectively. Table 1.0 shows the

activity concentrations of the natural radionuclides <sup>226</sup>Ra, <sup>232</sup>Th and <sup>40</sup>K and their coordinates in all the sampling sites and Table2.0 shows the mean activity concentrations and the range for the three natural radionuclides <sup>226</sup>Ra, <sup>232</sup>Th and <sup>40</sup>K in all the sampling sites.

**Table1.0 Activity Concentration of the natural radionuclides <sup>226</sup>Ra, <sup>232</sup>Th and <sup>40</sup>K and their coordinates.**

Sample Location	Sample code	<sup>226</sup> Ra (Bq/kg)	<sup>232</sup> Th (Bq/kg)	<sup>40</sup> K (Bq/kg)	Coordinates
GARHI A	SA <sub>1</sub>	44.84±2.20	42.07±0.57	272.78±11.04	N12° 22.784' E007° 27.987'
	SA <sub>2</sub>	57.70±3.82	96.00±2.85	800.77±12.59	N12° 22.787' E007° 27.905'
	SA <sub>3</sub>	39.62±4.51	163.28±3.30	704.66±14.61	N12° 22.642' E007° 27.926'
	SA <sub>4</sub>	23.87±1.04	41.73±2.16	286.93±	N12° 22.613' E007° 27.925'
	MEAN	41.51±2.89	85.77±2.22	516.29±12.48	
GARHI B	SB <sub>1</sub>	52.95±6.95	51.31±6.61	458.79±3.11	N12° 21.173' E007° 30.250'
	SB <sub>2</sub>	84.59±5.33	68.87±1.82	496.27±12.59	N12° 21.210' E007° 30.256'
	SB <sub>3</sub>	32.91±2.20	99.20±2.74	562.90±12.47	N12° 21.216' E007° 30.289'
	SB <sub>4</sub>	51.56±3.13	72.52±2.96	320.22±7.6	N12° 21.261' E007° 30.139'
	MEAN	55.50±4.40	291.9±3.53	459.56±8.5	
MAKERA	SC <sub>1</sub>	52.26±2.89	105.93±3.53	556.45±11.66	N12° 22.480' E007° 27.885'
	SC <sub>2</sub>	55.85±1.74	66.48±1.37	487.09±8.86	N12° 22.496' E007° 22.896'
	SC <sub>3</sub>	65.01±4.06	57.81±2.28	436.08±9.07	N12° 22.517' E007° 27.904'
	SC <sub>4</sub>	58.52±3.24	45.84±1.03	447.12±9.95	N12° 22.433' E007° 27.873'
	MEAN	57.91±2.98	69.02±2.05	481.69±10.07	
TABOBI	SD <sub>1</sub>	95.71±1.29	54.28±8.44	483.20±3.11	N12° 23.121' E007° 30.715'
	SD <sub>2</sub>	44.73±1.74	83.24±1.59	223.34±5.13	N12° 23.51' E007° 30.737'
	SD <sub>3</sub>	34.53±3.01	49.94±4.56	241.99±11.35	N12° 23.299' E007° 30.656'
	MEAN	43.74±2.01	62.49±4.86	316.18±6.53	

**Table2.0 Mean Activity Concentrations for the three natural radionuclides <sup>226</sup>Ra, <sup>232</sup>Th and <sup>40</sup>K.**

SITE	Activity Concentrations (Bq/kg)		<sup>226</sup> Ra		<sup>232</sup> Th		<sup>40</sup> K	
	MEAN	RANGE	MEAN	RANGE	MEAN	RANGE	MEAN	RANGE
SA	41.51±2.89	23.87-57.70	85.77±2.22	41.73-163.28	516.29±12.48	272.78-800.77		
SB	55.50±4.40	32.91-84.59	291.9±3.53	51.31-99.20	459.56±8.95	320.22-562.99		
SC	57.91±2.98	52.26-65.01	69.02±2.05	45.84-105.93	481.69±10.07	436.08-556.45		
SD	43.74±2.01	34.53-95.71	62.49±9.86	49.94-83.24	316.18±6.53	326.46-633.19		
AVERAGE	49.67±3.07	35.89-75.75	127.29±4.42	47.21-112.91	443.43±9.51	338.88-638.40		

Activity concentrations for <sup>40</sup>K are generally high than those of <sup>226</sup>Ra and <sup>232</sup>Th in all the sampling sites. The highest values of <sup>226</sup>Ra were found at site SC, It could be due to the presence of the loamy sediments [4]. While the highest value of <sup>232</sup>Th is found at site SB, this may be due to the high content of monazite [11]. There is generally higher activity concentration of <sup>40</sup>K at SA. These can be attributed to Dam from the intensive use of agrochemical such as NPK fertilizer for agricultural practice.

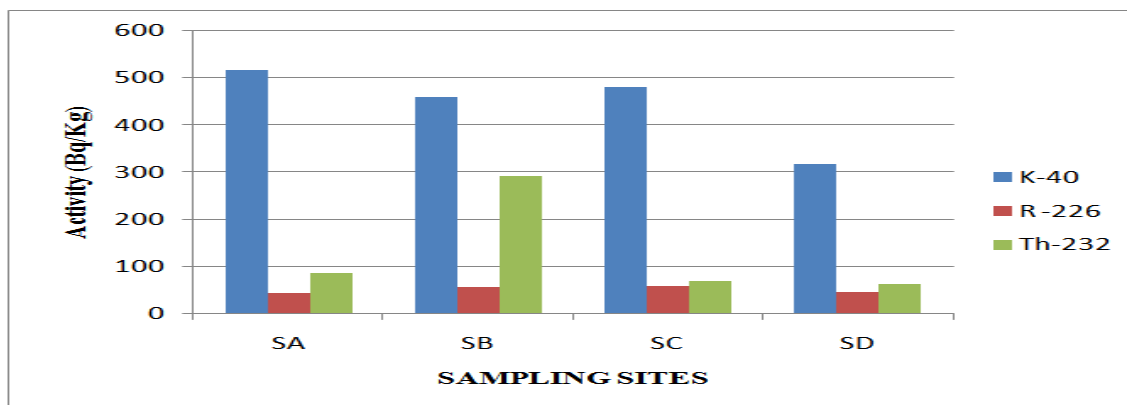


Figure 1.0: Activity concentrations of the natural radionuclides <sup>226</sup>Ra, <sup>232</sup>Th and <sup>40</sup>K in sediments samples.

4.2 Dose rate

The total dose rates from the sediments of Zobe Dam were calculated for all the sampling sites. The total dose rate was found to be 124.52±4.62 nGyh<sup>-1</sup> with the minimum value being 73.62 nGyh<sup>-1</sup> and the maximum 236.68 nGyh<sup>-1</sup>. Table 3.0 shows the average dose rates of the natural radionuclides in all the sampling sites and the total dose in Zobe Dam. The total dose rates were estimated using equation (3.0).

Table 3.0: Average dose rates of the natural radionuclides and the total dose rates measured in this work for all sampling sites.

Dose Rates (nG/h)				
SITES	<sup>226</sup> Ra	<sup>232</sup> Th	<sup>40</sup> K	TOTAL
SA	17.72±1.23	56.77±1.46	22.20±0.53	96.69
SB	23.69±1.87	193.23±2.33	19.76±0.36	236.68
SC	24.72±1.27	45.69±1.35	20.71±0.43	91.12
SD	18.67±0.85	41.36±6.52	13.59±0.28	73.62
AVERAGE	21.20±1.30	84.26±2.91	19.06±0.40	124.52

Contribution of each radionuclide to the gamma dose rate varied with the sampling sites. Figure 2.0 shows dose rates in which the sampling site SB has the value above the average for the whole Dam. The sampling site is on the southern region of Dam. The sampling sites SD and SC are within the worldwide value range which is from 18 nGyh<sup>-1</sup> to 93 nGyh<sup>-1</sup>. While the sampling sites SA and SB are higher than the worldwide value.

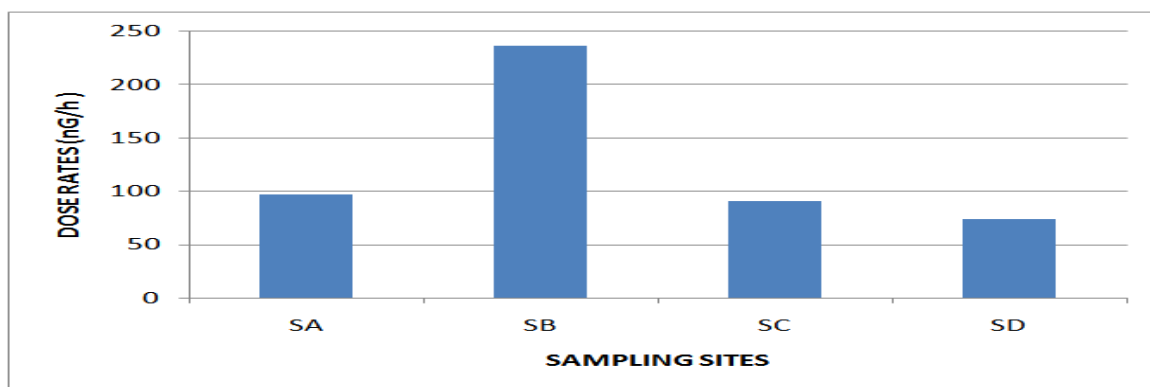


Figure 2.0: Dose rates for sediment samples measured in this work.

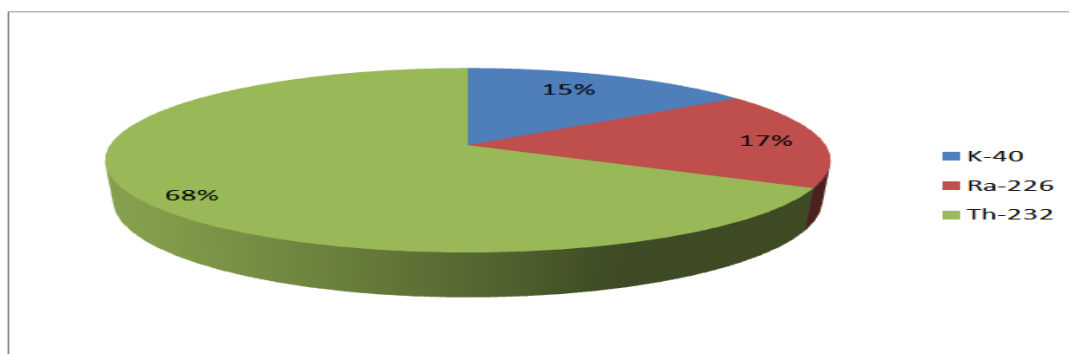


Figure 3.0: Estimate of the average dose rates contribution by the three radionuclides in sediment samples measured in this work.

**4.3 Annual Effective Dose Rate (AEDR), External Hazard and Internal Hazard index.**

The annual effective dose rates (AEDR), external hazard index ( $H_{ex}$ ) and internal hazard index ( $H_{in}$ ) were calculated for the sediments of Zobe Dam. The mean annual effective dose rate was found to be  $0.152 \pm 0.014$   $mSv\ y^{-1}$  with a minimum value of  $0.090 \pm 0.009$   $mSv\ y^{-1}$  at the sampling site SD at the northern side of the Dam and maximum value of  $0.2901 \pm 0.0056$   $mSv\ y^{-1}$  at the sampling site SB on the western side of the Dam. Table 4.0 shows the values of AEDR,  $H_{ex}$  and  $H_{in}$  values for all the sampling sites. The AEDR is below the maximum allowed limit of  $1$   $mSv\ y^{-1}$  of radiation exposure to the public [7].

The external ( $H_{ex}$ ) and internal ( $H_{in}$ ) hazard indices represent the risk associated from exposure of the radionuclides in the sediment samples. The external hazard index was found to be  $0.717 \pm 0.126$  with a minimum value of  $0.425 \pm 0.445$  at sampling site SD and maximum value of  $1.372 \pm 0.027$  at sampling site SB while the internal hazard index was found to be  $0.851 \pm 0.035$  with a minimum value of  $0.543 \pm 0.050$  at sampling site SD and maximum value of  $1.522 \pm 0.039$  at sampling site SB. This indicated that the risk associated with sediments sample is quite below the limit set by [6] for radiological exposure protection to the public which is unity. Since the value of the external hazard index is less than unity we can therefore say that the radiation hazard due the sediments of the Dam is low. However at the sampling site SB there are elevated values of external and internal hazard index which are above the unity and this indicate that the sediments sample at the site can pose a health risk to the public when use as building material. Figures 4.0, 5.0 and 6.0 shows the AEDR, external hazard and the internal hazard index for all the sampling sites.

Table 4.0: The annual effective dose rate (AEDR), external hazard index ( $H_{ex}$ ) and internal hazard index ( $H_{in}$ ) for sediment samples.

SITE	AEDR ( $mSv\ y^{-1}$ )	$H_{ex}$	$H_{in}$
SA	$0.119 \pm 0.039$	$0.550 \pm 0.018$	$0.662 \pm 0.026$
SB	$0.290 \pm 0.005$	$1.372 \pm 0.027$	$1.522 \pm 0.039$
SC	$0.112 \pm 0.003$	$0.523 \pm 0.017$	$0.679 \pm 0.026$
SD	$0.090 \pm 0.009$	$0.425 \pm 0.0445$	$0.543 \pm 0.050$
AVERAGE	$0.152 \pm 0.14$	$0.717 \pm 0.126$	$0.851 \pm 0.035$

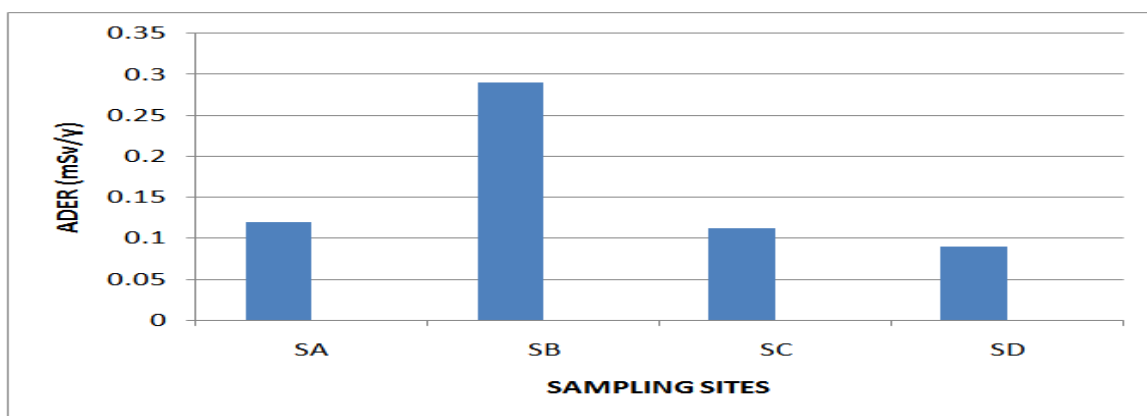


Figure 4.0: Annual Effective Dose Rate (AEDR) for sediment samples analysed in this work.

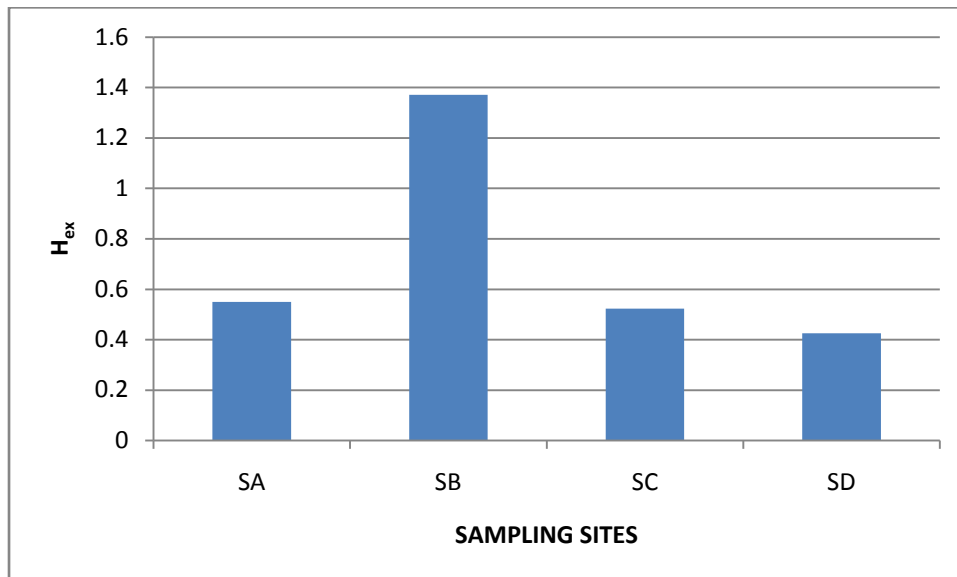


Figure 5.0: Estimate of the external hazard index for the sediment samples analysed in this work.

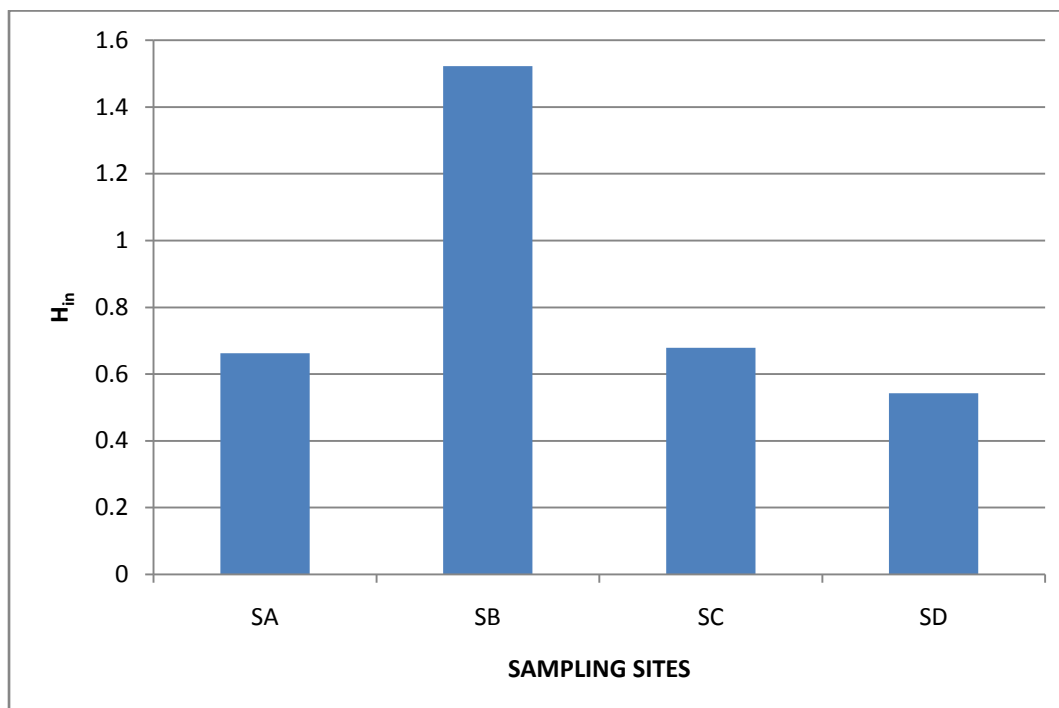


Figure 6.0: Estimate of the internal hazard index for the sediment samples analysed in this work.

#### V. Conclusion

The study showed that the radioactivity levels of  $^{226}\text{Ra}$ ,  $^{232}\text{Th}$  and  $^{40}\text{K}$  were  $49.67 \pm 3.07$  Bq/kg,  $127.29 \pm 4.42$  Bq/kg and  $434.43 \pm 9.51$  Bq/kg respectively and were comparable with the world average values. However, slight variation in the radioactivity content in soil observed with different locations worldwide mainly due to soil type, formation and transport process involved. This may be the reason for the variation. The mean absorbed dose rate obtained in the present study ( $124.52 \pm 4.61$  nGy/h) is comparable to the world average (55 nGy/h). The measured average annual effective dose rate in this study is 0.152 mSv/y, and is lower than the world average value 1 mSv/y [16]. The measured average values of external and internal hazard index found in this study are 0.717 and 0.851 (all are lower than unity), which indicate that the sediments in all the sampling sites can be used for safety construction of buildings. This information is important for the local people to utilize the Zobe Dam sediments.

## ACKNOWLEDGEMENTS

The authors are grateful to Department of Physics, Centre for Energy Research and Training, Ahmadu Bello University Zaria and Sokoto Rima Basin Development Project Dutsinma, Kastina State, Nigeria, for giving us access to their facility used during this research.

## REFERENCES

- [1] Bikit , N., Banzi, F.P., Kifanga, L.D., (2000). Natural radioactivity and radiation exposure at the Minjigu phosphate Mine in Tanzania. *Journal of Radiological Protection*, 20: 41-52
- [2] Beretka, J. and Mathew, P.J. (1985): Natural radioactivity of Australian building materials Industrial wastes and by-product. *Health physics* 48(1),87- 95.
- [3] CERT MANUAL (1999): Operation of Sodium Iodide-Thallium Gamma Spectrometry System Manual. Centre for Energy Research and Training, Ahmadu Bello University, Zaria
- [4] El-Gamal, S. Nasr, A. El-Taher (2007): Study of the spatial distribution of natural radioactivity In the upper Egypt Nile river sediments *Radiation Measurements*, 42, pp. 457-465
- [5] Ibeanu, I. G. E. (1999): Assessment of radiological effects in tin mining activities in jos and environs. PhD. Thesis, Ahmadu Bello University, Zaria. Pp 35,79. (unpublished)
- [6] ICRP (2000): Limits for intakes of Radionuclides by workers. International Commission on Radiological protection Committee II. Pergamon Press New York. Pp277
- [7] ICRP (1991) 1990 recommendations of the International Commission on Radiological Protection Pergamon Press, Oxford. Ann. ICRP, 21(1-3) (ICRP Publication 60).
- [8] Jibiri, N. N., Mabawonku, A.O., Oridate A.A. and Ujiagbedion (1999): 'Natural Radionuclide Conc. Levels in Soil and Water around a Cement Factory a Ewekoro, Ogun, Nigeria'*Nig. Jour. of Phy.*11(54), 12 – 16.
- [9] Kabir, K. A., Islam, S.M., and Rahma, M.M., (2008): Radioactivity Levels in Sediment Sample In the District of jessore, Bangladesh and Evaluation of Radiation Hazard, *Jahangirnagar University Journal of Science . 32(1) Pp. 81-92*
- [10] Mujahid and Hussain (2011): Measurement of Natural Radioactivity from soil samples of Sind Pakistan, *Radiation Protection Dosimetry* 145(4): page 351–355
- [11] Orgun, S., Singh, B., Kumar, A., (2007). Natural radioactivity measurements in soil sample From hamirpur district, Himadal pradseh, India. *Radiation measurement* 36: 547-
- [12] Olatunde Michael Oni, Idowu Peter Farai, Ayodeji Oladiran Awodugba (2011): Natural Radionuclide Concentrations and Radiological Impact Assessment of River Sediments of the Coastal Areas of Nigeria, *Journal of Environmental Protection* 2(4): page 418-423
- [13] Ramasamy, V., Senthil, S., Meenakshisundaram, V., and Gajendran, V., (2009): Measurement of natural radioactivity in beach sediments from North East Coast of Tamilnadu, India. *Research journal of applied sciences, Engineering and Technology* 1(2): 54-58, 2009.
- [14] Ravisankar R., Chandrasekaran A., Eswaran P., Rajalakshmi A., Vijayagopal P.,(2011): Natural Radioactivity Measurement in River Bed samples in and around Manaloorpet Riverbed Area, Tamilnadu, India, *International Journal of Science and Technology* 1 (1): page 38 -42
- [15] Taskin, H., Karavus M., Ay P., Topuzoglu A., Hindiroglu S. and Karahan G., (2009): Radionuclide concentrations in soil and lifetime cancer risk due to the gamma radioactivity in Kirklareli, Turkey. *Journal of Environmental Radioactivity. 100 (1):* page 49-53.
- [16] UNSCEAR, (2000): Sources effects and risks of ionizing radiation. United Nations Scientific Committee on Effects of Atomic Radiation, United Nations, New York, NY.

## Evaluation & Optimization of Software Engineering

Ashiqur Rahman<sup>1</sup>, Asaduzzaman Noman<sup>2</sup>, Atik Ahmed Sourav<sup>3</sup>,  
Shakh Md. Alimuzjaman Alim<sup>4</sup>,

<sup>1</sup>(M.Sc in Information Technology (IT), Jahangirnagar University, Bangladesh)

<sup>2</sup>(CSE, Royal University of Dhaka, Bangladesh)

<sup>3</sup>(CSE, Royal University of Dhaka, Bangladesh)

<sup>4</sup>(EEE, Royal University of Dhaka, Bangladesh)

**ABSTRACT:** The term is made of two words, software and engineering. Software is more than just a program code. A program is an executable code, which serves some computational purpose. Software is considered to be collection of executable programming code, associated libraries and documentations. Software, when made for a specific requirement is called software product. Engineering on the other hand, is all about developing products, using well-defined, scientific principles and methods. The outcome of software engineering is an efficient and reliable software product. IEEE defines software engineering as: The application of a systematic, disciplined, quantifiable approach to the development, operation and maintenance of software; that is, the application of engineering to software.

**Keywords** –Programming, IEEE, FORTRAN, COBOL, Client.

### I. INTRODUCTION

Software engineering is the branch of computer science that creates practical, cost-effective solutions to computing and information processing problems, preferentially by applying scientific knowledge, developing software systems in the service of mankind. This paper covers the fundamentals of software engineering, including understanding system requirements, finding appropriate engineering compromises, effective methods of design, coding, and testing, team software development, and the application of engineering tools. The process of developing a software product using software engineering principles and methods is referred to as software evolution. This includes the initial development of software and its maintenance and updates, till desired software product is developed, which satisfies the expected requirements. The process of developing a software product using software engineering principles and methods is referred to as software evolution. This includes the initial development of software and its maintenance and updates, till desired software product is developed, which satisfies the expected requirements

Software paradigms refer to the methods and steps, which are taken while designing the software.

- Requirement gathering
- Software design
- Programming

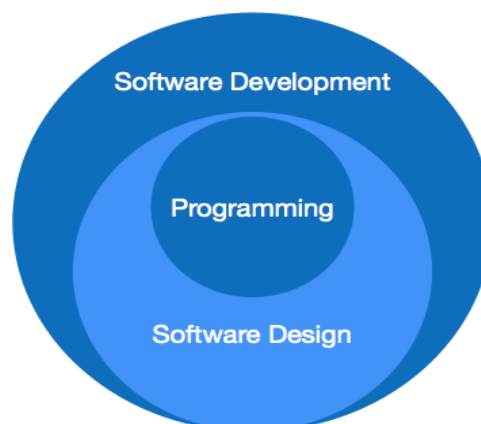


Figure 1: Software paradigm

## II. RELATED WORK

From its beginnings in the 1960s, writing software has evolved into a profession concerned with how best to maximize the quality of software and of how to create it. Quality can refer to how maintainable software is, to its stability, speed, usability, testability, readability, size, cost, security, and number of flaws or "bugs", as well as to less measurable qualities like elegance, conciseness, and customer satisfaction, among many other attributes. How best to create high quality software is a separate and controversial problem covering software design principles, so-called "best practices" for writing code, as well as broader management issues such as optimal team size, process, how best to deliver software on time and as quickly as possible, work-place "culture", hiring practices, and so forth. The most important development was that new computers were coming out almost every year or two, rendering existing ones obsolete. Software people had to rewrite all their programs to run on these new machines. Programmers did not have computers on their desks and had to go to the "machine room". Jobs were run by signing up for machine time or by operational staff. Jobs were run by putting punched cards for input into the machine's card reader and waiting for results to come back on the printer. The field was so new that the idea of management by schedule was non-existent. Making predictions of a project's completion date was almost impossible. Computer hardware was application-specific. Scientific and business tasks needed different machines. Due to the need to frequently translate old software to meet the needs of new machines, high-order languages like FORTRAN, COBOL, and ALGOL were developed. Hardware vendors gave away systems software for free as hardware could not be sold without software. A few companies sold the service of building custom software but no software companies were selling packaged software. The notion of reuse flourished. As software was free, user organizations commonly gave it away. Groups like IBM's scientific user group SHARE offered catalogues of reusable components. Academia did not yet teach the principles of computer science. Modular programming and data abstraction were already being used in programming. For decades, solving the software crisis was paramount to researchers and companies producing software tools. The cost of owning and maintaining software in the 1980s was twice as expensive as developing the software. During the 1990s, the cost of ownership and maintenance increased by 30% over the 1980s. • In 1995, statistics showed that half of surveyed development projects were operational, but were not considered successful. • The average software project overshoots its schedule by half. • Three-quarters of all large software products delivered to the customer are failures that are either not used at all, or do not meet the customer's requirements.

## III. WHY SOFTWARE ENGINEERING?

**Large software** - It is easier to build a wall than to a house or building, likewise, as the size of software become large engineering has to step to give it a scientific process.

**Scalability**- If the software process were not based on scientific and engineering concepts, it would be easier to re-create new software than to scale an existing one.

**Cost**- As hardware industry has shown its skills and huge manufacturing has lower down the price of computer and electronic hardware. But the cost of software remains high if proper process is not adapted.

**Dynamic Nature**- If the nature of software is always changing, new enhancements need to be done in the existing one. This is where software engineering plays a good role.

**Quality Management**- Better process of software development provides better and quality software product. A software product can be judged by what it offers and how well it can be used. This software must satisfy on the following grounds:

- Operational
- Transitional
- Maintenance

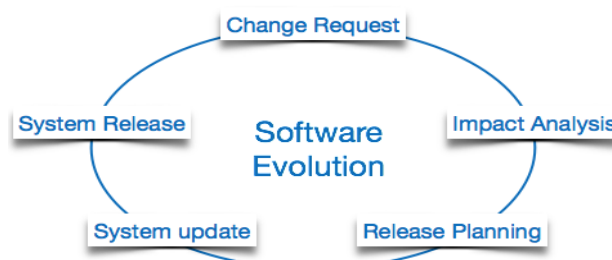


Figure 2: Software Evolution

- Process models define structured set of activities, tasks, milestones and work products required to develop high quality software.
- All software process models accommodate generic framework activities but each applies a different emphasis to these activities.

The deployment of the system includes changes and enhancements before the decommissioning or sunset of the system. Maintaining the system is an important aspect of SDLC. As key personnel change positions in the organization, new changes will be implemented, which will require system updates.

#### IV. OPERATIONAL, TRANSITIONAL & MAINTENANCE

Operational process tells us how well software works in operations. It can be measured on:

- Budget
- Usability
- Efficiency
- Correctness
- Functionality
- Dependability
- Security
- Safety

Transitional aspect is important when the software is moved from one platform to another:

- Portability
- Interoperability
- Reusability
- Adaptability

Maintenance aspect briefs about how well a software has the capabilities to maintain itself in the ever-changing environment:

- Modularity
- Maintainability
- Flexibility
- Scalability

#### V. SOFTWARE MYTHS

The development of software requires dedication and understanding on the developers' part. Many software problems arise due to myths that are formed during the initial stages of software development. Unlike ancient folklore that often provides valuable lessons, software myths propagate false beliefs and confusion in the minds of management, users and developers. Managers, who own software development responsibility, are often under strain and pressure to maintain a software budget, time constraints, improved quality, and many other considerations. Common management myths are listed below:

- Software standards provide software engineers with all the guidance they need - Learn to use them
- People with modern computers have all the software development tools they need - Need good CASE tools
- Adding people is a good way to catch up when a project is behind schedule - Late addition makes it later
- Giving software projects to outside parties to develop solves software project management problems - Need to learn how to manage and control software projects
- A general statement of objectives from the customer is all that is needed to begin a software project - spend time to have very good understanding of customer requirements
- Project requirements change continually and change is easy to accommodate in the software design
  - Understand the requirements first then write codes. It costs more to change later
- Once a program is written, the software engineer's work is finished
  - It is only the beginning
- There is no way to assess the quality of a piece of software until it is actually running on some machine. The only deliverable from a successful software project is the working program.
  - Practice formal/peer review
- Software engineering is all about the creation of large and unnecessary documentation not shorter development times or reduced costs
  - Better quality leads to reduced work



Figure 3: Flow chart of processing.

**VI. Acknowledgements Capability Maturity Model Integration**

Capability Maturity Model Integration (CMMI) is a process improvement training and appraisal program and service administered and marketed by Carnegie Mellon University (CMU) and required by many DoD and U.S. Government contracts, especially in software development. CMU claims CMMI can be used to guide process improvement across a project, division, or an entire organization. CMMI defines the following maturity levels for processes: Initial, Managed and Defined. Currently supported is CMMI Version 1.3. CMMI is registered in the U.S. Patent and Trademark Office by CMU. CMMI was developed by a group of experts from industry, government, and the Software Engineering Institute (SEI) at CMU. CMMI models provide guidance for developing or improving processes that meet the business goals of an organization. A CMMI model may also be used as a framework for appraising the process maturity of the organization. By January of 2013, the entire CMMI product suite was transferred from the SEI to the CMMI Institute, a newly created organization at Carnegie Mellon. CMMI originated in software engineering but has been highly generalized over the years to embrace other areas of interest, such as the development of hardware products, the delivery of all kinds of services, and the acquisition of products and services. The word "software" does not appear in definitions of CMMI. This generalization of improvement concepts makes CMMI extremely abstract. CMMI currently addresses three areas of interest:

1. Product and service development — CMMI for Development (CMMI-DEV),
2. Service establishment, management, — CMMI for Services (CMMI-SVC), and
3. Product and service acquisition — CMMI for Acquisition (CMMI-ACQ).

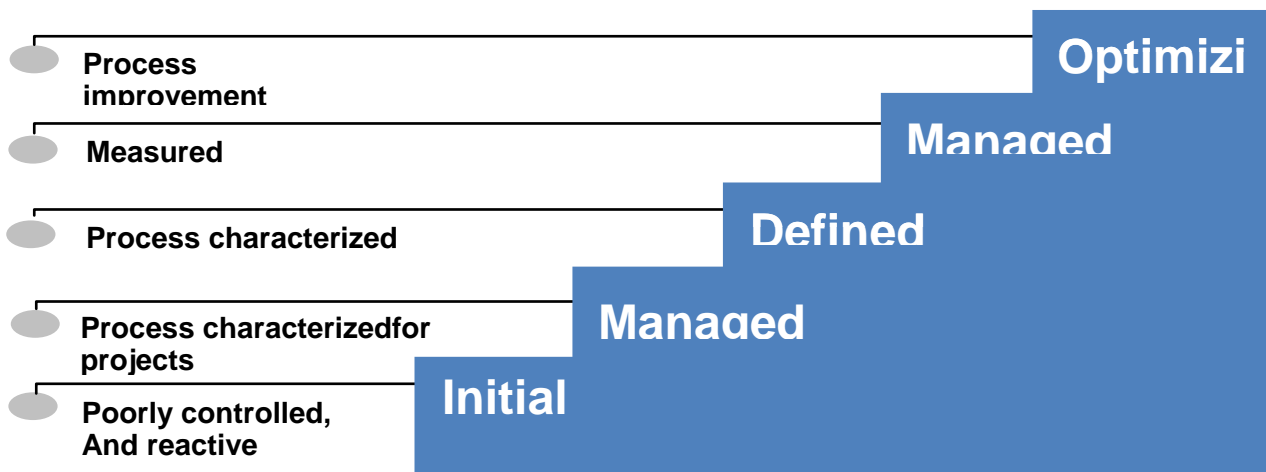


Figure 4: Maturity Levels

A process area (PA) is a cluster of related practices in an area that, when performed collectively, satisfy a set of goals considered important for making significant improvement in that area. Practices are actions to be performed to achieve the goals of a process area. All CMMI process areas are common to both continuous and staged representations. A process area is NOT a process description.

Level	Focus	Process Areas
5 Optimizing	<i>Continuous Process Improvement</i>	Organizational Innovation and Deployment Causal Analysis and Resolution
4 Quantitatively Managed	<i>Quantitative Management</i>	Organizational Process Performance Quantitative Project Management
3 Defined	<i>Process Standardization</i>	Requirements Development Technical Solution Product Integration Verification Validation Organizational Process Focus Organizational Process Definition Organizational Training Integrated Project Management for IPPD Risk Management Integrated Teaming Integrated Supplier Management Decision Analysis and Resolution Organizational Environment for Integration
2 Managed	<i>Basic Project Management</i>	Requirements Management Project Planning Project Monitoring and Control Supplier Agreement Management Measurement and Analysis Process and Product Quality Assurance Configuration Management
1 Initial		



Figure 5: Process Area



Figure 6: The Capability Levels

### V. CONCLUSION

Software engineering is about teams and it is about quality. The problems to solve are so complex or large, that a single developer cannot solve them anymore. Software engineering is also about communication. Teams do not consist only of developers, but also of testers, architects, system engineers, customer, project managers, etc. Software projects can be so large that we have to do careful planning. Implementation is no longer just writing code, but it is also following guidelines, writing documentation and also writing unit tests. But unit tests alone are not enough. The different pieces have to fit together. And we have to be able to spot problematic areas using metrics. Once we are finished coding, that does not mean that we are finished with the project: for large projects maintaining software can keep many people busy for a long time. Since there are so many factors influencing the success or failure of a project, we also need to learn a little about project management and its pitfalls, but especially what makes projects successful. And last but not least, a good software engineer, like any engineer, needs tools, and you need to know about them.

### REFERENCES

- [1] Victor R. Basili. The experimental paradigm in software engineering. In Experimental Software Engineering Issues: Critical Assessment and Future Directives. Proc of Dagstuhl-Workshop, H. Dieter Rombach, Victor R. Basili, and Richard Selby (eds), published as Lecture Notes in Computer Science #706, Springer-Verlag-1993.
- [2] Geoffrey Bowker and Susan Leigh Star: Sorting Things Out: Classification and Its Consequences. MIT Press, 1999.
- [3] Frederick P. Brooks, Jr. Grasping Reality through Illusion - Interactive Graphics Serving Science. Proc 1988 ACM SIGCHI Human Factors in Computer Systems Conf (CHI '88) pp. 1-11.
- [4] Rebecca Burnett. Technical Communication. Thomson Heinle 2001.
- [5] Thomas F. Gieryn. Cultural Boundaries of Science: Credibility on the line. Univ of Chicago Press, 1999.
- [6] ICSE 2002 Program Committee. Types of ICSE papers. <http://icse-conferences.org/2002/info/paperTypes.html>
- [7] Impact Project. Determining the impact of software engineering research upon practice. Panel summary, Proc. 23rd International Conference on Software Engineering (ICSE 2001), 2001.
- [8] Ellen Isaacs and John Tang. Why don't more non-North-American papers get accepted to CHI? <http://acm.org/sigchi/bulletin/1996.1/isaacs.html>

## Assessment of Physicochemical Parameters and Heavy Metals in Gombe Abattoir Wastewater

Nasiru A<sup>1</sup>, Osakwe C.E<sup>1</sup>, Lawal I.M<sup>2</sup> and Chinade A.U.<sup>2</sup>

<sup>1</sup>(Department of Civil Engineering, Modibbo Adama University of Technology Yola, Adamawa state, Nigeria)

<sup>2</sup>(Department of Civil Engineering, Abubakar Tafawa Balewa University, Bauchi, Bauchi state, Nigeria)

**ABSTRACT :** The physical parameters pH and Temperature of Gombe abattoir wastewater sample of 6.5 and 27.6°C respectively were within the WHO/USEPA discharge limits while turbidity, TSS, Conductivity and TDS with mean values of 1100NTU, 5600mg/L, 59mS/c and 38.5g/L respectively were also above the WHO/USEPA limits. For chemical parameters, concentration level of Nitrates (1034mg/L), Nitrogen (234mg/L), Ammonia (285mg/L), Ammonium (301mg/L), phosphate (163mg/L), phosphorus (53mg/L), and phosphorus-pentoxide (122mg/L) in the wastewater sample were above WHO/USEPA limits, only sulfate (44mg/L) that is below the WHO/USEPA limit of 250mg/L. The COD and BOD<sub>5</sub> values of 3539mg/L and 635mg/L respectively were also above the WHO/USEPA limits, Dissolved oxygen (DO) mean values of 2.3mg/L was below requirement of WHO/USEPA limits for the discharged of wastewater into river. The concentration of heavy metals in Gombe Abattoir wastewater sample determines are Copper (0.01ppm), Manganese (0.30ppm), Magnesium (9.60ppm), iron (0.20ppm), Chromium (0.01ppm), Cadmium (0.00ppm), Nickel (0.06ppm), and Lead (0.01ppm) were within the WHO/USEPA recommended standard limits, except the concentration of Zinc (0.26ppm) that was above the WHO/USEPA recommended limits of 0.10ppm, abattoir wastewater requires pretreatment before discharging into environment and more research should be conducted to reduce the abattoir wastewater concentration and its effect on the immediate environment.

**Keywords** – Abattoir, heavy metals, limits, pretreatment, wastewater

### I. INTRODUCTION

An abattoir is a special facility designed and licensed for receiving, holding, slaughtering and inspecting animal's meat and meat products before release to the public [1]. Abattoir waste generated as the result of abattoir operations is one of the greatest general environmental threat, this is because they actually pollute all phases of the environment namely land, water and air. Wastes emanating from slaughtered animals are basically in solid and liquid states. However, the gases and the odor emitted from putrefying wastes become very offensive to the nostrils, and can sometimes be source of localized air pollution. Almost each day, in all the urban and rural towns in Nigeria, animals are slaughtered and waste are generated in each day of the week, the meat and other extracts from the animals are made available to the public for consumption and the abattoir wastes originate from killing; hide removal or de-hairing, paunch handling, rendering, trimming, processing and clean-up operations in the abattoir. Fresh Abattoir wastewater is mainly composed of diluted blood, fat and suspended solids.

Generally, fresh abattoir effluent has been shown to contain solids, minerals, metals, and micro-organisms and to exert oxygen demand. On the other hand, aged and decomposing abattoir effluent is often malodorous [2]. In a study conducted by [3] on five abattoirs in Ibadan, it shown that pH levels were within acceptable range, all other standards were found to be in excess of 2000mg/L, suspended solids were between 590 to 1050 times the acceptable limits and phosphate levels ranged from 115-175 mg/L. Nitrate levels were not as extreme but all the sites were within six times the general discharge standard of 20mg/L. Comparatively, in a study conducted on some abattoirs by [4] in Quebec, Canada, the COD and TS was found to be between 2333-8620mg/L; SS was between 736-2099mg/L, Nitrogen and Phosphorus were 6.0 and 2.3g/L of COD. The COD of fresh blood that is universally put at 375,000mg/L was compared to the COD of manure put at 15,000-30,000 mg/L. It was established that abattoir effluents increase Nitrogen, phosphorus, solid and BOD levels of the receiving water body, potentially leading to eutrophication. Pathogens from cattle waste can also be transmitted to humans who are in contact with the water body [5].

Wrongful and unlawful discharge of blood and animal faeces into streams and rivers may cause oxygen-depletion as well as nutrient-over enrichment of the receiving system which could cause increased rate of toxin accumulation [6]. Humans may also be affected through outbreak of water borne diseases and some researchers point out that abattoir activities are responsible for the pollution of surface and underground waters as well as air quality which directly or indirectly affect the health of residents living within the vicinity of abattoirs ([7]; [8]; [9]). In addition, primary producers in affected water bodies may be destroyed by such pollutants, which may directly affect the aquatic ecosystem, with serious consequences on diet [10].

Gombe abattoir is situated in Gombe town, behind kasuwarkatako along AYU/TRIACTA quarry sites, BCJ area of Gombe local Government in Gombe state, Nigeria. With a total catchments area of about 52 km<sup>2</sup> (20 square mile), it lays between latitude 10° 17' 23"N and longitudes 11° 10' 2"E at an altitude of about 508m (1669 feet) above sea level. Animals (cows, goats, sheep, and camels) are slaughtered daily throughout the year. The wastewater generated flows directly into a stream behind the abattoir without treatments. Most of the activities of this Abattoir remain unregulated, due to this the present study therefore aimed at assessing the Abattoir wastewater samples from Gombe abattoir for physical and chemical parameters and the presence of Cu, Zn, Mn, Mg, Fe, Cr, Cd, Ni, and Pb in the abattoir wastewater. Data obtained could be important in providing basics for future wastewater management practices in the Abattoir and its impact to the immediate environment.

## II. METHODS AND MATERIALS

### 2.1 SAMPLE AREA AND COLLECTION

The abattoir wastewater sample was collected from the abattoir drainages in Gombe metropolis main abattoir building. Numbers of animals (cows, goats, sheep, and camels) are slaughtered in this abattoir. Abattoir wastewater sample was collected using grab/composite sampling where the sample was collected directed at the main drainage channels within the main abattoir building, the wastewater was collected in a 20 liters plastic container previously cleaned by washing with non-ionic detergent, rinsed with tap water and finally rinsed with deionized water prior to usage. During sampling, the sample container was rinsed with sample wastewater three times and then filled to the brim by grabbing about four liters at each different five points within the drainage channel and was later mixed thoroughly to obtained a composite sample of that wastewater. The sample was labeled and transported to the sanitary laboratory, Abubakar Tafawa Balewa University, Bauchi within 2 hours at about 4°C (kept in a cooler covered with ice water) prior to analysis under safe conditions in accordance with [11], on Sampling for water Quality.

The time in which the sample was collected from the abattoir wastewater was around 6:00am to 8:30am when the slaughtering activity is at its peak and when the effect of sun could not alter the chemistry of the wastewater. Samples were collected from the month of June to November 2015.



Plate 1: Abattoir Operations at Gombe Abattoir

Plate 2: Conducting Parameters Analysis of Abattoir Wastewater Using DR/890 Colorimeter

Plate 3: Conducting Titration for COD Determination of Abattoir Wastewater

### 2.2 DETERMINATION OF PHYSICAL AND CHEMICAL PARAMETERS

pH and Temperature were determined using Labtech Digital pH meter and compare with another pH meter MODEL PHB-4 pH meter serial no. 600910099001 for accuracy; while the levels of total dissolved solid (TDS) and electrical conductivity of abattoir wastewater were determined using a 430 pH/conductivity meter

JENWAY, serial No. 20051, (part No. 430-201, made in PRC). Dissolved oxygen was determined in this research by using dissolved oxygen meter HANNA HI 9146 serial no. 08689921 by Hanna® Instrument. For the determination of total suspended solid (TSS), 100ml of the wastewater samples were filtered through a pre weighed filtered paper. The filtered papers used were Whatman® 110mmØ by Whatman International LTD Maidstone, England with serial no. \*H71810011101-\*, the filter paper was then dried at 103-105°C. TSS was determined by using the following formula [12]:

$$TSS \left( \frac{mg}{l} \right) = \left( \frac{\text{final weight} - \text{initial weight}}{\text{amount of sample taken}} \right) * 1000 \quad (2.1)$$

Nitrate, total nitrogen, ammonium and ammonia were determined using cadmium reduction method 8039 ([13] and [14]), by using powder pillows Nitrate reagent CAT NO. 2106169, Sulfate was determined by using Sulfa Ver methods 8051 ([13] and [14]). USEPA accepted for reporting wastewater analysis by using powder pillows sulfaver® sulfate reagent CAT NO. 21067-69, Phosphate, phosphorus and phosphorus-pentoxide were determined by using orthophosphate phosVer 3 (Ascorbic Acid) Method 8048 (Powder Pillows) ([13] and [14]). USEPA accepted for reporting wastewater analysis by using powder pillows phosver® phosphate reagent CAT NO. 2106069 and Turbidity was estimated using absorbometric method 8237 ([13] and [14]). USEPA accepted for reporting wastewater analysis, the Nitrate, Sulfate, Phosphate and Turbidity were all determined using various methods with a DR/890 colorimeter of serial no. 130290694066, produced by Hach company world headquarters, Loveland, USA.

Titrimetric method is used in the determination of chemical oxygen demand (COD) and Biochemical oxygen demand (BOD<sub>5</sub>) was determined by using the United States environmental protection agency (USEPA) standard method: The test was done in accordance with [15].

### 2.3 DETERMINATION OF HEAVY METALS IN ABATTOIR WASTEWATER SAMPLES

Determination of Cu, Zn, Mn, Mg, Fe, Cr, Cd, Ni, and Pb were made directly on each final solution using MODEL 210VGP Atomic Absorption Spectrophotometer (AAS).

The samples (100ml) were transferred into a beaker and 1.6ml concentrated (HNO<sub>3</sub>) nitric acid was added. The beaker wall and watch glass were washed with distilled water and the samples were filtered using Whatman® 110mmØ by Whatman International LTD Maidstone, England with serial no. \*H71810011101-\* to remove some insoluble materials that could clog the atomizer. A blank sample was digested to allow a blank correction to be made. This was done by transferring 100ml of deionized water into a beaker and digested with 1ml of concentrated (HNO<sub>3</sub>) nitric acid.

## III. RESULTS AND DISCUSSIONS

### 3.1 THE ABATTOIR PHYSICO-CHEMICAL PARAMETERS

The pH of the Gombe abattoir wastewater sample from Table 1, pH values ranging from 6.5-7.0 obtained at 27.6°C. pH is the measure of acidity and alkalinity of water. However, the mean pH level of 6.5 is within the WHO/USEPA tolerance limits for the discharged of wastewater from all industries into a river. [16], [17].

The mean conductivity level in the abattoir wastewater sample was found to be 59mS/cm from Table 1; therefore the electrical conductivity of the Gombe abattoir wastewater sample is above WHO tolerance limits of 1mS/cm. Similarly, the mean turbidity value was 1100 NTU which was higher than the WHO/USEPA guideline of 5 NTU for the discharged of wastewater into river or stream.

The mean concentration of TDS in the abattoir wastewater sample was found to be 38.5g/L and was above WHO/USEPA limits of 2000mg/L (2g/L) and the mean TSS of 5600mg/L is however above the WHO/USEPA limits of 20mg/L.

The level of Nitrates in Gombe abattoir wastewater sample was observed to be 1034mg/L which is above 45mg/L discharge limits of WHO/USEPA, while that of Nitrogen, Ammonia and Ammonium were 234mg/L, 285mg/L and 301mg/L respectively which are also above the WHO/USEPA limits of 100mg/L, 5mg/L and 35mg/L respectively for the discharged of wastewater into river.

The mean concentration of phosphate in the abattoir wastewater obtained is 163mg/L which is above the WHO/USEPA limits of 5mg/L. The phosphorus P, and phosphorus-pentoxide P<sub>2</sub>O<sub>5</sub> of the abattoir wastewaters are 53mg/L and 122mg/L respectively for the discharged of wastewater into river, the levels of nitrate observed in this study in addition to phosphate levels can cause eutrophication and may pose a problem if discharged into river or stream.

The mean sulfate level of 44mg/L is below the WHO/USEPA limits of 250mg/L. Dissolved oxygen (DO) values obtained from the abattoir wastewater ranged between 1.2-3.8 mg/L. DO is a measure of the degree of pollution or waste loadings by organic matters, the standard for sustaining aquatic life is stipulated at 5mg/L a concentration below this value adversely affects aquatic biological life in the water, while concentration below

2mg/L may lead to death for most Aquatic life [18]. The mean DO value of 2.3mg/L was below the WHO and USEPA permissible limit of 4mg/L and 5mg/L respectively for the discharged of wastewater from industries into river.

From the results findings of this research, the abattoir wastewater COD mean values obtained was 3539mg/L and is higher than WHO/USEPA recommended standard limits of 1000mg/L for the discharged of wastewater into surface water respectively. More so, for BOD<sub>5</sub>, thus the mean BOD<sub>5</sub> of the abattoir wastewater sample was averagely 638mg/L and is higher than WHO/USEPA recommended standard limits of 20mg/L for the discharged of wastewater into surface water respectively.

**Table 1: Physicochemical Parameters of Gombe Abattoir Wastewater compared to WHO/USEPA Limit**

Parameter	Mean Value	WHO-USEPA limits	Remark
pH	6.5	6.5 - 9.5	Met Standard
Temperature (°C)	27.6	< 40	Met Standard
Conductivity (mS/cm)	59	1	Above Limits
TDS (g/L)	38.5	2	Above Limits
TSS (mg/L)	5600	20	Above Limits
Turbidity (NTU)	1100	5	Above Limits
N (mg/L)	234	100	Above Limits
NO <sub>3</sub> (mg/L)	1034	45	Above Limits
NH <sub>3</sub> (mg/L)	285	5	Above Limits
NH <sub>4</sub> (mg/L)	301	35	Above Limits
P (mg/L)	53	NA	-
P <sub>2</sub> O <sub>5</sub> (mg/L)	122	NA	-
PO <sub>4</sub> (mg/L)	163	5	Above Limits
SO <sub>4</sub> <sup>2-</sup> (mg/L)	44	250	Met Standard
COD (mg/L)	3539	1000	Above Limits
BOD <sub>5</sub> (mg/L)	638	20	Above Limits
DO (mg/L)	2.3	4	

**3.2 DETERMINATION OF HEAVY METALS IN ABATTOIR WASTEWATER**

The heavy metals presences in Gombe abattoir wastewater determines are Copper (Cu), Zinc (Zn), Manganese (Mn), Magnesium (Mg), iron (Fe), Chromium (Cr), Cadmium (Cd), Nickel (Ni), and Lead (Pb) and the heavy metal value for each metal is presented in fig. 1.

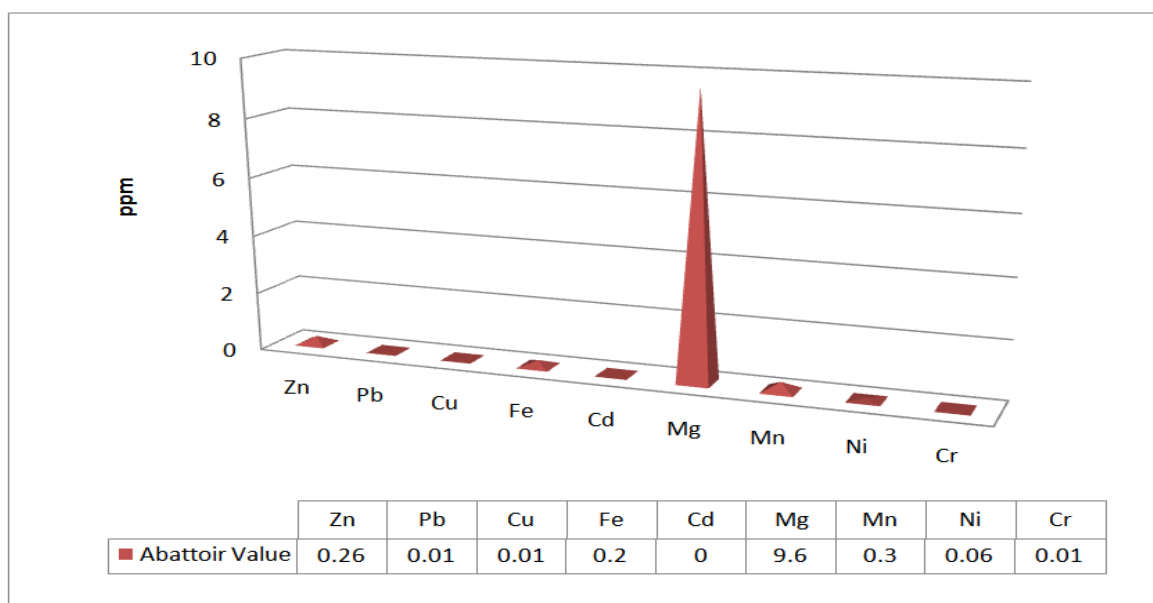


Figure 1: heavy metals values in Gombe abattoir wastewater

In the area of environmental pollution, there are few subjects that, during the latest years, have developed as rapidly as the study and research on toxic metals [19]. According to the World Health Organization (WHO), the metals of most immediate concern are Al, Cr, Mn, Fe, Co, Ni, Cu, Zn, Cd, Hg and Pb. It is apparent that the presence of a toxic metal may not represent a hazard if a threshold contents is below which there are no observable effects. It should be understood that some heavy metals, including Al, Cu, Cd, Fe, Pb, Mn and Ni are essential/beneficial or harmful in trace quantities [20].

**Table 2: Heavy Metals in Abattoir wastewater compared to standard**

Heavy metals	Abattoir Value	WHO-USEPA limits	REMARK
Zn	0.26	0.10	Above standard
Pb	0.01	0.10	Met Standard
Cu	0.01	0.05	Met Standard
Fe	0.20	0.30	Met Standard
Cd	0.00	0.003	Met Standard
Mg	9.60	N.A	Met Standard
Mn	0.30	0.40	Met Standard
Ni	0.06	0.10	Met Standard
Cr	0.01	0.10	Met Standard

The concentration of heavy metals in Abattoir wastewater sample is as presented in Table 2 which averagely shows that the levels of Pb, Cu, Cd, Mg, Mn, Ni and Cr were within the WHO/USEPA recommended standard limits. The concentrated level of Zn was found to be highly concentrated in the abattoir wastewater above the WHO/USEPA recommended standard limits of 0.1mg/L

#### IV. CONCLUSIONS

The physical parameters pH and Temperature of Gombe abattoir wastewater sample were within the WHO/USEPA tolerance discharge limits while turbidity, TSS, Conductivity and TDS were above the WHO/USEPA tolerance limits. For chemical parameters, concentration level of Nitrates (NO<sub>3</sub>), Nitrogen (N), Ammonia (NH<sub>3</sub>), Ammonium (NH<sub>4</sub>), phosphate (PO<sub>4</sub>), phosphorus (P), and phosphorus-pentoxide (P<sub>2</sub>O<sub>5</sub>) in the abattoir wastewater sample were above the WHO/USEPA tolerance limits for the discharged of wastewater into a river, only the concentrations of sulfate content that met the WHO/USEPA limits. The COD and BOD<sub>5</sub> values are also above the WHO/USEPA limits, Dissolved oxygen (DO) values obtained from the abattoir wastewater with mean value of 2.3mg/L which was below WHO/USEPA limits for the discharged of wastewater from industries into river, therefore it can be concluded that most of the physicochemical parameters of Gombe abattoir wastewater had not met the tolerance discharge limits and hence it requires pretreatment before discharging into the environment as it might cause eutrophication; deflection of oxygen in the stream and hence affect the aquatic ecosystem. The concentration of heavy metals in Gombe Abattoir wastewater sample determines are Copper (Cu), Zinc (Zn), Manganese (Mn), Magnesium (Mg), iron (Fe), Chromium (Cr), Cadmium (Cd), Nickel (Ni), and Lead (Pb) were within the WHO/USEPA recommended standard limits, except the concentration level of Zn that was found to have the higher concentration in the abattoir wastewater of 0.26 above the WHO/USEPA recommended standard limits of 0.10.

Therefore, this research will provide basics knowledge in field of abattoir waste management by providing basic data of the physicochemical parameters and heavy metals presence in abattoir wastewater and hence more research should be conducted on how to reduce the abattoir wastewater concentration and its effect on the immediate environment.

#### REFERENCES

- [1] D.O. Alonge, *Meat and Milk Hygiene in the Tropics* (Farmose Press, Ibadan, Nigeria, 2005)
- [2] S.L. Ezeoha, *Pollution and Biogas Production Potentials of Abattoir Wastes*, Masters's diss., University of Nigeria, Nsukka, Nigeria, 2000
- [3] A.Y. Sangodoyin, and O.M. Agbawe, Environmental Study on Surface and Groundwater Pollutants from Abattoir Effluents, *Bio resource Technology*, 41(2), 1992, 193-200.
- [4] G.S. Mittal, Characteristic of the Effluent Wastewater from Abattoirs for Land Application. *Journal of Food Reviews International*, Taylor and Francis group. 20(3), 2004, 229-256.
- [5] FEPA, *Strategic Options for the Redressing of Industrial Pollution*, Volume 2, Nigeria 1995.

- [6] M.I. Nwachukwu., S.B. Akinde., O.S. Udujih, and I.O. Nwachukwu, Effect of Abattoir Wastes on the Population of Proteolytic and Lipolytic Bacteria in a Recipient Water Body (Otamiri River), *Global Resources Journal of Science*, 1, 2011, 40-42.
- [7] C.L. Raymond, *Pollution Control for Agriculture* (Academic Press Inc, New York, 1977).
- [8] R.C. Patra., D. Swarup., R. Naresh., P. Kumar., D. Nandi., P. Shekhar., S. Roy, and S.L. Ali, Tail Hair as an Indicator of Environmental Exposure of Cows to Lead and Cadmium in Different Industrial Areas. *Ecotoxicology Environmental Safety*, 66, 2007, 127-131.
- [9] S.A. Odoemelan. and O. Ajunwa, Heavy Metal Status and Physicochemical Properties of Agricultural Soil Amended by Short term Application of Animal Manure, *Journal of Chemical Society. Niger*, 20, 2008, 60-63.
- [10] E.O.A. Aina, and N.O. Adedipe, *Water Quality Monitoring and Environmental Status in Nigeria* (FEPA Monograph, Lagos, 1991) 12-59.
- [11] Canadian Government, Ministry of Supply and Services, *Sampling for water Quality*, Environment Canada, 1983
- [12] R. Anon, *Standard Methods of Water and Wastewater Examination*, (American Public Health Association, Washington, DC. 18, 1992, 2-172)
- [13] American Public Health Association, *Standard Methods for the Examination of Water and Wastewater*, (American Public Health Association, America Water Works Association and Water Pollution Control Federation, Washington, DC. 14, 1976, 68-165)
- [14] DWAF. *Analytical Methods Manual. TR 151*, (Department of Water Affairs and Forestry, Pretoria, South Africa, 1992)
- [15] G.C. Delzer, and S.W. McKenzie, *Five-Day Biochemical Oxygen Demand*. (3rd Edition, USGS Twri Book 9–A7, 2003)
- [16] World Bank. *Nigeria, Strategic Options for Redressing Industrial Pollution* (Industry and Energy Operations Division, West Africa Department of World Bank, 11, 1994)
- [17] USEPA Volunteer Lake Monitoring A Methods Manual. EPA 440/4-91-002. (Office of Water, U.S Environmental Protection Agency: Washington, DC, 1999)
- [18] D. Chapman, *Water Quality Assessment*. (A Guide to the Use of Biota, Sediments and Water in Environmental Monitoring. E&FN Spon: London, UK, 2, 1997).
- [19] A.K. Bhattacharya, and C. Venkobachar, Removal of Cadmium (II) by Low Cost Adsorbents, *Journal of Environmental Engineering*, 110(1), 1984, 110-192.
- [20] P.W. Kirk, and J.N. Laster, Significance and Behaviors of Heavy Metals in Wastewater Treatment Processes, *Journal of Science and Total Environment*, 40, 1984 1-44.

## A Brief History of Virtual Pheromones in Engineering applications

Ioan Susnea<sup>1</sup>

<sup>1</sup>(Department of Computer and Information technology, University "Dunarea de Jos" of Galati, Romania)

**ABSTRACT:** In the past decades, numerous engineering designs attempted to imitate the operation mode of the natural pheromones, in applications ranging from robotics to packet routing in communication networks, and coordination in large human teams. This paper is a brief review – from an engineering perspective - of the state of the art in what concerns the implementations of the concept of “virtual pheromones” – the man-made counterpart of the biological pheromones. We provide an overview of the most significant solutions found in the vast literature dedicated to the means of coordination in multi agent systems, and try to identify the trends of evolution of the research in this field.

**Keywords :** Multi Agent Systems, virtual pheromones, stigmergy, Robotics, Behavioural Implicit Communication

### I. INTRODUCTION

The concept of *pheromones* is essential for understanding many fundamental biologic processes. Coined by Karlson & Luescher ([1]) in 1959, the term pheromones designates a class of chemical substances used by many animal species for intraspecific chemical communication. Animals often use pheromones to transmit chemical signals that serve for social organization (recognition of the members of the same family, kin, or colony), territorial behavior, finding and choosing mates, sending alarm messages, and for coordinating complex collective behaviors.

Etymologically, the term is derived from the Greek words *pherein* (to carry), and *hormon* (to stimulate, to excite) ([2]).

When perceived by other members of the same species, pheromones elicit specific reactions e.g. certain behavior patterns, or sometimes even developmental changes. The probability of the specific reaction is proportional with the pheromone intensity.

Once released in the environment, pheromones are subject to the following processes that describe their spatio-temporal evolution:

- spatial diffusion: this allows other agents to sense the pheromone at a certain distance from the source. Also, pheromone diffusion creates spatial intensity gradients, which contain important orientation clues for the sensing agents.
- aggregation: multiple sources of pheromones superpose their effects.
- evaporation: the intensity of a pheromone source decreases with time, thus eliminating obsolete information.

These simple processes, linked with certain behavior patterns, are the key for understanding the paradox of coordination in some insect colonies, capable of intelligent complex behavior, without the need of a central coordination mechanism, which intrigued the entomologists for over a century. A typical example of such coordination is the ant foraging behavior. When carrying food from a source to the nest, ants leave a trail of pheromones to indicate the path to the other ants.

The pheromone scent determines the other ants to adjust their behavior and to follow the existing trail, reinforcing it by depositing additional pheromone along the path, in a self-catalytic process. On the other hand, the pheromone evaporation creates a negative feedback loop in this process, making longer or less used paths to decay and eventually disappear.

As a result the majority of the ants will follow the best path between the food source and the nest. This mechanism of indirect coordination between the agents by means of traces created in a shared environment was first described by Grassé ([3]), who called it “stigmergy” (from the Greek words “stigma” – sign, mark, and ergon – work, action).

The biological stigmergy has been extensively studied ([4]), and the mechanism through which the ants eventually find the shortest path between the food source and the nest was formalized in what Dorigo called the “Ant Colony Optimization” algorithm ACO ([5]).

But the processes of decentralized self-organization in multi-agent systems composed of simple, ant-like agents go far beyond the ACO. These processes have been called with the generic name “swarm intelligence” ([6]), and later included a variety of other optimization algorithms (see [7]).

There are now thousands of research articles dedicated to the study of the processes related to swarm intelligence. This paper is only concerned with the engineering applications relying on the implementation of “virtual pheromones”, sometimes also called “digital pheromones” or just “synthetic pheromones”.

The remainder of this paper is structured as follows:

Section 2 contains a selection of the most interesting solutions involving virtual pheromones from a historical perspective, and in Section 3 we try to identify the trends of evolution of the research in this field, and formulate conclusions.

## II. AN OVERVIEW OF THE STATE OF THE ART FROM A HISTORICAL PERSPECTIVE

The idea to create simple, ant-like robotic agents capable of decentralized coordination dates back to 1980s, though the actual term of artificial, or virtual pheromones was used much later. In 1989, Steels ([8]) noted that the spatial propagation of sound creates a gradient field that can emulate the process of diffusion, and explored the possibility use this principle for creating robotic systems capable of self-organization.

In 1993 Drogoul & Ferber ([9]) suggested two possible ways to implement decentralized coordination in multi-agent systems composed of simple robots: by leaving “crumbs” along their path (like Tom Thumb, and other fairy tale characters used to do), or by creating chains, like dockers used to do between the ship and the wharves.

Parunak in [10] (1997) attempted to extract some general engineering principles from the analysis of the natural multi-agent systems. He emphasized the importance of the environment and proposed a structure of the multi-agents systems (MAS) as a three-tuple:

$$MAS = \langle \text{Agents}, \text{Environment}, \text{Coupling} \rangle$$

where “coupling” defines the interactions between the agents and the environment.

A variety of other studies from the same period (e.g. [11],[12]) reflect the growing interest in the study of “collective robotics”, and “robot colonies”, but the term “virtual pheromones” was not explicitly mentioned until 2001 ([13]). In this study, Payton et al. propose a solution wherein the “virtual pheromones” are short range infrared communication messages passed from one robot to another in a multi-hop communication network. The intrinsic directionality of the infrared communication was used to emulate spatial pheromone gradients, and relative distances between robots were estimated by counting the number of hops for each message.

Obviously, according to this model, the pheromones are tied to the robots, rather than being deployed in the environment, and the pheromone gradients change as the robots move.

To overcome this drawback, O’Hara et al. proposed in [14] a solution wherein the environment is pre-populated with a grid of beacons capable to store information and to communicate with the robots. A variant of this idea can be found in [15], where Hoff et al. assume that “during the execution of the algorithm [...], some robots will decide to stop their normal search behavior and become ‘pheromone robots’, also known as beacons, which means they stop moving and act as locations on which virtual pheromone can be stored.”

An interesting variation of the idea of deploying a sort of digital beacons throughout the environment can be found in [16], where Mamei & Zambonelli use RFID tags to store pheromone information. They also found an elegant solution to emulate the process of pheromone evaporation: the pheromone data structure stored in the RFID tags includes a time stamp indicating the moment of the most recent update of the pheromone. Assuming that the robots are equipped with a real-time clock, they can easily evaluate the pheromone decay through evaporation by comparing this time stamp with the current time.

Though the idea of using proximity RFID tags as physical support for digital pheromones has multiple advantages, it still has some drawbacks: RFID tags can be read one at a time (see fig. 1), so that the robot can only sense pheromone gradients by (randomly) moving from one tag to another.

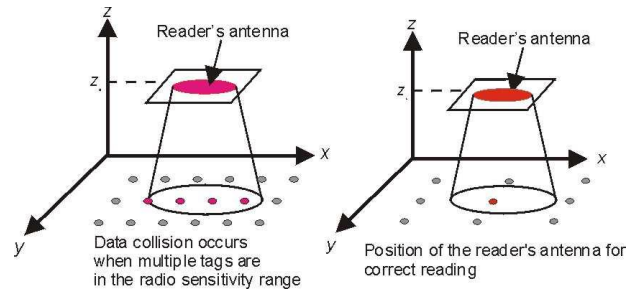


Figure 1: RFID readers can only access one tag at a time

We proposed a simple and efficient solution for this problem in [17], by using two reader antennas, located to a certain distance apart from one another, just like ants and other insects do to sense the pheromones (see fig. 2)

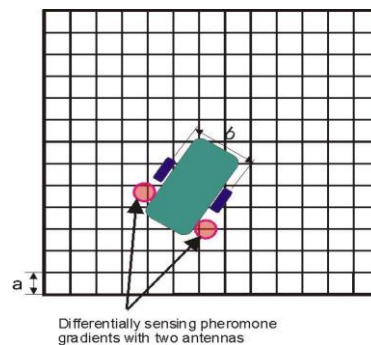


Figure 2: A better emulation of the process of pheromone diffusion with RFID technology by using differential sensing with two antennas

However, none of the above mentioned implementations emulate all of the transformations of biological pheromones (diffusion, aggregation, evaporation). Therefore, the quest for improving the model of the virtual pheromones continued to produce new solutions. An apparently good idea would be to instruct the robots to leave thermal traces by locally heating the ground along their path ([18]), but – considering the limited amount of energy available for the mobile robots – this solution is not feasible in practice.

In another implementation, described in [19], robots draw marks on the floor using a special disappearing ink. In [20] the marks on the floor are not drawn but projected by a computer that communicates with the robots and controls a video projector.

Other researchers tried to directly imitate the biological pheromones, by enabling robots to disperse and sense some chemical substances in the environment ([21],[22]), but it seems that there is still a long way to go for creating a reliable and cost effective artificial nose.

Considering the above examples, it becomes obvious that it is impractical for the agents to leave physical or chemical marks in the environment. It would be much more convenient to create a virtual environment for storing and manipulating the virtual pheromones. Therefore, Vaughan et al. ([23]) studied a scenario wherein the robots have their own localization means (odometry) and share a common *localization space*, defined as “any consistent spatial or topological representation of position. Such a space is shared if there is some [...] correlation between the representations maintained by two or more individuals. A prime example is the Global Positioning System (GPS). Two systems equipped with GPS share a metric localization space in planetary coordinates”.

In this approach, each robot periodically “drops crumbs” in this localization space by keeping a list of records of its coordinates and heading estimates as provided by the odometric system. In a subsequent communication process, these individual “private crumb lists” are fused into a “global crumb list” that guide the robots in their navigation tasks.

However, the task of creating and updating a global representation (or “map”) of the environment is quite complex and not really compatible with the idea of ant-like agents, capable only of local interactions with the environment. Therefore, in [24], we proposed a solution wherein the task of maintaining a global map of the environment is allocated to a central computer, called “pheromone server”. In this approach, the process of “dropping crumbs” is equivalent to sending a data packet to the pheromone server, containing the agent’s ID and current position. This creates a discrete pheromone source  $Sk$ , in a 2D map of the environment (see fig. 3)

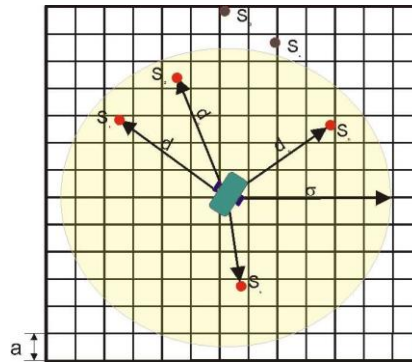


Figure 3: Notations used to describe the virtual pheromone model used in [24]

The major advantage of this scenario is that it allows a complete model of virtual pheromones, i.e. a model that reflects all the processes specific to the biological pheromones: dispersion aggregation, and evaporation.

Assuming a linear model, with the notations in fig. 3, the diffusion of the pheromone source  $S_k$  at the distance  $x$  can be described by:

$$p(x) = \begin{cases} p_k \left(1 - \frac{x}{\sigma}\right) & 0 < x < \sigma \\ 0 & x \geq \sigma \end{cases} \quad (1)$$

the aggregation of all the  $N$  sources:

$$P_R = \sum_{k=1}^N p_k \left(1 - \frac{d_k}{\sigma}\right) \quad (2)$$

and the evaporation:

$$P_R(t) = \sum_{k=1}^N p_k \left(1 - \frac{d_k}{\sigma}\right) \left(1 - \frac{t - t_k}{\tau}\right) \quad (3)$$

where  $t_k$  is the moment of creation of the source  $S_k$ , and  $\tau$  is an evaporation constant, and  $\sigma$  is the sensitivity range (i.e. the maximum distance from a pheromone source where the “scent” of the source can still be sensed).

All the examples described above can be included in the general category of applications called “swarm robotics”, but of course, swarm robotics is not limited to pheromone-based interactions. A recent comprehensive survey of the literature dedicated to swarm robotics is available in [25]. On the other side, the domain of possible applications of the virtual pheromones is not limited to robotics.

When both the agents and the environment are virtual (i.e. software simulated or implemented) there is plenty of room for applications involving stigmergy and virtual pheromones. Such application range from optimal routing in communication networks ([26], [27]), modeling and simulation of the crowd behavior, and smart evacuation systems ([28],[29],[30]), task allocation in flexible manufacturing systems ([31],[32]), to intelligent traffic control and congestion avoidance systems ([33],[34],[35]).

The solutions aimed to elicit stigmergic self-organization in multi-agent systems with human agents (e.g. [36],[37],[38]) rely on creating a virtual environment capable to capture and broadcast the Behavioural Implicit Communication (BIC) messages of the individual agents in the form of a shared global cognitive map that reflects the activity of all agents (see fig. 4).

Unlike the simple, ant-like agents, whose interactions with the environment are direct and local, human agents tend to use some technological means to interact with the environment, and build complex cognitive maps before taking actions. If these cognitive maps reflect the actions of the other agents, this may result in stigmergic behavior of the whole MAS ([38]).

Typical examples of applications built according to this model are the collaborative filtering systems used for data mining (39), or for the optimization of the educational paths in e-learning ([40],[41]).

Finally, it is worth to mention another class of applications involving virtual pheromones: those involving both human and robotic agents, or physical and virtual agents. A comprehensive survey regarding human interactions with robot swarms is available in [42], and an attempt to define a framework for creating hybrid systems with interacting physical and virtual agents is described in [43].

III. DISCUSSION AND CONCLUSION

The diversity of applications involving virtual pheromones illustrated in the previous paragraph, explains the interest of the researchers in defining a unified model for them.

One of the first unifying perspectives treats virtual pheromones as potential fields (see [44]), since the potential field is the closest physical concept that describes well the processes diffusion and superposition of effects.

In another approach, the process of sensing a spatial distribution of virtual pheromones is equivalent to a neural network. We suggested this in [24] (see fig. 5).

This analogy is investigated in depth in [45], where Mora et al. describe the implementation of a Kohonen Self Organizing Map (SOM) based on the concept of virtual pheromones.

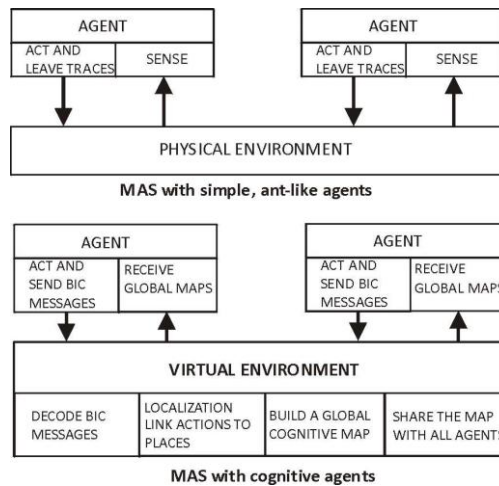


Figure 4: Capturing and broadcasting BIC messages may foster stigmergic interactions between intelligent agents (see [35]).

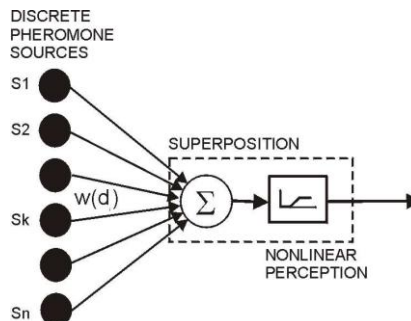


Figure 5: Sensing multiple pheromone sources is equivalent to the operation of a neuron

Parunak (in [46]) suggest an interpretation of the pheromone distributions as “probability fields”. A more rigorous study of the stochastic behavior of the ant system is available in [47], but the work on defining an ultimate mathematical model of the virtual pheromone is still in progress.

After reviewing the vast literature available on topics related to stigmergy and virtual pheromones, we believe that the most promising research direction remains the study of the so-called “cognitive stigmergy” ([48]) and the self-organization in MAS with intelligent agents.

The model of stigmergic interactions we proposed in [38] based on the automatic identification of the Behavioural Implicit Communication (BIC) messages, creates a strong link between the extremely fertile research field of activity recognition (see [49], [50]) and the equally rich in results field of the study of self-organization in MAS.

REFERENCES

[1] Karlson P. & Luescher M. ‘Pheromones’: a new term for a class of biologically active substances. *Nature*, 183, 1959, pp:155–156.  
 [2] Wyatt, T. D. (2003). *Pheromones and animal behaviour: communication by smell and taste*. Cambridge University Press.  
 [3] Grassé, P. P. La reconstruction du nid et les coordinations interindividuelles chez *Bellicositermes natalensis* et *Cubitermes* sp. la théorie de la stigmergie: Essai d'interprétation du comportement des termites constructeurs. *Insectes sociaux*, 6(1), 1959 : 41-80.

- [4] Theraulaz, G., & Bonabeau, E. (1999). A brief history of stigmergy. *Artificial life*, 5(2), 97-116.
- [5] Dorigo, M., Maniezzo, V., & Colomi, A. Ant system: optimization by a colony of cooperating agents. *Systems, Man, and Cybernetics, Part B: Cybernetics, IEEE Transactions on*, 26(1), 1996: 29-41.
- [6] Beni, G., & Wang, J. Swarm intelligence in cellular robotic systems. In *Robots and Biological Systems: Towards a New Bionics?* 1993 :703-712. Springer Berlin Heidelberg.
- [7] Yang, X. S., Cui, Z., Xiao, R., Gandomi, A. H., & Karamanoglu, M. (Eds.). *Swarm intelligence and bio-inspired computation: theory and applications*. 2013, Newnes.
- [8] Steels, L. Cooperation between distributed agents through self-organization. In Y. Demazeau, & J. P. Müller (Eds.), *Decentralized AI: proceedings of the First European Workshop on Modelling Autonomous Agents in a Multi-Agent World*, Cambridge, England, August 16–18, 1989.
- [9] Drogoul, A., & Ferber, J. Some Experiments with Foraging Robots. In *From Animals to Animats 2: Proceedings of the Second International Conference on Simulation of Adaptive Behavior* (Vol. 2, 1993 ). MIT Press.
- [10] Parunak, H. V. D. " Go to the ant": Engineering principles from natural multi-agent systems. *Annals of Operations Research*, 75, 1997: 69-101.
- [11] Arkin, R.C. and Bekey, G.A. (editors). *Robot Colonies*. Kluwer Academic Publishers, 1997.
- [12] Holland, O., & Melhuish, C. Stigmergy, self-organization, and sorting in collective robotics. *Artificial life*, 5(2), 1999 :173-202.
- [13] Payton, D. W., Daily, M. J., Hoff, B., Howard, M. D., & Lee, C. L. Pheromone robotics. In *Intelligent Systems and Smart Manufacturing 2001* :67-75. International Society for Optics and Photonics.
- [14] O'Hara, K. J., Walker, D. B., & Balch, T. R.. The GNATs—Low-cost Embedded Networks for Supporting Mobile Robots. In *Multi-Robot Systems. From Swarms to Intelligent Automata Volume III 2005* (:277-282). Springer Netherlands.
- [15] Hoff, N. R., Sagoff, A., Wood, R. J., & Nagpal, R. Two foraging algorithms for robot swarms using only local communication. In *Robotics and Biomimetics (ROBIO), 2010 IEEE International Conference on* (pp. 123-130). IEEE.
- [16] Mamei, M., & Zambonelli, F. Physical deployment of digital pheromones through RFID technology. In *Swarm Intelligence Symposium, 2005. SIS 2005. Proceedings 2005 IEEE* (pp. 281-288). IEEE.
- [17] Susnea, I., & Vasiliu, G. On defining and following robot paths in an RFID augmented environment. In *15th International Conference on System Theory, Control and Computing, 2011*
- [18] Russell, R. A.. Heat trails as short-lived navigational markers for mobile robots. In *Robotics and Automation, 1997. Proceedings., 1997 IEEE International Conference on* (Vol. 4, pp. 3534-3539). IEEE.
- [19] Mayet, R., Roberz, J., Schmickl, T., & Crailsheim, K. Antbots: A feasible visual emulation of pheromone trails for swarm robots. In *Swarm Intelligence 2010* (pp. 84-94). Springer Berlin Heidelberg.
- [20] Sugawara, K., Kazama, T., & Watanabe, T. Foraging behavior of interacting robots with virtual pheromone. In *Intelligent Robots and Systems, 2004. (IROS 2004). Proceedings. 2004 IEEE/RSJ International Conference on* (Vol. 3, pp. 3074-3079). IEEE.
- [21] Purnamadajaja, A. H., & Russell, R. A. Guiding robots' behaviors using pheromone communication. *Autonomous Robots*, 23(2), 2007 :113-130.
- [22] Ishida, H., Wada, Y., & Matsukura, H. Chemical sensing in robotic applications: A review. *Sensors Journal, IEEE*, 12(11), 2012 :3163-3173.
- [23] Vaughan, R. T., Støy, K., Sukhatme, G. S., & Matarić, M. J. Blazing a trail: insect-inspired resource transportation by a robot team. In *Distributed autonomous robotic systems 4 2010* (pp. 111-120). Springer Japan.
- [24] Susnea, I., Vasiliu, G., Filipescu, A., & Radaschin, A. Virtual pheromones for real-time control of autonomous mobile robots. *Studies in Informatics and Control*, 18(3), 2009:233-240.
- [25] Brambilla, M., Ferrante, E., Birattari, M., & Dorigo, M. Swarm robotics: a review from the swarm engineering perspective. *Swarm Intelligence*, 2013 7(1), :1-41.
- [26] Ducatelle, F., Di Caro, G., & Gambardella, L. M. Using ant agents to combine reactive and proactive strategies for routing in mobile ad-hoc networks. *International Journal of Computational Intelligence and Applications*, 5(02), 2005:169-184.
- [27] Roth, M., & Wicker, S. Termite: Ad-hoc networking with stigmergy. In *Global Telecommunications Conference, 2003. GLOBECOM'03. IEEE* (Vol. 5, pp. 2937-2941). IEEE.
- [28] Gaud, N., Galland, S., Gechter, F., Hilaire, V., & Koukam, A. Holonic multilevel simulation of complex systems: Application to real-time pedestrians simulation in virtual urban environment. *Simulation Modelling Practice and Theory*, 16(10), 2008: 1659-1676.
- [29] Henein, C. M., & White, T. Macroscopic effects of microscopic forces between agents in crowd models. *Physica A: statistical mechanics and its applications*, 373, 2007:694-712.
- [30] Rahman, A., Mahmood, A. K., & Schneider, E. (2008). Using agent-based simulation of human behavior to reduce evacuation time. In *Intelligent Agents and Multi-Agent Systems* (pp. 357-369). Springer Berlin Heidelberg.
- [31] Peeters, P., Van Brussel, H., Valckenaers, P., Wyns, J., Bongaerts, L., Kollingbaum, M., & Heikkilä, T. Pheromone based emergent shop floor control system for flexible flow shops. *Artificial Intelligence in Engineering*, 15(4), 2001:343-352.
- [32] Xiang, W., & Lee, H. P. Ant colony intelligence in multi-agent dynamic manufacturing scheduling. *Engineering Applications of Artificial Intelligence*, 21(1), 2008:73-85.
- [33] Ando, Y., Fukazawa, Y., Masutani, O., Iwasaki, H., & Honiden, S. Performance of pheromone model for predicting traffic congestion. In *Proceedings of the fifth international joint conference on Autonomous agents and multiagent systems 2006* (:73-80). ACM.
- [34] Narzt, W., Wilflingseder, U., Pomberger, G., Kolb, D., & Hortner, H. (2010). Self-organising congestion evasion strategies using ant-based pheromones. *Intelligent Transport Systems, IET*, 4(1), 93-102.
- [35] Susnea, I, Vasiliu G. Patent application „Vehicle Navigation System”, Romanian National Patent Office OSIM Application number A00960/11.10.2010.
- [36] Parunak, H. V. D. A survey of environments and mechanisms for human-human stigmergy. In *Environments for Multi-Agent Systems II* (2006: 163-186). Springer Berlin Heidelberg.
- [37] Susnea, I. Engineering Human Stigmergy. *International Journal of Computers Communications & Control*, 10(3), 2015:420-427.
- [38] Susnea, I., & Axenie, C. Cognitive Maps for Indirect Coordination of Intelligent Agents. *STUDIES IN INFORMATICS AND CONTROL*, 21(1), 2015:111-118.
- [39] Grosan, C., Abraham, A., & Chis, M. *Swarm intelligence in data mining* 2006:1-20. Springer Berlin Heidelberg.
- [40] Semet, Y., Yamont, Y., Biojout, R., Luton, E., & Collet, P. Artificial ant colonies and e-learning: An optimisation of pedagogical paths. In *10th International Conference on Human-Computer Interaction*. 2003
- [41] Susnea, I., Vasiliu, G., & Mitu, D. E. Enabling Self-Organization of the Educational Content in Ad Hoc Learning Networks. *Studies in Informatics and Control*, 22(2), 2013:143-152.

- [42] Kolling, A., Walker, P., Chakraborty, N., Sycara, K., & Lewis, M. Human Interaction With Robot Swarms: A Survey. In press, to appear in IEEE TRANSACTIONS ON HUMAN-MACHINE SYSTEMS.
- [43] Susnea, I. Vasiliu, G. "A framework for creating mixed robot formations with physical and virtual agents" *International Conference of the Air Force Academy —Henri Coanda, AFASES2011*, Brasov, 2011.
- [44] Van Dyke Parunak, H., Brueckner, S., & Sauter, J. Digital pheromone mechanisms for coordination of unmanned vehicles. In *Proceedings of the first international joint conference on Autonomous agents and multiagent systems: part 1* 2002: 449-450. ACM.
- [45] Mora, A. M., Fernandes, C. M., Merelo, J. J., Ramos, V., Laredo, J. L. J., & Rosa, A. C. KohonAnts: A Self-Organizing Ant Algorithm for Clustering and Pattern Classification. *Artificial Life*, 11, 2008:428.
- [46] Van Dyke Parunak, H. Interpreting digital pheromones as probability fields. In *Winter Simulation Conference* 2009: 1059-1068. Winter Simulation Conference.
- [47] Chialvo, D. R., & Millonas, M. M. How swarms build cognitive maps. In *The biology and technology of intelligent autonomous agents* 1995:439-450. Springer Berlin Heidelberg.
- [48] Ricci, A., Omicini, A., Viroli, M., Gardelli, L., & Oliva, E. Cognitive stigmergy: Towards a framework based on agents and artifacts. In *Environments for Multi-Agent Systems III* 2007: 124-140. Springer Berlin Heidelberg.
- [49] Turaga, P., Chellappa, R., Subrahmanian, V. S., & Udrea, O. Machine recognition of human activities: A survey. *Circuits and Systems for Video Technology, IEEE Transactions on*, 18(11), 2008:1473-1488.
- [50] Liao, L.. *Location-based activity recognition* (Doctoral dissertation, University of Washington, 2006)

## Cost Efficient Design Approach for Reversible Programmable Logic Arrays

Md. RiazurRahman

(Department of Computer Science and Engineering, Daffodil International University, Bangladesh)

**ABSTRACT** : Reversible programmable logic arrays (PLA) are at the heart of designing of efficient low power computers. This paper presents an efficient approach to design Reversible PLAs that maximizes the usability of garbage outputs and also reduces the number of ancilla inputs generated. The design for proposed essential components and the architecture of reversible grid network for designing AND and EX-OR planes are also presented. Several algorithms have been proposed and presented to describe the programming interfaces in context of Reversible PLAs construction. Lastly, recent result on the trade-off between cost factors of standard benchmark circuits shows that the proposed design clearly outperforms the existing ones in terms various cost factors.

**Keywords** : Reversible Logic Circuits, Quantum Computing, Low Power Computing.

### I. INTRODUCTION

During execution of every single instruction, stuff wastes  $kln(2)$  joule of energy that converted into heat due to per bit erase and reload where  $l$  is the operating temperature and  $k$  is the Boltzmann constant [1]. Solution to such input energy loss mechanism after publishing the tremendous approach called Reversible Computation was introduced by Bennett [2] in 1973. It opens the tunnel of designing robust architecture of low power consumption where total input energy loss is zero, supports the behaviour of optical computing, quantum computing, etc. Generic prototype of designing low power programmable devices [3] has obtained popularity in recent days. So, the development of reversible PLAs would be another application that enhances capability of low power computing. Proposed idea presents the novel architecture of PLAs in reversible computing by attaining 100% use of every logical units/gates that propagate all primary inputs to outputs. Proposed architecture reflects the following ideology:

- Maximize the usability of primary input signals
- Avoiding any type of EX-OR operations in AND plane
- Reduce number of garbage outputs and ancilla inputs

Rest of the paper has been organized as: section II has described reversible logic and the standards of measuring the performance of reversible circuits. Section III has presented the details of proposed gates and demonstrate organizational placement of logical units (gates) in Reversible PLAs grid. Section IV has illustrated the corresponding algorithms for constructing AND and EX-OR planes using reversible {UMG and UNG} and CNOT gates, respectively. Comparative performance analysis based on benchmark standard circuits has been showed in section V. Finally, section VI has concluded this paper with the summary and future directions. The contents of each section may be provided to understand easily about the paper.

### II. LITERATURE REVIEW

#### 2.1 Reversible Gates

Bidirectional or reversible circuit prevents input loss due to unique mapping between input and output states. Like classical computing, any reversible operational unit identity is called  $n \times n$ , i.e. any reversible gate contains:

- $n$ -input lines and  $n$ -output lines
- Unique mapping between input and output states

For example, controlled NOT (CNOT), widely known as Feynman gate [4] is reversible has two inputs (a, b) and two outputs (p, q) is shown in Fig. 1. Total number of input and output states are same (i.e. 4) and the mapping between input and output states is unique or vice versa.

There are many reversible gates have been populated based on conservative logic [5], universality of reversible circuit [6], fault tolerant mechanism [7], online testability [8], programmable devices [9], etc. Several reversible gates are self-reflexive, backs primary input signals by attaching self-copy and other gates stuck signals need extra circuitry to return in its initial state. In this paper, two new 3x3 reversible gates called Universal MUX (UMG) and Universal NOR (UNG) are used to design AND plane of reversible PLAs where UNG is self-reflexive reversible gate performs basic OR (or universal NOR) operation and returns primary inputs to output. On the other hand, UMG also performs AND operation and returns primary inputs as like UNG but not self-reflexive.

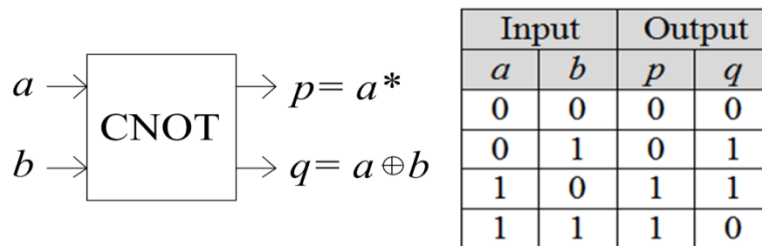


Fig. 1: Reversible CNOT and unique I/O states mapping

**2.2 Performance Measurement Standards**

Operational Competency of any circuit is always related to its technical design encroachment. In any particular technology, greater number of logical units slows down the strength of signal hampers net processing speed of circuit. But interestingly, logical minimization provides better opportunity to reduce the number of operational units and total cost.

**2.2.3 Total Number of Gates:**

In reversible circuit, the input loss is zero in ideal state but bending input signal to output lines absorbs energy and declines the strength of internal signal due to having unavoidable resistance. The total number of gates used in circuit is considered one of the worthy cost factor that controls performance of digital circuits [10].

**2.2.4 Quantum Cost:**

Every reversible circuit point's unique singular unitary matrix which can be accomplished with one or more 2x2 and 4x4 unitary matrices whose are also compatible to 1x1 and 2x2 basic primitives in Quantum Computing. Alternatively, the n-dimensional quantum primitive is identically formed of 2n x 2n dimensional unitary matrix. The total numbers of 2x2 quantum primitives are used to realize any reversible circuit is called Quantum Cost [11].

**2.2.5 Garbage Output and Ancilla Input:**

Unlike classical computing, reversible circuit requires extra output lines to map all input the states uniquely, called garbage output [12]. On the other hand, one or more input line(s) get saturated in constant level (i.e. 0 or 1) to perform specific operations is called Ancilla Input [13]. According to above definitions, the realization of 2-input EX-OR operation requires only one 2x2 reversible Feynman gate and the quantum cost of Feynman gate is 1 (single 2x2 quantum XOR gate is able to realize CNOT operation), the number of garbage output is 1 and finally, the number of ancilla input is zero.

**2.3 Review on Reversible PLAs**

In 2006, author of [14] has proposed the Reversible architecture of PLAs that was similar to classical PLA design [3] where AND plane consists of vertical complement and non-complement input lines and horizontal products lines spread over EX-OR plane. Toffoli gates were used to perform AND operation in AND plane whereas Feynman performed EX-OR operation in EX-OR plane. Additionally, Feynman gates were also used in AND plane for avoiding fan-out(s). The improved design of [14] was proposed in [15] brought prominent modification in the basic architecture of classical reversible PLA circuits by using only single line for each input literal in AND plane. Ref. [15] used MUX and Feynman gates to realize improved design of reversible PLAs

where AND plane also performed copy operation by using Feynman gates as the similar way in [14]. Both papers had used multiple output functions  $F$  (i.e. Eqn. 1) as a sample to represent their proposed designs and minimization methodologies.

$$F = \left\{ \begin{array}{l} f_1 = ab' \oplus ab'c \\ f_2 = ac \oplus a'b'c \\ f_3 = ab' \oplus ab'c \oplus bc' \\ f_4 = ac \\ f_5 = ab \oplus ac \oplus bc' \end{array} \right\} (1)$$

**2.4 Motivation of this Research Work**

Fundamentally, classical architecture of PLAs [3] was implemented by placing configurable switches at cross-point. These switches copy input signal multiple times increases fan-outs (which is restricted in Reversible Computing). The simplicity of AND, OR and NOT logic has been promoted by novel researchers to design such architecture of Programmable Logic Devices (PLD) in classical digital circuit [3]. But in reversible computing, the operability of basic bidirectional components is unavoidable when designing logic circuit such as Reversible Programmable Logic Arrays. In both [14] and [15], reversible PLAs focused the ideal zero energy dissipation due to use of large number of CNOT gates to recover fan-out(s) increases number of ancilla bits and garbage outputs. The idea of proposed research work comes through the reusability of garbage outputs as the input to next operational unit(s) that reduces the number of ancilla input at the same time.

**III. PROPOSED REVERSIBLE GATES AND PLAGRID**

In this section, two new reversible primitives (Universal MUX and Universal NOR gates) have been introduced followed by the demonstration of logical units placement in AND plane as well as the ordering principle of products generation.

**3.1 New Reversible Gates and Operational Templates**

**3.1.1 Reversible Universal MUX Gate (UMG):**

The input and output vectors of Universal MUX gate can be written as  $(a, b, c)$  and  $(p = a, q = b \oplus c, r = ab \oplus a'c)$ , respectively. The equivalent quantum representation of UMG is shown in Fig. 2.

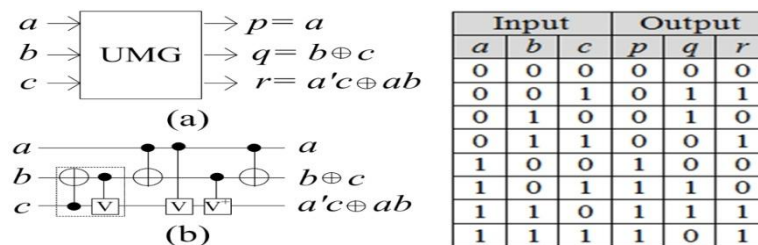


Fig. 2: Reversible Universal Multiplexer gate (UMG): (a) Block diagram of UMG and (b) Quantum realization of UMG; Truth table of UMG maps uniquely all the input states to output states

**3.1.2 Reversible Universal NOR Gate (UNG):**

In Boolean logic, NOR gate is a universal primitives can interpret the functionalities of all basic gates (AND, OR, NOT). Similarly, the input and output vectors of proposed 3x3 Universal NOR gate which perform NOR operation can be written as  $(a, b, c)$  and  $(p = a, q = b, r = (a + b) \oplus c)$ , respectively (shown in Fig. 3).

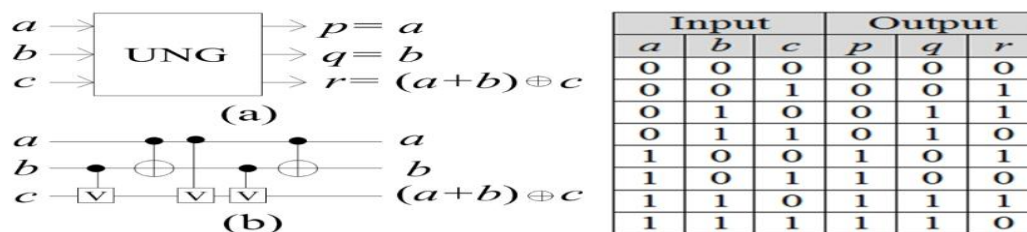


Fig. 3: Reversible Universal NOR gate (UNG): (a) Block diagram of UNG and (b) Quantum cost is 5; UNG maps input and output states uniquely

**3.1.3 Operational Procedures of Proposed Gates:**

Proposed UMG and UNG gates are used to perform AND operation of two literals (or a literal and a product). The forms of logical unit(s) which are used in proposed reversible PLAs have been selected based on following facts:

- Best orientation of Input and/or Output line(s)
- Projected output(s)(product/sum) of plane(AND/OR)

UMG performs MUX operation by setting input  $a$  as selection line and others ( $b$  and  $c$ ) as data. Proposed UMG is able to generate three terms of two inputs ( $ab, ab'$  and  $a'b$ ) are represented through templates  $\alpha, \beta$  and  $\gamma$  (swapping orientations are  $\alpha', \beta'$  and  $\gamma'$ ) as shown in Fig.4. UMG doesn't erase the input value of any operational unit while performing AND operation and those unused outputs can be used as the primary input to another reversible gate. UNG recover the limitation of UMG and the operational template is symbolized using  $\pi(\pi')$  (shown in Fig.5).

Algorithm 1 shows the methodology of selecting template (oriented form of logical unit) to perform AND operation of inputs  $p$  and  $q$  depending on the value of swapFlag. The statement, swapFlag = 0 indicates to perform AND operation by using  $\alpha', \beta'$  or  $\gamma'$  (otherwise  $\alpha, \beta, \gamma$  or  $\pi$ ).

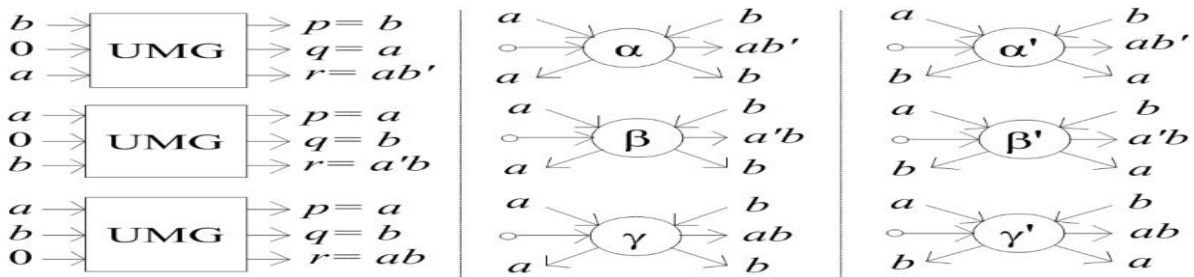


Fig. 4: Proposed templates of Universal MUX gate (UMG) that are used in proposed Reversible PLAs design

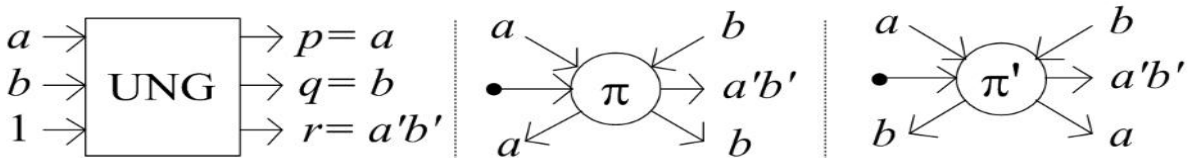


Fig. 5: Proposed templates of Universal NOR Gate (UNG) those are used in proposed Reversible PLAs design

**Algorithm 1: OpAND(p,q,swapFlag)**

Templates  $\{\alpha, \beta, \gamma, \pi\}$  (for swapping  $\{\alpha', \beta', \gamma', \pi'\}$ ) are used to AND  $\{p, q\}$  based on the value of  $swapFlag$ .

Start

1. If  $p$  is a literal in complemented form Then
2.     If  $q$  is in complemented form Then
3.         If swapFlag=0 Then use  $\pi'$  Else use  $\pi$
4.         End If
5.     Else
6.         If swapFlag=0 Then use  $\beta'$  Else use  $\beta$
7.         End If
8.     End If
9. Else
10.     If  $q$  is in complemented form Then
11.         If swapFlag=0 Then use  $\alpha'$  Else use  $\alpha$
12.         End If
13.     Else
14.         If swapFlag=0 Then use  $\gamma'$  Else use  $\gamma$
15.         End If

16. End If  
 17. End If  
 18. Return p, q

END

On the other hand, proposed EX-OR plane consists of only Feynman gates are used to perform XORing products. Three templates of Feynman gates have been used in proposed design are symbolized through symbols  $\Delta$ ,  $\lambda$  and  $\nabla$  perform NOT  $\{a, a'\}$ , EX-OR  $\{a, (a \oplus b)\}$  and COPY operation  $\{a, a\}$ , respectively (shown in Fig. 6).

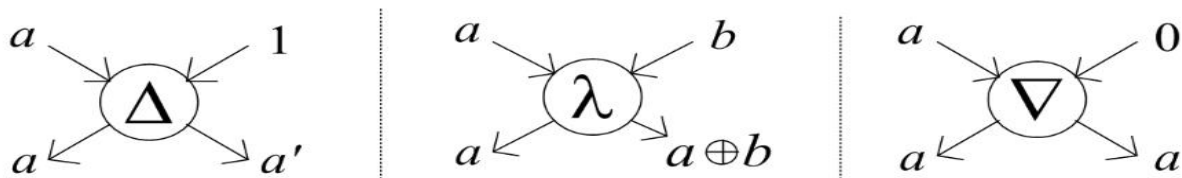


Fig. 6: Templates of CNOT gate are used to design EX-OR plane

### 3.2 Reversible PLAs Grid and Primitives Placement

Reversible gates are more powerful, perform multiple logic operations in a single cycle [10]. The orientation of input and product lines of proposed AND plane is pointed through solid lines (shown in Fig. 7a) where dotted lines indicate another pathway to swap input signals (shown in Fig. 7b) according to following algorithm (Algorithm 2).

#### Algorithm 2: Swap Literals ( $L_i, L_j$ )

Exchanging input signals  $\{L_i, L_j\}$  in lines,  $\{L_i, L_j\}$

Start

1. Set  $a :=$  signal at input line,  $L_i$
2. Set  $b :=$  signal at input line,  $L_j$
3.  $L_i := b$  and  $L_j := a$

End

Basically, swap operation of two literals be performed when the uses of any literal got ended for doing AND operation in AND plane. Swap Literals ( $L_i, L_j$ ) moves unused literals from left to right vertical tracks of AND Plane. Performing AND operation at any cross-point of two vertical lines binds single horizontal line to generate cumulative product and again, connecting another literals to cumulative product (if needed) to generate final product of AND plane.

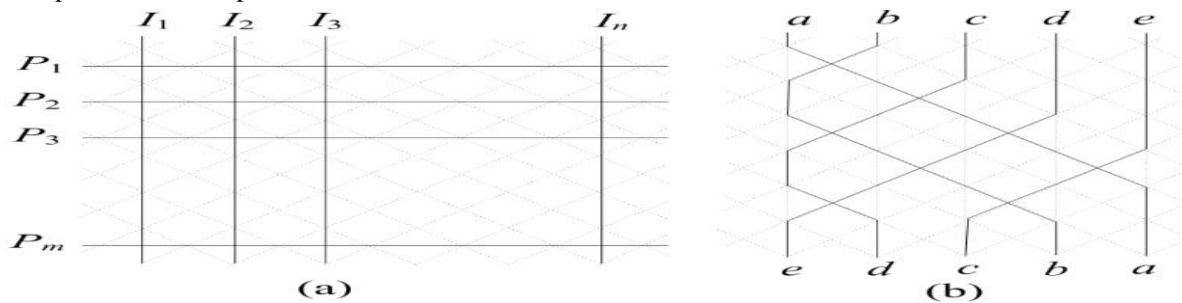


Fig. 7: Reversible PLAs Grid Architecture of AND plane: (a) Primary inputs and generated products passed through vertical and horizontal lines, respectively and (b) Swapping inputs

Ordering products takes crucial role to reduce the cost of products generation by using garbage output(s). Also, the usability of different templates provides mining opportunities optimizing the cost in physical layer. Resultant products contain a number of literals placed according to the order of input literals. For example, products ( $P_v$ ) consist of literals  $\{a, b \text{ and } c\}$  be produced in order, product(s) start with  $a$  followed by start with  $b$  followed by start with  $c$ . Algorithm 3 describes the methodology of placing products based on their usability. For example, product  $abcdbe$  generated before  $abc$ ,  $abd$  or  $ab$  which are consisted of less number of literals.

**Algorithm 3: OrderingProducts( $I_v, P_v$ )**

Products,  $P_v$  be ordered according to inputs,  $I_v$ .

**Start**

1. Set  $P_Q := \emptyset$  [ $P_Q$  is used to store products]
2. Sort  $P_v$  based on SizeOf( $P_i$ ) in descending order
3. For  $i=1$  to total Literals
4.     For  $j=1$  to total Products
5.         If  $I_i \in P_j$  and  $P_j \notin P_Q$  then Add  $P_j$  to  $P_Q$
6.         End If
7.     End Loop
8. End Loop
9. Set  $P_v := P_Q$

**End**

According to above algorithm (ALG. 3), the order of products consists of inputs  $a, b, c, d$  and  $e$  (only the non-complemented forms) can be graphed as shown in Fig. 8.

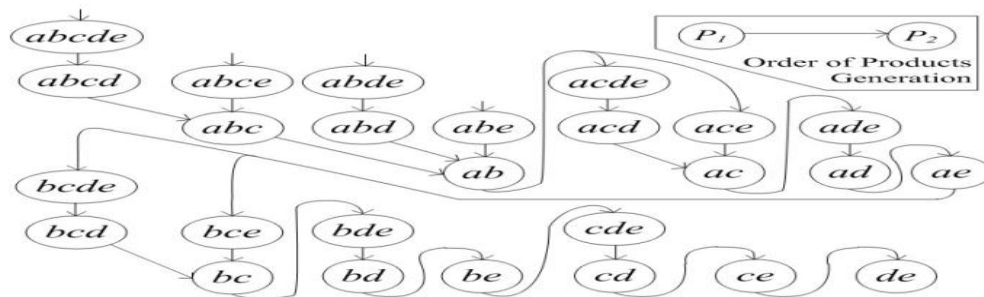


Fig. 8: The order of products consist of literals (a, b, c, d, e) is: {[abcde, abce, abde, abe], [abcd],[abc, abd], [ab], [acde, ace], [acd], [ac], [ade], [ad], [ae], [bcde, bce], [bcd], [bc], [bde], [bd], [be], [cde], [cd], [ce], [de]}. Products in the same group (for example [abcde, abce, abde, abe]) are independent can be generated in any order.

**IV. PROPOSED DESIGN OF AND AND OR PLANES**

In this section, proposed design of AND plane based has been described followed by the realization of EX-OR plane.

**4.1 Designing Reversible AND and EX-OR Planes**

AND plane dominates the performance and cost factors of reversible PLAs where every AND operation rises all cost factors compared to simple of EX-OR operation. Algorithm 4 presents the construction of proposed AND plane as well as the minimization of garbage outputs. The construction of AND plane includes, the ordering of products (Algorithm 3) followed by counting swapFlag and then invokes OpAND( $p, q, swapFlag$ ) (Algorithm 1). Input lines exchange signals (as Algorithm 2) after finishing the generation of all mutual product(s). Finally, Queue( $P_{QG}$ ) stores unused garbage products which are used in a afterwards as resultant products when they get similar to unexplored products.

**Algorithm 4: ConstructANDPlane( $I_v, P_v$ )**

This function constructs AND plane by taking set of input literals ( $I_v$ ) and generates products ( $P_v$ ) connecting multiple input lines ( $L_v$ ) by using UMG and UNG gates.

**Start**

1. OrderingProducts( $I_v, P_v$ )
2. Set  $P_{QG} := \emptyset$  and  $ndot := 0$  [ $P_{QG}$  stores garbage]
3. For  $g=1$  to total Literals-1
4.     For  $h=g+1$  to total Literals
5.         Set  $swapFlag := 0$
6.         For  $i=1$  to total Products
7.             If  $I_g I_h \in P_i$  Then  $swapFlag := swapFlag + 1$
8.         End If

```

9. End Loop
10. If swapFlag > 0 Then
11.   For i = 1 to totalProducts
12.     If SizeOf(Pi) > 1 Then
13.       If Pi ∈ POG Then Remove Pi from POG
14.       Else
15.         If IgIh ∈ Pi Then swapFlag := swapFlag - 1
16.           Set pivotP := OpAND(Ig, Ih, swapFlag)
17.           If SizeOf(Pi) > 2 Then
18.             For k = h + 1 to totalLiterals
19.               If Ik ∈ Pi Then
20.                 Set PG := pivotP
21.                 pivotP := OpAND(pivotP, Ik, false)
22.             End If
23.           End Loop
24.           Add PG to POG [Add new garbage to POG]
25.           End If
26.         End If
27.       End If
28.     Else ndot := ndot + 1 [ Use via (.)]
29.   End If
30. End Loop
31. Else SwapLiterals(LG, Lh) [No mutual products]
32. End If
33. End Loop
34. End Loop
End
    
```

**Theorem 1.** Let,  $n$  be the number of AND operations of  $m$  output functions and  $t$  be the number of AND operation of garbage outputs, ( $P_{OG}$ ) which are identical to any products then the minimum number of reversible gates to realize AND plane is  $(n-t)$ , the quantum cost is  $5(n-t)$ , the number of ancilla inputs is  $(n-t)$ .

**Proof:** As performing every reversible AND operation needs single UMG or UNG gate, results total number of gates to realize AND plane is  $n$ . But reusability of garbage reduces the number of acting AND operations to  $(n-t)$ . Similarly, the quantum cost of UMG or UNG is 5 sums-up the total quantum cost of circuit is  $5(n-t)$  and every reversible AND operation requires an ancilla bit summarize total number of ancilla inputs to  $(n-t)$ .

For multi-output function  $F$  in Eqn. (1), total number of AND operations ( $n$ ) is 7, the number of AND operation(s) in garbage which are similar to any product ( $t$ ) is 1. So, the number of gates  $= (n-t) = 7-1=6$ , quantum cost  $= 30$  and total ancilla inputs  $= 6$  (shown in Fig. 9).

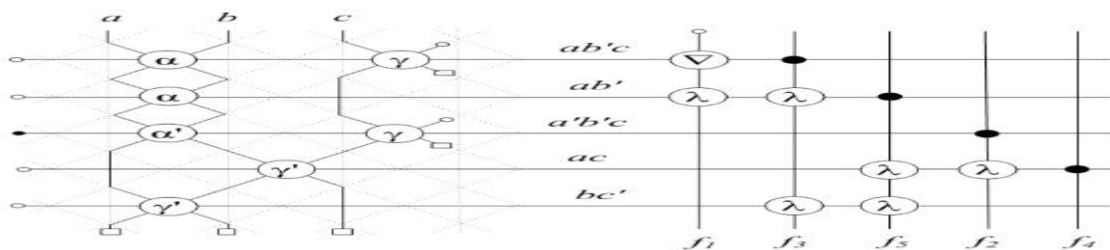


Fig. 9: Optimized version of reversible PLAs of multi-output function  $F$  in Eqn. (1)

**Theorem 2.** Let,  $p$  be the number of products (consist of more than two literals) of  $m$  output functions,  $q$  be the number of garbage outputs which are identical to any products and  $ndot$  be the number of cross-point then the number of garbage is  $p + totalLiterals - ndot - q$ .

Algorithm 5 describes the construction of EX-OR plane by using Feynman gates where  $\lambda$  connects product lines ( $P_i$ ) to corresponding function lines ( $F_j$ ) produces output signals and another identical copy of  $P_i$ .

**Algorithm 5: Construct XOR plane ( $P_v, F_v$ )**

EX-OR plane generates the final output of multi-output function, ( $F_v$ ) consists of products,  $P_v$ .

**Start**

1. Set  $F_Q := \emptyset$  and  $xdot := 0$
2. For  $i = 1$  to totalProducts
3.     For  $j = 1$  to totalFunctions
4.         If  $P_i \in F_j$  Then
5.             If  $F_i \notin F_Q$  Then
6.                 If  $\text{FreqOf}(P_i) == 1$  Then
7.                      $xdot := xdot + 1$
8.                     Else
9. Use  $\nabla$  [ Keep a copy of  $P_i$ ]
10.                     Set  $\text{FreqOf}(P_i) := \text{FreqOf}(P_i) - 1$
11.                     End If
12.                     Add  $F_i$  to  $F_Q$
13.                     Else Use  $\lambda$  [XORing  $P_i$  to  $F_j$  line]
14. End If
15. Else If  $P_i' \in F_j$  Then
16. Use  $\Delta$  [ Keep a copy of  $P_i$ ]
17. End If
18.     End Loop
19. End Loop

**End**

**Theorem 3.** Let,  $n$  be the number of EX-OR operations of  $m$  output functions and  $xdot$  be the number of cross-points, then the minimum number of Feynman gates to realize EX-OR plane is  $n + m - xdot$ , the quantum cost is  $n + m - xdot$ , total number of ancilla inputs is  $m - xdot$ .

According to proposed algorithms (ALG.4&5), the construction of multi-output function  $F$  in Equation (1) is shown in Fig.9 where garbage outputs are represented by using line ends with box. Table 1 summarizes that the proposed design of reversible PLAs requires less number of gates, garbage outputs and ancilla inputs as well as minimum quantum cost compared to existing design [15].

Table 1. Comparison between the proposed and existing [15] designs of multi-output function  $F$  in equation (1)

RPLAs Design	Total Gates (GA)	Garbage (GB)	Ancilla Input (AI)	Quantum Cost (QC)
Proposed	13	5	7	37
Existing [15]	18	10	12	39

**V. PERFORMANCE ANALYSIS**

The realization of benchmark circuits analysis based on proposed algorithms by using programming language Java (jdk1.7) on Netbeans IDE (8.0) in Window 7 Workstation is presented in Table 2. All the experiment results are tested on Intel(R) Core(TM) i3 CPU @3.30GHz with 2GB RAM. Table 2 shows the experimental results for different benchmark functions and the comparison with the existing method [15] where the required number of gates, garbage outputs and ancilla inputs are minimized in notable manner. Finally, the trade-off between quantum cost and other factors summarizes the better optimization of proposed design of reversible PLAs is presented.

Table 2. Experimental results using different benchmark functions

RPLAs	Total Gates (GA)		Garbage (GB)		Ancilla Input (AI)		Quantum Cost (QC)	
	Existing	Proposed	Existing	Proposed	Existing	Proposed	Existing	Proposed
5xp1	166	132	112	44	115	47	418	452
9sym	427	377	385	111	377	103	1405	1681
adr3	67	52	48	26	46	24	157	172
apex3	3998	3719	1799	520	1795	516	8654	9655
b12	159	127	132	56	167	50	453	495
bw	305	281	64	30	87	53	446	445
cordic	12162	11389	10640	1573	10661	1552	41694	50765
duke2	941	874	667	157	674	164	2735	3262
e64	2170	2074	2148	121	2148	121	8410	10282
inc4	16	11	10	4	11	5	34	35
inc5	23	16	16	6	17	7	53	56
misex1	88	74	51	25	50	24	193	206
misex2	199	165	176	79	149	52	122	673
pdc	3801	3451	3006	487	3030	511	12096	14115
rd53	56	44	42	23	40	21	134	141
rd73	187	150	141	68	137	64	487	550
rd84	328	267	265	114	261	110	928	1067
sasao	14	9	13	8	10	5	29	29
sao2	284	257	236	60	230	54	890	1065
t481	49	40	53	36	38	21	134	152
table3	2602	2439	1814	342	1814	342	7537	8995
table5	2539	2384	1819	319	1682	182	7516	8896
xor5	8	4	8	9	4	5	8	4
z5xp1	167	139	114	50	117	53	425	483
z9sym	427	377	385	111	377	103	1405	1681

## VI. CONCLUSION

Reversible computing is in high demands due to the increasing thirst for low power computation. The proposed design increases the reusability of garbage outputs which in turn enhances zero energy dissipation which is the primary concern for reversible computing. This work has introduced a novel approach to design reversible PLAs by proposing reversible PLAs grid and algorithms to construct AND and EX-OR planes with minimized gates and other cost factors which lead towards the advancement of reversible PLAs which will promote the development of Reversible Field Programmable Logic Arrays in the near future [9].

## References

- [1] R. Landauer, Irreversibility and heat generation in the computing process, *IBM J. of R&D*, vol. 5(3), pp. 183-191, 1961.
- [2] C.H. Bennett, Logical Reversibility of Computation, *IBM J. of Research and Development*, vol. 17(6), pp. 525-532, 1973.
- [3] H. Fleisher and L.I. Maissel, An Introduction to Array Logic, *IBM J. of Res. and Development*, vol. 19(2), pp. 98-109, 1975.
- [4] R.P. Feynman, Quantum Mechanical Computers, *Foundations of Physics*, vol. 16(6), pp. 507-531, 1986.
- [5] E. Fredkin and T. Toffoli, Conservative Logic, *International Journal of Theoretical Physics*, vol. 21, pp. 219-253, 1982.
- [6] T. Toffoli, Reversible Computing, *Lecture Notes in Comp. Sci. on Auto., Lang. and Prog.*, vol. 85, pp. 632-644, 1980.
- [7] B. Parhami, Fault-tolerant Reversible Circuits, *Proc. of 40<sup>th</sup> Asilomar conference on sig., sys. and comp.*, ACSSC'06, CA, pp. 1726-1729, 2006.
- [8] S.N. Mahammad and K. Veezhinathan, Constructing Online Testable Circuits Using Reversible Logic, *IEEE Trans. On Instrumentation and Measurement*, vol. 59(1), pp. 101-109, 2010.
- [9] A.S.M. Sayem and S.K. Mitra, Fault-tolerant Reversible Circuits, *Proc. Of IEEE Int'l conf. on computer sci. and automation engg.*, CSAE'11, Shanghai, China, pp. 251-255, 2011.
- [10] A.K. Biswas, M.M. Hasan, A.R. Chowdhury and H.M.H. Babu, Efficient Approaches for designing Reversible Binary Coded Decimal Adders, *Micro.J.*, vol. 39(12), pp. 1693-1703, 2008.
- [11] M. Perkowski and et al., A hierarchical approach to computer aided design of quantum circuits, *Proc. of 6<sup>th</sup> Int'l sym. on R. & M. of Future Comp. Tech.*, Germany, pp. 201-209, 2003.
- [12] M.R. Rahman, Cost Efficient Fault Tolerant Decoder in Reversible Logic Synthesis, *International Journal of Computer Applications*, vol. 108-2, pp. 7-12, 2014.
- [13] H. Thapliyal and N. Ranganathan, Design, synthesis and test of reversible circuits for emerging nanotechnologies, *Proc. of IEEE comp. soc., annual sym. on VLSI, USA*, pp. 5-6, 2012.
- [14] A.R. Chowdhury and R. Nazmul and H.M.H. Babu, A new approach to synthesize multiple-output functions using reversible programmable logic arrays, *Proc. of 19<sup>th</sup> Int'l conf. on VLSI Design (VLSID'06)*, India, pp. 311-316, 2006.
- [15] S.K. Mitra and L. Jamal and M. Kaneko and H.M.H. Babu, An efficient approach for designing and minimizing reversible programmable logic arrays, *Proc. of the Great Lakes sym. on VLSI*, ACM, New York, NY, USA, pp. 215-220, 2012.

## Development of Evaluation Models for Estimation of Economic Values of Natural Gas Fractionation in the Niger Delta

Udie, A. C.<sup>1</sup>, Nwakaudu, S. M.<sup>2</sup>.

<sup>1</sup>(Department of Petroleum Engineering, Federal University of Technology Owerri (FUTO), Nigeria

<sup>2</sup>(Department of Chemical Engineering, Federal University of Technology Owerri (FUTO), Nigeria)

**Abstract:** Natural gas fractionation components and economic values models have been developed in the Niger Delta. The importance is to enhance diversifying utilization, reduce gas flaring, creates fast development, impacts on building the Nation's economy, industrialization and jobs creation in the country. This was possible calculated average Natural gas values, weight, heating value, specific gravity and ratio of the gas components (LNG, LPG and condensate). The resulted fractionation ratio is 85.76% of LNG, 11.61% of LPG and 2.28% of condensate (liquid) with a revenue generation of LNG USD1.85/SCF, LPG ₦ 0.41/SCF and ₦ 0.38/SCF. The revenue per give time depends on demand and supply.

**Keywords:** Economic values of natural gas fractionation ratio, liquefied natural gas, liquefied petroleum gas and condensate components

### I. Introduction

Natural gas is a compound of carbon and hydrogen as the major elements and some impurities such as:  $H_2S$ ,  $CO_2$ ,  $N_2$  and water vapour ( $H_2O_{(g)}$ ) as manor components. The compound CH-bond is called hydrocarbon and combusts in oxygen to produce carbon dioxide ( $CO_2$ ), water vapour and appreciable energy released that can be used in generating heat, electricity cooking and condensate for gas based power plant for electricity generation as well. Natural gas is found in porous rocks (Reservoirs) either associated with crude oil (called associated gas), in gas reservoir with no crude oil (called non-associated gas) or Coal Beds (called coal bed Methane, CBM). The challenge in this work is to find out the natural gas useful fractions ratios for diversifying utilization and Successful fractionation enhances proper ratios estimations and modelling which results in economic evaluations. Natural gas fractionation is done to multiply its utilization.

#### i. Liquefied Natural Gas (LNG)

This is natural gas component which contains methane ( $C_1H_4$ ) and ethane ( $C_2H_6$ ) only. This component can be liquefied or solidified (chips) for easy transportation management with reduced boil-off value. The major use of LNG is heat energy generation for industrial manufacturing plants (fertilizer manufacturing plant, petrochemicals, soap, and may others) and gas base power plant for electric energy generation.

#### ii. Liquefied Petroleum Gas (LPG)

This is natural gas component which contains propane ( $C_3H_8$ ) and butane ( $C_4H_{10}$ ) only. The major uses of LPG are as cooking gas and industrial tarnishes.

#### iii. Condensate

This component is the hydrocarbons mixture of pentane ( $C_5H_{12}$ ), hexane ( $C_6H_{14}$ ) and heptanes plus ( $C_7+$ ) used mainly for crude oil stabilization and gas base power plant fuel for generating electric energy for sustainability of life in a country or community.

Many authors worked on gas recovery, processing and sales. Udie and Nwakaudu, (2015)<sup>[1]</sup> worked on natural gas fractionation in Nigeria for diversifying utilization showed that it contains three useful components or ratios (LNG, LPG and Condensate). Rankine, (Mid-19th century)<sup>[2]</sup>, a British Physicist and Engineer, 1820-1872 designed an absolute temperature scale in which each degree equals one degree on the Fahrenheit scale, with the freezing point of water being  $491.67^\circ$  and its boiling point  $671.67^\circ$ . Baryon Cycly (Mid-20<sup>th</sup> Century)<sup>[3]</sup>

discovered the Subatomic particle that undergoes strong interactions”, with a mass greater than or equal to that of the proton, and consists of three quarks. Here It is a gas turbine using compression skid, combustion skid and exhaust unit, releasing heat for electrical generation. National Petroleum Council, NPC, (1984)<sup>[4]</sup>, studied the economics of enhanced oil recovery and developed models for oil marketing. The models were accepted worldwide and they were adopted by OPEC for Oil. Mathematically:  $Rev = X_s(S - 0.02(40 - API))$ . Zanker, (1973)<sup>[5]</sup>, provided methods for estimation of NGL recovery fractionator trays efficiencies. He stated that there was no good prior method of estimating tray efficiencies for unsteady or different separations. The reason was that many factors affect tray efficiency: relative vapour and liquid holding of the tray, physical characteristics of liquid (foaming Viscosity and surface tension), trays characteristics, mechanical design as well as installation. Another factor was the thermodynamic properties used to determine the number of theoretical trays. They recommended O’Connell correlation model. Tray efficiency of 75 – 85%,  $\mu = 0.088cp$ ,  $\alpha = 1.695$  and  $\alpha \mu = 0.15$ :  $T_{NT} = \frac{32-1bioler}{0.8}$ . Williams, (1996)<sup>[6]</sup> work showed that Liquids recovery in gas-condensate reservoirs is classified under low hydrocarbons fluids reservoirs (marginal oil field), because the techniques, quantity and expenses for liquid (oil) recovery in gas condensate reservoir are off the conventional recovery methods. The quantity of oil to be recovered using gas-injection depends on the quantity of the injected gas invasion and by volumetric depletion depends on the reservoir pressure. The gas invasion value depends on the void spaces in a reservoir to be replaced as a displacing agent. Gas injection gears towards an overall recovery factor of 0.46 to 0.48. The control or dependant parameters are rock permeability uniformity, displacement and injected-gas invasion/swept efficiencies. The recovery value is due to pressure maintenance, sweep efficiency and displacement by the injected gas vapour. If pressure is not enhanced (maintained), low recovery would establish itself through retrograde condensation in the gas-condensate reservoir. Gas re-cycling is only fairly good in a gas condensate with gas-cap, which is overlying by an oil-zone that is also overlain by an active water-drive. In this case the pressure is supported by the aquifer. In the absence of active water-drive, oil-zone can be depleted first, allowing the gas-cap to expand and sweep through the oil-zone, maximizing the recovery. This is because in the absence of active water-drive, the application of gas re-cycling would cause oil to zone into shrink gas-cap and/or the original oil-zone initially displaced by gas, resulting in low recovery. Johnson and Morgan, (1985)<sup>[7]</sup> worked on gas fractionation control and found out that it operates by using a controlled temperature gradient from top to bottom. The composition of the distillate product is fixed by its bubble point The Bottom is controlled by bubble pint and top by dew point. Izuwa, et al (2014)<sup>[8]</sup> studied optimum recovery of condensate in gas-condensate reservoirs and found out that the highest injection rate was not the optimum recovery factor. They concluded that optimum recovery was by a combination of many factors. Izuwa and Obah, (2014)<sup>[9]</sup> developed a model by integration of exponent design fluid characteristic and reservoir compositional simulation. These predictive models were used to assess the effects of the reservoir production parameters on condensate recovery. They concluded that recycling was best above dew-point pressure. Maddox and Morgan, (1998)<sup>[10]</sup> worked on gas treatment and sulphur recovery and stated that fractionation is a sluggish device, so liquid hold up is fairly large since flow rates are relatively low compared to its flow inventory. They recommended that fractionation should be operated so that the material and energy balances around it are satisfied on a steady state basis. This is because any momentary upsets cause internal unstable operation. Hauseh, (1986)<sup>[11]</sup>, developed a General Pressure Drop Correlation (GPDC) model which is widely used today to size packed Tower for water content adjustment in gas processing and conditioning. The flood point is a function of liquid rate, packing characteristics, Gas and Liquid densities and liquid viscosity. Mathematically:  $y = \frac{AF G^2 v^{0.1}}{\rho_g(\rho_L - \rho_g)}$  and  $x = \frac{L}{G} \left(\frac{\rho_v}{\rho_L}\right)^{0.5}$ . Hubard, (1997)<sup>[12]</sup>, studied an independent appraisal of gas dehydration using reflux and fractionation type stabilizers in crude oil and condensate stabilization process. He recommended stabilizer in place of stage separator. The reasons were that stabilizers are more economical and have higher efficiency than stage separators. Brown, (1990)<sup>[13]</sup> Compared sizes of hydrocarbons separator and explained that large capacity separators have more foam Problems and recommended sizeable ones or fractionation type stabilizer units. Udie, et al, (2014)<sup>[14]</sup>, did a comparative study of techniques for condensate recovery and found out that the highest recovery technique was water injection at dew-point pressure. Their result showed that 62% of gas, 25% condensate (liquid) and 13% residual saturation.

## II. MATERIALS AND METHODS

### 2.1 Materials

The material used in this work were mainly sample data obtained from the inlets and outlets of stages-separators and West African Gas Pipeline feed-up (node) in the Niger Delta. Table 2.1 shows details sample data.

Table 2.1: Gas Sample Analysis Record from Separators and WAGP Gas Sample in Niger Delta

Gas Sample Component	Stage Separators Gas Sample				WAGP Gas Sample Composition				
	Well-1 % Mole	Well - 2 % Mole	Well - 3 % Mole	Well - 4 % Mole	Well - 5 % Mole	Well - 6 % Mole	Well - 7 % Mole	Well - 8 % Mole	Wee-9 % Mole
CO <sub>2</sub>	4.39	4.02	4.11	1.85	2.852	3.220	0.51	1.22	1.65
N <sub>2</sub>	4.61	4.53	4.05	0.04	0.130	0.058	0.13	0.13	0.08
H <sub>2</sub> S	-	-	-	-	-	-	-	-	-
C <sub>1</sub>	76.41	78.22	80.79	86.85	80.28	83.87	85.37	88.96	89.77
C <sub>2</sub>	8.35	8.12	7.66	5.33	8.68	6.89	6.70	5.26	3.95
C <sub>3</sub>	4.08	3.57	2.62	3.54	4.90	3.42	4.09	2.70	2.64
iC <sub>4</sub>	0.64	0.05	0.28	0.62	-	-	-	-	-
nC <sub>4</sub>	0.93	0.68	0.34	1.05	2.23	1.60	2.21	1.14	1.20
iC <sub>5</sub>	0.22	0.14	0.06	0.30	-	-	-	-	-
nC <sub>5</sub>	0.16	0.10	0.04	0.28	0.68	0.52	0.99	0.31	0.35
C <sub>6</sub>	0.07	0.06	0.02	0.14	0.25	0.423	0.00	0.28	0.36
C <sub>7</sub> +	0.14	0.06	0.03	-	-	-	-	-	-
H <sub>2</sub> O	-	-	-	-	-	-	-	-	-
Total	1.00	1.00	1.00	1.00	1.00	1.00	1.00	1.00	1/00

2.2: Natural Gas Fractionation Ratios Estimation Procedure

2.2.1: Calculation of the Values using Stage Separator Samples

The Weight ( $M_{gi}$ ), Gross Heating Value ( $GHV_i$ ) and Specific Gravity ( $\gamma_{gi}$ ) of the Natural Gas were estimated using samples collected from stages-separators. These samples data were each collated or grouped into three components liquefied natural gas (LNP), liquefied petroleum gas (LPG) and condensate (Liquid). The ratio of each component was calculated using well-1 to well-9. Table 2.2 shows the estimation procedure of Well-1 to Well-4. The averages of these values,  $M_{gi}$ ,  $GHV_i$  and  $\gamma_{gi}$  were also calculated using eqn2,5 and eqn2.6 on each separator values.

Table 2.2a Well-1 Weight, Heating Value and Specific Gravity Estimation

Natural Gas Components	% Mole $y_i$	Mass, g $M_i$	Weight $y_i M_i$	(GHV) <sub>i</sub> Btu/scf	Net Heat $y_i (GHV)_i$
CO <sub>2</sub>	0.0439	44.01	1.9320	-	-
H <sub>2</sub> S	-	34.08	-	-	-
N <sub>2</sub>	0.0461	28.01	1.2913	-	-
C <sub>1</sub>	0.7641	16.04	12.2562	1007.7	769.9836
C <sub>2</sub>	0.0835	30.07	2.5108	1768.8	147.6948
C <sub>3</sub>	0.0408	44.10	1.7993	2517.4	102.7099
iC <sub>4</sub>	0.0064	55.14	0.3520	3257.4	20.8474
nC <sub>4</sub>	0.0093	55.14	0.5128	3257.4	30.2938
iC <sub>5</sub>	0.0022	72.20	0.0588	4071.8	8.9580
nC <sub>5</sub>	0.0016	72.20	0.1165	4071.8	6.5149
C <sub>6</sub>	0.0007	86.12	0.0603	4886.2	3.4203
C <sub>7</sub> +	0.0014	101.00	0.1414	5435.2	7.6993
H <sub>2</sub> O	-	18.08	-	-	-
Total	1.0000	-	21.1313	-	1098.0320

Table 2.2b Well-2 Weight, Heating Value and Specific Gravity Estimation

Natural Gas Components	% Mole $y_i$	Mass, g $M_i$	Weight $y_i M_i$	(GHV) <sub>i</sub> Btu/scf	Net Heat $y_i (GHV)_i$
CO <sub>2</sub>	0.0402	44.01	1.7692	-	-
H <sub>2</sub> S	-	34.08	-	-	-
N <sub>2</sub>	0.0453	28.01	1.2689	-	-
C <sub>1</sub>	0.7822	16.04	12.5465	1007.7	788.2220
C <sub>2</sub>	0.0812	30.07	2.4417	1768.8	143.6266
C <sub>3</sub>	0.0357	44.10	1.5540	2517.4	89.8722
iC <sub>4</sub>	0.0005	55.14	0.0276	3257.4	1.6287
nC <sub>4</sub>	0.0068	55.14	0.3750	3257.4	22.1502
iC <sub>5</sub>	0.0014	72.20	0.1011	4071.8	5.7005
nC <sub>5</sub>	0.0010	72.20	0.0722	4071.8	4.0718
C <sub>6</sub>	0.0006	86.12	0.0517	4886.2	2.9317
C <sub>7</sub> +	0.0006	101.00	0.0606	5435.2	3.2611
H <sub>2</sub> O	-	18.08	-	-	-
Total	1.0000	-	20.2588	-	1061.4647

Table 2.2c Well-3 Weight, Heating Value and Specific Gravity Estimation

Natural Gas Components	% Mole $y_i$	Mass, g $M_i$	Weight $y_i M_i$	(GHV) $_i$ Btu/scf	Net Heat $y_i$ (GHV) $_i$
CO2	0.0411	44.01	1.8088	-	-
H2S	-	34.08	-	-	-
N2	0.0405	28.01	1.1344	-	-
C1	0.8079	16.04	12.9587	1007.7	814.1208
C2	0.0866	30.07	2.3034	1768.8	135.4901
C3	0.0363	44.10	1.1554	2517.4	65.9559
iC4	0.0028	55.14	0.1544	3257.4	9.1207
nC4	0.0034	55.14	0.1875	3257.4	11.0752
iC5	0.0006	72.20	0.0433	4071.8	2.4431
nC5	0.0004	72.20	0.0289	4071.8	1.6287
C6	0.0002	86.12	0.0172	4886.2	0.9772
C7+	0.0003	101.00	0.0303	5435.2	1.6306
H2O	-	18.08	-	-	-
	1.0000	-	19.8223	-	1042.4418

Table 2.2d: Well-4 Weight, Heating Value and Specific Gravity Estimation

Natural Gas Components	% Mole $y_i$	Mass, g $M_i$	Weight $y_i M_i$	(GHV) $_i$ Btu/scf	Net Heat $y_i$ (GHV) $_i$
CO2	0.0185	44.01	0.8142	-	-
H2S	-	34.08	-	-	-
N2	0.0004	28.01	0.0112	-	-
C1	0.8635	16.04	13.8505	1007.7	814.1208
C2	0.0533	30.07	1.6027	1768.8	135.4901
C3	0.0354	44.10	1.5560	2517.4	65.9559
iC4	0.0062	55.14	0.3419	3257.4	9.1207
nC4	0.0105	55.14	0.5790	3257.4	11.0752
iC5	0.0030	72.20	0.2166	4071.8	2.4431
nC5	0.0028	72.20	0.2022	4071.8	1.6287
C6	0.0014	86.12	0.1206	4886.2	0.9772
C7+	-	101.00	-	5435.2	-
H2O	-	18.08	-	-	-
	1.0000	-	19.2949	-	1138.3877

Gas Weight,  $M_{gi} = \sum(y_i M_i) g$  [2.1]

Gross Heating Value,  $GHV = \sum y_i (GHV)_i$  MBtu/scf [2.2]

$\gamma_{gi} = \frac{\sum(y_i M_i)}{M_{air}} = \frac{\sum_i^n (y_i M_i)}{29} = 0.69$  [2.3]

Gas Density,  $\gamma_g = \frac{\sum(y_i M_i)}{M_{air}} = \frac{\sum(y_i M_i)}{29}$  [2.4]

Stages Separators Average Gas Values

$M_{gs} = \frac{\sum_i^n (y_i M_i)}{n_w} = \frac{21.1313+20.2588+19.8223+19.2949}{4} = 20.13g$  [2.5]

$(GHV)_{sg} = \frac{\sum_i^n y_i (GHV)_i}{n_w} = \frac{1098.0320+1061.4647+1042.4418+1138.3877}{4} = 1085.0736 MBtu/scf$  [2.6]

2.2.2: Calculation of the Values using West African Gas Pipeline (WAGPS)

Weight ( $M_{gi}$ ), Gross Heating Value ( $GHV_i$ ) and Specific Gravity ( $\gamma_{gi}$ ) of Natural gas were also estimated using samples collected from the West African Gas Pipeline (WAGPS) feed-up (node). Table 2.3 shows the estimation procedure of Well-5 to Well-9. The averages of these values,  $M_{gi}$ ,  $GHV_i$  and  $\gamma_{gi}$  were also calculated using eqn2,9 and eqn2.10 on each separator values.

Table 2.3a: Well-5 Weight, Heating Value and Specific Gravity Estimation

<i>Natural Gas Components</i>	<i>% Mole yi</i>	<i>Mass, g Mi</i>	<i>Weight yi Mi</i>	<i>(GHV)i Btu/scf</i>	<i>Net Heat yi (GHV)i</i>
CO2	0.0285	44.01	1.4171	-	-
H2S	-	34.08	-	-	-
N2	0.0058	28.01	0.1625	-	-
C1	0.8387	16.04	13.4527	1007.7	808.9816
C2	0.0689	30.07	2.0718	1768.8	153.5318
C3	0.0342	44.10	1.5051	2517.4	123.3526
C4	0.0160	55.14	0.8822	3257.4	72.6400
C5	0.0052	72.20	0.3754	4071.8	11.4010
C6+	0.0042	86.12	0.3617	4886.2	12.2155
H2O	-	18.08	-	-	-
	1.0000	-	20.8301	-	1182.1225

Table 2.3b: Well-6 Weight, Heating Value and Specific Gravity Estimation

<i>Natural Gas Components</i>	<i>% Mole yi</i>	<i>Mass, g Mi</i>	<i>Weight yi Mi</i>	<i>(GHV)i Btu/scf</i>	<i>Net Heat yi (GHV)i</i>
CO2	0.0322	44.01	1.2543	-	-
H2S	-	34.08	-	-	-
N2	0.0013	28.01	0.0364	-	-
C1	0.8028	16.04	12.8769	1007.7	845.1580
C2	0.0868	30.07	2.6101	1768.8	121.8703
C3	0.0490	44.10	2.1565	2517.4	86.0951
C4	0.0223	55.14	1.2296	3257.4	52.1184
C5	0.0068	72.20	0.4910	4071.8	21.1734
C6+	0.0025	86.12	0.2153	4886.2	20.5220
H2O	-	18.08	-	-	-
	1.0000	-	20.2285	-	1146.9372

Table 2.3c: Well-7 Weight, Heating Value and Specific Gravity Estimation

<i>Natural Gas Components</i>	<i>% Mole yi</i>	<i>Mass, g Mi</i>	<i>Weight yi Mi</i>	<i>(GHV)i Btu/scf</i>	<i>Net Heat yi (GHV)i</i>
CO2	0.0051	44.01	0.2245	-	-
H2S	-	34.08	-	-	-
N2	0.0013	28.01	0.0364	-	-
C1	0.8537	16.04	13.6933	1007.7	860.2735
C2	0.0670	30.07	2.0147	1768.8	118.5096
C3	0.0409	44.10	1.8037	2517.4	102.9517
C4	0.0221	55.14	1.2186	3257.4	71.9885
C5	0.0099	72.20	0.7148	4071.8	40.3108
C6+	-	86.12	-	4886.2	-
H2O	-	18.08	-	-	-
	1.0000	-	19.7060	-	1194.0441

**Table 2.3d: Well-8 Weight, Heating Value and Specific Gravity Estimation**

Natural Gas Components	% Mole $y_i$	Mass, g $M_i$	Weight $y_i M_i$	(GHV) $_i$ Btu/scf	Net Heat $y_i$ (GHV) $_i$
CO2	0.0122	44.01	0.5369	-	-
H2S	-	34.08	-	-	-
N2	0.0013	28.01	0.0364	-	-
C1	0.8896	16.04	14.2692	1007.7	896.4499
C2	0.0526	30.07	1.5817	1768.8	93.0389
C3	0.0270	44.10	1.1907	2517.4	67.9698
C4	0.0114	55.14	0.6286	3257.4	37.1344
C5	0.0031	72.20	0.2238	4071.8	12.6226
C6+	0.0028	86.12	0.2411	4886.2	13.6814
H2O	-	18.08	-	-	-
	1.0000	-	18.7084	-	1117.8970

**Table 2.3e: Well-9 Weight, Heating Value and Specific Gravity Estimation**

Natural Gas Components	% Mole $y_i$	Mass, g $M_i$	Weight $y_i M_i$	(GHV) $_i$ Btu/scf	Net Heat $y_i$ (GHV) $_i$
CO2	0.0165	44.01	0.7262	-	-
H2S	-	34.08	-	-	-
N2	0.0008	28.01	0.0224	-	-
C1	0.8977	16.04	14.3991	1007.7	904.6023
C2	0.0395	30.07	1.1878	1768.8	69.8676
C3	0.0264	44.10	1.1642	2517.4	66.4594
C4	0.0120	55.14	0.6617	3257.4	39.0888
C5	0.0035	72.20	0.2527	4071.8	14.2513
C6+	0.0036	86.12	0.3100	4886.2	17.5903
H2O	-	18.08	-	-	-
	1.0000	-	18.7241	-	1111.8697

$$\text{Gas Weight, } M_{pgi} = \sum(y_i M_i) \text{ g} \tag{2.5}$$

$$\text{Gross Heating Value, (GHV)}_{pg} = \sum y_i (\text{GHV})_i \text{ MBtu/scf} \tag{2.6}$$

$$\gamma_{pgi} = \frac{\sum(y_i M_i)}{M_{air}} = \frac{\sum_1^n (y_i M_i)}{29} = 0.69 \tag{2.7}$$

$$\text{Gas Density, } \gamma_{pg} = \frac{\sum(y_i M_i)}{M_{air}} = \frac{\sum(y_i M_i)}{29} \tag{2.8}$$

**West African Gas Pipeline Average Gas Values**

$$M_{gp} = \frac{\sum_1^n (y_i M_i)}{n_w} = \frac{20.8301 + 20.2285 + 19.7060 + 18.7084 + 18.7241}{5} = 20.13 \tag{2.9}$$

$$(\text{GHV})_{gp} = \frac{\sum_1^n y_i (\text{GHV})_i}{n_w} = \frac{1182.1225 + 1146.9372 + 1194.0441 + 1117.8970 + 1111.8697}{5} = 1150.5741 \text{ MBtu/scf} \tag{2.10}$$

**2.2.3 Calculation of the Niger Delta Gas Average Values**

Average values of Weight ( $M_{gi}$ ), Gross Heating Value ( $(\text{GHV})_i$ ) and Specific Gravity ( $\gamma_{gi}$ ) were calculated using the mean values from stages-separators and West African Gas Pipeline (WAGPS) system.

$$M_g = \frac{1}{n} \sum_1^n (y_i M_i) = \frac{1}{2} [(y_i M_i)_s + (y_i M_i)_p] = 19.883 \text{ g} = 0.02 \text{ Kg/scf}$$

$$\gamma_g = \frac{\sum_1^n (y_i M_i)}{M_{air}} = \frac{1}{2} \frac{[(y_i M_i)_s + (y_i M_i)_p]}{29} = 0.69$$

$$(GHV)_g = \frac{\sum_1^n y_i(GHV)_i}{n_w} = \frac{1}{n_w} [y_i(GHV)_s + y_i(GHV)_p] = 1117.8 \text{Btu/scf}$$

$$= 1.12 \text{ MBtu/scf}$$

**2.3 Development of the Natural Gas Fractions Evaluation Models**

Using separators weight values (Well-1 to Well-4), the percentage weight of LPG and gross heating values of LNP and condensate were obtained. Similarly using the WAGPS weight values (Well-5 to Well-9), the percentage weight of LPG, gross heating values of LNP and condensate were also obtained. Conventionally the means of the gas lines were calculated.

**Separator Gas Lines (Well-1 to Well-4)**

LPG:  $\% M_g = \frac{\sum_1^n \% M_{gi}}{n} = \frac{\% M_{g1} + \% M_{g2} + \% M_{g3} + \dots + \% M_{gn}}{n} = 10.75\%$  [2.11]

LNG:  $\%(GHV)_g = \frac{\sum_1^n \%(GHV)_{gi}}{n} = 86.75\%$  [2.12]

CONDENSATE:  $\%(GHV)_c = \frac{\sum_1^n \%(GHV)_{ci}}{n} = 1.71\%$  [2.13]

**WAGPS (Well-5 to Well-9)**

LPG:  $\% M_g = \frac{\sum_1^n \% M_{gi}}{n} = \frac{\% M_{g1} + \% M_{g2} + \% M_{g3} + \dots + \% M_{gn}}{n} = 12.47\%$

LNG:  $\%(GHV)_g = \frac{\sum_1^n \%(GHV)_{gi}}{n} = 84.77\%$

CONDENSATE:  $\%(GHV)_c = \frac{\sum_1^n \%(GHV)_{ci}}{n} = 2.28\%$

**Niger Delta Natural Fractionation Ratio (G<sub>fn</sub>)**

LPG:  $G_{fn} = \frac{1}{n} \sum_1^n M_{gi} = \frac{1}{2} [M_{gs} + M_{gw}] = 11.61 \% M_g$  [2.14]

LNG:  $G_{fn} = \frac{1}{n} \sum_1^n \%(GHV)_i = \frac{1}{2} [\%(GHV)_{gs} + \%(GHV)_{gw}]$  [2.15]

COND :  $G_{fn} = \frac{1}{n} \sum_1^n \%(GHV)_i = \frac{1}{2} [\%(GHV)_{cs} + \%(GHV)_{cw}] = 2.28 \% \text{MBtu}$  [2.16]  
 $= 85.76 \% \text{MBtu}$

**2.4 Revenue from the Proceeds of Natural Gas Fractionation**

**Procedure**

- Daily Natural Gas Volume, V<sub>g</sub>, MMscf, Market Sale Price, S<sub>G</sub> and Inflection, F<sub>in</sub> = 8%
- Market Modifying Factor, X<sub>G</sub> = 1.0 for sweet Gas and 0.9 for Sour Gas
- Average or conventional modifier, X<sub>G</sub> = 0.95 since Nigeria gas is sweet
- Natural Gas Fraction Ratio, G<sub>fn</sub> = 85.76%V<sub>g</sub> for LNG, G<sub>fn</sub> = 11.61%V<sub>g</sub> for LPG and G<sub>fn</sub> = 2.28%V<sub>g</sub> for Condensate
- Nigerian Gas Heating Value, H<sub>v</sub> = 1.12 MBtu and Weight of Gas, M<sub>g</sub> = 0.02 Kg

**General Revenue generating Evaluation Models for Condensate (liquid) in the Niger Delta**

$$\left[ \begin{matrix} \text{Revenue} \\ \text{unit time} \end{matrix} \right] = \left[ \begin{matrix} \text{Market} \\ \text{Modifier} \end{matrix} \right] \left[ \begin{matrix} \text{Inflection} \\ \% \text{ Value,} \end{matrix} \right] \left[ \begin{matrix} \text{Gas} \\ \text{Ratio} \end{matrix} \right] \left[ \begin{matrix} \text{Volume} \\ \text{of Gas} \end{matrix} \right] \left[ \begin{matrix} \text{Gas} \\ \text{Price} \end{matrix} \right] \left[ \begin{matrix} \text{Heating} \\ \text{Value} \end{matrix} \right]$$

$$\text{Rev} = [X_G] * [F_{in}] S_G * [G_{fn}] V_g * [H_v] \quad [2.17]$$

$$= [0.95] * [1 - 0.08] S_G * [0.0228] V_g * [1.12]$$

$$\text{Rev} = 0.023 V_g S_G \quad [2.18]$$

**General Revenue generating Evaluation Models for LNG in the Niger Delta**

$$\left[ \begin{matrix} \text{Revenue} \\ \text{unit time} \end{matrix} \right] = \left[ \begin{matrix} \text{Market} \\ \text{Modifier} \end{matrix} \right] \left[ \begin{matrix} \text{Inflection} \\ \% \text{ Value,} \end{matrix} \right] \left[ \begin{matrix} \text{Gas} \\ \text{Ratio} \end{matrix} \right] \left[ \begin{matrix} \text{Volume} \\ \text{of Gas} \end{matrix} \right] \left[ \begin{matrix} \text{Gas} \\ \text{Price} \end{matrix} \right] \left[ \begin{matrix} \text{Heating} \\ \text{Value} \end{matrix} \right]$$

$$\text{Rev} = [X_G] * [F_{in}] S_G * [G_{fn}] V_g * [H_v] \quad [2.19]$$

$$= [0.95] * [1 - 0.08] S_G * [0.8576] V_g * [1.12]$$

$$\text{Rev} = 0.8395 V_g S_G \quad [2.20]$$

**Revenue generating Evaluation Models for Cooking Gas in the Niger Delta**

$$\left[ \begin{matrix} \text{Revenue} \\ \text{unit time} \end{matrix} \right] = \left[ \begin{matrix} \text{Market} \\ \text{Modifier} \end{matrix} \right] \left[ \begin{matrix} \text{Inflection} \\ \% \text{ Value,} \end{matrix} \right] \left[ \begin{matrix} \text{Gas} \\ \text{Ratio} \end{matrix} \right] \left[ \begin{matrix} \text{Volume} \\ \text{of Gas} \end{matrix} \right] \left[ \begin{matrix} \text{Gas} \\ \text{Price} \end{matrix} \right] \left[ \begin{matrix} \text{Wieht} \\ \text{of Gas} \end{matrix} \right]$$

$$\begin{aligned} \text{Rev} &= [X_G] * [F_{in}]S_G * [G_{fn}]V_g * [M_g] & [2.21] \\ &= [0.95] * [1 - 0.08]S_G * [0.1161]V_g * [0.02] \end{aligned}$$

$$\text{Rev} = 0.00203 V_g S_G \quad [2.22]$$

**2.5 Models Applications using Daily Gas Volume Assumptions**

- Daily Gas Supply and Demand is between 1 to 250MMscf/d
- The revenue inflection is only 8%
- Taxation: Income tax is 10% of the Revenue and State tax is 8% of the Revenue
- Capital Expenses (CAPEX) and Operation Expenses (OPEX) must be calculated
- Overhead is 10% of the OPEX and amortization must be calculated with a Bank
- CAPEX value is the loan obtained from a bank to set up the business, so it is the amortization value.

**Economic Values from the Proceeds of Natural Gas Fractionation**

The estimation of revenue generation from the proceeds accounts for the business income before taxation. Raw LNG is mainly for export selling at USD2.5/SCF or as heating value,  $H_v = USD11/MBtu$ . In domestic utilization heating value is for electricity generation using LNG or condensate in power base plants selling at N16.44/MBtu. LPG is used as cooking gas selling at N200/Kg. These are the current prices of natural gas proceeds from the fractionation components.

Table 2.5: Models Applications using Daily Gas Volume

Daily Gas Volume $V_g$ , MMscf	Fraction	Evaluation Model	Unit Price $S_G$ ,	Revenue	
				Internal ₦ * 10 <sup>6</sup>	Export USD * 10 <sup>6</sup>
50	LNG	Rev = 0.8395 $V_g S_G$	USD2.5/SCF	-	104.94
	LPG	Rev = 0.00203 $V_g S_G$	N200/Kg	20.30	-
	Condt	Rev = 0.0230 $V_g S_G$	N16.44/MBtu	18.91	-
<b>Total</b>				<b>40.21</b>	<b>104.94</b>
100	LNG	Rev = 0.8395 $V_g S_G$	USD2.5/SCF	-	209.88
	LPG	Rev = 0.00203 $V_g S_G$	N200/Kg	40.60	-
	Condt	Rev = 0.0230 $V_g S_G$	N16.44/MBtu	37.81	-
<b>Total</b>				<b>78.41</b>	<b>209.88</b>
150	LNG	Rev = 0.8395 $V_g S_G$	USD2.5/SCF	-	314.81
	LPG	Rev = 0.00203 $V_g S_G$	N200/Kg	60.90	-
	Condt	Rev = 0.0230 $V_g S_G$	N16.44/MBtu	56.72	-
<b>Total</b>				<b>117.62</b>	<b>314.81</b>
200	LNG	Rev = 0.8395 $V_g S_G$	USD2.5/SCF	-	419.75
	LPG	Rev = 0.00203 $V_g S_G$	N200/Kg	81.20	-
	Condt	Rev = 0.0230 $V_g S_G$	N16.44/MBtu	75.62	-
<b>Total</b>				<b>156.82</b>	<b>419.75</b>
250	LNG	Rev = 0.8395 $V_g S_G$	USD2.5/SCF	-	524.69
	LPG	Rev = 0.00203 $V_g S_G$	N200/Kg	101.50	-
	Condt	Rev = 0.0230 $V_g S_G$	N16.44/MBtu	94.53	-
<b>Total</b>				<b>196.03</b>	<b>524.69</b>

**III. Results and Discussion**

**Results**

Table 3.1 shows the Niger Delta average gas Weight ( $M_{gi}$ ), Gross Heating Value ( $GHV_i$ ) and Specific Gravity ( $\gamma_{gi}$ ). Table 3.2 shows the Niger Delta fractionation components ratios in percentages. Table 3.3 shows the developed models for estimation of revenue generation from the proceeds of the Niger Delta natural gas system. Table 3.4 shows the application of the models on daily gas demand and supply results estimated before tax. Figure 3.1 shows the graphical representation of daily gas (export, USD/day and domestic utilization, ₦/day) revenue generation from the proceeds.

Table 3.1: Niger Delta Natural gas average Values

Value	Gas Weight ( $M_{gi}$ ), Kg/SCF	Gross Heating Value ( $GHV_i$ ), MBtu/SCF	Specific Gravity ( $\gamma_{gi}$ )
	0.02	1.12	0.69

Table 3.2: Ratios of the Niger Delta Natural Gas Fractionation Components

components	Liquefied Natural Gas (LNG)	Liquefied Petroleum Gas (LPG)	Condensate (Liquid)
Ratio	85.76%	11.61%	2.28%

Table 3.3: Revenue Estimation Models from the proceeds of the Niger Delta natural gas

Equation	Component	Evaluation Model
2.18	Condensate (Liquid)	Rev = 0.0230 $V_g S_G$
2.20	Liquefied Natural Gas (LNG)	Rev = 0.8395 $V_g S_G$
2.22	Liquefied Petroleum Gas (LPG)	Rev = 0.00203 $V_g S_G$

Table 3.4: Results of Revenue from Proceeds Using the Gas Fractionation Models

Daily Gas Volume $V_g$ , MMscf/d	Domestic Utilization Revenue, ₦ * 10 <sup>6</sup> /d	Gas for Export Revenue, USD * 10 <sup>6</sup>
0	0	0
5	4.02	10.49
10	7.84	20.99
15	11.76	31.48
20	15.58	41.98
25	19.60	53.47
30	23.52	62.96
35	27.44	73.46
40	31.36	83.95
45	35.29	94.44
50	40.21	104.94
100	78.41	209.88
150	117.62	314.81
200	156.82	419.75
250	196.03	524.69

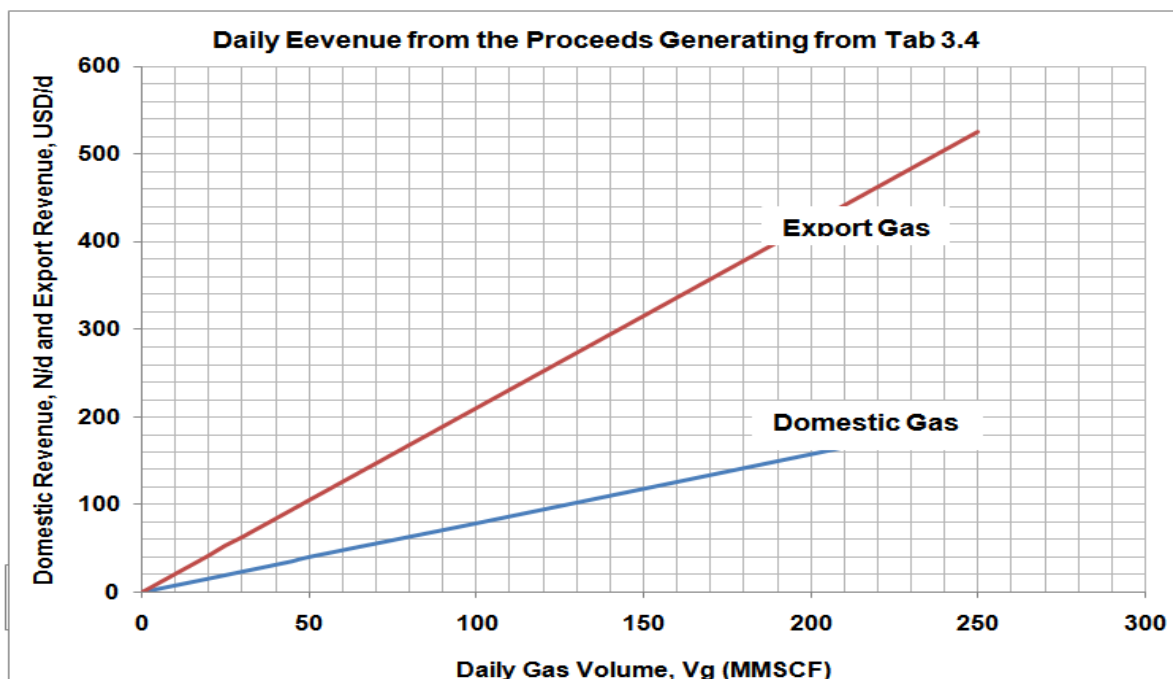


Fig 3.1: Daily Revenue from Proceeds Using the Gas Fractionation Models

### Discussion

The average values calculated on Table 3.1 show that Niger Delta natural gas weight is 0.02Kg/scf, heating value is 1.12MBtu/scf and the specific gravity is 0.69. The resulted ratio of the Niger Delta natural gas fractionation components on Table 3.2 shows that LNG is 85.76%, LPG is 11.61% and condensate (liquid) is 2.28%. Revenue estimation evaluation models on Table 3.4 are fractionation components for triple utilization of natural gas of a Nation. This enhances industrialization system. Figure 3.1 shows that economic values of both domestic gas utilization and export gas could be estimated base on daily natural gas volume supplied. Using table 3.1 and table 3.2 the average weight is 0.02Kg and 11.61% of this is the cooking gas (LPG), Average heating value is 1.12MBtu, 85.76% of this is LNG and 2.28 of this is condensate (liquid)

## IV. Conclusion and Recommendations

### Conclusion

Models for estimation of revenue from the proceeds of natural gas fractionation components in the Niger Delta were developed. This was possible using the natural gas average values gas weight, heating value, specific gravity and the ratio of the gas fractions components were first calculated. Natural gas fractionation components models in the Niger Delta enhance economic values estimation from the proceeds of natural gas of the nation. The yearly revenue depends on the demand and supply and the economic value depends on the CAPEX, OPEX and government taxation policy. The importance of this work is to enhance estimation of revenue of the proceeds from natural gas fractionation in the Niger Delta. The revenue value is the business income.

### Recommendations

This research did not work on yearly revalue, capital expenses (CAPEX) or operation expenses (OPEX) for business formation, so I recommend that economic models be developed for estimating yearly revenue of the proceeds from gas fractionation components in the Niger Delta. This will encourage many investors into gas business in Nigeria.

## REFERENCES

- [1] **Udie, A. C. and Nwankaudu, S. M., (2016)** "Models for Natural Gas Fractionation in Nigeria for Diversifying Utilization" futo Journals Series Vol-1, issue 2, Feb., 2016.
- [2] **Rankine, W. J. M., (Mid-19th century)**, "A British Physicist and Engineer, 1820-1872" designed an absolute temperature scale in which each degree equals one degree on the Fahrenheit scale, with the freezing point of water being 491.67° and its boiling point 671.67°.
- [3] **Baryon Cycly, (Mid-20<sup>th</sup> Century)** "Subatomic particle that undergoes strong interactions", with a mass greater than or equal to that of the proton, and consists of three quarks. Here It is a gas turbine using compression skid, combustion skid and exhaust unit, releasing heat for electrical generation.
- [4] **National Petroleum Council, NPC, (1984)** ""Economics of Enhanced oil Recovery" U. S. Report DOE/ET/12072-2 Washinton, D. C. U.S. 19 - 20
- [5] **Zanker, A. (1973)** "Estimation of NGL Recovery Tray" Chem. Eng Prog., 3th Sept., 1973. 38
- [6] **William, C. L., (1996)** "Standard Handbook of petroleum and Natural Gas Engineering" Copyright (C) 1996 by Gulf Publishing Company Houston, Texas; 319 - 325
- [7] **Johnson, J. E. and Morgan, J., (1985)** "Graphical Techniques for Process Engineering" Chem Eng Prog. V92, No.14, July, 8 1985. 72 – 83.
- [8] **Izuwa, N. C., Obah, B. and Appah, D. C. (2014)** " Optimum Gas Production in Gas Condensate Reservoirs" SPE 172453, NAICE August, 2014.
- [9] **Izuwa, N. C.,and Obah, B. (2014)** "Optimum Recovery of Condensate in Gas-Condensate Reservoirs through Gas-Cycling" Petroleum Technical Development Journal (PTDJ) and International Journal V1, Jan., 2014
- [10] **Maddox, R. N. and Morgan, R. J. (1998)** "Gas Treating and Sulfour Recovery", Vol. 4 of gas conditioning and processing series, John M. Cambell and Company, Norman, Oklahoma.
- [11] **Hauseh, G. W., (1986)** "Tower Packing in the Gas Processing Industry" 36<sup>th</sup> Cond. Conf, 3<sup>rd</sup> March, 1986, UNI-OKLa, Norman, Oklahoma.
- [12] **Hubard, R. A. (1997)** "An Independent Approach of Gas Dehydration Process" European GPA, Antwerp, Belgium.
- [13] **Brown, M. R., (1990)** "Large Capacity Separators More Suseptible to Foam Problem" Report National Tank Co. Tusla, OK, 28<sup>th</sup> Sept, 1990. 60
- [14] **Udie, A. C. Nwankuadu, M. S. and Anyadiegwu, C. I. C., (2014)** " Improving Condensate Recovery Using Water Injection Model at Dew-Point Pressure" American Journal of Engineering Research (AJER) e-ISSN : 2320-0847 p-ISSN : 2320-0936 Volume-03, Issue-02, -54 - 62 [www.ajer.org](http://www.ajer.org)

## Study the effect of cryogenic cooling on orthogonal machining Process

Arvind Kaushal<sup>1</sup>, Ajay Vardhan<sup>2</sup>, A.C.Tiwari<sup>3</sup>, S.K.Saluja<sup>4</sup>

<sup>1</sup> lecturer Department of mechanical Engineering, Indira Gandhi Engineering College Sagar(MP) , INDIA

<sup>2</sup> lecturer Department of mechanical Engineering, Rajiv Gandhi Proudyogiki Vishwavidyalaya , (BHOPAL), INDIA

<sup>3</sup> Professor Department of mechanical Engineering, Rajiv Gandhi Proudyogiki Vishwavidyalaya , (BHOPAL), INDIA

<sup>4</sup> Professor Department of mechanical Engineering, Indira Gandhi Engineering College Sagar(MP) , INDIA

**Abstract :** *In present scenario , all the manufacturing organization aims to maximize the productivity of organization in respect of all the aspect of manufacturing process, in case of machining process, it associated with various factors which affect the productivity directly in sense of tool life . Temperature, cutting forces, shear angle, work-piece surface finishing & accuracy, amount of power consumed in machining process and other thing also. All the factors might be optimized by applying effective and efficient amount of coolant throughout the process, to get desired efficiency of process. A coolant play a vital role in machining operation but which must have specific properties which have been reviewed in previous article of various student , research scholars , scientist and industrial candidates .in this research paper , we were focusing on the effect of cryogenic cooling on cutting temperature , cutting forces , chip behavior , shear angle , when alloy steel EN-8 and aluminum alloy 6061-T89 was machined by carbide cutting tool (coated & uncoated ) & applying liquid nitrogen as a coolant and observed that temperature was decreased during the machining process about 16% to 27% and cutting forces improved to 13%when the machining was performed , the same without cooling of EN-8 alloy, similarly on the other hand in case of aluminum alloy 6061-T89 , temperature was decreased to 25% to 37% and cutting force improved to 9% .*

**Key word:** *cryogenic cooling, productivity, cutting temperature, liquid nitrogen coolant, cutting forces*

### I. Introduction

Cryogenics in the context of scientific sense is usually referring to events occurring at temperature  $-153^{\circ}\text{C}$  or lower [1]. In the usual meaning of cryogenic liquids, chemicals such as liquid nitrogen, oxygen, helium, methane, carbon dioxide, ethane and argon are the area of interest. The proposed work , mainly concentrated upon liquid nitrogen (LN<sub>2</sub>) . The modern manufacturing world of producing and processing metals, offers a great variety of alternatives to produce a product demanded by the market. Turning, milling and drilling are among the most common methods exercised in order to shape and form metals to meet the requirements of the market. Myriads of factors affect the final outcome and productivity in manufacturing processes and higher demands are constantly forcing the industry to improve and optimize working methods [2]. Cutting fluids which are provided to the cutting zone in metal cutting are one of the most important elements in machining metal parts. The main purpose of cutting fluids is to provide cooling and lubrication in the cutting zone, work piece, tool or the chip [3]. They are either classified as coolants, lubricants or a chemical formulation of cutting fluids which are designed to provide both cooling and lubrication. Coolants are usually water-based solutions or water emulsions and lubricants are usually oil-based fluids. Cooling-lubrication cutting fluids are most commonly oil-based and contain dozens of chemicals which can be hazardous for the environment [4, 5]. Environmental issues and sustainability demands are growing and have become an inseparable part of modern manufacturing. The industry is being forced to come up with innovative and sustainable solutions to sustain its level of competitiveness. Using cryogenic cooling liquids is an environmentally friendly method of providing cooling and lubrication to the cutting zone. Under certain parameters, cryogenic cooling has shown clear superiority over conventional oil-based coolants with pressure additives. E.g. the cooling efficiency is normally much higher and in some cases the conventional cutting fluids fail to provide desirable control of cutting temperature due to their lack of ability to penetrate sufficiently to the chip-tool interface [6]. Research and experiments with

cryogenic gases as cooling and lubrication can be dated back to the 1950's and is still being developed by scientists today [7]. The technique has not been fully adapted by the industry but has shown some great potential within certain combination of materials, cutting tools and machining methods [5]. Among the most common materials showing promising results associated with cryogenic cooling are difficult-to-machine materials such as nickel-based alloys, titanium-based alloys and hardened steels [8, 9]. In the criteria for machinability there are usually few factors involved in the judgment. The factors are:

- Chip form
- Magnitude of cutting forces
- Vibration of machining system
- Tool wear
- Surface finish
- Dimensional deviation

These are all issues that have been proven to be influenced positively by cryogenic cooling.

### 1.1 Cryogenic technology

Several cryogenic liquids are available but for machining operations, CO<sub>2</sub> and LN<sub>2</sub> are almost exclusively used. How the liquid nitrogen ( LN<sub>2</sub> ) control the temperature rise , the complete mechanism regarding the context is given below in deep .

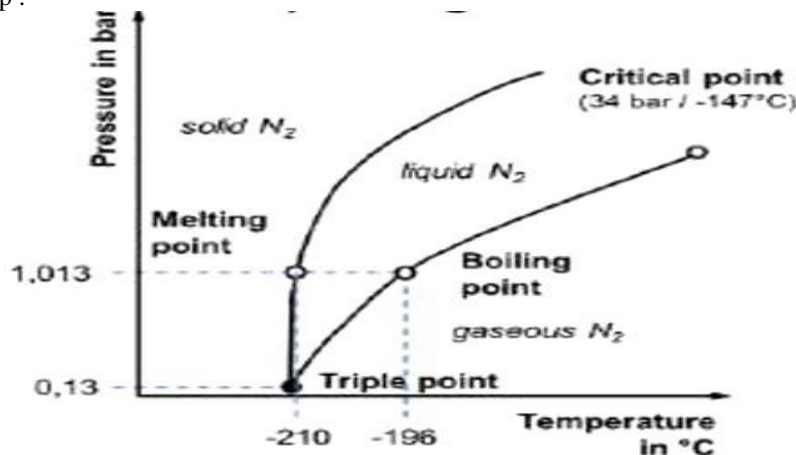


Figure -1 phase diagram for liquid nitrogen gas

### 1.2 (Liquid Nitrogen Gas) LN<sub>2</sub>

Figure -1 shows the phase diagram for LN<sub>2</sub>. The triple point, occurring at pressure 0, 13 bar and -210°C, is the state where nitrogen can be found at all forms. LN<sub>2</sub> is nitrogen in a liquid state at a very low temperature and usually stored in isolated tanks at very high pressure. When the media enters the ambient temperature and the pressure drops (1, 01325 bar), the nitrogen starts boiling at -196°C [15]. In cutting processes it absorbs the heat dissipated from the cutting process and evaporates into nitrogen gas and becomes a part of the air. It is safe non-combustible chemical and leaves no harmful residue to the environment since it becomes a part of the other 79% of nitrogen in the atmosphere [3, 16, 17]. However, in some cases when LN<sub>2</sub> comes in contact with hot surfaces it starts boiling and vaporizing, an insulating film of gas forms and surrounds the part, reducing the cooling effect [15].

## II. Literature review

Literature review provide a correct path & background for futuristic approach in the research work, following are very important review of researcher, scholars and scientist in the field of metal machining process, whose thought & ideas give us a constant guidance as well as motivation .The purpose of the application of the cutting fluids in metal cutting was stated as reducing cutting temperature by cooling and friction between the tool, chip and work piece by lubrication [6]. Chip formation and curl, which affects the size of the crater wear and the strength of the cutting tool edge, is also affected when coolant is carried out during machining. Generally, a reduction in temperature results in a decrease in wear rate and an increase in tool life. Seah et al. examined water-soluble lubricating on tool wear in turning of AISI 4340 and AISI 1045 steel with an uncoated tungsten carbide insert. They found that there was no significant difference between the cases where coolant was used and that of dry cutting. In fact, they showed that it aggravated flank and crater wear in some of the cutting

conditions [8]. It was also proved that the conventional cooling action worsened the surface roughness when compared with dry cutting [9]. The main functions of cryogenic cooling in metal cutting were defined by Hong and Zhao [28] as removing heat effectively from the cutting zone, hence lowering cutting temperatures, modifying the frictional characteristics at the tool/chip interfaces, changing the properties of the work piece and the tool material. In cryogenic pre-cooling, the work piece and chip cooling method, the aim is to cool work piece or chip to Change properties of material from ductile to brittle because, the ductile chip material can become brittle when the chip temperature is lowered [46]. Chip formation and its effect on productivity in metal cutting have been proved by Jawahir [47] and control and breaking of chips during cutting will increase performance of machining. Hong et al. [46, 50] developed a cryogen delivery system. In this system, LN2 was supplied to chip faces to improve the chip breakability. In this design, the size, shape and position of the nozzle were selected so that the LN2 jet covered the chip arc, and liquid flow was oriented parallel to the axial line of the curved chip faces. Wang and Rajurkar [54–56] designed a liquid nitrogen circulation system on the tool for conductive cooling of the cutting edge. Ahmed et al. [51] modified a tool holder with two designs for cryogenic machining. In one of their design, the discharging gas was directed away from the work piece for maintaining ductility of materials. Piling up of nitrogen below the insert and thus keeping the tool insert at low temperatures were targeted without evaporating. So, the design is suitable for conductive remote cooling of the cutting edge. Hong and Broome, LN2 was injected with three nozzles to the cutting zone; in a *\_Z* direction, parallel to the spindle axis, or in *\_X* direction, perpendicular to the spindle axis, on the tool rake face and flank face, similarly [60]. In design of Dhar et al. [61–63], LN2 jets were targeted along the rake and flank surfaces, parallel to the main and auxiliary cutting edges too. In another design, Venugopal et al. [64] used LN2 jets through a nozzle on the face and flank of the cutting tool. Zurecki et al. [57] made a tool life comparison between cryogenic nitrogen cooled Al<sub>2</sub>O<sub>3</sub>-based cutting tools and conventionally cooled CBN tools in machining of hardened steel. They applied cryogenic coolant by spraying with a nozzle to the rake surface of the tool. They found that cryogenic cooled Al<sub>2</sub>O<sub>3</sub>-based cutting tools endured longer than the conventionally cooled CBN tools. Hong et al. [95] presented an experimental sliding contact test setup on CNC turning centre composed of a carbide tool and Ti-6Al-4V titanium alloy and AISI 1018 low carbon steel disks. Their findings showed that the LN2 lubricated contact produced lower friction coefficient than the dry sliding contact and the emulsion-lubricated contact for both disk materials. Wang et al [1] have carried out turning of ceramics [Si<sub>3</sub>N<sub>4</sub>] with Polycrystalline Cubic Boron Nitride [PCBN] under cryogenic cutting conditions and reported that liquid nitrogen cooling system reduced the cutting tool temperature and tool wear over dry machining Hong and Ding [2] conducted an experiment with various cooling approaches in cryogenic machining of Ti-6Al-4V. Temperatures in cryogenic machining were compared with conventional dry cutting and emulsion cooling. It was showed that a small amount of liquid nitrogen applied locally to the cutting edge is superior to emulsion cutting in lowering the cutting temperature. Dhar and Kamruzzaman [5] conducted an experiment on cryogenic cooling and stated that benefits of cryogenic cooling are mainly by substantially reducing the cutting temperature, which improves the chip-tool interaction and maintains sharpness of the cutting edge and accuracy as compared to dry and wet machining. **Prudvi Reddy et al [1] indicate that** Cryogenic cooling result in increased in grinding ratio as well as effective cooling of grinding zone indicated by Scanning Electron Microscope (SEM), shows cryogenic cooling enhances life of grinding wheel and reduction in grinding temperatures. In an investigation of **Ranajit Ghosh et al [2]** For sinter hardened material machining, only specific type of cutting tool materials can be used like Poly Cubic Boron Nitric (PCBN). Due to conventional cooling techniques, negative effects of tool wear, deformation of tool wear, slow cutting speed, etc. were caused higher abrasive resistance and lower flank wear due to elimination of hardness of cutting tool. Improvement in life of tool was found to be 135%. In an another investigation of **D. Umbrello et al [3] he perform,** of cryogenic cooling on surface integrity on AISI 52100 steel of hard machining. Reduction in white layer formation and residual stresses due to cryogenic coolants was noticed. Cryogenic cooling helps to improve surface integrity during machining of hard components'. **Pradeep Kumar et al [4]** investigate the effect on orthogonal machining processes by liquid nitrogen (LN2) cooling. The main objective of researcher behind presenting this paper is to study the effects of cryogenic coolants on various aspects of machining on work piece such as cutting temperatures, shear angle, cutting force and chip thickness also in orthogonal manufacturing of AISI 1045 and Al 6061- T6 alloy. & concluded that Reduction in cutting temperature was found to be 19-40%. Cutting forces were increased by 10%. Chip thickness is increased by 25%. Shear angle was increased to 30%.

### Cryogenic Cooling Process

Cryogenic cooling techniques involve various methods:

- ❖ Pre cooling of work piece by cryogenic fluids
- ❖ Direct cryogenic cooling
- ❖ Indirect cryogenic cooling
- ❖ Jet cryogenic cooling

**Experimental setup**

Machining is the operation of removal of unwanted material from the block of metal to get desired shape & size as per the design specification, the overall operation is known as metal cutting throughout the machining process high heat is generated which affects the productivity directly, due to the decrease tool life, surface finishing of work piece, increase in cutting forces, friction between tool & rake face of the tool and so many other factor also. In present work alloy steel EN-8 & aluminum alloy 6061-T89, is used as test specimen whose dimension and related machining parameters are given below in table -1 when machining is going cryogenic cooling is applied through nozzle of liquid nitrogen between tool chip interface, the cryogenic cooling set up is given in figure- 2 similarly the orthogonal machining process is given in figure-3

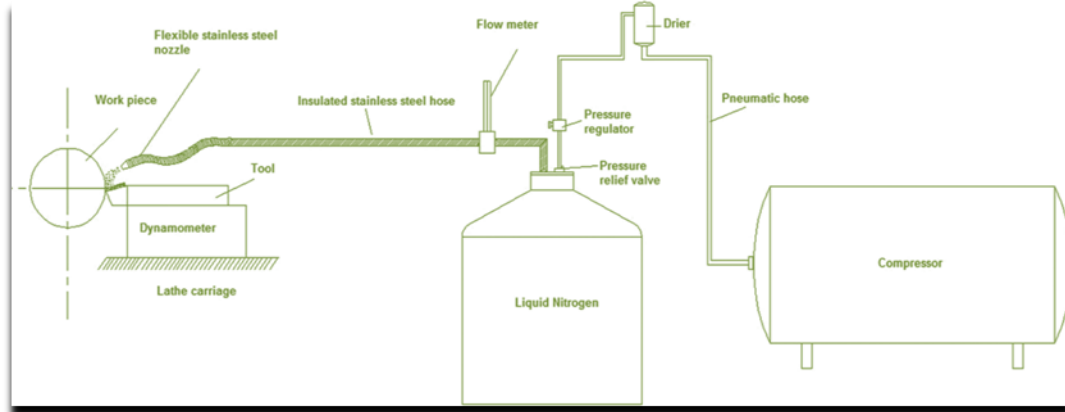


**Figure -2 cryogenic cooling setup of liquid nitrogen**

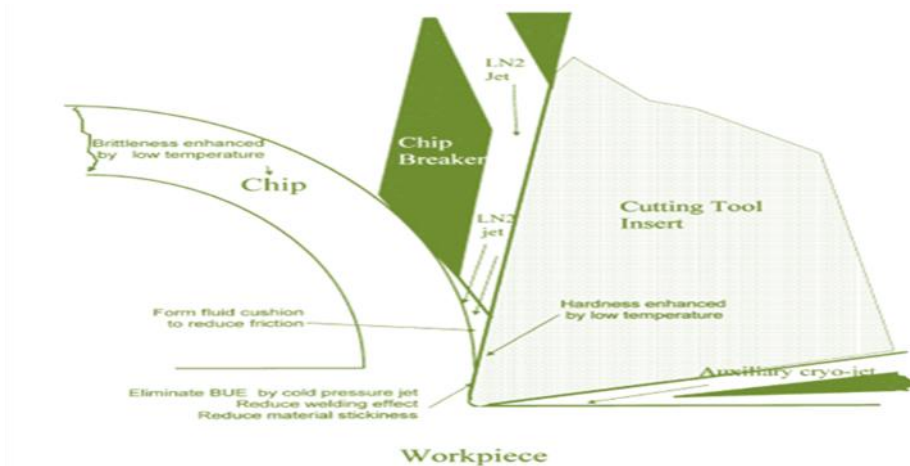


**Figure- 3 A schematic diagram of the orthogonal cryogenic machining process**

**Work – piece dimension**

<b>work-piece dimension</b>	<b>Test specimen- I</b>	<b>Test specimen- II</b>
Work-piece metal	EN-8 (ALLOY STEEL)	Aluminum alloy --6061-T89
Length of work-piece in MM	225 mm	230 mm
Diameter of work-piece in MM.	50 mm	50 mm

**Cutting tool & cutting tool parameter:-**

Tool name & cutting parameter	For test specimen-I	For test specimen-II
Cutting tool name	Carbide cutting tool	Plain carbide cutting tool
Cutting velocity (m/min)	50 and 180	50 and 180
Feed rate (mm/rev)	0.079 , 0.110 , 0.148	0.079 , 0.110 , 0.148
Coolant used	Dry cooling on tool chip interface	Dry cooling on tool chip interface
Coolant used ( Liquid Nitrogen)	Between tool chip interface	Between tool chip interface

**Table – 1 work-piece dimension & cutting tool parameter****Measuring equipment method****Cutting force measurement**

Measurement of cutting force in machining process is very complex in nature; dynamometer is used to fulfill the requirement purpose –which is piezo electric three component dynamometer

**Temperature measurement**

temperature measurement in metal machining also a very complicated & complex task , there are generally two method which is direct method and indirect method , in this case non-contact pyrometer is used which is indirect one

**Cryogenic cooling effect on temperature**

Whenever machining operation is going on , metal is being operated thus high heat is generated which affect the surface finishing as well as performance of machining operation , in order to reduce the effect of temperature we are applying liquid nitrogen as a coolant on chip tool interface whose effect is noticed and temperature is

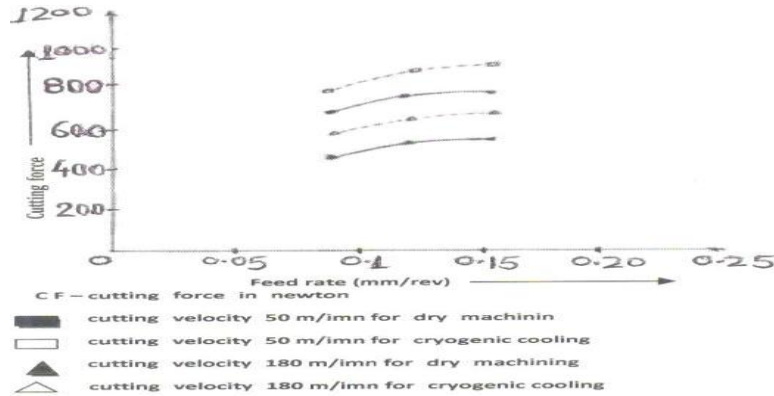
<b>Cutting velocity</b>	50	50	50	180	180	180
<b>Feed rate</b>	0.079	0.110	0.148	0.079	0.11	0.148
<b>Temperature reduced For EN-8(%)</b>	26.37	25.21	24.92	20.56	18.2	16.89
<b>Temperature reduced For 6061-T89 (%)</b>	37.12	35.65	33.13	30.52	28.4	26.98
<b>Temperature in dry machining (EN-8)</b>	130.16	120.81	129.0	104.86	105	105.92
<b>Temperature in dry machining (6061-T89)</b>	102.62	102.8	104.0	103.86	104	103.77

reduced . Summary of result is tabulated below in table-2

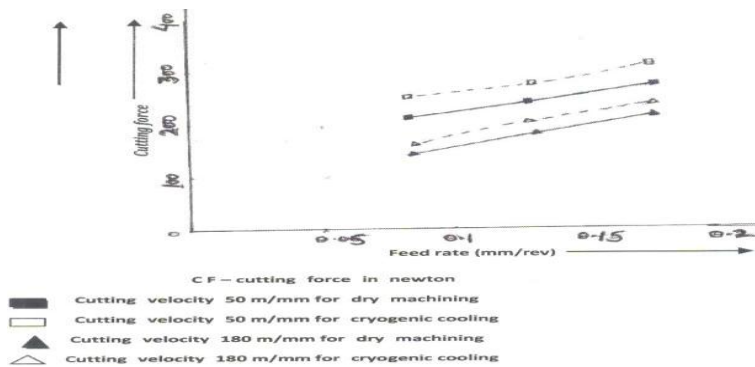
**Cutting force analyses**

During the machining operation high heat generated to overcome the high heat we applied here a liquid nitrogen as a cutting fluid whose effect is to control temperature as well as the work-piece foreign material that is removed from block of metal represent less sticky behavior and also work-piece become harder and hence increased cutting force and less sticky between tool chip interface table shows the resulting data,

Specimen material	Cutting force improved
EN-8	13%
6061-T89	9%



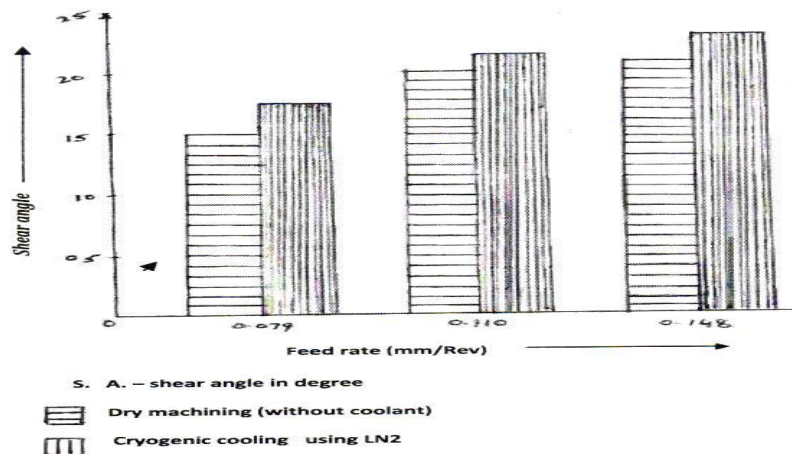
Graph -3 showing the relative position of effected forces under dry and cryogenic cooling On alloy steel EN-8



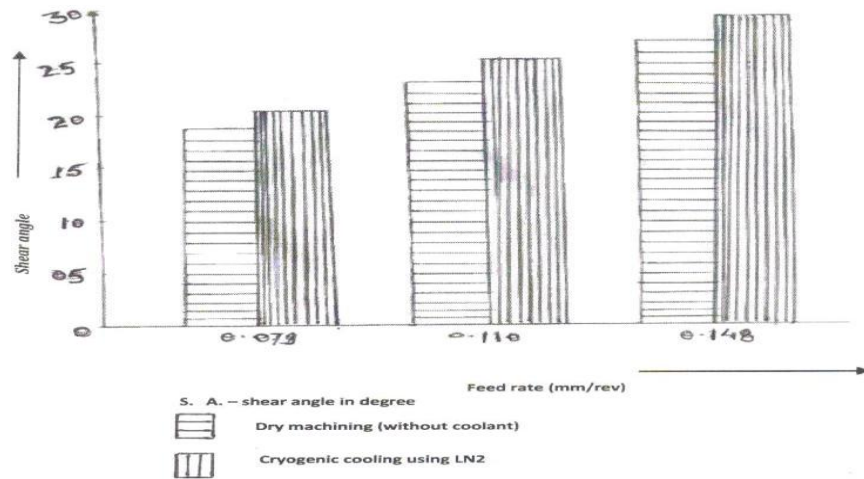
Graph -4 showing the relative position of effected forces under dry and cryogenic cooling On alloy steel 6061-T89

Analyses of shear angle variation due to the effect of cryogenic cooling

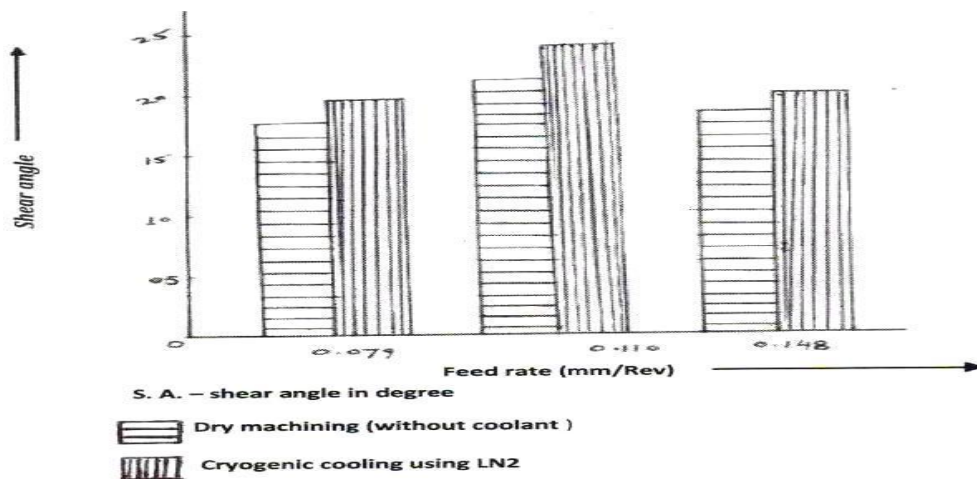
When test specimen 1 & 2 are machined, at different feed rate and cutting velocities with consideration of dry and cryogenic cooling. it is observed that shear angle is increased due to the reduction of cutting temperature in cutting zone of metal as well as dimension of chip also changed i.e. thickness is reduced , the variation of shear angle is achieved between range of 13% to 27% for test specimen- 1 & test specimen-2 respectively. And hence shear angle alteration directly affect the dimension of chip & its behavior. Graph -5 & 6 shows the relative position of shear angle variation at different feed rate & cutting speed for EN-8 alloy steel similarly graph - 7 & 8 for aluminum alloy 6061 -T89 respectively.



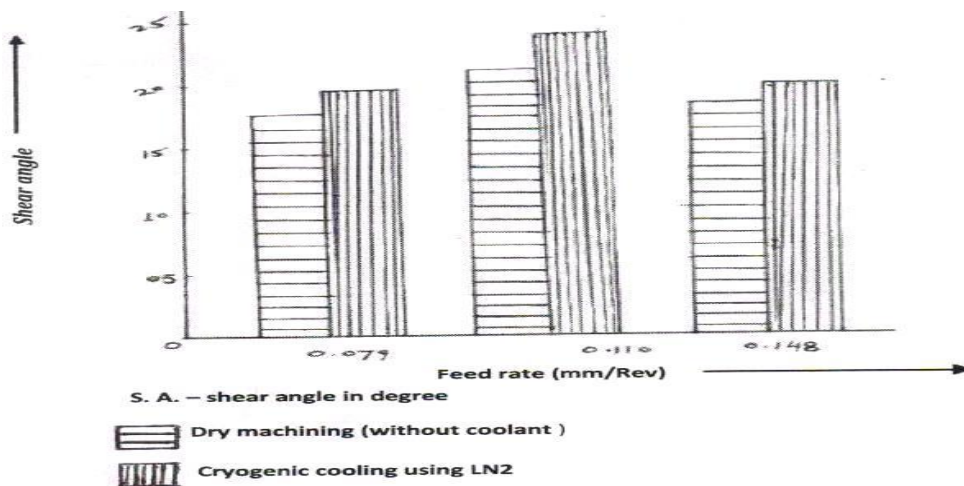
Graph - 5 shows plot between shear angle & feed rate for cutting speed 50 (m/min) when machined EN-8



Graph – 6 shows plot between shear angle & feed rate for cutting speed 180 (m/min) when Machined EN-8



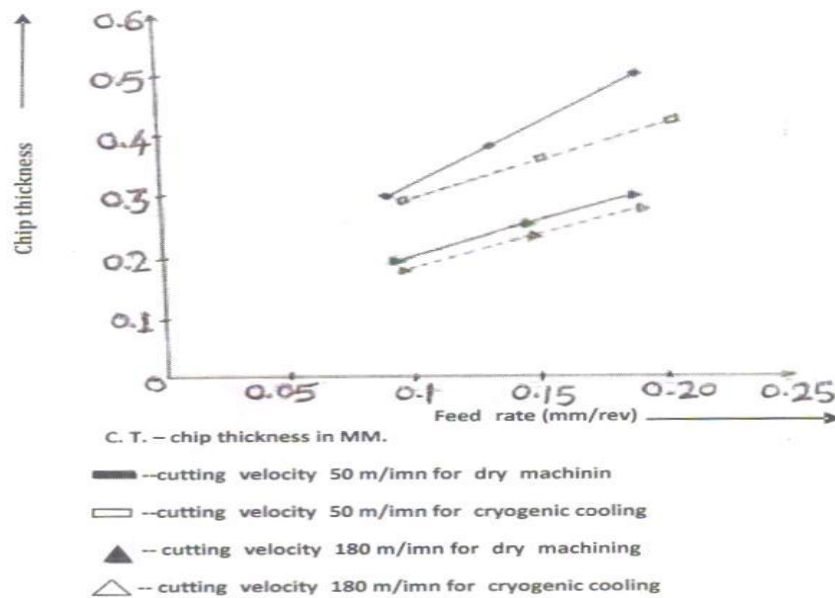
Graph – 7 shows plot between shear angle & feed rate for cutting speed 50 (m/min) when Machined Aluminum 6061-T 89



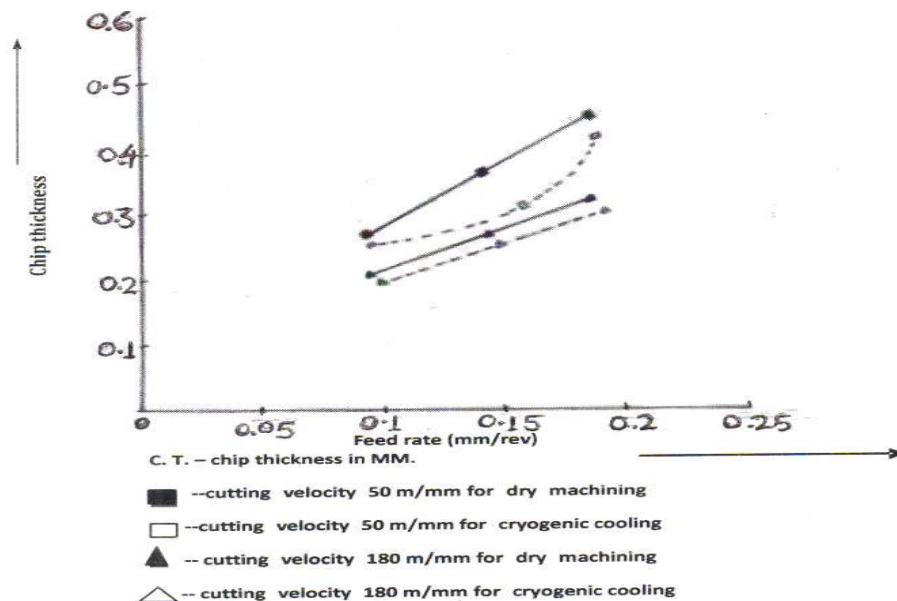
Graph – 8 shows plot between shear angle & feed rate for cutting speed 180 (m/min) when Machined Aluminum 6061-T 8

**Analyses the effect of cryogenic cooling on chip behavior**

During the machining process, high heat generation takes place when liquid nitrogen is applied it is reducing temperature, minimizing the friction at tool chip interface, thus it also work as lubricant during machining operation. The generation of high heat associated the process is responsible for chip dimension if temperature is high thickness of chip will be larger on the other hand temperature is in decreasing order then thickness will be lesser ,in other word we can say that during dry machining process thickness of chip will be larger & minimum when cryogenic cooling is provided when both test specimen machined at different feed and cutting velocity it is observed that reduction achieved between 15 % to 23 % respectively. The behavior of the chip with respect to different feed rate can be clearly understand by following graph , the graph – 9 represent the chip thickness behavior of EN- 8 alloy steel when machined at dry state and under cryogenic cooling similarly graph- 10 associated with the aluminum alloy 6064-T89.



**Graph –9 represent chip thickness V/s feed rate under dry and cryogenic cooling for EN -8**



**Graph – 10 represent chip thickness V/s feed rate under dry and cryogenic cooling for aluminum Alloy 6061–T 89**

## V. Conclusion

The above orthogonal metal machining experiment of EN – 8 & Aluminum alloy 6061 – T 89 is performed under the dry state and the cryogenic cooling state , with respect to the study following conclusion is comes on the front line .

- Machinability of any metal is depends upon the various factor like cutting velocity , feed , depth of cut & characteristic's of work piece material , throughout the machining process high heat generated when we put the coolant it can be limited , if cryogenic cooling is perform by LN<sub>2</sub> temperature is reduced about 16 % to 27% . the temperature of variation depends upon the value of cutting parameter.
- The value of associated cutting cutting forces is increased by 13% and 9% if cryogenic cooling is done for alloy steel EN-8 & aluminum alloy 6061 –T 89 respectively.
- The chip thickness is reduced about 15 % to 23% in respect of dry machining state of EN – 8 & AL-6061 T89.
- The shear angle variation by cryogenic cooling is achieved about range of 13% to 27% for respective test specimens

## Acknowledgement

This work is carried out with the assistance of **Indira Gandhi Government Engineering College Sagar (MP)**, I am very thankful to all the respected faculty member of department as well as colleagues

## References

- [1] Wang, K.P. Rajurkar, and M. Murugappan, "Cryogenic PCBN turning of ceramics (Si<sub>3</sub>N<sub>4</sub>)," *Wear*, Vol. 195, pp 1-6, 1996. Z.Y.
- [2] Shane Y. Hong and Yucheng Ding, "Cooling approaches and cutting temperatures in cryogenic machining of Ti-6Al 4V," *International Journal of Machine Tools and Manufacture*, Vol. 41, pp. 1417-1437, 2001.
- [3] Shane Y. Hong, Yucheng Ding and Woo-cheol jeong, "Friction and cutting forces in cryogenic machining of Ti- 6Al-4V," *International Journal of Machine Tools and Manufacture*, Vol. 41, pp. 2271- 2285, 2001.
- [4] N.R. Dhar, S. Paul and A.B. Chattopadhyay, "Machining of AISI 4140 steel under cryogenic cooling – tool wear, surface roughness and dimensional deviation," *Journal of Materials Processing technology*, Vol. 123, pp. 483-489, 2002.
- [5] N.R. Dhar and M. Kamruzzaman, "Cutting temperature, tool wear, surface roughness and dimensional deviation in turning AISI-4037 steel under cryogenic condition," *International Journal of Machine Tools and Manufacture*, Vol. 47, pp. 754-759, 2007.
- [6] K. A. Venugopal, S. Paul and A.B. Chattopadhyay, "Growth of tool wear in turning of Ti-6Al-4V alloy under cryogenic cooling," *Wear*, Vol. 262, pp. 1071-1078, 2007
- [7] A.R. Machado, J. Wallbank, Machining of titanium and its alloys: a review, *Proc. Inst. Mech. Eng.* 204 (1990) 53.
- [8] P.D. Hartung, B.M. Kramer, Tool wear in titanium machining, *Ann. CIRP* 31 (1982) 75–80.
- [9] M.J. Donachie Jr., in: ASM (Ed.), *Titanium, a Technical Guide*, 1982, p. 163.
- [10] R. Komanduri, B.F. von Turkovich, New observation on the mechanism of chip formation when machining titanium alloys, *Wear* 69 (1981) 179–188.
- [11] E.H. Rennhack, N.D. Carlsted, Effect of temperature on the lathe machining characteristics of Ti-6-4, in: *Ann. Trans. Technol. Conf.*, 1974, p.
- [12] Prudvi Redd grinding of hardened bearing steels". *Procedia Material Science* 5 (2014) 2622- 2628y P, A. Ghosh: "Effect of cryogenic cooling on spindle power and G-ratio in
- [13] RanajitGhosh, Bruce Lindsley: "Role of Cryogenic cooling in machining of sinter Hardened materials
- [14] D. Umbrello, Z. Pu, S. Caruso J. C. quteiro, A.D. Jayal, O.W. Dillon Jr. I.S. Jawahir: "effects of cryogenic cooling on surface integrity of hard machining *Procedia Engineering* 19 (2011) 371 -376
- [15] M. Dhananchezein, M. Pradeep Kumar, A. rajadurai: "Experimental investigation of Cryogenic cooling by liquid nitrogen in the orthogonal machining process"
- [16] S. Y. Hong, Economical and ecological cryogenic machining, *Journal of Manufacturing Science and Engineering* 123 (2) (2001) 331–338
- [17] A.B. Chattopadhyay, A. Bose, A.K. Chattopdhyay, Improvements in grinding steels by Cryogenic cooling, *Precision Engineering* 7 (2) (1985) 93–98.
- [18] S. Paul, A.B. Chattopadhyay, Effects of cryogenic cooling by liquid nitrogen jet on forces, temperature and surface residual stresses in grinding, *Cryogenics* 35 (8) (1995) 515–523.
- [19] S. Paul, A.B. Chattopadhyay, The effect of cryogenic cooling on grinding forces, *International Journal of Machine Tools and Manufacture* 36 (1) (1996) 63–72
- [20] S. Paul, A.B. Chattopadhyay, Environmentally conscious machining and grinding with Cryogenic with cryogenic cooling, *Machining Science and Technolog*10 (2006) 87– 131.
- [21] Dhar, N.R., Kamruzzamanb, M. (2007) Cutting temperature, tool wear, surface roughness and dimensional deviation in turning AISI-4037 steel under cryogenic condition, *International Journal of Machine Tools & Manufacture*, vol. 47, p. 754-759.
- [22] S.Hong, Economical and ecological cryogenic machining, *J. Manuf. Sci. Eng.* 123(2001)
- [23] Hong, S., Cryogenic machining, US Patent No. 5,901,623, May 11, 1999
- [24] K. Uehara, S. Kumagai, Chip formation, surface roughness and cutting force in cryogenic Machining, *Ann. CIRP* 17 (1968) 409.
- [25] Yong SY, Zhao Z (1999). Thermal aspects, material considerations and Cooling strategies in cryogenic machining. *Clean Products and Processes* 1: 107-116.
- [26] S.Y. Hong, Y. Ding, Micro-temperature manipulation in cryogenic machining of low carbon Steel, *Journal of Materials Processing technology* 116 (2001) 22–30.
- [27] M.B. Silva, J. Wall bank, Cutting temperature: prediction and measurement methods— a review, *Journal of Materials Processing Technology* 88 (1999) 195–202.

## Variation of stresses at different nodal points in a isotropic beam using ANSYS

Shabbir Ahmed Osmani<sup>1</sup>

<sup>1</sup>Department of Civil Engineering, Leading University, Sylhet, Bangladesh.

**ABSTRACT:** Compression and tension phenomena are being developed in the analysis of beams using different approaches. Different approaches sometimes result in vary close variations with each other. The simulation software ANSYS uses the finite element concept to visualize the stress and its variation and comparison at different nodes. This paper illustrates the conditions where the bending stresses getting minimized and maximized as the changes in nodal distance. It shows that the neutral axis has the least bending stresses where the outmost fibers give the maximum. And also the theoretical calculations comply with the finite element results up to certain conditions.

**KEYWORDS:** Finite element, ANSYS, bending stress, meshing.

### I. INTRODUCTION:

A part of a structure like beams have been using in the modeling of structural finite element analysis [1]. Finite Element Analysis aims to mathematically model a physical body that cannot be solved with satisfied result by other means. And FEA is an effective method of determining the static performance of structures for three reasons which are saving in design time, cost effective in construction and increase the safety of the structure[2]. A member subjected to bending moment and shear force undergoes certain deformations. The material of the member will offer resistance or stresses against these deformations[3]. Using FEA, the mathematical modeling of the body is done by splitting the body into small and smaller parts whose performance and response can be modeled simply finite elements. FEA analysis, and the most reliable, is still the static structural analysis limited to:-

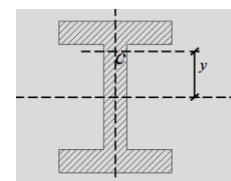
- elastic, homogeneous, isotropic materials & linear material properties
- small deflections: geometry changes can be ignored
- all material well below yield: no plastic deformation

The ANSYS 15.0 meshing application is a separate ANSYS Workbench application[4]. The Meshing application is data-integrated with ANSYS Workbench, meaning that although the interface remains separate, the data from the application communicates with the native ANSYS Workbench data. Here construction geometry is used to insert a path which means of creating a path between nodes of a meshed model. And this practice will give linearized stress in axial direction.

The theoretical flexure formula shows that

$\sigma = \frac{M y}{I}$  where  $\sigma$  is the bending stress in a particular cross section(i.e. Figure 2.1),  $M$  is the moment developed due to applied loads,  $y$  is the distance from the neutral axis to the upper(compressive) fiber or lower(tensile) fiber and  $I$  is the moment of inertia in  $xx$  direction[5][3].

Figure 2.1



The calculations are done considering a uniform rectangular cross-sectional beam of linear elastic isotropic homogeneous materials. The beam is assumed to be mass less, inextensible having developed no strains [6].

**II. BEAM ANALYSIS IN ANSYS:**

Typical section is shown in Fig. 2.1 which is to be used here.

Material = Structural steel, Modulus of Elasticity=  $29 \times 10^3$  ksi. Poisson's ratio: 0.3

**TABLE: 2.1**

Flange width	8 in	Web thickness	0.5 in
Flange thickness	0.5 in	Total height	18 in
Length of the beam	180 in		
Nonlinear Effects	Yes		

**Fig. 2.2**

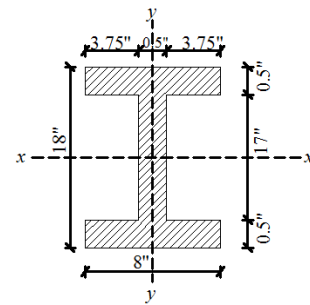


**TABLE: 2.2**

FEA by ANSYS	
Nodes	252673
Elements	54720

Now beam has been defined with four axial(cross sectional) linear paths to show its range of bending stresses. The table below shows the details:

**TABLE: 2.3**

Object Name	Axial at 90 in	Axial at 60 in	Axial at 30 in	Axial at 10 in
State	Fully Defined			
<b>Definition</b>				
Path Type	Two Points			
Path Coordinate System	Global Coordinate System			
Number of Sampling Points	47.			
Suppressed	No			
<b>Start</b>				
Coordinate System	Global Coordinate System			
Start X Coordinate	0. in			0 in
Start Y Coordinate	18. in			
Start Z Coordinate	90. in	60. in	30. in	10. in
Location	Defined			
<b>End</b>				
Coordinate System	Global Coordinate System			
End X Coordinate	0. in			0 in
End Y Coordinate	0 in			
End Z Coordinate	90. in	60. in	30. in	10. in
Location	Defined			

**III. CONFIGURATION WITH ANSYS:**

A. Location of linear paths:

In the starting of analysis the following Fig. 3.1.1, 3.1.2, 3.1.3 and 3.1.4 show that the location of axially linear path for stress analysis which complying the table 2.3.

Fig. 3.1.1: Bending stress, Axial at 90 in

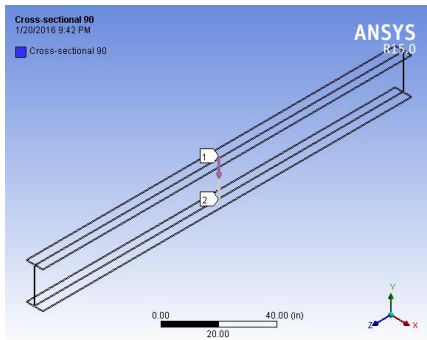


Fig. 3.1.2: Bending stress, Axial at 60 in

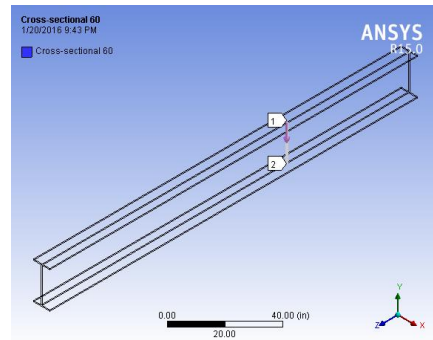


Figure 3.1.3: Bending stress, Axial at 30 in

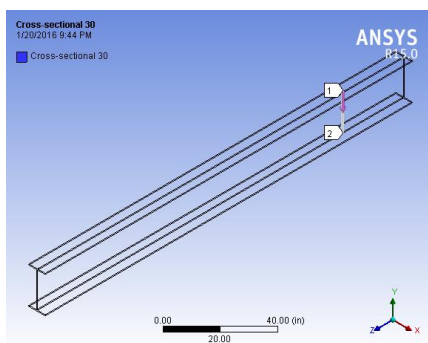
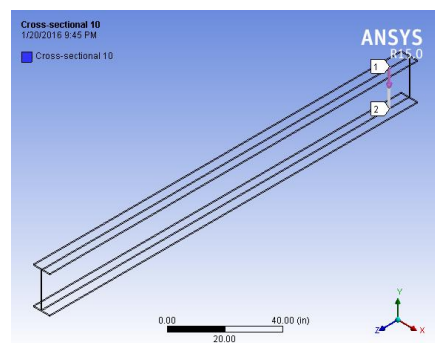


Figure 3.1.4: Bending stress, Axial at 10 in



**B: Bending stresses:**

Using the flexure formula to find out the bending stresses, here four locations are considered. First one is at 90 in., 2nd one is 60 in., 3rd one is 30 in. and 4th one is at 10 in. from the right face as shown in Fig. 3.2.1

Fig. 3.2.1 Location of stresses

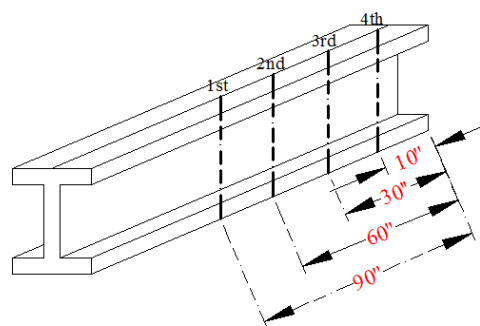


Fig. 3.2.2 to Fig. 3.2.5 shows the changes in stresses along the centroidal vertical axis in ANSYS. Here it is shown that as it moves far from the centre span, the stress varies. And more interesting thing is that the maximum stress is developed at the outer fibre in either compressive or tensile zone. But when it moves from centre either towards right or left, the bending stress decreases. And this is of course comply with the theoretical concept that the bending moment also decreases.

The table 3.1 below shows some points where comparison of stresses have been done by hand calculation and ANSYS. And the visual output have been made in Fig. 3.2.6 to Fig. 3.2.9. These Figures confirm that the stresses those developed by ANSYS, also comply with the theoretical calculation.

Fig. 3.2.2: Changes in stresses, Axial 90

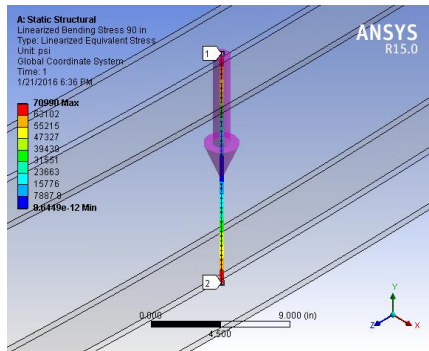


Fig. 3.2.3: Changes in stresses, Axial 60

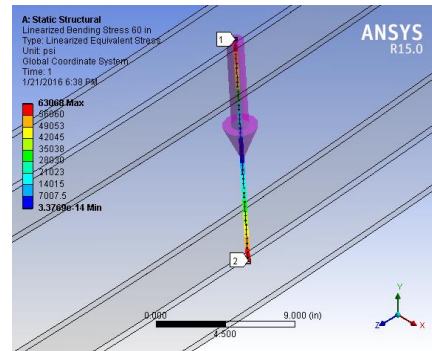


Fig. 3.2.4: Changes in stresses, Axial 30

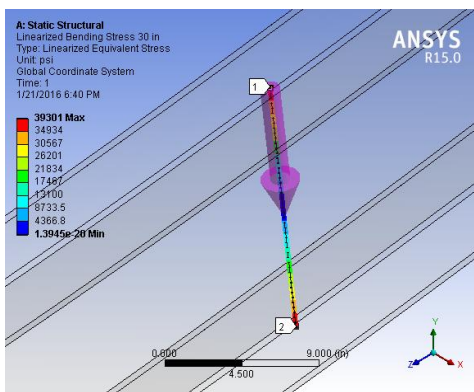


Fig. 3.2.5: Changes in stresses, Axial 10

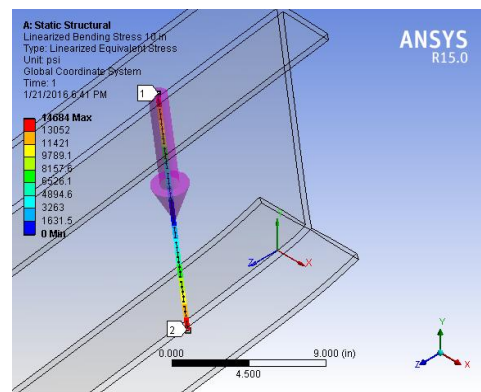


TABLE: 3.1

Distance from upper or lower fibre [in]	At 90 in		At 60 in		At 30 in		At 10 in	
	Theoretical [psi]	ANSYS [psi]						
0	71350.80	70990	63422.93	63068	39639.33	39301	14974.86	14684
1.5	59459.00	59158	52852.44	52556	33032.77	32751	12479.05	12236
2.25	53513.10	53243	47567.20	47301	29729.49	29476	11231.14	11013
3	47567.20	47327	42281.95	42045	26426.22	26201	9983.24	9789.1
3.75	41621.30	41411	36996.71	36790	23122.94	22925	8735.33	8565.5
4.5	35675.40	35495	31711.46	31534	19819.66	19650	7487.43	7341.9
5.25	29729.50	29579	26426.22	26278	16516.38	16375	6239.52	6118.2
6	23783.60	23663	21140.98	21023	13213.11	13100	4991.62	4894.6
6.75	17837.70	17748	15855.73	15767	9909.83	9825.2	3743.71	3670.9
7.5	11891.80	11832	10570.49	10511	6606.55	6550.1	2495.81	2447.3
8.25	5945.90	5915.8	5285.24	5255.6	3303.27	3275.1	1247.90	1223.6
9	0.00	0.0	0.00	0.0	0.0	0.0	0.00	0.0

Fig. 3.2.6: Comparison of stresses, Axial 90

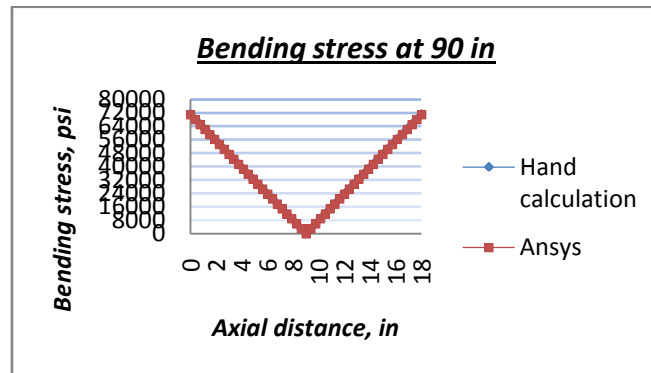


Fig. 3.2.7: Comparison of stresses, Axial 60

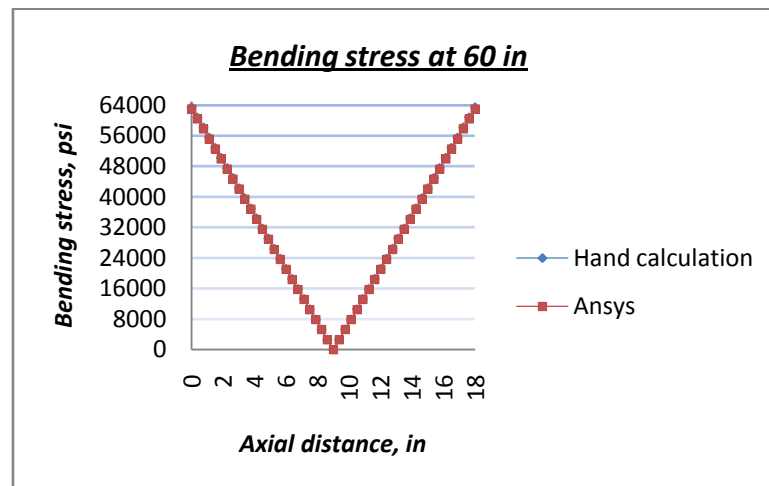


Fig. 3.2.8: Comparison of stresses, Axial 30

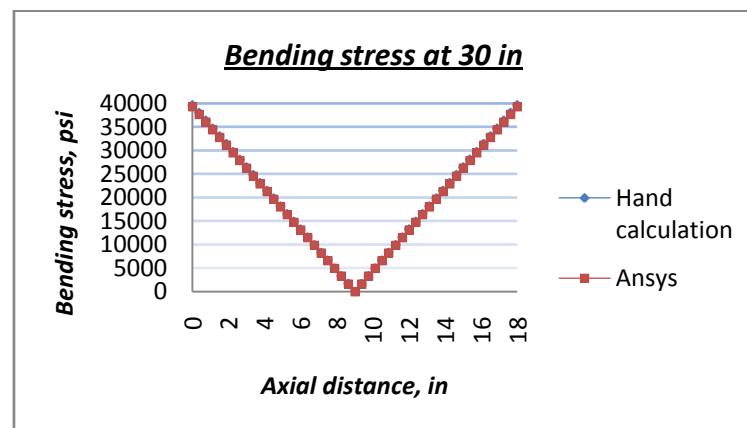
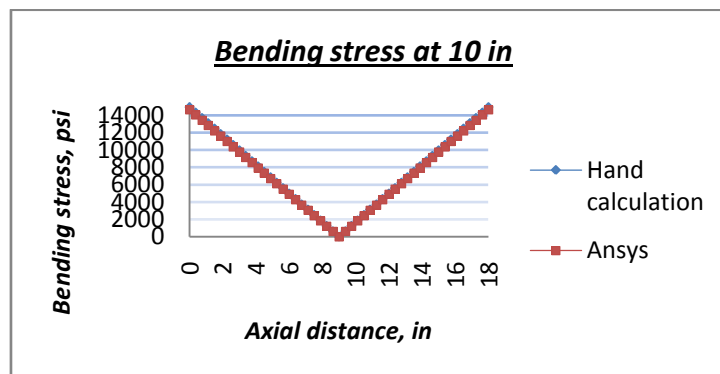


Fig. 3.2.9: Comparison of stresses, Axial 10



All figures show that the axial distance at 9 in has zero bending stress. And if any point below or above the neutral axis is considered, then it gives more stress and it increases linearly to outermost fibre.

#### IV. CONCLUSION:

The relation between bending stresses and bending moment has been expressed by flexural relation. That is the elastic deformations plus Hooke's law determine the manner of stress variation. Again the theoretical relation indicates that the flexure stress in any section varies directly with the distance of the section from the neutral axis. And this is also true for ANSYS. However this analysis allows to stand with the theoretical background of flexure formula when finite element analysis would considered.

#### References:

- [1] A solid-beam finite element and non-linear constitutive modeling J. Frischkorn, S. Reese Comput. Methods Appl. Mech. Engrg. 265 (2013) 195–212.
- [2] S. Abhinav Kasat & Valsson Varghese, "Finite Element analysis of prestressed concrete beams", International Journal of Advanced Technology in Civil Engineering, Vol. No. 1, Issue no.- 3,4, Page no. 29-33, 2012.
- [3] Strength of Material by S.Ramamrutham, pg:235 Dhanpat Rai Publishing Company 15th edition.
- [4] ANSYS. (Help Documentation).
- [5] Timoshenko, S., (1953), History of strength of materials, McGraw-Hill New York.
- [6] Timoshenko, S.P. and D.H. Young. Elements of Strength of Materials, 5th edition. (MKS System).
- [7] JN Mahto, SC Roy, J Kushwaha and RS Prasad, "Displacement Analysis of Cantilever Beam using Fem Package", International Journal of Mechanical Engineering & Technology (IJMET), Volume 4, Issue 3, 2013, pp. 75 - 78, ISSN Print: 0976 – 6340, ISSN Online: 0976 –6359.
- [8] ACI 318-89, 1992, "Building Code Requirements for Reinforced Concrete," A CI Manual of Concrete Practice Part 3-1992, American Concrete Institute.

## Is there a way to provide mobility in a spatial direction within the virtual environment provided by Google Cardboard Virtual Reality System?

Gourav Acharya

Department of Computer Engineering, Mukesh Patel School of Technology Management & Engineering, NMIMS, Mumbai, India

**ABSTRACT:** Google cardboard is a unique Virtual Reality System that's one of the first to provide the virtual experience via a smartphone using Gyroscope and Accelerometer built into the system. Even after being an effective system there's no way to emulate mobility in the virtual environment when it comes to activities such as running, walking and jumping. Walking in the virtual reality is achieved either by focusing on a target object or the environment is designed to move linearly automatically to give the sensation of mobility with neck movements to act as rudders-enabling users to experience the view at their own comfort in 360 degrees, yet unable to further advance the experience by letting them control their spatial body movement too. The study initiates with understanding how recognition takes place in a smartphone using the in-built accelerometer. It is derived that for measuring locomotion of body in any direction the device should be placed in that moving part of body but the smartphone in cardboard resides in the headgear. As the extremely low pricing of Cardboard is its redeeming quality; solutions like sensors and treadmill as input though effective are considered overpriced. A tangible mechanical system made of a cheap lightweight material that interacts through the screen sensitive strip built into the cardboard could be a possible solution. This solution is investigated through a study on how the body behaves while walking and the relative motion of its various body parts with respect to each other and how walking in virtual environment changes the gait of a person. The hindrance to natural movement in virtual environment is not only technical but also a consequence of human health, so finally a comparative study on simulator sickness brought on by different locomotion scenarios in virtual and real environment addresses this.

**Keywords:** Virtual Reality, Virtual Experience, Walking, Cardboard, Google Cardboard, Accelerometer, Smartphone.

### I. Introduction

Virtual reality or VR, also referred to as immersive media is a collection or a singular system that aims to stimulate physical presence in a virtual computer generated environment. The sensory modes of input to the person inside such an environment includes auditory, olfactory, visual or in some extreme cases gustation. With its widely accepted inception in the 1968 by Professor Ivan Sutherland and his student Bob Sproull with their Head mounted display Sword of Damocles which took up the whole room and was considerably huge for an HMD; the Virtual Reality gears have come a long way since then.

The Google Cardboard introduced in 2014 at the Google I/O developer's conference and created by David Coz and Damien Henry (Google engineers at the Google Cultural Institute Paris) in the same year, is one such revolutionary device which is immensely unique from the other devices in the same field. While other systems seek to make The Virtual Experience more immersive by incorporating as much of hardware and software as they can Google Cardboard has achieved a surprisingly efficient System at the percent of the cost and with the most simplistic of materials.

Google Cardboard is a cardboard cut-out which mostly exists as a do it yourself kit (DIY). It has 2 binocular sized holes where 2-34 mm diameter biconvex lenses are set at the suitable distance just as in a pair of glasses. The front side consisting of these lens spaces gets covered by a sheet of foldable cardboard from the front. Between the lens holes and the sheet there's just enough place for the smartphone to be inserted. The Cardboard lenses do the job of focusing the rays coming from the screen to the eye and projecting a virtual image which the

user feels himself inside of. It is equipped with either a magnetic button or screen sensitive strip to interact with the virtual elements.

Such a simple concept of focusing the image from the phone screen onto the user and giving him the virtual experience by allowing him to move his head in different directions and subsequently seeing that particular part of the virtual field is what makes cardboard unique. They took an existing smartphone system and used it to make a virtual system a common man can afford.

But with the reduced cost come limitations. The user is able to change his viewing direction with his neck movements but is unable to control his movement with such control. Yes he can move because of some tweaks like focusing on a target object which triggers movement towards that object or in that particular direction. But an **Authentic walking experience** which will enable him to move with the movement of his legs is not seen as of yet in the various applications tested. This paper seeks to find the reason to the above mentioned problem based on the comprehensive study done by various research studies.

## II. Studies Conducted

### 2.1 Activity Recognition using Cell Phone Accelerometers [1]

#### 2.1.1 Brief Description

The goal of WISDM (Wireless Sensor Data Mining)[1] project as described in the paper was to explore the research issues related to mining sensor data from mobile devices and to build useful applications using accelerometer as the sensor in study. Their study differs from previous study in the manner that they are using a single device to measure user activity rather than several placed across the body. They enlisted the help of twenty-nine volunteer subjects who carried the Android phone in their front

Pants leg pocket and were asked to walk, jog, ascend stairs, descend stairs, sit, and stand for specific periods of time. The data collection was controlled by a simple application created on android that registered the user's name and some other details and started and stopped the collecting of data. Sensor allocated was accelerometer.

The activities they carried out were observe and the data collected was in the form of spatial acceleration in 3 axes. Z-forwardly-vertical and x-horizontal. They made graphs of acceleration vs time and proceeded to observe where during mobility exercises like walking and running and jogging the periodic spikes occur. Y axis gave the most increased values as it was always being acted upon by the gravitational acceleration, then reduced was z and further very less was x. The data was collected in raw format and then converted to example samples. These samples were described in a table. Then they plotted other tables based on accuracy and confusion matrices which represented the confusion in the ability of the results to determine if the person was going upstairs or downstairs. This was verified using the walking statistics as walking is thrice as more while going up then going down. Many other such projects are mentioned and references for their research have been provided.

#### 2.1.2 Observations

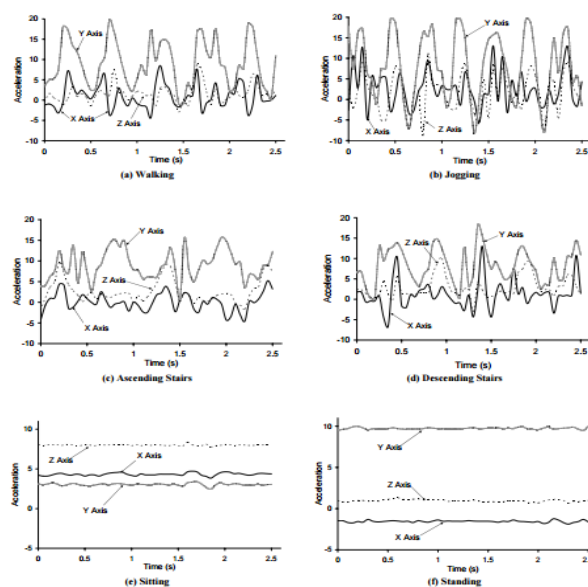


Figure 1: Acceleration Plots for the Six Activities (a-f) [1]

The plots depict how the accelerations in the different spatial directions vary with time. Y axis gave the most increased values as it was always being acted upon by the gravitational acceleration, then reduced was z and further very less was x.

### 2.1.1 Inferences

The inferences made from the research paper are as follows:-

- I. The most important inference gained from the research paper was that the accelerometer detects the acceleration of the phone and not the part of body it is attached to. Now since cardboard keeps the phone in itself and its head mounted, the user's leg movement will not be detected at all.
- II. Accelerometers are used to determine the orientation of device as they can sense the gravitational acceleration.
- III. Accelerometers are used to determine the orientation of device as they can sense the gravitational acceleration.
- IV. They measure accelerations in 3 spatial directions, namely x, y and z.
- V. On the basis of walk, jog, ascend stairs, descend stairs, sit, and stand one can prepare the factors/parameters that affect the accelerometers values.
- VI. All 3 axis will have a spike during the mobility actions in the decreasing order of the amplitudes  $y > z > x$  if we consider y to be vertical z to be forward and x to be horizontal.
- VII. Standing and sitting lead to the minimum of amplitude variations in the axis.
- VIII. A need for confusion matrix exists to determine which operation is being performed. Like in the case of ascending or descending the stairs. Multiple data has to be analysed including walking. Walking is 3 times more while climbing then descending.
- IX. The accuracy of determining the operation based on the accelerometer values is approximately 90%.

## 2.2 Effects of walking velocity on vertical head and body movements during locomotion [2]

### 2.2.1 Brief Description

It is usually concluded that the vestibular system plays a minimal role in maintaining posture and balance during walking [2]. In contrast, it has been suggested that the motion pattern of the upper part of the body is important for reducing energy consumption [2]. The study performed in this review is to establish a quantitative understanding of arm movement functions that can be obtained in terms of the relationship between arm movement and walking stability, this data will prove invaluable not only in the field of robotics research, but also in other fields such as sports physiology research, and medical research related to rehabilitation.

The main impact it will have on the overall study is to provide a way to determine which part of the upper human body best responds to the body movement so as to devise a mechanical model to implement the system of walking in virtual reality.

Aim of the study was to attempt to establish a relationship between:-

- a. Stride Length
- b. Stepping frequency
- c. Vertical head translation
- d. pitch rotation for head and torso
- e. Head point

### 2.2.2 Experiment and Measurement

A study on 9 healthy subjects of similar height strapped with headband, heel markers and chest plate to keep track of translations was conducted. For each stride cycle the stride length, frequency, SLI (stride length index), pitch for torso and head, Head point Variations are recorded. These factors were mapped with walking speed.

The Measurement Apparatus in the study:-

- 1) Body movements were measured with a video-based motion analysis System (OPTOTRAK 3020, Northern Digital Inc., Canada)[2]
- 2) It was placed approximately 4 m from the subject.
- 3) Eight IR markers were placed on the headband
- 4) Four markers on the small plate attached to the chest.

The markers were 8 mm in diameter and 5 g in weight, and were connected to a strobe unit (94 g) that was worn on the subject's belt. The strobe unit was connected to a central control unit that fed the three-dimensional position data of each marker to a computer at a strobe rate of 150 Hz [2]. The markers and strobe unit did not interfere with natural movements of the head.

The different coordinate frames are visible in the figure 2. The vertical head translations along with the pitch rotation of head and body was measured in this experiment.

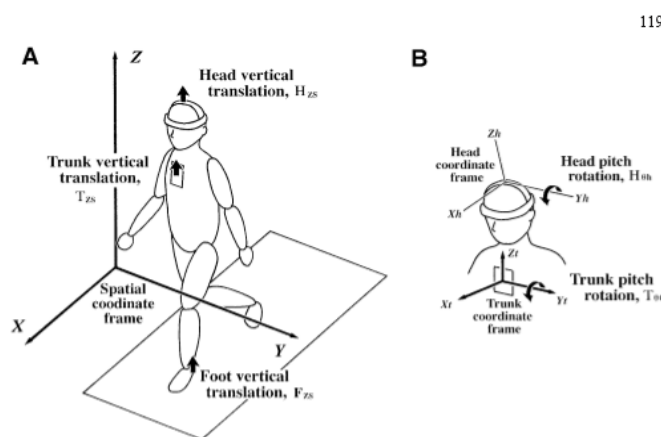


**Figure 2: 1A, B Coordinate frames used in this study. A Vertical translation of the head (HZS), trunk (TZS) and foot (FZS) were measured in space-fixed coordinate frame [2] . B Pitch rotations of the trunk (T  $\theta$  t) and head (H  $\theta$  h)were estimated as rotations about bodyfixed Y-axes [2]**

### 2.2.3 Observations

Each trial lasted 30 s and contained 15–30 complete stride cycles, depending on walking velocity. Stride length and step frequency are functions of walking velocity and were determined by the heel strike. Stride length and frequency are function of walking velocity given by  $V = F \cdot S$ . The stride length index

Given by:

$$SLI = (\log(S2/S1) / \log(V2/V1)) * 100$$

If the value is:

- a. 50 % --> Half Stride Length contribution
- b. 0 % ---> Only Frequency contribution
- c. 100% --> Only Stride Length contribution

All the data under uniform gait was considered for the 10 sec intervals

It was observed that the Stride Length during gait monotonically increased as a function of walking velocity for all the subjects. Same goes for mean stride length. And same for Stride Frequency for all regardless of height. The contribution of Stride length was determined by SLI. Between 1.0m/s-1.6m/s SLI-greater than 50% when SLI<50% frequency of steps changes. Finally, at 2m/s stride length saturates so Velocity varied only with frequency. At 1.2 m/s SLI was maximum.

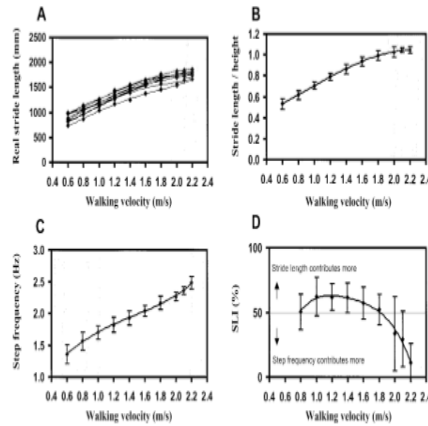


Figure 3: A Stride length of the nine subjects as a function of walking velocity. B Mean and SD of the relative stride length (calculated from the ratio of stride length to the subject’s height) [2]. Stride length saturated above 2.0 m/s (shaded area). C Step frequency as a function of walking velocity. The rate of change of frequency was largest below 1.2 and above 1.8 m/s (shaded areas) [2]. D Stride length index (SLI), estimated using Eq. 1 in “Materials and methods.” The curves in B, C, and D were fit by 4th-degree polynomials so that trends in the data could be observed. [2]

All the data under uniform gait was considered for the 10 sec intervals

It was observed that the Stride Length during gait monotonically increased as a function of walking velocity for all the subjects. Same goes for mean stride length. And same for Stride Frequency for all regardless of height. The contribution of Stride length was determined by SLI. Between 1.0m/s-1.6m/s SLI-greater than 50% when SLI<50% frequency of steps changes. Finally, at 2m/s stride length saturates so Velocity varied only with frequency. At 1.2 m/s SLI was maximum.

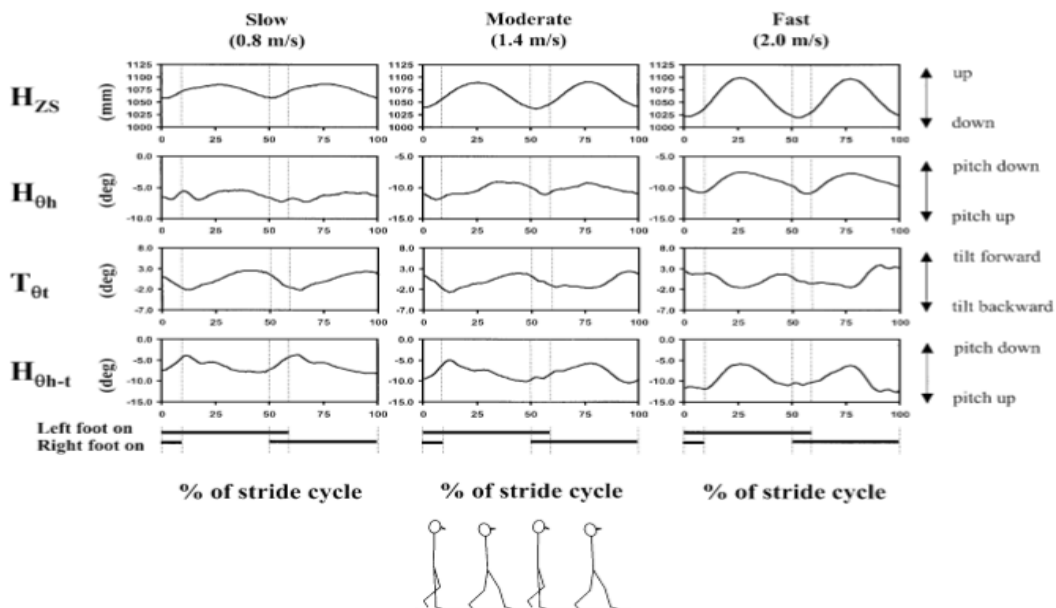


Figure 4: Typical averaged waveforms of H<sub>ZS</sub>, H<sub>0h</sub>, T<sub>0t</sub> and H<sub>0h-t</sub> for slow, moderate and fast walking from one subject (SM). The abscissa is the percentage of one stride cycle, which began with left heel strike and ended with next heel strike of the same foot. Each stride waveform is the average from 15–30 walking cycles, depending on the walking speed. The angular rotations of the head and trunk were zero (the reference position) when subjects were stationary looking at the visual target. Note that nose-down pitch rotations are positive [2]

The above figure shows how the vertical translation of head and torso along with their pitch rotations vary during walking. During stationary the angular rotations are taken as 0 of the body and the head and once the movement begins the rotation and translation is measured relative to it. One stride cycle starts from one heel strike to the next heel strike of the same foot.

During each stride cycle when the maximum force is given to the favoured foot to propel the person forward it is then that a considerable head translation towards the ground sets in. The person looks down to accommodate the head point view. Same goes for the head pitch as the head rotates about the axis when it propels itself forward. A similar variation is seen for the torso.

During the act of propulsion the torso tilts ahead to create the momentum of the movement and then it tilts back to conserve the inertia.

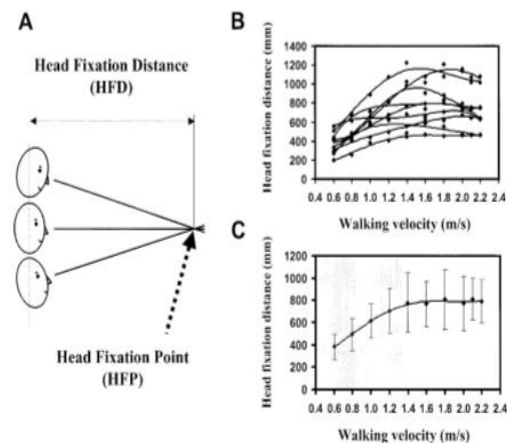


Figure 5: A The head fixation point (HFP) was defined as the point where the head roll axis intersects during compensatory pitch rotation and vertical translation of the head, and was estimated by triangulation. The head fixation distance (HFD) is the distance from the subject to HFP. B Distance from the head to the HFP as a function of walking velocity for each subject. C Mean distance to the HFP of all nine subjects. The distance to the HFP was relatively constant above 1.2 m/s (unshaded area) [2]

The point we look at while walking also drives the operation forward. If we look farther then according to the data the velocity increases in the same manner

As we see farther away from the target our speed keeps increasing until it reaches somewhat of a constant curve.

#### 2.2.4 Inferences

The inferences made from the research paper are as follows:-

The most important inference gained got from the research paper was that there are multiple upper body parts which are affected in multiple ways through locomotion.

The factors getting affected or affecting the study's stability are:

- Stride Length
- Stepping frequency
- Vertical head translation
- pitch rotation for head and torso
- Head point

Stride length and stepping frequency are related to the translation and rotation of head

Height does not vary the head point or the frequency very much.

The factors vary differently for different walking speeds which can provide me with a continuous function to provide mechanical responses for different speeds.

## 2.3 Real Walking Increases Simulator Sickness in Navigationally Complex Virtual Environments [3]

### 2.3.1 Brief Description

Movement in a virtual environment can generate various types of simulation sickness like disorientation, nausea etc. This paper serves as a comparative study to determine which out of real world, natural walking in virtual world and simulation walking cause the most amount of sickness.

Navigation is the key component to gauge the immersive nature of a virtual environment. The main component, walking is used in this study to drive the discussion forward. There have been carried out many experiments on the study of motion sickness prior to this one. Zambaka and Suma [3] are two researchers who've conducted tests in this field but have done so in a small environment, restrictive in terms of time and space. So consequently their deductions or observations were severely limited and hence they couldn't reach a final conclusion or rather didn't see any such difference in the simulation sickness in the 3 conditions. A researcher by the name of Chance established that in some cases the natural walking in a simulated environment was less prone to sickness than the simulated one.

So due to lack of a proper measuring gauge or questionnaire the team led the study to warrant their question.

The method conducted consisted of a creation of a maze in their lab, a real tangible maze. It was followed by the designing of an almost similar maze in a virtual reality software. The test subjects chosen were allowed a period of five minutes to travel in either of the 3 conditions in randomized order. Where the three conditions were:-

VNW: Natural walking in virtual environment

VSW: Simulated walking in virtual environment

RW: Real walking in real environment

They were also given a one minute test time to get used to the simulation software. The Kennedy-Lane Simulator Sickness Questionnaire (SSQ) [3] was given before and after the testing and the overall sickness score along with that in each condition was recorded for each type of discomfort i.e. nausea disorientation and oculomotor discomfort.

### 2.3.2 Observations

The result on the 90 test subjects where 30 were in each condition showed drastic deviation in some cases and none in others. The results were influenced on the basis of the travel technique; the total and the individual simulator sickness changed. None of the deviations were much significant except for disorientation during VNW.

So Natural walking in virtual environment produces the most sickness while that in real and simulated remains the same and in some cases even lessens. So this proves that simulated walking is a better way to navigate highly complex mazes and probably because the physical effort required is less.

		Before	After
<b>Overall</b>	RW	18.95	12.72
	VNW	18.20	29.17
	VSW	15.46	14.46
<b>Disorientation</b>	RW	12.99	11.60
	VNW	14.85	37.11
	VSW	13.92	14.84
<b>Nausea</b>	RW	13.99	10.81
	VNW	10.81	19.72
	VSW	8.59	9.22
<b>Oculomotor</b>	RW	18.95	10.86
	VNW	19.96	23.25
	VSW	16.42	13.90

Table 1: Mean Simulator Sickness result [3]

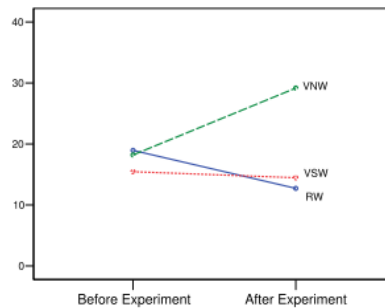


Figure 6: Overall Simulator Sickness Score [3]

## 2.4 The influence of virtual reality systems on walking behaviour: A toolset to support application design

### 2.4.1 Brief Description

The paper deals with the effect of a number of factors within VR systems on walking and movement perception [4]. Even normal walking is hindered due to any injury to the legs or any form of disease that can reduce or change walking patterns. The walking in a virtual environment is dependent on walking interface, visual gain, and audio tempo [4]. The relationship between walk length and stride length and the tempo or frequency is altered by the walking interface and visual gain [4]. Our own perception of how we are moving is altered by what we see from the corner of the eyes or how far wide we can see, the brightness, the size of what we see etc.

This study will help understand the various factors to be kept in mind while designing the solution to the problem. A mechanical solution was the way to solve the problem as of yet, envisioning ideal conditions and assuming that **the walking in real and virtual environment won't vary at all. But it does.**

The study begins with the description of the various factors that can cause the variation in walking in virtual reality including perception, interface and tempo, stride length etc.

Virtual rehabilitation helps keep the injured person engaged and takes his mind off the pain. So research into this matter to provide efficient and friendly systems/applications is necessary. Cadence is the frequency of heel taps on the ground between the stride of the two legs while stride length is the length from the left footfall to the right during one step. It has been seen that the walk ratio which is the relationship between the walk stride and cadence remains same for a range of speeds, so for a consistent experience walk ratio and speed should remain similar.

Real world movement is controlled by vestibular and stimuli and visual perception but since these might change in the virtual reality it's difficult to emulate actual walking. But there are systems that can change the variables like the interface, the environment to provide every kind of virtual terrain to alter the perception of the user and suit real conditions.

The input devices to measure user movement can be of 3 general types:-

- 1) Mechanical: Restricts user movement a lot so not a valid way to study walking behaviour.
- 2) Sensor based: Freedom is unlimited but the position of sensors also matter, some movements may require the use of changing body pattern to match sensor pattern. Also fear of falling off can also affect change in walking pattern in virtual environment.
- 3) Using Treadmill: The most convenient way to measure the movement since it provides a linear direction to measure, it can be changed to match user autonomy over movement. Also require less space and give the feel of walking over ground. This system has been employed in the study.

Output devices:-

For giving feedback to the users the main channels are the visual and auditory. So, big flat screens or head mounted displays and speakers or headphones are used. Factors such as display size, field of view, display resolution, refresh rate and color fidelity all vary between different output devices [4]. Since the input device is a treadmill hence it's necessary that the user knows his bounds, a head mounted display though provides an extreme immersion it also provides perception distortion and the inability of the user to judge real world obstacles. Hence Screens put around the user are much more efficient on this manner. Due to Lack of studies it's

not clear how the difference between the two will affect user pattern. By thorough testing the decisive field view that provides natural perception would be in the range of 80° and 200°.

The display taken into consideration is stereoscopic since studies show that it increases depth perception and the visual perception varies greatly.

Virtual Environment:-

The video content provided by the environment is usually filled with abstract or literal cues. Like dots moving behind will give the illusion of walking hence the user will move forward consequently but other studies have used actual literal environments like a street or a rollercoaster to invite user to move. Peripheral video matters as it affects user perception of a situation. Also the contrast of the abstract cues like dots changes the user speed like brighter dots appear to move faster.

Audio input like music or external noise can also affect gait as the user can be disturbed while walking or increase his tempo based on the beats of the music. Again enough study has not been conducted regarding this problem.

Calibration and scaling also form an important factor for user walking pattern as the size of the entities in the virtual environment should be as real as possible to sate the mind of any confusion and hence disrupting a certain Candace. The user also expects things to scale as he/she approaches or moves back. Not in the least the speed at which the virtual environment displays the environment going by can also lead to increase or decrease of speeds.

### 2.4.2 Observations and Inferences

Table 2: A TOOLSET TO DETERMINE THE EFFECT OF VARIOUS VR FACTORS ON WALK SPEED, WALK RATIO; VISUAL FLOW PWERCEPTION, IMMERSION AND SPACE/TRACKING REQUIREMENTS [4]

VR factor		Effect on walk speed	Effect on normal walk ratio	Effect on self-motion perception	Effect on immersion	Space / tracking required
Walking interface	Free walking (with HMD)	May lead to 'cautious walking' (+)	No data	HMD required - see separate heading	HMD required - see separate heading	Large spaces. Tracking can be complex.
	Self-paced treadmill	Baseline walk speed reduced by around 25%	Normal walk ratio maintained	Self-speed estimation increased by around 10%	Natural walking may increase immersion (+)	Can be used in restricted spaces
	Motorised treadmill	Walk speed pre-set by operator	Walk ratio decreased by around 10%	Fixed speed may reduce immersion (+)		
Visual content	Peripheral visual cues	Lack of cues may affect visual flow - see visual gain	No direct effect	Increased accuracy of self-motion perception	No direct effect	N/A
	Correct scaling of geometry	No data			Increases immersion	
	High visual contrast	No direct effect	High contrast gives impression of faster visual flow	No direct effect		
	Visual gain	Visual gain 0.5:1.0 increases walk speed by around 10% (*)	Lower visual gain increases stride length	Visual gain between 1.5:1.0 and 2.4:1.0 appears 'normal'	Lower visual gain may decrease immersion (+)	

Visual delivery	Head mounted display (HMD)	No direct effect. Cautious walking more likely (+)	No direct effect	Reduced accuracy of depth and motion perception	Higher immersion than flat screen	Head tracking necessary
	Large-screen display	No direct effect. Needs to be used with stepping in place or treadmill	No direct effect	Less perceptual distortion than HMD. Wider FOV possible	Less immersive than HMD	No head tracking required.
	Stereoscopic projection	No direct effect	No direct effect	Increased accuracy of self-motion perception	Increased immersion	N/A
	Monoscopic projection	May reduce the effect of visual flow modulation	No direct effect	Decreased accuracy of self-motion perception	Decreased immersion	
	Field of View (FOV)	FOV < 80° reduces peripheral flow and thus may reduce visual flow modulation effect	No direct effect	Increased accuracy of self-motion perception with FOV > 80°	Increased immersion with wider FOV	N/A
Audio content	Tempo	Increased walk speed by 15% with tempo 25% above baseline cadence	Normal walk ratio maintained	No data	No data	N/A

### III. Discussion

**Table 3: Comparison of Different Methods**

	Ease of Implementation	Cost of implementation	Effect of External Factors	Tangibility	Error finding	Workload
Software Solution	Hard	No cost	No effect	Non Tangible	Hard because exists in complex code.	The real workloads are infinite as the user can do any action.
Mechanical Model	Easy	Negligible cost	Humidity affects	Tangible	Errors are all mechanical so easy to fix.	Real workload is restricted to normal user movement.

The table depicts the comparison between different Solutions that can be employed implemented to solve the problem of walking in virtual reality.

Though the Software solution will be more flexible and efficient by a large degree; it'll also be harder to implement. Too many workloads to process and the error handling becomes difficult,

The mechanical model will be cheap, Tangible and mostly error free. But it'll restrict user workload and can be affected by external factors like humidity and precipitation etc.

### IV. Conclusion

It is possible to implement a system which will enable us to carry out mobile activities like walking, running jumping etc. The system can be implemented

By either software or hardware method. The software method though more flexible in terms of the movement scenarios it's able to provide is hard to implement because of the limited amount of Application programming interfaces(API's) present. Also it's difficult to work with the smartphone accelerometer as it can detect even the most smallest of acceleration vectors hence ruining the movement. The accelerometer also detects the movement of the body part which it's attached to so leg movement will be hard to detect.

The mechanical model is easier to implement. It can consist of a tangible connecting device made of a flexible material that will connect the legs, hands or some other organ of the body which responds to the walking stimuli like head as discussed in [2]. It would be less prone to errors as it's a physical device. But it'll be hard to determine the performance metrics during the research as its dependent on many factors such as pitch, stride length and stride frequency etc.

The idea of walking in virtual reality using your legs can provide quite an immersive experience but this can also lead to increase in the amount of simulator sickness that arises from the increased mode of input by the user through his legs. He/ She will feel disoriented and nauseous by the amount of control they have in the virtual environment.

### References

- [1] Jennifer R. Kwapisz, Gary M. Weiss, Samuel A. Moore, "Activity Recognition using Cell Phone Accelerometers" ,on cis.fordham.edu, 2010.
- [2] Eishi Hirasaki, Steven T. Moore, Theodore Raphan and Bernard Cohen, "Effects of walking velocity on vertical head and body movements during locomotion" Exp Brain Res (1999) 127:117--130 \copyright Springer-Verlag 1999.
- [3] Evan A. Suma, Samantha L. Finkelstein, Myra Reid, Amy Ulinski and Larry F. Hodges" Real Walking Increases Simulator Sickness in Navigationally Complex Virtual Environments", in <http://people.ict.usc.edu/>, 2009.
- [4] Powell, W.A. and Stevens, B. "The influence of virtual reality systems on walking behavior: A toolset to support application design", in Virtual Rehabilitation (ICVR), 2013 International Conference, p.p(270 -- 276), 26-29 Aug. 2013.

## Development of Visually Impaired Guided System Using GPS, Sensors and Wireless Detection

Emmanuel Kobina Payne<sup>1</sup>, Dennis Joe Harmah<sup>2</sup>

<sup>1</sup>(Department of Electrical & Electronic Engineering, Takoradi Polytechnic, Takoradi, Ghana)

<sup>2</sup>(Department of Biomedical Engineering, All Nations University College, Koforidua, Ghana)

**ABSTRACT:** Visually impaired is the loss of vision of a person or a significant limitation of visual capability. Without any form of assistance, most visually impaired people have to stress their other senses mostly the ears in an attempt to detect any possible obstacles in their path. Advances in modern technology has provided an improved navigation capabilities such as the use of ultrasound sensors and electronics to assist the visually impaired to navigate independently and to enhance security and safety. This paper presents the use of new technologically developed voice guided walking stick to improve the mobility of visually impaired people. This focuses on detecting the direction and position of obstacles ahead using ultrasonic and infrared sensors and finding locations with the aid of voice prompt and GPS.

**Keywords** - Detection, Enhancement, Technology, Visually Impaired

### I. INTRODUCTION

Visual impairment is the loss of vision of a person or a significant limitation of visual capability resulting from disease, trauma, or congenital condition that cannot be corrected by conventional means such as refractive correction, medication or surgery [1].

The levels of impairments can be classified into three groups namely;

- Partially sighted: Visual problems caused by age related muscular degeneration, diabetic retinopathy, corneal clouding or childhood blindness. This indicates some type of visual problem, with the need of a person to receive special attention in direction of movements [4].
- Low vision: This applies to individuals with sight who are unable to read the newspaper at a normal viewing distance unless with the aid of eyeglasses or contact lenses. It can be divided into, myopic (short-sighted) unable to see distance objects clearly and hyperopic (long-sighted) unable to see close objects clearly. [2].
- Total blindness: This is when one is unable to sense light or a complete vision loss. This can be as a result of the following disorders; albinism, cataracts, stroke, prematurity, glaucoma, congenital disorders, infection and retinal degeneration [3].

For a visually impaired person to navigate an environment with human assistance, the person must have adequate information about the travel path and also be able to detect obstacles within the navigation range. Without any form of assistance, most visually impaired people have to stress their other senses mostly the ears in an attempt to detect any possible obstacles in their path. There are various methods devised to aid visually impaired individuals, such as the walking canes, guide dogs and help of another human with perfect sight. The most important drawbacks of these aids are lack of necessary skills and information. Advances in modern technology has provided improved navigation capabilities such as the use of ultrasound sensors and electronic travel aids to assist the visually impaired to navigate independently [4].

However, the developed technology as walking stick to improve the mobility of visually impaired people focuses on detecting the direction and position of obstacles ahead using ultrasonic and infrared sensors [5] finding locations with some limitations and alert prompts challenges. The aforementioned designed challenges impede the movement of the visually impaired individuals hence making it difficult to identify the best route to get to the specified location independently because of technological lapses in development. The one inexistent does not have it all. It can only detect distance or obstacles and not both [6&7]. Besides, it has no GPS neither voice prompts, hence the challenges the already inexistent electronic aid poses to visually impaired persons.

The proposed development aims to resolve the limitation by incorporating an ultrasonic sensor for detecting distance and infrared sensor for detecting obstacles at close range on a single walking aid. These different sensors will compensate each other in case of failure, thus not only aid in obstacle detection and will also reduce cost. The device is of multi-functional purpose as it is also improved with extra features of GPS for providing information of geographical areas with voice prompts. This minimizes navigation difficulties the visual impaired persons are subjected to. The performance of this technologically advanced stick is further enhanced with an alert light, an emergency alarm and voice guidance played from a wireless headset.

## II. SYSTEM DEVELOPMENT CONCEPT

### Design Consideration

Consideration is been given to the identification of specific requirements and then formulate set of specifications required for actual construction of the product. Appropriate materials with their specification were given priority. This presented the product material selection criteria to meet expected outcome.

### Design Components Data Considerations

Choices of components operating characteristics were considered. Below, empirical data for components and attributes;

The forward voltage drops ( $V_f$ ) of an LED is typically 2V, and LEDs typically require about 10mA – 30 mA of current for good lighting. To conserve power for the device and still get a good glow out of our LEDs, decision was made to operate the LEDs at 10mA. Using this information and the fact that the LEDs operate from the 5V regulated source, the value of an ideal current limiter for the LEDs is obtained from Ohm's Law formula. Using the multi meter, the current for the used LED is 24mA. This design operates on two voltages, which are 3.3volts and 5volts which depends on the components selected. The voltages are specified on the manufacturer's data sheet for the components. The following are the components with their specific voltages:

Table 1: Components Operating Voltage Characteristics

Components Operating with 3.3V	Components Operating with 5V
Ultrasonic sensor	GPS
Microcontroller	Infrared sensor
Vibration motor	LED (night lights)
Emergency alarm	
Audio player	
Bluetooth module	
Light sensor (Light Dependent Resistor)	

### System Specification

The table shows the physical specifications for the proposed development

Table 2: System Specifications

Factor	Specification
System technology	Microcontroller-based design using the PIC16F877A
User interfaces	Bluetooth Audio Vibration motor SPST switches for overall (power) control
System Operating Voltage Range	5V – 9V
Packaging/presentation	Standard walking stick with the control and user interface modules attached
Usage	Indoor, Outdoor

### Development Materials Selection

The materials required for the development were selected based on suitability, simplicity of use by the visually impaired person, development resources and cost. The following are the list of the major materials:

- Microcontroller (PIC16F877A)
- Infrared Sensor (Sharp GP2Y0A02YK IR module)
- Ultrasonic sensor (Ultrasonic Range Finder EZ1 module)
- Bluetooth Audio Module (Roving Network RN-52 audio Bluetooth module)
- Global Positioning System (GPS) Module (GP-635T GPS receiver module)
- Adjustable Walking Stick.

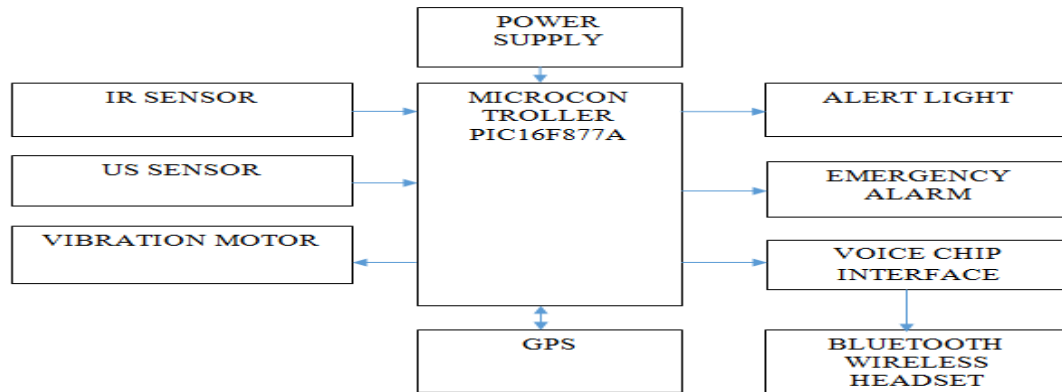


Figure 1: Design Block Diagram

**Device Implementation**

The artefact was constructed in stages, following a divide and conquers method. The product had two high-level components hardware and software. Either of these was built in stage and the two integrated finally for testing.

**Hardware Development**

The stages of hardware construction were the following:

A) Stick modification

An adjustable walking stick was acquired which was improvised for sensors and other components to be fitted on. The unmodified stick as shown in figure below yet to be worked on. It was then modified locally to have the components mounted on.



Figure 2: Modified stick

The circuit was hardwired on a protoboard as the main circuit board. This comprises of the power supply unit, the control circuitry (microcontroller), and connection headers for an extension board. The extension board is a second circuit board which houses all the communication components (the bluetooth module, sound module, and GPS receiver). These individual components are presented in the following figures.

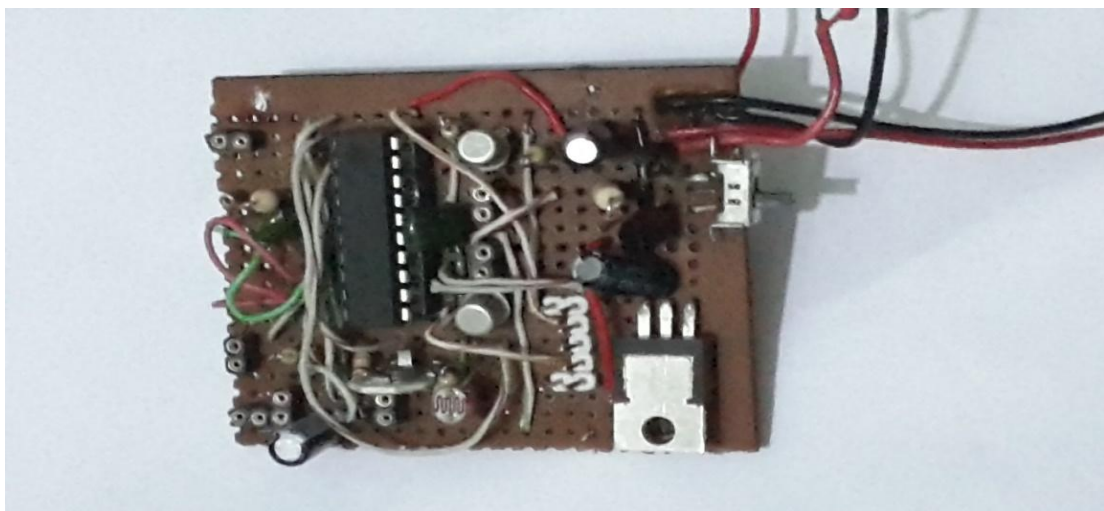


Figure 3: Main Circuit Board

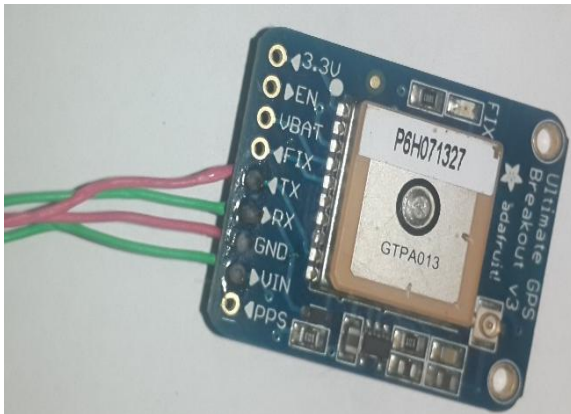


Figure 4.a: GPS Receiver



Figure 4.b: Bluetooth Module

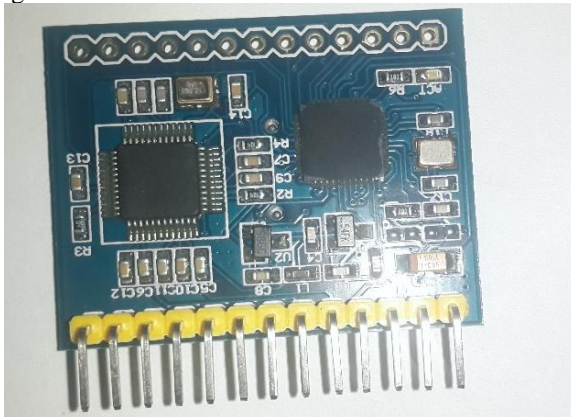


Figure 4.c: Audio Player



Figure 4.d: Infrared Sensor



Figure 4.e: Ultrasonic Sensor



Figure 4.f: Extension Board

**B) Assembly**

After preparing the stick and constructing the circuits, everything was brought together to make the final hardware artefact. This step comprised of inserting the sensor modules and LEDs, routing connecting wires through the stick, and attaching the circuit board and vibrating motor.

**Packaged Artefact**

The final package of the device as presented in the figure below.

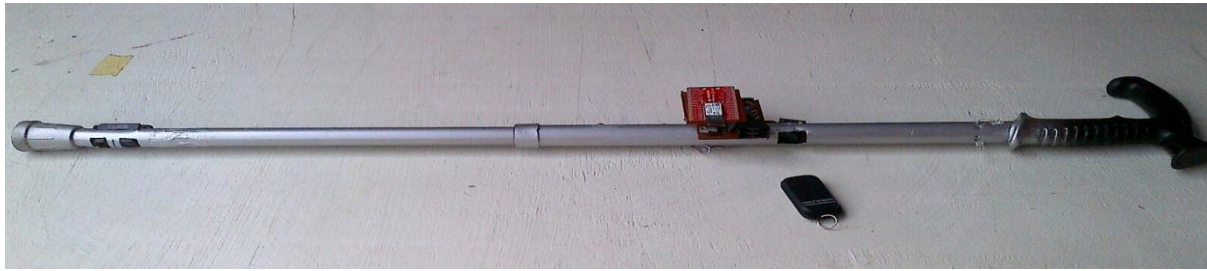


Figure 5: Final Package of the System

### Software Development

The control software of the system was built on a PC with the MikroC Pro development environment from Mikroelektronika Systems. The source code was crafted in MikroC Pro's text editor, compiled to Intel HEX format, and uploaded to the on-board microcontroller using a flash programmer from Mikroelektronika Systems.

## III. SYSTEM PERFORMANCE AND ANALYSIS

### System Testing

The system was subjected to various tests for purposes of functional assessment and performance. The major expected areas of testing were short circuits, open circuits, and dry joints. These were tested with digital multi-meter for assurance, where minor faults were identified and rectified. Software errors were of two kinds, builds errors and run-time errors. The build errors were isolated and fixed on the development system but the run-time errors were only detected at the time testing the unified system (hardware with software loaded) for functionality. Solution was preferred the run-time errors by logic change, source code editing, and re-building of the software, and uploading of HEX file to the system board.

### System Operation

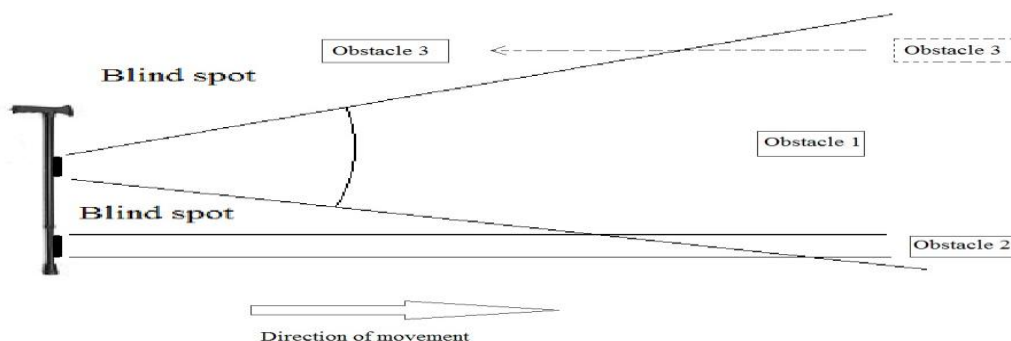


Figure 6: Interaction of Infrared and Ultrasonic Sensors in Obstacle Detection

The figure 6: above shows how the two sensors of the system interact. The infrared sensor is highly directional, so it only detects obstacles that are in its line of sight (LoS). In the figure, obstacle 2 will easily be picked up by the infrared sensor once it gets within the range of the infrared sensor, provided it stays on the same path.

The ultrasonic sensor on the other hand gives out a signal that spreads out from the sensor in a beam of a dynamic beam angle, according to the ultrasonic sensor data sheet, "the actual beam angle changes over the full range" [12]. From the figure 6, obstacles 1, 2, and 3, are all within the sweep of the ultrasonic sensor and will be picked it up. Obstacle 2 is also detectable by the infrared sensor within a certain range, but the two outputs of the two sensors are logically O-Red in the software, so no conflict occurs.

The spread of the ultrasonic beam is such that objects that are farther from the source usually have a wider coverage. Since the beam diverges from the source, the obstacle detection system has blind spots on either side of the ultrasonic beam, spots in which neither the ultrasonic sensor nor the infrared sensor can detect an obstacle. But this is not a serious limitation because obstacles which move into the blind spot will usually move through the sweep of the ultrasonic beam first

### System Performance Characteristics

This represents the characteristics of results that were obtained from the major components after testing the system.

Table 3: Obstacle Detection and Ranging

Obstacle Distance	Vibration 'ON' Period (in milliseconds)	Vibration 'OFF' Period (in milliseconds)	Audio Announcement
> 90cm	0	Fully off	None
30cm - 90cm	100	900	Obstacle ahead
0 - 30cm	500	500	Obstacle getting closer

Table 4: Night Alerts

Ambient Light Intensity (in lux)	Alert Status
>700	LED blinks at a rate of 2 per second
< 700	LED stops blinking (if it was blinking before). LED stays off

Table 5: GPS Location Service

Location	Audio Announcement
Present location e.g Takoradi Polytechnic	Approaching Takoradi Polytechnic New site main campus

The table below shows the number of characteristics that were used in order to obtain the response, comfortability and accuracy of results for the design.

Table 6: Usability Results

System/Sub-system	No. of Subjects	Accuracy of results	Responsiveness	Comfortability
Obstacle Detection	5	Good	Good	Not very good
Audio	4	Good	Good	Very good
GPS Location	4	Good	Somehow	Good
Night Alerts	7	Not very good	Good	Very good

## IV. CONCLUSION

The work that was done during this development generally revolved around deducing and formalizing the particular features that the product must have in order to fulfil the desired objective. The voice guided walking stick for the visually impaired incorporated with a GPS was successively designed and implemented. As earlier estimated, the study requirements expected are:

- The system was able to detect obstacles and issue guidance messages to the user as appropriate.
- The voice guidance subsystem was able to communicate guidance messages wirelessly for better audibility in all environments.
- The system was able to vibrate when an obstacle is found within a pre-specified range.

The GPS module in the system is intended to offer location services to the user which is very significant. The embedded GPS module communicates with dedicated satellites around the globe and sends location co-ordinates to the microcontroller. Ideally, the microcontroller should convert these co-ordinates to location information by looking up for the co-ordinates in a geographic information system (GIS) like Google Maps where available. This design is of great benefit to the visually impaired when it comes to independent mobility. With the combination of the two sensors, the GPS, emergency alarm and alert light, the visually impaired will be able to move around with ease and confidence in their environment.

## REFERENCES

- [1] "Change the Definition of Blindness" (PDF). World Health Organization. Retrieved 28 November 2015.
- [2] <<http://www.wikipedia.org>.
- [3] "Visual Impairment and Blindness Fact Sheet N282". August 2014. Retrieved 23 May 2015.
- [4] Global Data On Visual Impairments 2010(PDF). WHO. 2012. p. 6.
- [5] Divya, Srirama (2010). Ultrasonic and Voice Based Walking Stick for The Blind. GokarajuRangaraju Institute of Engineering and Technology.
- [6] S. Gangwar, (2011) "Smart Stick for The Blind", New Delhi, Sept. 26.
- [7] A. R. G. Ramirez, R. F. L. da Silva, M. J. C. A. D. C. de Albornoz, (2012) "Evaluation of Electronic Haptic Device for Blind and Visually Impaired People" Journal of Medical and Biological Engineering, Vol.32, No.6, 423-428.
- [8] Vigneshwari C, Vimala V, Sumithra G "Sensor Based Assistance System for Visually Impaired" (2013) International Journal of Engineering Trends and Technology (IJETT) – Volume 4 Issue 10 - Oct 2013 ISSN: 2231-5381 <http://www.ijettjournal.org>

- [9] O. O. Oladayo “A Multidimensional Walking Aid For Visually Impaired Using Ultrasonic Sensors Network With Voice Guidance” (2014) I.J. Intelligent Systems And Applications, 2014,08, 53-59 published online July 2014 in mecs (<http://www.mecs-press.org>)
- [10] L. Zaratang, D. Kimbin (2015) “Sensor Stick Walking Aid for The Blind” International Journal of Research in Engineering and Science (ijres) issn (online): 2320-9364, issn (Print): 2320-9356 www.ijres.org Volume 3 Issue 3. March. 2015.
- [11] ADH 2012 ADH Technology Co. Ltd, *GP-635T Data Sheet*, 2012, <http://www.adh-tech.com.tw>
- [12] [Sharp 2015] Sharp World, *GP2Y0A02YK Data Sheet*, 2015, <[http://sharp-world.com/products/device/lineup/data/pdf/datasheet/gp2y0a02\\_e.pdf](http://sharp-world.com/products/device/lineup/data/pdf/datasheet/gp2y0a02_e.pdf)>
- [13] [Sparkfun2015] Sparkfun Electronics, *RN-52 Bluetooth Hookup Guide*, 2015, <<https://learn.sparkfun.com/tutorials/rn-52-bluetooth-hookup-guide>>

## Numerical Investigation of inlet distortion on the flowfield within the NASA rotor67

HengMing Zhang<sup>1</sup>, XiuQuan Huang<sup>1</sup>, Xiang Zhang<sup>1</sup>, QingZhen Yang<sup>1</sup>

<sup>1</sup>(School of power and energy, Northwestern Polytechnical University, China)

**ABSTRACT:** Based on Harmonic Balance method, this paper studies the effect of inlet distortion on the performance of NASA Rotor67. Two kinds of inlet distortion with different sinusoidal forms of circumferential total pressure distribution have been applied on the inflowing boundary. The numerical results show that the solver based on frequency domain is capable of simulating the nonuniform flow in circumferential direction and can capture the detailed propagation of inlet distortion in the blade passage very well. The analysis shows that low frequency inlet distortion lead to a higher loss, while both inlet distortion have the similar total pressure ratio characteristic. There is little difference in stall margin of compressor for two types of inlet distortion. And for both types of inlet total pressure distribution, the low total pressure inlet zone is the source of high intension of tip clearance flow which results in the entropy production.

**Keywords** - Inlet distortion, Rotor67, Harmonic balance, Unsteady flow, Performance

### I. INTRODUCTION

Inlet distortion is very common in the actual flight of the aircraft and tends to be inevitable, e.g., the changing of flight attitude and flow separation in inlet duct. The nonuniform inlet flow can lead to performance degradation of fan/compressor. The studies about inlet distortion can be traced back to the middle of last century[1]. In earlier studies, experiments and simplified models were applied on researches about the effects of interaction between inlet distortion and compressor/fan. For instance, comparing with experimental results, Korn validated the reliability and accuracy of "parallel compressor" model in predicting inlet distortion induced stall[2]. And the results showed that this model agreed well with circumferential distortion test data on the single compressor stage, while it failed being used to estimate the multistage compressor. To investigate the effects of the inlet distortion on compressor stability, a series of experiments have been conducted by Greitzer[3]-[5]. Until the 90s of last century, some researchers began to exploit the Computational Fluid Dynamics(CFD) to study the inlet distortion of compressor/fan. For instance, combining CFD technique, Joubert[6] established two method to predict the compressor/fan inlet distortion. One method adopted two-dimension Euler unsteady calculation, another method combined "actuator disks" method and three-dimension Euler calculation. His analysis demonstrated that it was necessary for prediction of inlet distortion to establish study on three-dimension numerical simulation and "actuator disks" ignored the detailed flowfield in the blade. To control the inlet distortion induced compressor stall, the effect of casing treatment on inlet distortion has been investigated experimentally by Dong[7]. And The stall margin enhancement with a kind of stall precursor-suppressed (SPS) casing treatment has been found in their experiments.

Many researches about inlet distortion of compressor/fan have been completed by experiments and some simplified models. But few studies were completed by numerical simulation due to the very high computation cost, though the unsteady Reynold-averaged Navier-Stokes computation technique nowadays is mature and reliable for the researches about inlet distortion. To reduce calculation amount, the Hamornic Balance(HB) method[8] based on frequency domain has been adopted in this paper. And the numerical investigation of inlet distortion on the performance of compressor has been presented.

### II. COMPUTATIONAL APPROACH

The model equation of HB method is derived from the unsteady Reynolds Averaged Navier-Stokes equations(U-RANS). The integrated U-RANS equations could be expressed as follow:

$$\frac{\partial}{\partial t} \iiint_{\delta V} U dV + \iint_{\delta A} (F - Uv_{mg}) \cdot ndA = \iiint_{\delta V} (S_i + S_v) dV \tag{1}$$

Where,  $U$  are the conservative variables,  $F$  are the convective terms,  $Uv_{mg}$  are the flux terms from the grid moving,  $S_i$  are the centrifugal source terms and  $S_v$  are the viscous terms. The basic idea of Harmonic balance method is that the conservative variables could be decomposed into a time-averaged value and a sum of periodic perturbations, expressed as the fourier series form:

$$U = U_0 + \sum_{n=1}^N (A_n \sin(\omega_n t) + B_n \cos(\omega_n t)) \tag{2}$$

$U_0$  is the zero-order fourier coefficient, which represents the time-averaged value of conservative variables. And  $A_n$  and  $B_n$  are the N'th order fourier coefficient,  $\omega_n$  is the N'th angular frequency respect to  $A_n$  and  $B_n$ .  $U^*$  is a vector which consists of  $2N+1$  samples corresponding to different time, and  $\tilde{U}$  is the vector of fourier coefficients.

$$U^* = E \tilde{U} \tag{3}$$

Where,  $U^* = [U_1 \ U_2 \ U_3 \ \dots \ U_{2N} \ U_{2N+1}]^T$

$$\tilde{U} = [U_0 \ A_1 \ B_1 \ \dots \ A_N \ B_N]^T$$

$E$  is the fourier matrix. And substituting Eq. 3 into Eq.1, the governing equations could be derived as follow:

$$\frac{\partial}{\partial \tau} \iiint_{\delta V} U^* dV + \iint_{\delta A} (F^* - U^* v_{mg}) \cdot ndA = \iiint_{\delta V} (S_i^* + S_v^* + DU^*) dV \tag{4}$$

Where,  $DU^* = \frac{\partial E}{\partial t} E^{-1} U^*$ ,  $D$  is the frequency domain operator.

Eq(4) is the final set of equations that this article would to solve. So the number of simultaneous equations for HB method is  $2N+1$ . By employing the phase-lag boundary condition, the HB unsteady calculation can be conducted on a single-passage mesh. As a result, the amount of unsteady computation is as  $2N+1$  as that of steady. The accuracy and stability of HB method has been validated by Gopinath [9].

As for the numerical method, the central difference method with second-order accuracy and lower-upper symmetric Gauss-Seidel (LU-SGS) implicit time integration have been applied in this article. In order to reduce time cost, local time stepping, implicit residual smoothing and multigrid techniques are employed to accelerate convergence. The one-equation S-A model is chosen as turbulence model to calculate turbulence viscosity coefficient, which is widely used in turbomachinery numerical simulation.

### III. TEST CASE AND VALIDATION

The test case in this paper is NASA Rotor67. It is a transonic compressor rotor. And because the detailed experimental data of Rotor67 could easily be found in the NASA technical report[9], Rotor 67 becomes one of the most popular research objects in turbomachinery field. The design parameters of NASA Rotor67 are showed in table 1.

Table 1. NASA Rotor67 Design Parameters

Number of Blade		22
Blade Speed(rpm)		16043
Massflow(kg/s)		33.25
Total Pressure Ratio		1.63
Tip Speed(m/s)		429
Tip Mach Number		1.38
Aspect Ratio		1.56
Solidity	Tip	3.11
	Root	1.29
Hub-to-tip Radii Ratio	Inlet	0.375
	Outlet	0.478
Blade Tip Diameter(cm)	Inlet	51.4
	Outlet	48.5

Because of the adoption of phase-lag condition, the single passage grid could be used in the numerical simulation. The H-type mesh topology has been applied to generation of grid. The grid number of Rotor67 is

about  $5.4 \times 10^6$  with 65 grid points at radial direction, which is more enough to meet the requirement of grid independence. The blade-to-blade grid and validation of mesh independence has been showed in Fig.1

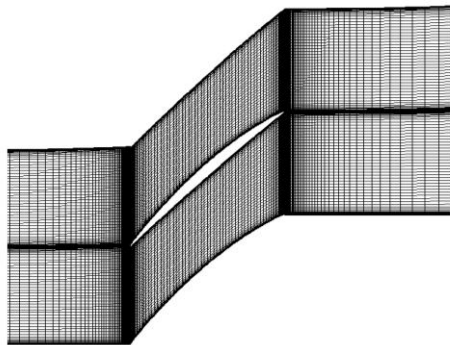
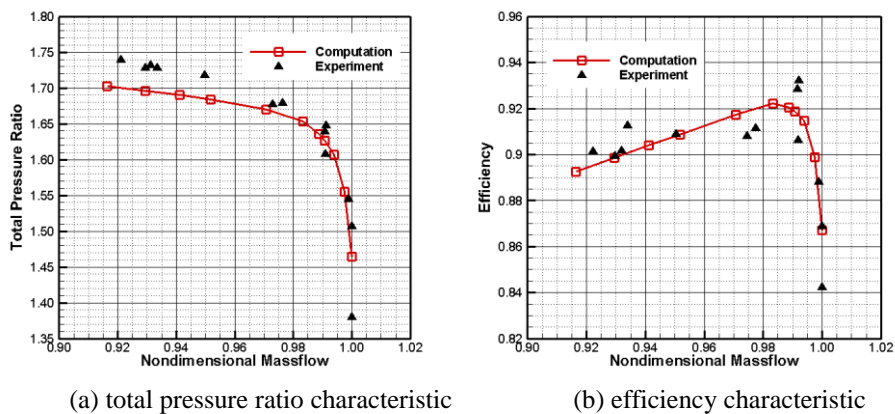


Figure 1. Grid at blade-to-blade surface

To make sure the numerical simulation results reliable, it is necessary to compare the numerical and experimental data. Fig. 2 shows the total pressure ratio characteristic and efficiency characteristic.



(a) total pressure ratio characteristic

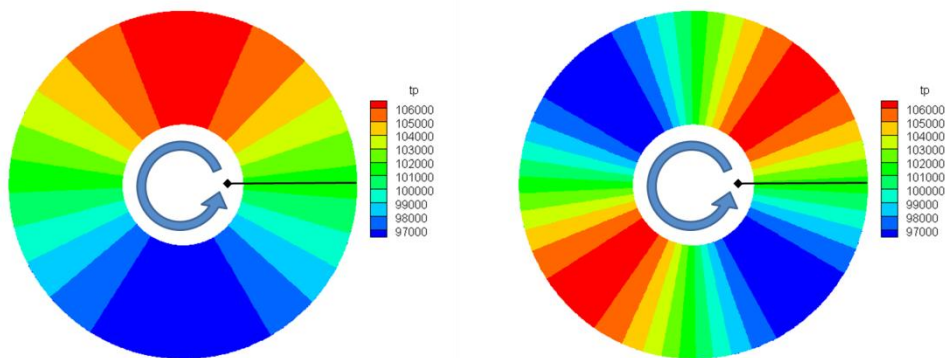
(b) efficiency characteristic

Figure 2. Rotor67 characteristics: experiment and computation

It is clear that the total pressure ratio of numerical simulation near stall boundary is little lower than that of experiment. However, the trend of computation is coincident with experiment. Also, the efficiency characteristic curve of computation agrees well with experimental results. So the numerical method and the solver adopted in this article are credible and trustworth.

#### IV. RESULTS

Adopting the mesh described above, two unsteady simulations based on harmonic balance method have been proceeding with two kinds of sinusoidal inlet distortion respectively. The inlet total pressure distribution contour are displayed in Fig.3.



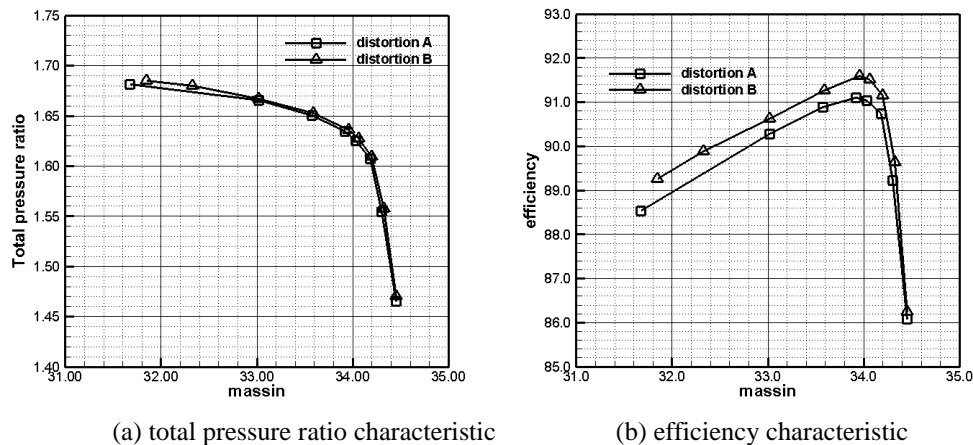
(a) distortion A

(b) distortion B

Figure 3. Inlet total pressure distribution: distortion A and distortion B

For two kinds of inlet distortion, the variations of amplitude are both 5 percentages of atmospheric pressure(101325pa) and the averaged inlet total pressure are both 101325pa. So the only different between two inlet distortion forms is the frequency. For distortion A, Rotor67 would experience one period when it rotates one revolution around its axis. And for distortion B, two sinusoidal waves sweep the blades during one revolution.

Fig. 4 compares the Rotor67 performances from distortion A and distortion B numerical simulations at designed rotational speed. It is clear that the total pressure ratio characteristic curve of distortion A agrees well with that of distortion B, while the differences of efficiency characteristic between distortion A and distortion B is obvious. Specifically, at choked operating point, the efficiency of distortion A and distortion B is nearly the same. However, with the operating point toward stall boundary, the efficiency of distortion B is higher than that of distortion A and this tendency is increasingly apparent.



(a) total pressure ratio characteristic (b) efficiency characteristic  
 Figure 4. Rotor67 characteristics: distortion A and B

Entropy is often used to characterize the loss in turbomachinery flow study. So to know more about the rotor response to inlet distortion and deepen understanding about the interaction mechanism between the inlet distortion and blade flowfield, the instantaneous entropy distributions for both distortion forms at 99% span at near design operating point are presented in Fig. 5.

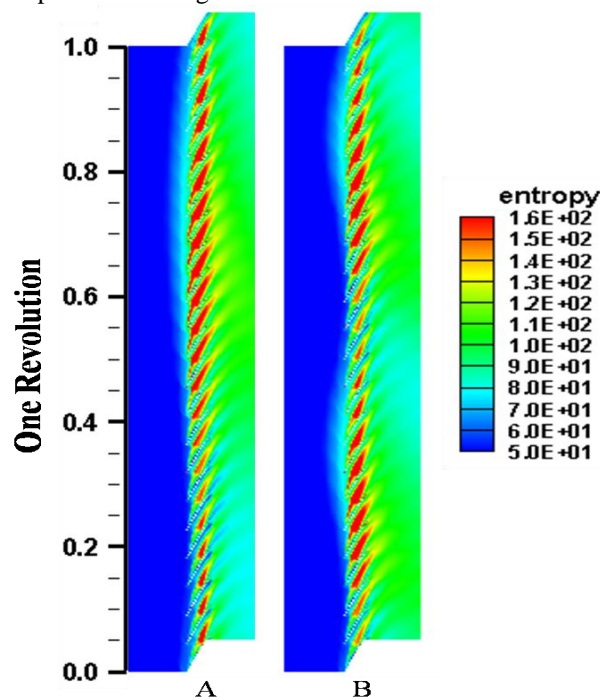


Figure 5. Entropy instantaneous distribution at the 99% spanwise location at design condition

Fig. 5 shows that the variations of entropy in a full annular of both distortion forms are also sinusoidal, which keep consistent with their inlet distortion waves. So the sinusoidal form inlet distortion lead to an almost sinusoidal form variation of flowfield.

Specially, it is easy to recognize that the stripy high entropy area in Fig.5 is due to the tip clearance flow. So the intensity of tip leakage is changing with time in sine form.

Also, combining the Fig. 5 and Fig. 3, it could be found that the high entropy areas in Fig. 5 are corresponding to the low total pressure areas in Fig. 3, which indicates that low total pressure inlet could lead to loss increment.

## V. CONCLUSION

Harmonic balance method could be used to numerical simulate inlet distortion efficiently and reliably. By HB technique, the NASA Rotor67 encountering two kinds of sinusoidal inlet distortion with different frequencies has been investigated. The results demonstrate that the frequency of inlet distortion has considerable influence on efficiency of Rotor67, while its impact on stall margin of Rotor67 is limited. Additionally, low pressure domain of inflowing boundary could strengthen the tip clearance massflow and lead to obvious entropy production. And the effects would be more significant for low frequency inlet distortion.

## REFERENCES

- [1] Conrad, E. William, and Adam E. Sobolewski, Investigation of Effects of Inlet-Air Velocity Distortion on Performance of Turbojet Engine, 1950.
- [2] Korn, James A, Compressor Distortion Estimates Using Parallel Compressor Theory and Stall Delay, *Journal of Aircraft*, 11(9), 1974, 584-586.
- [3] Callahan G M, Stenning A H, Attenuation of inlet flow distortion upstream of axial flow compressors, *Journal of Aircraft*, 8(4), 1971, 227-233.
- [4] Horlock J H, Greitzer E M, Henderson R E, The response of turbomachine blades to low frequency inlet distortions, *Journal of Engineering for Power*, 99(2) , 1977, 195-203.
- [5] Hynes T P, Greitzer E M, A method for assessing effects of circumferential flow distortion on compressor stability, *Journal of Turbomachinery*, 109(3), 1987, 371-379.
- [6] Joubert H, Flowfield calculation in compressor operating with distorted inlet flow, *ASME 1990 International Gas Turbine and Aeroengine Congress and Exposition*. American Society of Mechanical Engineers, Brussels, Belgium, 1990, V001T01A065-V001T01A065
- [7] Dong X, Sun D, Li F, et al, Effects of Rotating Inlet Distortion on Compressor Stability With Stall Precursor-Suppressed Casing Treatment. *Journal of Fluids Engineering*, 137(11) , 2015, 111101.
- [8] Hall K C, Thomas J P, Clark W S, Computation of unsteady nonlinear flows in cascades using a harmonic balance technique, *AIAA journal*, 40(5), 2002, 879-886.
- [9] Gopinath A, Van Der Weide E, Alonso J J, et al. Three-dimensional unsteady multi-stage turbomachinery simulations using the harmonic balance technique[C]//45th AIAA Aerospace Sciences Meeting and Exhibit. 2007, 892.

## Investigation into Unsteady Blade Row Interaction Effects of a Two-Stage Counter-Rotating Lift-Fan by Harmonic Balance Method

Xiang Zhang<sup>1</sup>, XiuQuan Huang<sup>1</sup>, HengMing Zhang<sup>1</sup>, YuChun Chen<sup>1</sup>

<sup>1</sup>(School of power and energy, Northwestern Polytechnical University, China)

**ABSTRACT:** Applying the harmonic balance method, an effective computational method in simulating time-periodic unsteady flows, this article studied the unsteady blade row interaction effects of a two-stage counter-rotating lift-fan. The unsteady flow in the 1st blade row was represented by one harmonic wave, while the unsteady flow of the 2nd blade row was modeled using three harmonic waves. The results show that: (1) the isentropic efficiency and lift force are proportional to the rotate speed, with the maximum of 88.35% and 130.04N respectively at the design speed; (2) the harmonic balance method predicts a higher isentropic efficiency of the 2nd rotor below its mid-span than the steady study, while a contrary observation is obtained above the mid-span; (3) the harmonic balance method is efficient and reliable to simulate the time-periodic unsteady blade row interaction.

**Keywords -** Harmonic Balance, Unsteady Flow, Lift-Fan, Counter-Rotating, Blade Row Interaction

### I. INTRODUCTION

Lift fan as the direct lift device, has a broad prospect in military and civil applications. In recent years, it has been successfully used in the vertical take-off and landing (VTOL) aircraft. A typical example is the Mule series VTOL unmanned aerial vehicles (UAV) developed by Israel Urban Aero. The maximum take-off weight of Mule is 1,130kg with a cargo capacity of 226kg. Another example is the counter-rotating lift fan in F-35B designed by Lockheed Martin Corporation.

In this article, a two-stage counter-rotating lift fan, designed to power a small flying saucer, is studied. By canceling the stators, the counter-rotating fan is more compact, and the flow unsteadiness induced the blade row interaction is strong. Recently, more research effort has been spent to investigate the unsteady flow in counter-rotating fans.

Most of unsteady flow field simulations are based on time domain, which are high computational time costly and hinder engineering application. The unsteady effects of turbomachinery can be divided into conditioned unsteady and inherent unsteady. The conditioned unsteady effects means the unsteady phenomenon would happen at specified working condition, for example, rotating stall and surge, while the inherent unsteady effects arise from blade row interaction, which makes the flow change periodically. And the inherent unsteady effects are considered to be the dominant part in the turbomachinery unsteady flow. For these characteristics of the unsteady flow in turbomachinery, an effective method with the ability to capture the inherent unsteady effects is proposed, which represents these changing flow variables by Fourier series approximately. By that, the unsteady calculation can be translated from time domain to frequency domain and reaches the objective of time savings. The frequency domain methods include the time-linearized linear/nonlinear harmonic method, the Harmonic Balance Method, the Nonlinear Frequency Domain method and the Nonlinear Harmonic Phase Solution method. The time-linearized equations were obtained by subtracting the time-averaged equations from the original unsteady flow equations and neglecting the nonlinear terms (Adamczyk, 1985[1]). And Hall and Lorence[2] expressed this unsteady time-linearized equations as one harmonic. With the harmonic formulation, the time domain unsteady time-linearized equations could be converted into steady like equations about the harmonic amplitude in the frequency domain. The use of the Fourier transformation technique was further exploited by Hall[3] and McMullen[4]. Hall proposed the Harmonic Balance Method, while McMullen proposed the Nonlinear Frequency Domain method. And the latest Nonlinear Harmonic Phase Solution method is coined by He[5].

This article adopts the Harmonic Balance method for unsteady flow field simulation. This method expresses an unsteady flow solution as a whole in Fourier series, giving rise to work out the time derivative in the unsteady flow equations using the flow solution at equally spaced phases in a period of unsteadiness. Fourier transformation is utilized to get the time derivatives of the conservative flow variables in terms of the flow solution variables at those discrete phases.

**II. PHYSICAL MODEL AND SOLUTION METHOD**

Integrating the unsteady Reynolds-averaged Navier-Stokes (U-RANS) equations over a control volume, we could obtain the following semi-discrete finite-volume form equations:

$$V \frac{\partial \mathbf{W}}{\partial t} + R(\mathbf{W}) = 0 \tag{1}$$

where  $\mathbf{W}$  is the conservative flow variables, including the fluid density, momentum, total energy and turbulent variables depending on the model;  $V$  represents the volume of the grid cell and  $R$  is the residual resulting from the discretization of the fluxes and the source terms (comprising the turbulent equations).

Assuming the flow variables are composed of non-harmonically related frequencies, these variables could be expressed approximately as follow :

$$\mathbf{W}(t) \approx \sum_{k=-N}^N \hat{\mathbf{W}}_k e^{i\omega_k t} \tag{2}$$

$$\mathbf{R}(t) \approx \sum_{k=-N}^N \hat{\mathbf{R}}_k e^{i\omega_k t} \tag{3}$$

where  $\hat{\mathbf{W}}_k$  and  $\hat{\mathbf{R}}_k$  are the coefficients of the Fourier series for the frequency  $\Gamma_k = \omega_k / 2\pi$ . Plugging the Eq.(2) and the Eq. (3) into Eq.(1) yields

$$\sum_{k=-N}^N (i\omega_k V \hat{\mathbf{W}}_k + \hat{\mathbf{R}}_k) e^{i\omega_k t} = 0 \tag{4}$$

The formula(4) could be changed into  $2N+1$  frequency domain equations by harmonic balance. However it is very different to solve it. By inverse discrete Fourier transformation, we could sample these equations in time onto a set of  $2N+1$  time levels. The following matrix formulation is obtained:

$$F^{-1} \cdot (iVP \hat{\mathbf{W}}^* + \hat{\mathbf{R}}^*) = 0 \tag{5}$$

$F^{-1}$  is an inverse discrete Fourier transform matrix (IDFT) :

$$F^{-1} = \begin{bmatrix} e^{i\omega_{-N}t_0} & \dots & e^{i\omega_0t_0} & \dots & e^{i\omega_Nt_0} \\ \vdots & & \vdots & & \vdots \\ e^{i\omega_{-N}t_k} & \dots & e^{i\omega_0t_k} & \dots & e^{i\omega_Nt_k} \\ \vdots & & \vdots & & \vdots \\ e^{i\omega_{-N}t_{2N}} & \dots & e^{i\omega_0t_{2N}} & \dots & e^{i\omega_Nt_{2N}} \end{bmatrix}$$

Where,

$$\omega_0 = 0, t_0 = 0, \omega_{-N} = -\omega_N$$

$$P = \text{diag}(-\omega_N, \dots, \omega_0, \dots, \omega_N)$$

$$\hat{\mathbf{W}}^* = [\hat{W}_{-N}, \dots, \hat{W}_0, \dots, \hat{W}_N]^T, \hat{\mathbf{R}}^* = [\hat{R}_{-N}, \dots, \hat{R}_0, \dots, \hat{R}_N]^T$$

So the Fourier coefficients can be computed by

$$\hat{\mathbf{W}}^* = F \mathbf{W}^* \tag{6}$$

$$\hat{\mathbf{R}}^* = F \mathbf{R}^* \tag{7}$$

$$W^* = [W(t_0), \dots, W(t_i), \dots, W(t_{2N})]^T; R^* = [R(t_0), \dots, R(t_i), \dots, R(t_{2N})]^T$$

applying these relationships, the governing equations could be given by:

$$iVF^{-1}PFW^* + R^* = 0$$

By introducing the pseudo-time derivative term to the above equations, we can solve these equations by a time marching method.

As for spatial discretization, the central difference method with a second order and fourth order blended artificial viscosity is adopted. About temporal discretization, this article applies the four-stage Runge-Kutta method with second-order accuracy. In order to reduce time cost, local time stepping, implicit residual smoothing and multi-grid techniques are employed to accelerate convergence. The one-equation S-A model is chosen as turbulence model.

There are four types of boundary conditions. At the subsonic inlet boundary, the total pressure, total temperature and flow angles are specified, while the static pressure is prescribed at the outlet boundary. The non-reflecting boundary described by Giles[6] has been applied at both inlet and outlet boundary. The periodical boundary condition in a single blade passage computation for unsteady is different from the steady one. It is necessary to use the phase-lag condition[7] to take the space-time periodicity into account. Applying this condition in equation(2), we can obtain that:

$$\hat{W}_k(\theta + \Delta\theta, t) = \hat{W}_k(\theta, t) \cdot \exp(i\beta_k)$$

Where,  $\beta_k$  is the inner blade phase angle. Combining the Fourier transform equation(6), the periodical boundary condition in this article could be given by:

$$W^*(\theta + \square\theta) = F^{-1}MFW^*(\theta)$$

Where,  $M = \text{diag}(-\beta_N, \dots, \beta_0, \dots, \beta_N)$

### III. CASE DESCRIPTION

An original-designed two-stage counter-rotating lift fan is studied in the present work, which is the central part of the propulsion system. The 3D solid modeling drawing of this fan is showed in Fig.1.



Figure 1. Two-Stage Counter-Rotating Lift Fan

This fan is small with a constant shroud-contour radii of 75mm. The rate of mass flow and total pressure ratio at design point is 1.8 kg/s and 1.08 respectively. Before simulating this fan with harmonic balance method, we should give the frequencies of unsteady disturbance. According to Tyler and Sofrin[8], in multi-stage environment, the kth frequencies of jth row could be given by:

$$\omega_k^j = \sum_{i=1}^{NR} n_{k,i} B_i (BPF_i - BPF_j) \tag{8}$$

Where BPF means blade passing frequency, NR is blade count. The  $n_{k,i}$  represents  $k$  sets of user-defined integers that drive the frequency combinations.

Table 1 Parameters about the unsteady frequency

	Design Rotation Speed(RPM)	Blade Count	BPF(Hz)
Row 1	-19100	7	318.3
Row 2	13200	8	220.0

According to the parameters in Table 1, specified  $n_{1,2}=1$  for blade row 1, then we can get that  $\omega_1^1=4306.7\text{Hz}$ , specified  $n_{1,1}=1, 2, 3$  for blade row 2, then we can get that  $\omega_1^2 = 3768.3\text{Hz}, 7536.7\text{Hz}, 11305.0\text{Hz}$ .

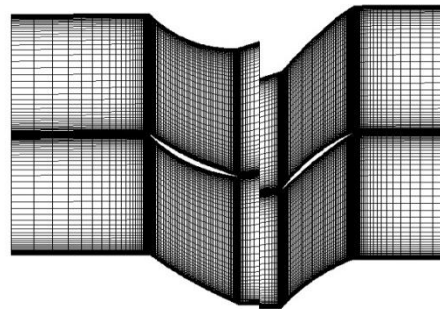


Figure 2. Computational Grid

Because of the adoption of phase-lag boundary condition, a single passage computational domain is used. In present work, single H block are applied on spatial discretization for each blade row. Both single H block have the same grid points in three direction, with  $57 \times 129 \times 65$  nodes in the circumferential, axial and radial direction respectively. The mesh is showed in Fig. 2.

#### IV. RESULTS AND DISCUSSION

Considering the atmosphere condition that the lift fan works at, total pressure (101325Pa) and total temperature (288.15K) is given at inlet and static pressure (101325Pa) is fixed at outlet. Then keeping the boundary conditions unchanged, several simulations using harmonic balance method have been finished at different rotation speed. The characteristic of lift force and isentropic efficiency varying with rotation speed is illustrated in Fig.3.

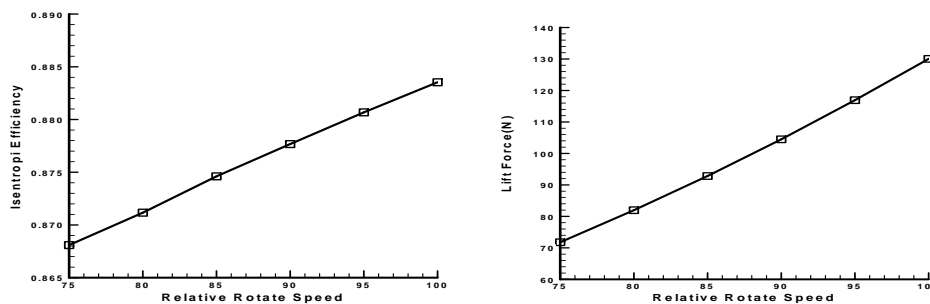


Figure 3. Lift Fan Characteristic: Lift Force and Isentropic Efficiency

The relative rotation speed is scaled by design rotation speed. Fig. 3 shows that the isentropic efficiency and lift force is almost linearly associated with the rotate speed. And the efficiency and lift force reach peak at design rotation speed, with 0.8835 and 130.04(N) respectively.

For further analysis, this article takes the working condition, i.e. design point, as the research object. By reconstructing the flow solution from harmonic balance in time, we can gain the time-varying flow variables. Fig. 4 shows the time-varying isentropic efficiency of row 1 and row 2.

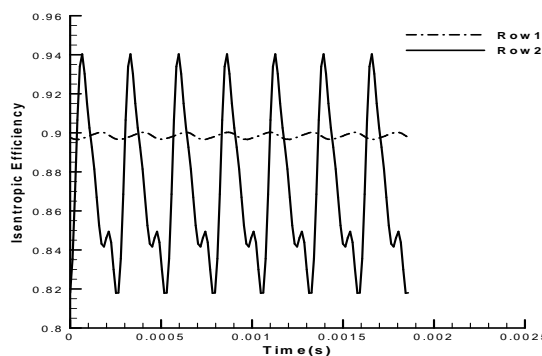


Figure 4. Variation of Isentropic Efficiency along Time at Design Point

From Fig. 4, it is clear that the isentropic efficiency in row 1 changed between 0.897 and 0.900, while it changed between 0.818 and 0.940 for row 2. So the changing amplitude for row 2(0.122) is almost as 40 times as that for row 1(0.003). This indicates that the flow unsteadiness in row 2 outweigh the flow unsteadiness in row 1.

The reason is that the dominant unsteady perturbation of row 1 is an acoustic disturbance (pressure wave), which is from row 2 and propagate both upstream and downstream for subsonic flow. And the unsteady perturbation of row 2 is composed of acoustic disturbance and entropy disturbance. The entropy disturbance is caused by the wake of row 1 and convects at a local flow velocity, running downstream. Entropy has a close relationship with the isentropic efficiency. As a result, the downstream of entropy disturbance of second row experiences a bigger variation of isentropic efficiency. The entropy could be compute as follow:

$$entropy = C_p \ln \frac{T}{T_{ref}} - R_g \ln \frac{P}{P_{ref}}$$

Where,  $T_{ref}$  is the reference temperature and  $P_{ref}$  is the reference pressure. In present work,  $T_{ref}$  equals inlet total temperature(288.16K) and  $P_{ref}$  equals inlet total pressure (101325Pa). Fig. 5 shows the process of wake entropy flow chopped by the second stage rotor.

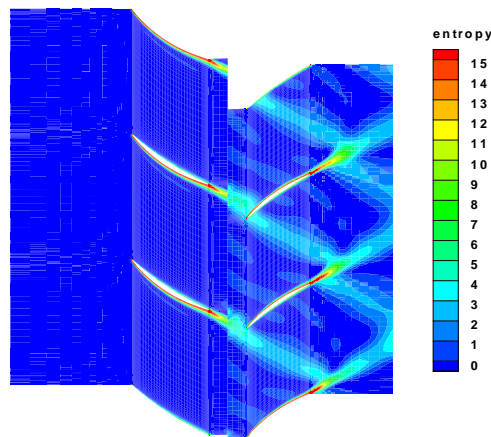


Figure 5. Instantaneous Entropy Contour of at 50% Span

In view of the small unsteady effects of row 1 and the difficulty of ensuring the performance of the second row of counter-rotating compressor/fan, it is more meaningful to study the unsteady effects of the second row. The follow part would focus on the unsteady flow field of the second row at design rotation speed.

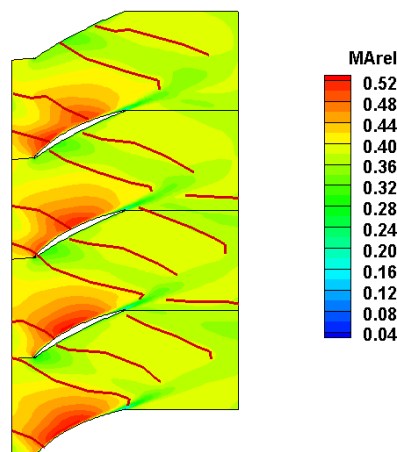


Figure 6. Instantaneous Relative Mach Number Contour at 20% Span of Row 2

Fig. 6 shows the instantaneous relative mach number contour of row 2, and the red solid lines represent the row1 wake shape. We can see that the originally arc-shaped relative-high mach regions are deformed by the rotor wakes. When the wakes pass through these arc regions, the area of these regions become smaller. It results from the negative jet described by Fig. 7.

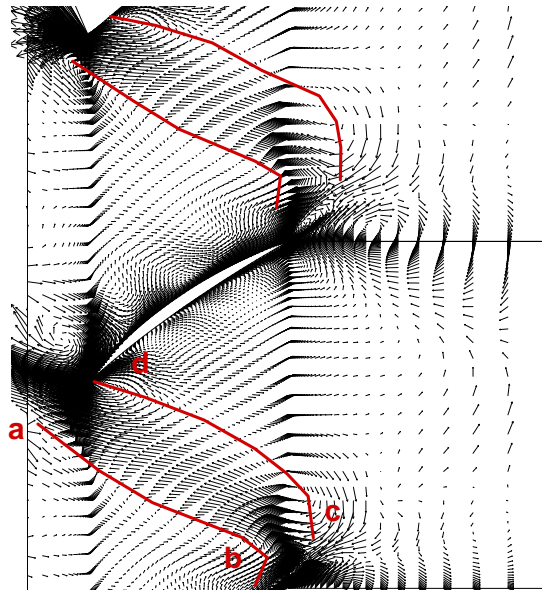


Figure 7. Instantaneous Velocity Vector Perturbation Field at 50% Span

The perturbation field is defined as the difference between an instantaneous solution and the time-averaged one. The wakes appear as a jet pointing upstream toward the trailing edge of the blade it originated from. So the direction of disturbance velocity is opposing the direction of mean flow velocity. As a result, it lessens the mach number and causes the deformation of high relative mach number region. According to the model of Smith[9], the circulation across the wake segment a-b-c-d remains constant :

$$\Gamma = \oint_{\Omega} U ds = ab\Delta U = \text{constant}$$

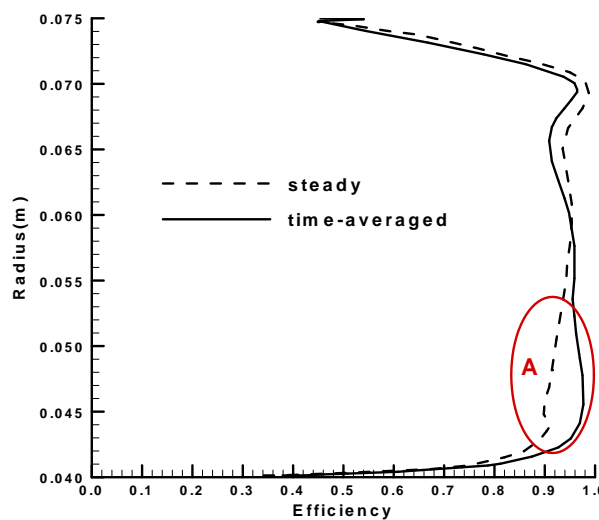


Figure. 8 Distribution of Isentropic Efficiency along Blade Span

Under the assumption of incompressible and inviscid flow, to have the constant circulation, the velocity defect in the wake has to change inverse proportion to the wakes length. As the wake segment passes through the downstream passage, it would be tilted and stretched because of the difference in velocity between suction and pressure side and the diffusive shape of vane. So the wake length grows longer, which results in smaller velocity defect and less flow loss. This is called wake recovery. Though the velocity difference between suction and pressure surface is small for the test case in this paper, this phenomenon can also be found in Fig. 5 by careful observation. For further study of the influences of the unsteady disturbance on the efficiency, the comparison of isentropic efficiency along the blade span between time-averaged HB solution and steady solution is illustrated in Fig. 8.

It could be found that the isentropic efficiency obtained by HB below mid-span is higher than that from steady calculation, while a contrary relationship exists above mid-span. To explain this interesting phenomenon, a parameter  $k$  which could be used to describe the intensity of unsteady disturbance is introduced here:

$$k = \sqrt{u'^2 + v'^2 + w'^2} / U_{\text{tip}}$$

Where,  $u'$ 、 $v'$ 、 $w'$  are the fluctuating velocity in three directions respectively,  $U_{\text{tip}}$  is the blade tip speed (103m/s in this work). The instantaneous contour of  $k$  at row2 inlet is showed in Fig. 9.

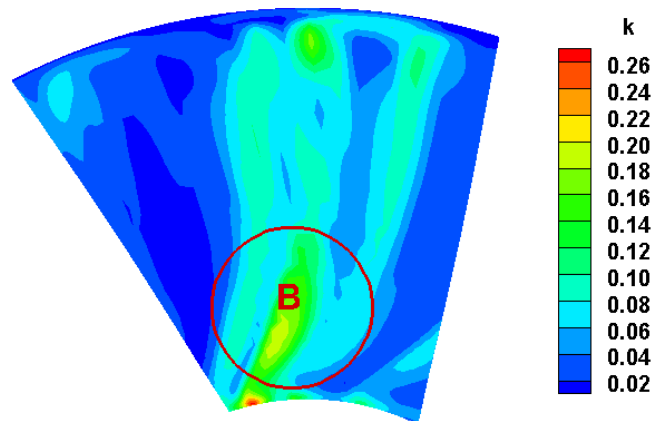


Figure. 9 Contour of  $k$  at Row2 Inlet

The wake from row 1 can be identified clearly in Fig.9, and it shows that the disturbance caused by the upstream wake is the dominant part of unsteady perturbation. Meanwhile, Fig.9 also indicates that the intensity of wake disturbance weakens along blade span. Combining Fig.8 and Fig.9, it can be found that a higher value of  $k$  is corresponding to higher efficiency below mid-span, i.e., the circle region B in Fig.9 agrees with the ellipse region A in Fig.8. However, this law is invalid above mid-span.

For most of transonic compressors/fans, the work is done by changing the velocity direction near blade root and by shock compression near blade tip. So the difference of velocity between suction and pressure side is bigger at the position near blade root. It results that the upstream wake near the stall is tilted and stretched more than that near the blade tip. Consequently, the wake recovery near blade root is stronger and the isentropic efficiency is higher.

As for the low efficiency near blade tip comprising the steady one, it should be attributed to a couple of reasons. The first reason is explained as above, i.e. the feeble wake recovery. The second reason is that the upstream wake interacts with the boundary and the downstream wake.

Fig. 10 shows the entropy contours at three moments. Firstly, taking a look at the contours at 85% span, it is clear that, at time A, the entropy flow caused by upstream wake is in blade passage, and it thickens the boundary layer on the suction surface and leads to efficiency loss (entropy production). At time B, the wake entropy flow passes through the row 2 wake and enlarges the area of high entropy value. At time C, the wake entropy continues to spread and interact with the row2 wake. It is obviously that the process of interaction between row 1 wake and row 2 wake increases entropy a lot and leads to serious efficiency loss at 85% blade span. Then turning attention to the contours at 15% span, though there is a similar phenomenon in Fig.10, the entropy increased by the wake interaction is tiny and the resulting efficiency loss is exceeded by efficiency gains due to the strong wake recovery. Above all, the wake recovery is dominant below mid-span, while the wake interaction is dominant above mid-span.

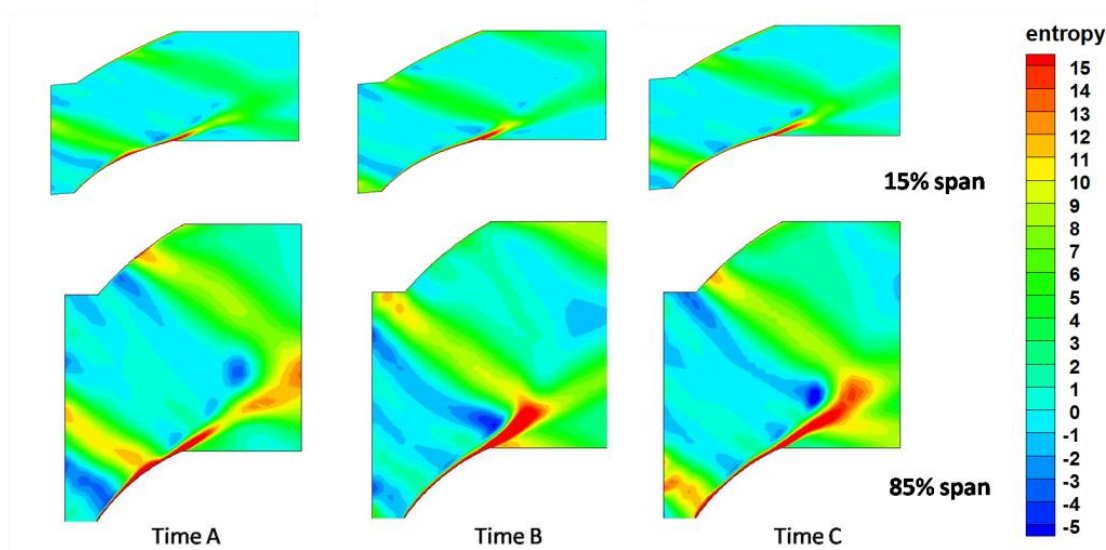


Figure. 10 Entropy of Three Moments at 15% and 85% Blade Span

## V. CONCLUSION

This paper applies harmonic balance method to simulate the original-designed two stage counter-rotating fan. The unsteady characteristic, row interaction and wake spread have been studied, the discussions show that: the upstream wake improves the efficiency of row 2 below the mid-span because of the wake recovery, while it lowers the efficiency above the mid-span because of interaction between row1 and row 2 wake; It is meaningful to study how to make use of the unsteady effects; The harmonic balance method is efficient and reliable to simulate the periodic unsteady blade row interaction.

## REFERENCES

- [1] Adamczy, J. J., Model Equations for Simulating Flows in Multistage Turbomachinery. *ASME Paper*, 85-GT-226, 1985
- [2] Hall, K., Lorence, C., Calculation of Three-dimensional Unsteady Flows In Turbomachinery Using the Linearized Harmonic Euler equations. *Journal of Turbomachinery*, 115(4), 1993, 800-809
- [3] Hall, K., Thomas, J., Clark, W., Computation of Unsteady Nonlinear Flows in Cascades using a Harmonic Balance Technique. *AIAA Journal*, 40(5), 2002, 879-886
- [4] McMullen, M., Jameson, A., Alonso, J., Demonstration of Nonlinear Frequency Domain Methods. *AIAA Journal*, 40(7), 2006, 1428-1435
- [5] He, L., Harmonic Solution of Unsteady Flow around Blade with Separation. *AIAA Journal*, 46(6), 2008, 1299-1307
- [6] Giles, M. B., Nonreflecting Boundary Conditions for Euler Equation Calculations, *AIAA Journal*, 28(12), 1990, 2050-2058
- [7] Erdos, J.I., Alznert, E., McNally, W., Numerical Solution of Periodic Transonic Flow through a Fan Stage, *AIAA Journal*, 15(11), 1977, 1559-1568
- [8] Tyler, J., Sofrin, T., Axial Flow Compressor Noise Studies. *Society of Automotive Engineers Transactions*, 70, 1962, 307-332
- [9] Smith, L.H., Wake Dissipation in Turbomachines, *Journal of Basic Engineering*, Vol. 88D, 1966, 688-690

## View of Flood Disaster Management in Indonesia and the Key Solutions

Ratih Indri Hapsari<sup>1</sup>, Mohammad Zenurianto<sup>1</sup>

*1(Department of Civil Engineering, State Polytechnic of Malang, Indonesia)*

**ABSTRACT:** Over the years, Indonesia has seen many flood disasters that have brought about great losses. The aim of this study is to address key issues that lead to flooding problems in Indonesia in response to the challenge of recurrent flood events. An overview of the past flood disaster profiles and ongoing flood management are presented. The problems with the current situation are identified and the critical solutions are recommended to manage flooding and mitigate the negative impact in a more sustainable way. This study shows that man-made factors, natural causes, and managerial issues are the factors that have contributed to the problem. The coordination and the public awareness are the challenges in improving the flood management. Efforts have been made to alleviate the problems through legal framework establishment, community participation programs, and flood-control projects. In the post-disaster stage, the authorities and public have been quite responsive. However, prevention and preparedness are still lacking. The overall current flood disaster management may lead to more recurrent events and cause severe impacts. Sustainable actions are needed to solve these problems that include environment-based flood integrated countermeasures, improving water retarding function, eradication of deforestation, meteorological and hydrological prediction, and political will and law enforcement.

**Keywords** –Flood disaster, Indonesia, disaster management, environment, flood countermeasures

### I. INTRODUCTION

Flooding has been recognized as one of the worst disasters[1]. It is one of the most frequent and expensive natural disasters in the world. Hundreds of millions of people around the world have been affected by floods. Floods lead to social and physical losses and may have significant impact on the economic condition of a nation. The worldwide distribution of natural disasters in the last decade, categorized by disaster type, is depicted in Fig. 1. It is noticeable that flooding is the most chronic natural disasters in terms of the number of occurrences and the impact on humans.

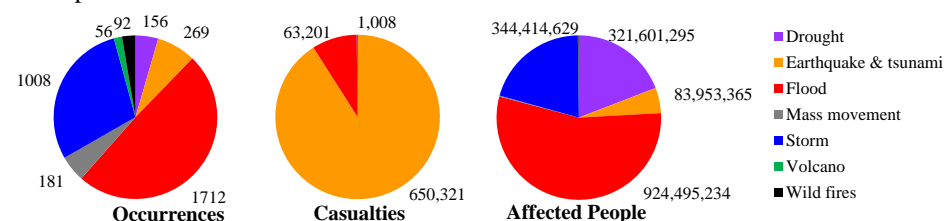


Figure 1. Worldwide natural disaster (2004–2013)[2]

Indonesia is an equatorial, tropical country with around 17,000 islands. With a total population of approximately 237 million people, it is the fourth most populous country in the world. Indonesia is frequently hit by natural disasters. Almost regularly, Indonesia experiences floods, landslides, earthquakes, tornados, cyclones, tidal bores, and droughts. In the last decade, Indonesia has faced frequent, recurrent flooding every year in many parts of the country[2][3]. Compared with other countries, Indonesia is considerably more vulnerable to flooding disasters[4]. It ranks third and seventh in the world in terms of flood occurrence and the number of people affected, respectively (Fig. 2).

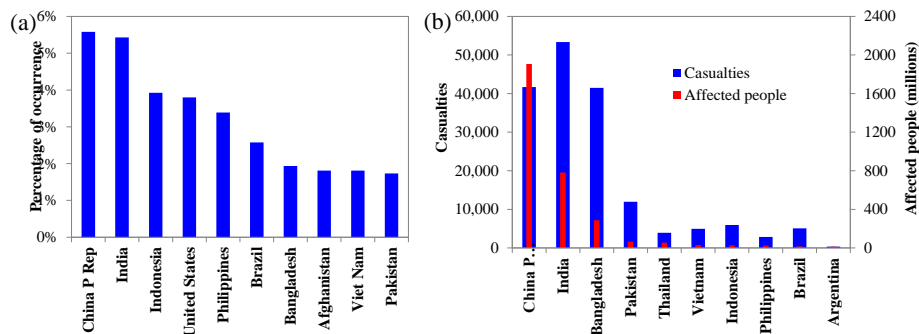


Figure 2. (a) Percentage of worldwide flood occurrence by country (1970–2011); (b) Number of casualties and affected people due to floods by country (1970–2011)[2]

Flood disaster management in Indonesia has not been as widely implemented as expected[5][6][7]. Between 2004 to 2013, flood occurred annually and affected more than 12 million people[8]. Annual incidences of flooding were worst in 2008 and 2009; however, these events only appeared as “routine” mass media coverage[9][10][11]. Environmental scientists believe that an increase in population, exacerbated by the effects of climate change, have contributed to these flooding catastrophes[12][13]. Although much work has been done by the government of Indonesia (GOI) to manage the flood problem, the complex issues, including budget allocation issue, awareness issue, and the need for expertise, remain challenges in achieving efficient flood risk management[5][7][14][9].

A few studies based on the flooding issues in Indonesia have been conducted, each dealing with various aspects of the problem. Some studies have researched the technical and engineering aspects of flooding, e.g. flood modeling, GIS utilisation, hazard mapping, and prediction [17][15][16]. Other studies have discussed flooding impacts, including physical damage, health risks, economic damage, and numerous other factors [14][18]. Several papers concerning the social and managerial aspects of flooding in Indonesia, such as public participation, non-physical countermeasures, governance, and regulatory issues, have also been written [5][17][9][12][19]. Some of these studies focused on a particular part of the country rather than the entire country. Scientific papers, in particular, still have limited discussions on concrete and deliverable solution that might be realized to reduce flood occurrence based on identification of the flooding problems.

With respect to the background described above, the objectives of this paper include: to identify the cause of subsequent flood disasters in Indonesia based on the profiles of past flood events and the present state of flood disaster risk management; to evaluate the effectiveness of current flood disaster management, and; to formulate the concrete solutions of reducing flood risk in Indonesia. The critical information provided in this paper and the proposed solutions are expected to be useful for the country to cope with future flood problems.

## II.METHODOLOGY

### 2.1 Profile of Indonesia as Study Area

Indonesia is an island nation in South East Asia, located in the equator lying between 11°S to 6°N and 95°E to 141°E. Indonesia’s total land area is 1,919,440 km<sup>2</sup>, making the world’s 14<sup>th</sup> largest country by total area, and includes 93,000 km<sup>2</sup> of inland water or accounts for 4.88% of country area. The population, as recorded by Statistics Indonesia in 2011 is 237,424,363, with the average population density of 125/km<sup>2</sup>. The population is heavily concentrated at Java Island. Its population is 139 million inhabitants or accounts for 57% of Indonesia’s population, making the world most populous island. The capital, Jakarta, is located in the western part of Java Island. Indonesia is classified as developing country with lower middle income. It has emerging market economy with current average per capita GDP is \$3,464. Abundant natural resources contribute significantly to Indonesia’s total wealth.

Indonesia has a special characteristic of climate including the influence of monsoon season, tropical climate, and oceanic climate[20]. The climate in Indonesia is predominantly tropical, with two distinct monsoonal wet and dry seasons. The wet season starts from November and ends at March, which brings the rains, and the rest is the dry season. Its special climate characteristic contributes to the vulnerability to hydrological/climatological disaster. Average annual rainfall is considered quite high, which measures as much as 2000–3500 mm in the lowlands but up to 6000 mm in the mountainous area. From average precipitation amount of 2700 mm, about 90% becomes overland flow as a surface runoff, while the remaining of about 278 mm goes through infiltration/percolation[33]. Indonesia is a humid tropical country with average humidity of about 80%. Temperature usually ranges from 26 to 30°C and varies little throughout the years.

In the 1950s, the landscape of Indonesia was mostly covered by tropical rain forest for approximately 77% of the country[21]. However, the area of natural forest cover decreases significantly year by year. Currently, forest comprises only 51.8% of total land area. Between 1950 and 1985, Indonesia lost 27% of its forest area or 0.77% per year. Large scale deforestation driven by the expansion of urban and agriculture area as well as timber cutting. Moreover, destruction due to wildfires is a serious problem in Indonesia. The quite high growth of population in Indonesia of 1.9% highly contributes to the forest land conversion into other land uses.

**2.2 Data Collection and Research Method**

Secondary data in the form of records of flood disaster events and the consequences is obtained from Indonesian Disaster Data and Information Database (DIBI) provided by Indonesian National Board for Disaster Management (BNPB) (Indonesian National Board for Disaster Management, 2014). Facts on flood events in the regions collected from emergency situation reports are also used. Primary data is used in this study to provide the study with specific information about the effectiveness of existing countermeasure, current management being implemented, and public perception on flood disaster. This data was collected through field survey and discussion with local people and also with authority during October 2015.

The profiles of past flood events and the present state of flood disaster risk management are investigated through a review of database, literature, and interview result. The underlying causes are identified and the current management of these causes is described using content analysis. On the basis of the present status, the effectiveness of current flood disaster management is analyzed, and future needs are pointed out. Finally, some insights for further improvement of flood management in technical and regulatory arrangements directed toward the sustainable flood countermeasures are discussed.

**III. FACTS ON INDONESIA’S FLOOD DISASTER**

**3.1 Flood Disaster Profile in Indonesia**

Indonesia is found to be vulnerable to a variety of natural disasters such as drought, earthquake and tsunami, and flood. Figure 3 shows the chart of occurrences of disaster events and the total loss for each disaster type within 1974 to 2013, which is obtained from DIBI. Flood is defined as significant rise of water level in a stream, lake, reservoir, or coastal region. The criteria for defining flood incidents are those that have ten or more people reported killed, more than a hundred people reported affected, declaration of a state of emergency, or call for international assistance. Based on these criteria, the pie chart indicates that the flood is the most frequent disaster in Indonesia.

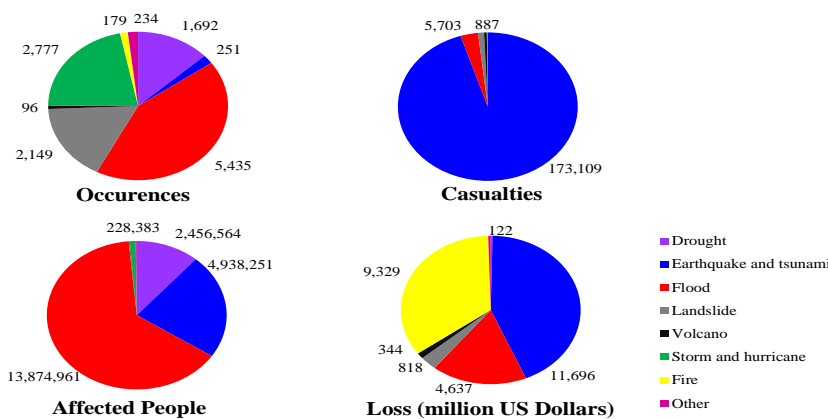


Figure 3. Natural disaster events, loss, casualties, and affected people by disaster type in Indonesia (1974–2013) (Source: National Disaster Management Agency, 2014)

In 2007, 2008, 2009, 2010, 2011, 2012, and 2013 the reported flood occurrence in Indonesia were 338, 490, 381, 990, 553, 540, and 520 events respectively, showing the tendency of increasing. In the tremendous incidents in 2008, 191 people were killed and more than 150 thousand people were affected. In that year, the most serious floods were happened at Situbondo Regency at East Java Province and Jakarta capital city. The 2010 is identified as the year that suffered most from floods in the last five years that killed 502 people. Many floods took place repetitively in some provinces like East Java (January, February, May, June), West Java (February, March, May, September), Central Java (almost all months), and Jakarta capital city (February and October). The numbers of flood occurrence in Java islands are considered quite big, as in East Java Province alone in 2010 the number of flood is 10 events. Over last 40 years, Central Java Province has had the highest occurrences of flood (740), followed by East Java (662), and West Java (535)[8].

The flood disaster severity is determined based on its negative impact, usually including casualties, affected people, and economic damage. Flood is responsible to the second deadliest disaster in Indonesia's history of past 40 years. In terms of the number of casualties, it is in the second most severe disaster after tsunami (mostly contributed by 2004 Indian Ocean earthquake and tsunami). In terms of the damage, flood is in the third most expensive disaster after tsunami and wildfire. Millions of people in Indonesia have been affected by flood in last five decades, giving the flood the most serious disaster in terms of the number of affected people.

### 3.2 Impact of Flood Disaster

Flood catastrophe could lead to some severe negative consequences directly and indirectly that include social, environmental, and economic impacts. These impacts vary with different severity according to the distance, vulnerability, and flood extent[7][17][11][12][18]. Major flood causes health problems, including community disease, injuries, and disabilities. The worst effect a flood creates is the loss of human life due to fast-flowing water and waterborne disease. In addition to the physical problem, the flood causes psychological stress. Lost the family member, evacuation, interruption of work, loss of home and livelihood may cause the enduring psychological impacts. One of the negative environmental disruptions due to flooding is the contamination of soil and water with hazardous substances because of the abnormal drainage system. Flood also destroys ecological habitat, resulting in the loss of animal and plant. Aside from the devastation in response to large floodwater, landslide and sedimentation brought by flood appear as another concern for environment. High velocity flooding may directly destruct the physical properties such as streamside, housing, infrastructure, and agriculture land. The failure of those assets and the cost to repair the destroyed construction brings the monetary losses[22]. Furthermore, the flood-related supply disruptions severely impede the economic activity of Indonesia[23].

Recurrent flood occurrences that have been faced between 2004 and 2013 in every year across the country have brought significant damages and losses. No less than 1500 people have been killed and around 12 million people have been affected. Table I shows the data of damages and losses in this period obtained from DIBI[8]. In Jakarta, flood in January and February 2007 is considered to be the greatest flooding in last three centuries. Flood induced by high rainfall with 195 mm/day rate has inundated about 40% to 70% of the capital city area and about 320,000 people were driven from the houses by floods. The flood disaster took 80 lives in total due to being swept, flood-related disease, and electric stun. The total monetary loss due to 2007 flood is estimated to be in the range of more than 400 million US dollars. On October 2010 a devastating flood struck TelukWondama Regency at Papua Province. Heavy rains caused destructive flash floods, landslides, and mudslides, which have killed at least 161 people. The flood caused damages to major infrastructure facility include the airport and brought more than 30 million US dollars in losses[24]. In 2013, Jakarta has suffered from severe flooding again, which caused 33,500 people were displaced. In this year, the maximum daily rainfall of 168 was somewhat lower than 2007 flood event; however, it was distributed evenly over the region. In the middle of 2013, Ambon City flooding has caused the death of 11 people. In the end of 2013 and beginning of 2014, many cities have experienced flooding, including Manado City at North Sulawesi Province, Medan at North Sumatera Province, Kudus at Central Java, and Samarinda at East Kalimantan.

Table I. Flood damages and loss in Indonesia between 2004 and 2013

Damage	Quantity
People killed	1,546
People injured	105,180
People evacuated	3,007,125
People affected	12,771,746
Houses damaged	2,268,356
Schools damaged	6,251
Bridges damaged	454
Land damaged	1,161,170 Ha

Source: National Disaster Management Agency, 2014.

### 3.3 Present Status of the On-Going Management Measures

The current organisation is Indonesian National Board for *Disaster* Management (BNPB), a ministerial level non-departmental government institution[24]. According to the Law of Republic of Indonesia Number 24 of 2007 concerning disaster management[25], the roles of BNPB in disaster countermeasures cover three stages: pre, during, and post disaster circumstances. In the less disaster prone area, pre-disaster tasks comprise of

preventing the disaster by protecting natural resources from overexploitation, planning the disaster countermeasures plans, increasing community resilience, estimating the disaster impact, analyzing the disaster risk and reduction, and conducting the education. Countermeasures in disaster-prone area typically embrace all aspects of preparedness and mitigation. Observation and prediction, emergency response plan, and early warning system are the elements of disaster preparedness under BNPB responsibility. Works done during disaster are focused on damage analysis and rescue and evacuation. The post-disaster responses enable the disaster area recovery through rehabilitation and reconstruction. They are made up by physical elements consisting of environment, facility, infrastructure, and residential recovery in addition to non-physical ones such as social, psychological, economy, culture, governance, and public service.

The implementation of disaster management at sub-national levels is handled by the representative of BNPB in every province and regency/municipality, known as Regional Board of Disaster Management (BPBD)[21][25]. In general, the responsibilities of BPBD are identical to those of BNPB, but they are different in the jurisdiction level. The BPBDs play major roles in the disaster management activities in their respective areas backed up by BNPB and Indonesian military, thereby the BPBD is expected to act quickly with well thought-out plans. The mandates of the government, whether central or local, are set out in the establishment of BNPB or BPBDs and their disaster management policies to maintain public welfare. Furthermore, the governments have responsibility to include disaster countermeasures and disaster risk reduction in the developmental works with allocating specific budgets for those purposes.

In the implementation of disaster management, BNPB works along with related state-owned and non-state-owned corporations. Regarding prediction of flood, BNPB collaborates with Meteorological, Climatological, and Geophysical Agency (BMKG), Coordination Agency for Surveys and Mapping, Ministry of Public Works, and its local office in every region, river basin management authorities, and so forth. Indonesia Red Cross Society, National Search and Rescue Agency, Ministry of Social Affairs are the main institutions concerning to flood emergency response. The mechanisms of collaboration to those institutions are governed generally.

### 3.4 Past and Current Efforts of Flood Alleviation

There have been some recent efforts to alleviate the wide range of flood problem through structural measures at national level, either independently or by assistance of international agencies. For instance, land use spatial planning in Jakarta Flood East Canal Project, integrated water resources management carried out by Brantas River Basin authorities, provision of adequate coastal inundation problem at low-lying area of Semarang, and resettlement of river squatter in Solo River[26][11]. Some major river including Ciliwung River, Brantas River, and Citarum River have been equipped by system for flood warning for operational purpose[9][11]. However, instead of rainfall short-range forecasting, they are supplied by real time rainfall monitoring, long-range rainfall forecasts, or even none, possibly due to lack of expertise. Technical cooperation with some developed countries is undertaken in establishing model for flash flood disaster mitigation management with empowering local government or society and also in other fields. On the water resources side, some projects to promote water supply and demand efficiency were launched including stream normalisation from Mt. Merapi volcanic debris and dredging of some vital reservoirs, such as Sutami Dam at Brantas River Basin[11][27]. Rainwater harvesting is encouraged as part of flood and drought management such as in Semarang city[7][17]. Within the last couple of years, significant investments and efforts toward Jakarta flood reduction has been made. It includes the large scale dredging project and squatter clearance, pump revitalisation, promoting the construction of 2 million infiltration wells.

Recently, raising public participation program has become attention of GOI. Many actions have been done to promote the consciousness in flood hazards and to increase community preparedness in managing the surroundings hazards, for instance public empowerment for disaster risk reduction in Jakarta, dissemination of flood knowledge to the community, conducting workshop of local government and community leader, and education through formal and religious organization[9][7][12][28]. In order to increase the resilience in facing flood disaster, the government has been encouraging the public to have self-initiative in facing their surrounding flood hazard by their own local resources, or known as of community based disaster management. In addition to the improvement of the governance matters, recently Indonesia has noted much advancement in the research of flood disaster prevention, which should contribute to the development of effective and efficient flood countermeasures plan. Strengthening the national disaster database in Indonesia through DIBI Project introduced by UNDP and GOI is one attempt to facilitate risk assessment and pre-disaster decision making. Some scientific meetings have been conducted to discuss the flood disaster in Indonesia as well as integrated flood and drought management, e.g. the establishment of Indonesia's Partnership for Disaster Risk Reduction[25].

As found previously, in the strike of disaster, the authorities often are quite responsive to the events. Local military force and volunteer rescue workers provide rescue and evacuation service organized by local government quickly. In the TelukWondamaflash-flood case, the Ministry of Health through provincial health

office, district health office, and port health office has responded to the situation by supplying medical services and logistic within one-day aftermath the disaster[29]. No less than 10 thousand people, that consists of armed forces, civilian defense unit, red cross, search and rescue agency, and other units have been assigned by the GOI to assist the flood emergency responses at the 2007 Jakarta flood[30].

Although much effort and resources have been expended for post-disaster response, the prevention and preparedness actions are seen to be lacking. The policy has been addressed to emphasize natural hazards rather than the cause of vulnerability[6]. Inconducive conditions for designing substantive plan are identified, which leads to the weak planning in both central and regional levels. Despite the established legal framework in the areas of disaster preparedness as elaborated in the review of policies and institutional capacity for early warning and disaster management in Indonesia[31], there remain difficulties towards the implementation of disaster management regulation. Indeed, today, the people obedience to law and professionalism in law enforcement in Indonesia remain low. Lack of coordination is still found between the central and provincial governments as well as with the counterparts. Along with decentralisation policy, Indonesia's disaster management is now in the transition from the centrally planned to the empowerment of local institution[23]. Notwithstanding the above, BNPB are continually to improve the system towards a more efficient coordination among elements. On the policy maker side, regional sectors often consider that the disaster handling is the tasks of BNPB and central government rather than synergistic mutual cooperation.

#### IV. ANALYSIS OF MAJOR CAUSES OF FLOOD DISASTER SEVERITY IN INDONESIA

In this section, the underlying causes of severe flooding in Indonesia and the current handling of these causes are identified. The analysis is conducted based on the review of the past flood events and the present state of flood disaster risk management. The effectiveness of current flood disaster management is analyzed based on the present status. The content analysis reveals several causes of damaging floods which are described below.

##### 4.1 Natural Caused

Flood is said to be natural if the cause is high rainfall intensity. Being the country with high annual rainfall, the problem of flood in Indonesia becomes serious[23]. Wet monsoon brings much rainfall through moist southwest wind that contributes highly to the flood in Indonesia[20]. Beside rain seasonal variability due to monsoon, the rainfall pattern also has unique interannual variability influenced mainly by ENSO. The variability of rainfall patterns varies in different areas of Indonesia at different times. The climate change likely triggers a number of flood occurrences[11][13][12]. Under climate change, the hydrological variables tend to have large spatial and temporal variability and the chance of extreme rainfall is significantly increasing, which make prediction is more difficult. There are more than 5590 small and big rivers in Indonesia[27], of which about 30% pass high density population. Except those located in Kalimantan, most of them have limited water conveying capacity. Moreover, generally, rivers are originated from the volcanic mountains that may convey much quantities of sediment. Hence, along with high rainfall in the catchment, the rivers pose more flood hazard due to river sedimentation. The determinants of flooding could be the combinations of those conditions and some other factors, such as the existence of low lying area, tidal effect, or river morphological factor.

##### 4.2 Human Caused

Occasionally, flood is a natural phenomenon driven by rain. However, when the flood becomes recurring events with frequency more than its return period, factors linked to society or anthropogenic factors may be part of the cause. Overpopulation and its accompanying urbanisation pose significant risk of flood[9][12][22][27]. Along with the high population growth which is closely connected with industrialisation and poverty, the spatial layout would change. The need of more land has driven the deforestation. Land use alterations that are not considerably schemed contribute primarily to the forest degradation problem[11][21][23]. Furthermore, in many cases, watersheds are increasingly being degraded by extensive encroaching practices, such as illegal logging and uncontrolled land use change. Meanwhile, forest is essential to absorb the rainwater into the ground and vegetation helps to intercept the rainwater. Flooding will happen if the soil is saturated so that the rain water has no space to be collected on the ground. At the same time, the channel capacity is not sufficient to convey the excess water. In many urban areas the squatter settlements in the river passage are quite extensive, which causes channel narrowing[6]. There is significant evidence that this human activity along the river banks exacerbates the problem of flooding. These situations are widely found in Java Island and have brought many flood incidents as reported within past fifty years. In the big rivers, the erosion and sedimentation are also the contributing factor to the flooding problem. The large flood transports the sediment from upstream and deposit on river bed, which consequently makes the river shallower. The habit of the people to throw the solid waste to the river body has received the high attention[27]. Due to the blockage of drainage with the garbage, the rainwater has no space to drain and eventually overwhelms the floodplain. Flood hazard map provided by

Indonesian National Board for Disaster Management highlights the region prone to flooding considering the contributing factors to flood[24], which shows that 309 out of 497 cities/regencies of the territory of Indonesia are at medium to high risk to flood threats.

The structural countermeasures have been the focus of recent flood handling programs. The planning of river works for prevention at the level of the whole river basin is indeed very essential. In many places in Indonesia, however, they are undertaken partially[14][9][24] and decided by local stakeholders' own account. Socio-economic feasibility is often insufficient, which makes the master plan exists more as a blueprint than as a thorough plan[23]. For many years, newly built flood control structures are destroyed by flood or else becomes the cause of flooding due to improper design without considering the aspect of design sustainability. Moreover, the delivery of implementation scheme is usually slow due to insufficient expertise[9][23]. In any case, ineffective existing flood management has contributed to the recurrent flood problem. Governance and accountability are still the glaring challenges encountered by Indonesia today in improving natural disaster management.

#### 4.3 Contributing Factors to the Damaging Flood

Flood-related problem in Indonesia is liable to be the result of a combination of some factors indirectly. Besides the above mentioned factors, there are other aspects contributing to the damaging flood. In almost all cases, high death toll results from lack of flood warning[23]. In order to provide a critical warning, there is a need for accurate and timely meteorological-hydrological prediction. However, generally, weather forecast provided by meteorological agency can only predict storm in relatively large spatial scale and give general alert [11][16][23]. Proper flood hazard mapping is still insufficient in regional scale, which may result in delayed flood responses. In the case that the system is well provided, the lack of understanding of forecasting and warning system by the lower organisation levels and low public responsiveness in early warning mechanism may hinder their full and effective implementation[21][23]. In fact, there are still unclear or overlapping role of authorities during emergency situation[9]. Schematic drawing showing factors contributing the flood disaster occurrences in Indonesia is given on Figure 4.

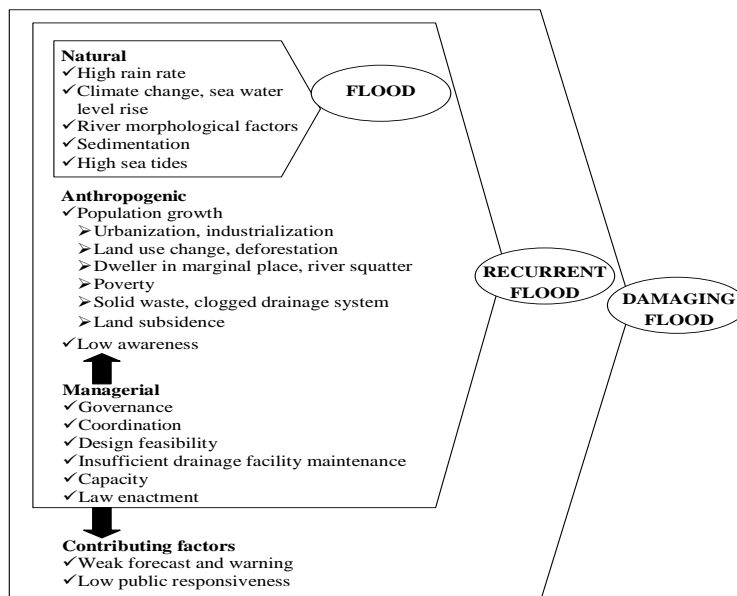


Figure 4. Factors and circumstances contributing to the flood in Indonesia

### V. PROPOSED SOLUTIONS TO ACHIEVE EFFICIENT AND SUCCESSFUL FLOOD MANAGEMENT AND MITIGATION

Having the detailed knowledge of shortcoming of the existing system as elaborated previously, the subsequent attempts in improving the current management aimed at flood risk reduction could be formulated. This part offers integrated recommendation for resolving the urgent flood disaster problems in Indonesia upon analyzing the aforementioned state and problems. Recently, the international flood management has shifted toward more integrated one[19]. The key solutions are focused on the deliverable *solutions for sustainable development*.

In order to stop the flooding from occurring recurrently in the region vulnerable to flood, such as Jakarta, the physical measures through construction works are now being conducted. Levee construction, dredging, shortcut or inter-catchment water transfer, and floodgate along the river should provide defense against the inundation. Deep tunnel reservoir system which is currently proposed will greatly prevent the Jakarta municipality from flooding. Nevertheless, flood physical countermeasures have a limited capacity and economical constraints. The government should run large budget for structural measure.

### 5.1 River Restoration Program

As a matter of fact, drainage channel widening is not always a good solution. The large scale dredging throughout the channel provides the bigger channel capacity. In the low-flow condition, it causes the sediment accumulation therein, which requires additional maintenances. The dredging should be conducted only in the narrow part of the channel for the removal of the bottleneck. The river normalisation without enough assessment of river characteristic greatly changes the natural condition of the stream. It may even worsen the effects of extreme natural events if the structures fail to overcome the flooding. Regarding this matter, river restoration concept aiming to bring back the river to the natural states is recommended rather than the river engineering concept. Instead of increasing the channel capacity, the river normalisation is carried not only aiming to, but even further to provide wider riparian zone for protecting the environment. In addition, the relocation of the people from river bank as a part of channel normalisation works is needed based on the social engineering technique. The government housing policies should aim to encourage people living in the vertical housing in order to promote the urban basin revitalisation.

### 5.2 Basin-Scale Environment-Based Flood Countermeasures Plan

For upper of Greater Jakarta and other areas such as Bojonegoro, Manado, Samarinda, or Medan which has riverine flooding problem, the proposed idea is providing the environment-based flood integrated countermeasures plan in the river basins. For example, in Samarinda city, Karangmumus River, as a sub catchment of Mahakam River which is in critical condition is set as a pilot project. The idea is restoring the river bank by well preserving the riparian area. The vegetation surrounding the streams protects the environment, support the biodiversity, and increase the hydraulic resistance from flood. The natural preserved meander has big roles in flood risk reduction through preventing the erosion and sedimentation as well as providing the space for reserving the water. In accordance with this program, the traditional flood measures which now exist in the target area is adapted for supporting the idea of developing the basin-scale environment-based flood countermeasures plan initiated with a pilot project. In fact, Dayak community which is the main ethnic group in East Kalimantan has local wisdom of land utilisation. The Dayak common law regulates the forest utilisation and the activities to create a precondition for living in balance with environment. Involving the local people is a way to bring about the public participation in this program.

### 5.3 Improving Water Retarding Function

The flood hard countermeasure in Jakarta particularly has been focused primarily on conveying away the water as quickly as possible through the flood canals. In fact, it is important to understand that the rain water is not a waste but a source of groundwater recharge. The structural works providing river normal capacity in carrying the water should be balanced with the system to retain the water.

A natural way to reduce the runoff and increase the storm-water infiltration is by decreasing the whole catchment runoff coefficient through providing green space, which highly contributes to the reduced storm runoff. The man-made facilities include the household scale water harvesting such as recharge through infiltration pit and hole or the more sophisticated techniques such as detention pond and retention basin. In a condition where the river water volume is extremely big to be handled by the existing facilities, wetland and meander are significant to reduce runoff as well as recharge the groundwater resources. Applying the bioengineering technique in the basin-scale environment-based flood countermeasures plan project improves the basin retarding function, which can maintain the higher base flow during dry season and slow water releasing during the high flow.

In the advanced countries which are particularly less vulnerable to flood disaster, there are some strategies of flood control that put forward the harmony with natural environment. In Japan, along with control works introduce at the rivers, watershed protection is formally implemented forming the integrated flood disaster prevention actions. In order to reduce the level of vulnerability of flood in Indonesia, some good practices of watershed protection in Japan can be adopted. However, it should be noted that as a developing country, Indonesia has limitation to take full advantage of the scientific efforts. The selection and adoption of the possible means to be introduced in Indonesia case needs different strategies. Park retarding basin and school yard reservoir are the infrastructures recently introduced to the public facilities at urban river basins in Japan. The idea of school yard storage facilities is utilizing the outdoor sports fields to restore the storm water

temporarily during heavy rain. The construction includes depression reservoir or underground storage tank provided with discharge facilities and dyke around the storage location. This can be applied also in other public facilities, such as park or parking area. Figure 5 shows the illustration of this infrastructure.

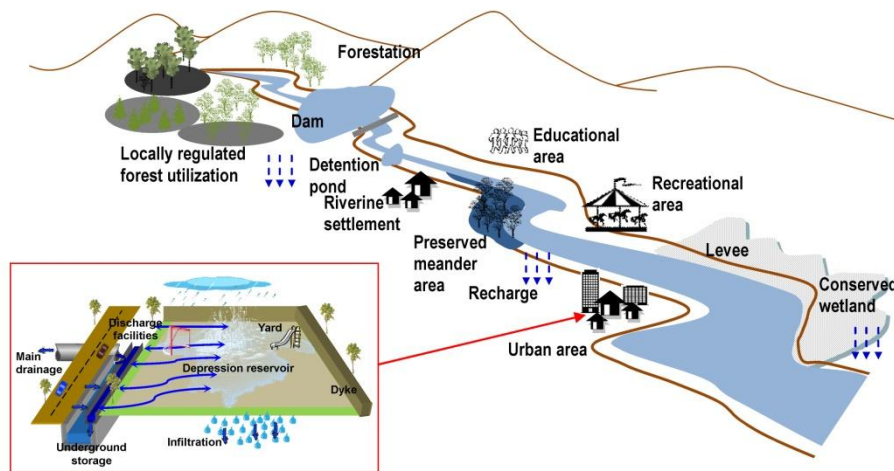


Figure 5. Basin-scale environment-based flood countermeasures plan and yard retarding basin

Even though this measure does not necessarily substantially reduce frequency of flooding, it contributes to the decrease of amount of storm water. It gives the added benefit by allowing the retardation of rapid drain into the river, water reuse, and finally groundwater recharges. By constructing storage facilities in 0.5 hectare school yard, the stored storm water is about 1000 m<sup>3</sup>. This amount is the equivalent of water needed for 5000 times of bathing. With more than 500 number of school in southern Jakarta, restoring the storm water by utilizing the schools yard could significantly alleviate the flood problem in the downstream of Ciliwung River. This illustration helps convincing the administrators to provide these systems. If such practice is successfully implemented, either with government subsidy, external support, or self-funding, it reflects the public concern over the flooding. Whilst there is a need to allow sufficient time for the familiarisation of the full system, the government might bring out a green building ordinance which establishes the standard for improving construction to allow much water to be conserved.

At the same time, this system also facilitates flood and drought management to overcome water shortage persists in many regions in Indonesia. The principle is providing more places to store safely the excess water during wet periods and allocating it efficiently during dry periods. Whilst construction of the large dams may be criticized because of the adverse environmental and social impact, as well as the financial aspect, the small reservoir locally called “embung” can be proposed. In order to promote the water conservation, there should be a policy of water conservation in Indonesia to encourage all citizens to reduce the runoff coefficient of each land plot in a basin as well as rain water harvesting.

In the case of constructing the flood countermeasure works, thorough and comprehensive planning, construction, and maintenance are indeed very essential to ensure their effectiveness. The environmental options in the flood physical countermeasures should be also included. It is expected the measures would sustain its long-term usefulness without adversely affecting other region or environment. As noted before, in post-disaster situations, when the damages restoration is required quickly, the quality of the construction is often ruled out. In effect, the reconstruction efforts are supposed to result in less-hazard-resistant structure. Care must be taken in designing the control works, whether the constructions will accommodate the dominant flood or design flood. Therefore, the fund wastages, which frequently occur due to ignorance of importance of sustainability, could be minimized.

#### 5.4 Public Awareness and Participation

Non-structural measures could offset the tremendous expenditure of control works. Moreover, structural measures alone, which are effective in only certain flood magnitude, may not be sufficient. The big effort put on structural measures may cause a false sense of security of the public. Therefore, in parallel with the river restoration program, another important point is awareness on the cause of disaster related to human activity. Flood happens regularly, and the campaign of man-caused flood has been held extensively over recent years in Indonesia through government and NGO, but public awareness remains low. Even so, the disaster education should still be implemented vigorously to ensure its entrenchment. Flood awareness is the basis of the developing public attitude to flood problem, and this is a prerequisite of community participation in flood prevention.

We identify two ways to increase public awareness in flood disaster. First, the adequate environmental education has an important role in the flood management program. It includes the insertion of ecological content in mainstream formal education, training of community group, target group training for professional and employee for capacity development. Having made this point, public awareness fosters active participation of the community in the design of local strategies for flood control, known as community-based disaster management. In this notion, teacher, priest, and community leader as influential patrons play vital roles in bringing awareness in the society.

Second, the objective of developing basin-scale environment-based flood countermeasures plan is not only for flood control, but also raising public awareness. Providing the recreational area which allows the people to access the riparian area would become the part of the efforts. This area is arranged to have environmental education programs, which aims to increase people's knowledge and awareness about the environment and flood hazard. The components of the program are introduction of watershed management, river engineering to against flooding, local tradition, and flood drills. Maintaining the healthy of riparian area and showing the interconnection with other natural resources will encourage the people to conservation concern in the river basin.

Such symbiotic relationship between maintaining urban life for economic growth and conserving the natural resources in river basin is a great potential to contribute to the sustainable flood countermeasures. In parallel with flood hazard reduction, the benefit of the proposed program is an investment in public awareness enhancement that generates more resilient floodplain. The basin-scale environment-based flood countermeasures plan as illustrated in Figure 5 is expected to stimulate the greater resultants to the broader community by gradual accumulation of public positive response.

### 5.5 Deforestation Issues

Promoting forest conservation by eradicating illegal logging is the critical step toward solving the menace of flooding in Indonesia. The condition in Indonesia is quite difficult where population increasing threatens natural resource. With proper spatial planning, the area could become urbanized without deforestation, and accordingly all the nature places in cities are thoroughly schemed as well. In order to ensure that the plan is executed as intended, oversee its implementation is no less important than the planning itself. In this regard, enforcing law of illegal deforestation plays important roles.

### 5.6 Meteorological-hydrological Forecasting

Preparing accurate and quick forecasting of severe rainfall and flood in operational setting provided by BMKG could help reducing the risk of flood catastrophe. Further, the adverse weather information should be provided at small scales in such a way that it can encompass the localized regions in the short term, i.e. a week to months in advance. In such a context, the forecasting can be viewed as an attempt to provide flood hazards outlook and warning in specific region or catchment. In Indonesia, each major river is managed by one river agency or organisation in charge of "in-stream" water resources management, water allocation, and infrastructure management within a particular basin. This agency could have an opportunity to play important roles in facilitating the flood prediction within one river basin system supplied by weather forecast product. Once the warning is issued by the agency, the responsibility for responding to the emergency situation addressed to the people is held by BPBD along with local government. In turn, support from local government is needed to raise the community capacity in reacting to the warning. Cooperation with international organisation with respect to assistance in finance, cutting-edge technology transfer, and capacity-building expertise will be necessary to realizing the idea.

### 5.7 Political Will and Law Enforcement

Programs of improving flood disaster management are substantially in line with Indonesia national developmental needs. Consequently, governmental at all levels must include them into overall development plan and formulate the policies. Furthermore, the program should include the provision of equitable development to all areas, especially at islands outside Java-Bali. One of the essential steps towards the successful program would be to increase the coordination and integration between central and local governments as well as between related state-owned and non-state-owned corporations. Strengthening the commitment of *policy* makers for development and implementation of the strategic approach to solve flooding problem accompanied by law enforcement are absolutely compulsory.

## VI. CONCLUSIONS

This paper addresses the issues of flood disaster threats in Indonesia. A comprehensive review of progress achieved in dealing with flood management and their effectiveness are presented in detail. Flooding in Indonesia is a recurring event, and each year, floods cause losses in terms of human lives, infrastructure, livelihoods, and social and economic disruption. Man-made factors such as poor planning and management

compounded by natural factors are considered to account for this catastrophe. Overpopulation and its accompanying urbanisation are significant contributing factors. A legal framework in the areas of disaster preparedness has been established, and improvements in governance matters are being sought continuously. Basically, natural disaster prevention, mitigation, and rehabilitation are handled by BNPB, a ministerial-level government institution. It is supported by legal measures, special budget allocation, and professional experts. Nevertheless, there remain lack of coordination and difficulties towards the implementation of disaster management regulation. In the aftermath of a disaster, the people and authorities are quite responsive. However, the review identifies a lack of prevention and preparedness actions. On analyzing the aforementioned state and problems, the key solutions that are focused is the development of environment-based flood countermeasures plan which is initiated with basin-scale pilot project. The idea is restoring the river and maintaining the riparian area. Local people and their indigenous practices for flood mitigation should be involved to allow for the public participation. The promotion of storm water harvesting may not be an easy task; however, we consider that it to be the best solution to deal with water resource's constraints that lie ahead. Simultaneously, raising public awareness through environmental and flood hazard education should be integrated. Furthermore, eradication of deforestation is the critical step towards solving the flood problem; otherwise, human security in Indonesia will be endangered. Reliable flood forecasting and warning should contribute by alerting people about an impending flood rather than just reacting to the disaster. To conclude, political will and law enforcement are imperative in order to solve the flood disaster problems in Indonesia. The deeper discussion on technical arrangement of flood plain management through integrated flood and drought management will be explored in a future study.

### REFERENCES

- [1] Few, R. Flood hazards, vulnerability, and risk reduction, in Few, R. and Mattheis, F. (Eds.), *Flood Hazards and Health: Responding to Present and Future Risks*, Earthscan, London, 2006, 8-27.
- [3] Tse, C. W. Do Natural Disasters Really Lead to Forced Migration? Evidence from Indonesia in *Proceeding of Northeast Universities Development Consortium Conference*, New Heaven, USA, 2011.
- [2] Centre for Research on the Epidemiology of Disasters (CRED). *EM-DAT (The International Disaster Database)* [online]. EMDAT, Brussels <http://www.emdat.be/>, 2014.
- [4] Dutta, D. and Herath, S. Trend of floods in Asia and flood risk management with integrated river basin approach in *Proceeding of the 2<sup>nd</sup> International Conference of Asia-Pacific Hydrology and Water Resources Association*, Singapore, 55–63, 2005.
- [5] Wardani, S. P. R., and R. J. Kodoatie. Disaster Management in Central Java Province, Indonesia in *Proceeding of the 2<sup>nd</sup> International Conference on Geotechnical Engineering for Disaster Mitigation and Rehabilitation*, Beijing, China, 2008.
- [6] Texier, P. Floods in Jakarta: When the extreme reveals daily structural constraints and mismanagement., *Disaster Prevention and Management*, 17(3) [online]<http://www.emeraldinsight.com/doi/abs/10.1108/09653560810887284> (Accessed 10 November 2015), 2008.
- [7] Marfai, M. A., L. King, J. Sartohadi, Sudrajat, S. R. Budiani, and F. Yulianto. The impact of tidal flooding on a coastal community in Semarang, Indonesia., *The Environmentalist*, 28(3) [online] <http://link.springer.com/article/10.1007%2Fs10669-007-9134-4#page-1> (Accessed 10 November 2015), 2008.
- [8] Indonesian National Board for Disaster Management. *Indonesian Disaster Information and Data* [online]. BNPB, Jakarta. <http://dibi.bnpb.go.id/DesInventar/dashboard.jsp>, 2014.
- [9] Rahayu, H. P., and S. Nasu. S. Good practices of enhancement early warning system for high populated cities - A case study for Jakarta Flood in *Proceeding of Society for Social Management Systems International Symposium*, Kochi, Japan, 2010, SMS10-163.
- [10] National Aeronautics and Space Administration (NASA). *Heavy Rainfall Floods Indonesia* [online] NASA Earth Observatory, USA. <http://earthobservatory.nasa.gov/IOTD/view.php?id=8376>, 2008.
- [11] Hidayat, F., H. M. Sungguh, and Harianto. Impact of climate change on floods in Bengawan Solo and Brantas River Basins, Indonesia in *Proceeding of 13<sup>th</sup> International River Symposium*, Brisbane, Australia, 2008.
- [12] Harwitasari, D., and J. A. van Ast. Climate change adaptation in practice: Peoples responses to tidal flooding in Semarang., Indonesia. *Journal of Flood Risk Management*, 4(3) [online] <http://onlinelibrary.wiley.com/doi/10.1111/j.1753-318X.2011.01104.x/abstract> (Accessed 10 November 2015), 2011.
- [13] Manuta, J., and L. Lebel. Climate change and the risks of flood disasters in Asia: Crafting adaptive and just institutions in *Proceeding of Human Security and Climate Change: An International Workshop*, Oslo, Norway, 2005.
- [14] Marfai, M. A., L. King, L. P. Singh, D. Mardiatno, J. Sartohadi, D. S. Hadmoko, and A. Dewi. Natural hazards in Central Java Province, Indonesia: An overview., *Environmental Geology*, 56(2) [online] (Accessed 10 November 2015), 2008.
- [15] Farid, M., A. Mano, and K. Udo. *Urban flood inundation model for high density building area*, *Journal of Disaster Research*, 7(5) [online]<https://www.fujipress.jp/finder/xslt.php?mode=present&inputfile=DSSTR000700050004.xml> (Accessed 10 November 2015), 2012.
- [16] Otok, B.W., and Suhartono. Development of rainfall forecasting model in Indonesia by using ASTAR, transfer function, and ARIMA Methods., *European Journal of Scientific Research*, 38(3) [online] Development of rainfall forecasting model in Indonesia by using ASTAR, transfer function, and ARIMA Methods (Accessed 10 November 2015), 2009.
- [17] Marfai, M. A., and L. King. Coastal flood management in Semarang, Indonesia., *Environmental Geology*, 55(7) [online] <http://link.springer.com/article/10.1007%2Fs00254-007-1101-3#page-1> (Accessed 10 November 2015), 2008.
- [18] Phanuwat, C., S. Takizawa, K. Oguma, H. Katayama, A. Yunika, and Y. Ohgaki. Monitoring of human enteric viruses and coliform bacteria in waters after urban flood in Jakarta, Indonesia., *Water Science and Technology*, 54(3) [online]<http://www.ncbi.nlm.nih.gov/pubmed/17037154> (Accessed 10 November 2015), 2006.
- [19] Ward, P. J., Pauw, W. P., van Buuren, M. W., and Marfai, M. A. Governance of flood risk management in t Time of climate change: the cases of Jakarta and Rotterdam, *Environmental Politics*, 22(3) [online]<http://www.tandfonline.com/doi/abs/10.1080/09644016.2012.683155?journalCode=fenp20#.VkJc2NrkK00> (Accessed 10 November 2015), 2013.

- [20] Aldrian, E., L. D. Gates, and F. H. Widodo. *Variability of Indonesian rainfall and the influence of ENSO and resolution in ECHAM4 simulations and in the reanalyzes*. Report No. 346 [online]. Max-Planck-Institut für Meteorologie, Hamburg. [https://www.mpimet.mpg.de/fileadmin/publikationen/Reports/max\\_scirep\\_346.pdf](https://www.mpimet.mpg.de/fileadmin/publikationen/Reports/max_scirep_346.pdf) (Accessed 10 November 2015), 2003.
- [21] Forest Watch Indonesia and Global Forest Watch (FWI/GFW). *The State of the Forest Indonesia* [online]. Forest Watch Indonesia, Bogor; Global Forest Watch, Washington DC, 2002.
- [22] Kusumastuti, R.D., S. S. Wibowo, and R. Insanita. Relief logistics practices in Indonesia: A survey in *Proceeding of 5<sup>th</sup> International Conference on Business and Management Research 2010*, Jakarta, Indonesia, 2010.
- [23] Sutardi. *Action Report toward Flood Disaster Reduction-Indonesian Case* [online]. Indonesia Water Partnership, Jakarta. <http://www.internationalfloodnetwork.org/AR2006/AR06Sutardi.pdf> (Accessed 10 November 2015), 2006.
- [24] Indonesian National Board for Disaster Management. *Map of Flood Hazard Index in Indonesia* [online]. BNPB, Jakarta. <http://geospasial.bnpb.go.id/2010/02/19/peta-indeks-ancaman-banjir-di-indonesia/>, 2009.
- [25] Law of Republic of Indonesia (LRI). *Law of Republic of Indonesia Number 24 of 2007 Concerning Disaster Management*. [online], 2007
- [25] United Nations Development Programme (UNDP). *Lessons Learned: Indonesias Partnership for Disaster Risk Reduction*. The National Platform for Disaster Risk Reduction and the University Forum, 2009.
- [26] Asia Disaster Preparedness Center (ADPC). *Policy and Institutional Arrangement for Disaster Management in Indonesia* [online]. Southeast Asia Section Publications, Bangkok. <http://www.adpc.net/pdr-sea/publications/6-PIA-Ind.pdf>, 2001.
- [27] Sutardi. *Water Resources Management towards Enhancement of Effective Water Governance in Indonesia* [online]. Country Report for 3<sup>rd</sup> World Water Forum, World Water Council, Kyoto. [http://www.worldwatercouncil.org/fileadmin/www/Library/Publications\\_and\\_reports/country\\_reports/report\\_Indonesia.pdf](http://www.worldwatercouncil.org/fileadmin/www/Library/Publications_and_reports/country_reports/report_Indonesia.pdf) (Accessed 10 November 2015), 2003.
- [28] Pribadi, K.S., and A. Mariani. *Implementing community-based disaster risk reduction in Indonesia: The role of research institutions and religious-based organizations* [online]. Disaster Reduction Hyperbase, Asian Application, Japan. [http://drh.bosai.go.jp/files/3f11992da3de433954239df73ce8bc31e85ee4df7\\_PT2\\_P.pdf](http://drh.bosai.go.jp/files/3f11992da3de433954239df73ce8bc31e85ee4df7_PT2_P.pdf) (Accessed 10 November 2015), 2007
- [29] WHO. *Emergency Situation Report of Flash Flood in Teluk Wondama District, West Papua Province, Indonesia*. [online] WHO, Emergency and Humanitarian Action. [http://www.searo.who.int/LinkFiles/Indonesia\\_ESR-1FF-Papua-05-10-2010.pdf](http://www.searo.who.int/LinkFiles/Indonesia_ESR-1FF-Papua-05-10-2010.pdf), 2010.
- [30] WHO. *Emergency Situation Report No. 5 of Floods in Jakarta Province, Indonesia*. [online] <http://www.who.or.id/eng/contents/esr/ESR%20%2805%29%20Floods%20in%20DKI%20Jakarta%20Province.%20Updated%2009%2002%2007.pdf>, 2007.
- [31] United States Agency for International Development (USAID). *Review of Policies and Institutional Capacity for Early Warning and Disaster Management in Indonesia*. [online] U.S. Indian Ocean Tsunami Warning System Document, 2007.
- [33] The Water Dialogues. *Indonesia Contextual Analysis in Water Supply and Sanitation Sector* [online] [www.waterdialogues.org/documents/8.6ContextualAnalysis.pdf](http://www.waterdialogues.org/documents/8.6ContextualAnalysis.pdf), 2009.

## Thermal Comfort Temperature Range for Industry Workers in a Factory in Malaysia

A.Z.A. SAIFULLAH<sup>1</sup>, Y.H. YAU<sup>2</sup>, B.T. CHEW<sup>3</sup>

<sup>1</sup>Professor & Chair, Department of Mechanical Engineering, IUBAT – International University of Business Agriculture and Technology, Dhaka 1230, Bangladesh

<sup>2</sup>Department of Mechanical Engineering, University of Malaya,  
50603 Kuala Lumpur, Malaysia

<sup>3</sup>Department of Mechanical Engineering, University of Malaya,  
50603 Kuala Lumpur, Malaysia

**ABSTRACT:** A field study was carried out to assess the comfortable conditions of the working environment of a production factory in Kuala Langat, Malaysia. Malaysia is a hot and humid climatic country with high average outdoor temperature of 23.7<sup>o</sup>C - 31.3<sup>o</sup>C and average humidity of 75% RH - 95% RH throughout a day. Heating, ventilating and air-conditioning (HVAC) system of a factory must be well-designed to provide comfortable conditions to the workers. Survey was conducted by randomly picking up the employees in the desired space. The air quality of the space that is temperature, humidity, CO and CO<sub>2</sub> level, as well as dust particles of the plant was measured. The workers' thermal satisfaction was studied by using seven-point thermal sensation scale proposed by ASHRAE standard 55 (2004). Adaptive model was employed to determine the neutrality temperature. The comfortable temperature range for the workers of the factory was determined to be from 21.5<sup>o</sup>C to 23<sup>o</sup>C with humidity of 45% RH to 60% RH.

**Keywords:** Malaysia, factory workers, HVAC, air quality, ASHRAE seven-point thermal sensation scale, adaptive model.

### I. INTRODUCTION

The number of HVAC systems of various buildings has been significantly increased for their growing importance along with the rapid industrialization of developing countries (Nicol and Roaf, 1996), (Szokolay, 1991). Study has shown that the energy use for HVAC has now become one of the largest sectors in energy consumption (Humphreys, 1976). Malaysia, a country located in south-east Asia, lies north to the equator with 7° latitude, has a tropical climate. Malaysia has a hot and humid weather all the time (de Dear and Brager, 2002). Hence consumption of energy is too high to produce comfortable air-conditioned (AC) environment for working space in the factories.

Nowadays, HVAC system is a primary concern in every building, since the energy consumption in electricity has the highest percentage in HVAC among all building services installations as well as electric appliances. HVAC system of a building plays an important role in providing a comfortable environment by controlling temperature, humidity, air motion, radiant sources, odour and noise of the space (Yamtraipat *et al.*, 2005). Comfort is a major concern in a working space to provide satisfaction to all workers. Study has shown that the productivity level of employees is related to the level of thermal comfort (TC) (de Dear and Brager, 2002), (Abdul Rahman and Kannan, 1997). The humidity ratio is one of the major concerns in production especially for manufacture of semiconductors and foods, because the ambient humidity is around 80% RH. RH levels affect the respiratory system of human body and encourage the growth of harmful matter such as mold and mildew. Besides, many pests such as dust mites, bacteria, and viruses thrive at environment of high RH (Canter, 1983). Working environment above 32<sup>o</sup>C is considered as high temperature environment and environment with humidity above 60% RH can be considered as high humidity environment, based on the relationship between environmental temperature and human thermal balance (Mathews *et al.*, 2001).

The main objective of this research is to find the desirable comfort temperature range for workers in a factory in Kuala Langat, Malaysia. Measurement of various aspects of TC for environment, namely temperature, air velocity, dust particle, CO<sub>2</sub> level contains and RH was done at the plant.

## II. METHODOLOGY AND ESTIMATION

The methodology used in the study is as given below:

1. A factory was chosen and the details of all type of workers and room specifications were found out.
2. Field survey was conducted to find the TC temperature range for factory workers for different types of rooms. This includes measuring the data on temperature, air quality, and air flow characteristic. Survey-questionnaires were also distributed among the workers to have them expressed their comfort level.
3. All measurements of the factory were compared with standard comfort level of ASHRAE Standard 55 to find their suitability for warm humid tropical climatic conditions.

### 2.1 WARM HUMID TROPICAL CLIMATIC CONDITIONS

The study is focused on warm humid tropical climatic location near the equator. Such countries are Malaysia, Singapore, and Indonesia in South-East Asia. There is almost no distinction between summer, winter, autumn or spring in these regions. Basically, the whole year round is a permanent summer with high temperature, with the exception of periods during the wet season and places at higher altitudes. In many tropical regions, people identify two seasons: wet and dry. However, most places close to the equator are wet throughout the year, and seasons can vary depending on a variety of factors including elevation and proximity to an ocean. Even though it is situated at the equator it might not be the hottest region in the world, since the rainy and humid conditions cools down the air.

As for the study conducted in Malaysia, average temperature is around 27°C year round with heavy rains from November to February. The warmer months are not extremely hot, while the cooler months appear to be similar to warm summer conditions in this 4 seasonal country. Light clothes are worn throughout the year since the temperature difference between day and night is insignificant.

### 2.2 THE FACTORY ENVIRONMENT AND THE WORKERS

The factory environment considered in this research involve those workers who work in the production line in Malaysia, where their work is considered as light work and does not pollute the indoor air. The main concern is the increase of moisture or humidity due to the respiration of the workers and the temperature rise due to heat gain from building and machines. Such condition thus needs fresh or outdoor air to balance the indoor air content and quality. A “factory worker” here is classified as an employee who is directly involved in production related activities of the factory establishment excluding any work at supervisory or administrative level (Wijewardane and Jayasinghe, 2008).

The thermal perceptions of the occupants are affected by the factors such as demographics (gender, age, economic status), context (building design, building function, season, climate, semantics, social condition), and cognition (attitude, preference, and expectations). People interact with and change their environment in consistent with their past experiences, future plans and intentions, and hence their perception on TC could be affected by such factors too (Baker, 1993), (Oseland, 1994).

Therefore, one’s satisfaction towards TC is not fixed. It could be calculated with some parameters given, but it does not apply for the whole life. It changes from time to time depending on the current and past experience, cultural and technical practices.

### 2.3 FIELD SURVEY

In the factory, survey was done in both office building and production line building. The production line building is identified as Semicond 1 (zone 1, production line), Semicond 1 (zone 2, production line) and Semicond 4 (first floor, production line). Survey was done first in the office building. There is high density of workers in this building and its temperature is a bit high compared to the manufacturing plant. The latter is of lower density of workers, but has many types of equipment that need low temperature to maintain their functionality. The location of the factory is at Kuala Langat, 2°55' N and 101° 28' E with average climatic data as shown in Table 1.

The office building together with its high density of workers, fluorescent lighting, electrical equipment such as computers and photocopy machine were selected during the survey. The idea is, this entire factory would increase the heat gain within the space, which has a significant effect on TC.

For the production line building, although the density of workers is lower but the number of equipments is so large which causes the area need a higher cooling effect to remove the heat generated by the equipments.

The TC of the workers had been determined by the survey-questionnaire that was distributed to the workers. Both male and female workers were selected for the questionnaire, because the number of male and female in this factory is almost the same. The seven point scale for comfort vote proposed by ASHRAE Standard 55 was used to determine the TC in the area. This would give a wide range for response in the research. 'Slightly cool', 'neutral', and 'slightly warm' were considered as thermally acceptable conditions.

The survey was conducted in a sunny day. The outdoor temperature varied from 31°C (10.00 am) to 32.6°C (3.45 pm). The maximum outdoor temperature was 40.3°C (11.50 am). The indoor temperature of Semicond 4 building varied from 21.6 to 22.5°C and that of Semicond 1 building varied from 20 to 23.4°C. This survey was using ASHRAE Standard 55 in determining the objective of the research. It is about indoor temperature and humidity at a certain area and a subjective survey which is the questionnaire. In this survey, many data had been collected on relative humidity, dry bulb temperature, mean radiant temperature, air flow rate, air velocity and particles in the space, etc. All the data were measured by digital equipments and were combined together in Microsoft Excel. Outdoor humidity was also recorded. The questionnaire survey was carried out at the same time when objective measurements were going on. Activity and clothing value for the workers were also evaluated according to ASHRAE Standard 55.

**Table 1. The average climatic data for Kuala Langkat with 2°55'N latitude 101°28'E longitude**

Month	Mean daily temperature (°C)		Relative humidity (%)			
	Max	Min	Min	Mean	Max	Mean
January	31.9	25.9	82.6		98.6	
February	32.8	26.3	81.2		98.2	
March	33.0	26.6	82.5		98.4	
April	32.8	26.8	84.9		98.4	
May	32.7	27.0	84.3		98.2	
June	32.3	26.7	83.9		98.1	
July	31.9	26.4	83.4		97.8	
August	32.0	26.4	83.1		97.9	
September	31.9	26.2	84.6		98.3	
October	31.7	26.2	85.5		98.7	
November	31.2	25.9	86.9		98.9	
December	31.2	25.8	85.7		98.9	

Source: Director General Meteorological Services- Malaysia

### III. RESULTS AND DISCUSSION

#### 3.1 FINDINGS

Seven point scale for comfort vote proposed by ASHRAE Standard 55 was used considering 'slightly cool', 'neutral' and 'slightly warm' as acceptable range for TC. In the questionnaire survey, for Semicond 1 – zone 1, 73% of occupants' vote for 'cool' condition on the scale is shown in Table 2. This result tells us that the workers were thermally distressed. For Semicond 1 – zone 2, 91.6% of the occupants' vote was for 'slightly cool' on the scale. For Semicond 4- level 1, 33% vote was for 'neutral', 25% vote for 'slightly cool', 25% vote for 'slightly warm'. This tells us that this area has acceptable thermal comfort conditions.

**Table 2. Results of survey**

Location	Average Temp (C°)	(-3) Cold	(-2) Cool	(-1) Slightly Cool	0 Neutral	(+1) Slightly Warm	(+2) Warm	(+3) Hot	Number of Subjects
Semicond 1 (zone 1)	23.0	0 0%	11 73%	3 20%	0 0%	1 7%	0 0%	0 0%	15
Semicond 1 (zone 2)	21.5	0 0%	0 0%	11 92%	1 8%	0 0%	0 0%	0 0%	12
Semicond 4 (level 1)	23.0	0 0%	1 8%	3 25%	4 33%	3 25%	1 8%	0 0%	12

Humidity – 49.5-50.5%; metabolic rate – 1.7-2.2; clothing – 0.67 clo (Overalls, long-sleeve shirt, Lab Cot); average outdoor temperature – 34.2°C at 51.6% relative humidity.

### 3.2 VALIDATION WITH LARGER FACTORY

For validation purpose, another test was conducted in the production line (Semicond 4) with a larger workforce. The survey was carried out also on a working day representing the normal daily routine. Workers were asked to do their normal work, while indicating the comfort vote. On a typical day, the temperature range inside the factory was 21.6 °C to 22.5°C from 10 a.m. to 4 p.m. Therefore, the temperature-changing rate was very small and that eased the task of questioning a large number of workers. Supervisors from the factory were informed about the procedure and requested to administrate the seven point scale comfort vote. The survey was conducted in a sunny day. The outside temperature range varied from 31°C (10.00am) to 32.6°C (3.45pm). The maximum temperature for outdoor was 40.3°C (11.50 pm). With the large sample also, it was indicated that temperature in the range of 21.5 °C to 23°C was acceptable by up to 80% of the occupants. This indicates that the prediction of the smaller sample tallies very well with the large sample. Thus, a temperature up to 23°C can be considered acceptable for factory workers who are accustomed to warm humid tropical climatic conditions.

### 3.3 A COMPARISON WITH COMFORT MODELS

Adaptive models are applied to define the neutral temperature as a function of outdoor, indoor or both temperatures. Some of them present a higher accuracy in certain conditions and, as a result, these principal models were employed for this study. Auliciems and de Dear developed the relations for predicting group neutralities based on mean indoor and outdoor temperatures which were employed by the ASHRAE as shown in eq. (1). Other adaptive models have been also proposed by Humphreys (1976) and Nicol and Roaf (1996). Szokolay (1991) developed the model to determine the comfort zone in psychometric chart by determining neutrality temperature, using equation below to indicate the center point for comfort zone. Szokolay (1991) indicated also the range of about  $\pm 2^\circ\text{C}$  about neutrality temperature. However, before applying these models, we must remember that occupants must be engaged in near sedentary activity (1-1.3 met).

$$T_n = 17.6 + 0.31T_o \quad (1)$$

where

$T_n$  = Neutrality temperature [°C],  $T_o$  = Arithmetic average of the mean daily minimum and mean daily maximum outdoor (dry bulb) temperatures for the month in question [°C].

But, considering the tropical climate change that was possibly adapted, de Dear and Brager (2002) proposed the deviation of about  $\pm 3.5^\circ\text{C}$  about the neutrality temperature, which gives the range of 7°C.

From Table 3, on the day this research was conducted, the mean value of outdoor dry bulb temperature was about 34°C, which gives the neutrality temperature to be 28°C. This is relevant to the neutrality temperatures (24.6 °C, 26.1 °C and 27.4°C) for Malaysia (Abdul Rahman and Kannan, 1997). The thermal sensation voting indicates that the acceptable comfort temperature for all workers is up to 23°C, which is in the range proposed by de Dear and Brager (2002). This proves the applicability of their recommendation.

**Table 3. Outdoor temperature and relative humidity**

Time	Temperature	Humidity
10.00	31.0	57.7
11.10	34.2	50.1
12.10	37.0	48.3
12.40	39.4	45.8
15.00	30.8	52.2
15.45	32.6	55.2

Yamtraipat *et al.* (2005) conducted research about the acceptable comfort temperature of large number of respondents in different climatic regions of Thailand. The survey was conducted using different types of AC buildings from the private and public sectors. The highest mean indoor temperature for thermal acceptability of the subjects was 26°C, 27.4 °C and 26.4°C for zone H1, H2 and H3 respectively. They concluded that the recommended nationwide indoor set point for AC buildings in Thailand is 26°C, which was accepted by most of the subjects in every climatic zone (80% of votes), and the appropriate relative humidity range should be between 50% and 60%. Since Malaysia is neighbor to Thailand, the climatic condition of these two countries is

not much different as well. And, these values can be referred as benchmark to the acceptable temperature and RH. Based on thermal sensation voting at the factory in Malaysia, most of the staff felt comfort with the temperature of 22.6°C, and humidity range of 45% RH to 55% RH which is not much different with the research done by Yamtraipat *et al.* (2005).

#### IV. CONCLUSION

From the study, it is revealed that the factory workers in clean room could feel reasonably comfortable up to a temperature of 21.5°C - 23°C with humidity of 45% RH to 60% RH. This is a very important finding, since this guideline can be used for establishing TC by introducing some features to the factory. A higher level of TC would increase the productivity of the factory.

Applications of findings are

Once the air quality and the temperature range for TC of factory workers in warm humid tropical climates is found, these can be used to promote some of the features to the factory to achieve the goal. Some of the examples are:

1. In order to reach the TC temperature range, the number of the machines must be controlled in every section of the factory. The machines in the factory may be treated as heated bodies in the factory and a good locating strategy should be considered as highly desirable.
2. A better clothing material for clean room would assure the workers to feel more comfortable. Clothing includes coveralls, shoe & boot covers, facemasks, gloves & disposable garments.
3. It would be necessary to ensure that the outdoor temperature remains relatively low. In this context, the use of plenty of vegetation is highly desirable. Thus, reservation of strips of sufficient width such as 10m or more between factories for planting multiple rows of trees can be recommended.
4. The use of plenty of insulation in the roofs and walls of factory buildings can be considered as extreme necessity, since the above upper limit of comfort will be valid only in the absence of heated bodies.

#### REFERENCES

- [1] Abdul Rahman S, Kannan KS. 1997, A Study of Thermal Comfort in Naturally Ventilated Classrooms: Towards New Indoor Temperature Standards, *Asia Pacific Conference on the Built Environment*, Kuala Lumpur, Malaysia.
- [2] Baker NV. 1993, Thermal comfort evaluation for passive cooling - A PASCOOL task, *Proc Conf. Solar Energy in Architecture and Planning*, Florence, Stephens HS and Associates, Bedford, UK.
- [3] Canter D. 1983, The purposive evaluation of places: a facet approach, *Environment and Behavior*. 15(6): 659-698.
- [4] de Dear RJ, Brager GS. 2002, Thermal comfort in naturally ventilated buildings: revisions to ASHRAE Standard 55, *Energy and Buildings*. 34(6): 549-561.
- [5] Humphreys MA. 1976, Comfortable indoor temperatures related to the outdoor air temperature, *Building Service Engineer*. 44: 5-27.
- [6] Mathews EH, Botha CP, Arndt DC, Malan A. 2001, HVAC control strategies to enhance comfort and minimize energy usage, *Energy and Buildings*. 33: 853-863.
- [7] Nicol F, Roaf S. 1996, Pioneering new indoor temperature standard: the Pakistan project, *Energy and Buildings*. 23: 169-174.
- [8] Oseland NA. 1994, A comparison of the predicted and reported thermal sensation vote in homes during winter and summer, *Energy and Buildings*. 21(1): 45-54.
- [9] Szokolay SV. 1991, Heating and cooling of buildings. In: Cowen HJ, Editor, *Handbook of architectural technology*, Van Nostrand Reinhold, New York.
- [10] Wijewardane S, Jayasinghe MTR. 2008, Thermal comfort temperature range for factory workers in warm humid tropical climates, *Renewable Energy*. 33(9): 2057-2063.
- [11] Yamtraipat N, Khedari J, Hirunlabh J. 2005, Thermal comfort standards for air conditioned buildings in hot and humid Thailand considering additional factors of acclimatization and education level, *Solar Energy*. 78(4): 504-517.

## Krill Oil Quantification in CS/TPP Nanoparticles Using Novel One Step Fourier Transform Infrared Spectroscopy

Junaid Haider<sup>a</sup>, Hamid Majeed<sup>a</sup>, Hafiz Rizwan Sharif<sup>a</sup>, Muhammad Shamoona<sup>a</sup>,  
Haroon Jamshaid Qazi<sup>b</sup>, Ali Haider<sup>c</sup>, Jianguo Ma<sup>a</sup>, Fang Zhong<sup>\*a</sup>

<sup>a</sup>State Key Laboratory of Food Science and Technology, School of Food Science and Technology, Jiangnan University, Wuxi 214122, Jiangsu, P.R China.

<sup>b</sup>Department of Food Science and Human Nutrition, University of Veterinary and Animal Sciences, Lahore, Pakistan.

<sup>c</sup>Department of Clinical Medicine and Surgery, University of Veterinary and Animal Sciences, Lahore, Pakistan.

\*Correspondence author: (Fang Zhong; E-mail: [fzhong@jiangnan.edu.cn](mailto:fzhong@jiangnan.edu.cn))

**ABSTRACT:** Recent success in quantitative analysis of essential fatty acid compositions in encapsulated Krill oil (KO) supplement, we extended the application of Fourier transform infrared spectroscopic technique for rapid determination of KO loading efficiency from the intact biodegradable CS/TPP nanoparticles. Beer-Lambert law was applied in the quantification following selection of a few wave number combinations. The optimized spectral region to attain linear calibration curve for KO/CS-TPP nanoparticles with regression coefficient of  $R^2=0.9959$  for determination of KO. The result revealed successful encapsulation of KO in CS/TPP nanoparticles with loading efficiency of  $22.2 \pm 0.26$  %. Further, to validate the FTIR method for KO contents analysis, gravimetric method was compared that confirmed the same quantity of KO. This method is fast and easy to apply and does not require sample processing. Therefore, current findings confirmed the advantage of FTIR technique in quantification of KO and other bioactive constituents directly and efficiently with no extra sample preparation procedures.

**Keywords:** Krill oil, CS/TPP nanoparticles, Fourier transform infrared spectroscopy (FTIR), Atomic force microscopy (AFM), Loading efficiency

### I. INTRODUCTION

Krill oil (KO) is a rich alternative source of polyunsaturated fatty acids (PUFAs) besides algal and fish oil mainly of which are docosahexaenoic acid (DHA) and eicosapentaenoic acid (EPA) (Bustos, Romo, Yáñez, Díaz, & Romo, 2003). DHA and EPA have recently gained a significant attention for their use as nutritional supplements, functional foods and pharmaceutical ingredients (Yao, Xiao, & McClements, 2014). The dietary intake of DHA and EPA, particularly from Western life style diet, is considerably lower than recommended levels and their conversion from precursor  $\alpha$ -linolenic acid (ALA) in the body is also far from to cover up the deficit (Burdge & Calder, 2005). KO also has a significant level of other constituents (200-400 ppm) such as various potent antioxidants and astaxanthin (provitamin E) (Kolakowska, Kolakowski, & Szczygielski, 1994). The unique phospholipids (naturally rich in omega-3 fatty acids and diverse antioxidants) profile of KO offers a wide range of benefits as compared with usual fish oil. It highly facilitates the absorptive passage of fatty acids through epithelium, increasing bioavailability and improving the  $\Omega$ -3: $\Omega$ -6 fatty acids ratio (Schuchardt & Hahn, 2013; Werner, Havinga, Kuipers, & Verkade, 2004). EPA, DHA and astaxanthin are highly unsaturated in their nature and prone to degradation. KO fortified sea food products are even more susceptible to undergo the oxidation degradation as compared to those which are enriched with other n-3 rich oil (Pietrowski, Tahergorabi, Matak, Tou, & Jaczynski, 2011). PUFAs rapidly oxidized products at trace level can produce off flavour and other quality disadvantages within the food products. This rationale bases the foundation for development of a delivery system that may enhance its solubility in water as well as minimize oxidation at the same time for future use of KO in food applications.

Stabilising through micro-encapsulation seems to be a reasonable approach that enables the successful incorporation of PUFAs into a wide variety of food products (Barrow, Nolan, & Jin, 2007). To protect the core

loaded bioactive compounds from the harsh environmental conditions, polymeric nanoparticles development as encapsulants or "shell" is being implemented in the food industry as well as many other related industries (Acosta, 2009; Chen, Remondetto, & Subirade, 2006; Duclairoir, Orecchioni, Depraetere, Osterstock, & Nakache, 2003; Guterres, Alves, & Pohlmann, 2007; Jang & Lee, 2008; Pinto Reis, Neufeld, Ribeiro, & Veiga, 2006; Rothenfluh, Bermudez, O'Neil, & Hubbell, 2008). A two-step emulsion and ionic-gelation method has been reported to synthesize chitosan (CS) nanoparticles which are non-toxic, organic solvent free and convenient for targeted delivery of bioactive compounds (Malafaya, Silva, & Reis, 2007; Yang et al., 2011). This method was based on the principle of ionic interactions between the positively charged primary amino groups of CS and the negatively charged groups of polyanion such as sodium tripolyphosphate (TPP; the most extensively used ion cross-linking agent) (Shu & Zhu, 2002).

Traditional time consuming gas chromatography and gravimetric analysis have been used widely to determine the oil contents in variety of samples by many researchers (Aziz, Gill, Dutilleul, Neufeld, & Kermasha, 2014; Indarti, Majid, Hashim, & Chong, 2005; Liu, Low, & Nickerson, 2010; Ulberth & Henninger, 1992). But these methods considered being time consuming, invasive, indirect and involving the use of hazardous solvents that is not environment friendly. Therefore, an alternative quantification method based on Fourier transform infrared (FTIR) spectroscopy has been employed in this study. FTIR spectroscopy has gained much popularity for its use in many researches as a quantitative tool owing to its rapid and non-destructive nature, simple sample preparation, ease of use and less or no solvent consumption for monitoring quality (Anzanello, Fogliatto, Ortiz, Limberger, & Mariotti, 2014; Blanco, Valdés, Bayod, Fernández-Marí, & Llorente, 2004; Kondepati, Keese, Michael Heise, & Backhaus, 2006; Ortiz et al., 2013; Rodionova et al., 2005) as well as quantity of the raw materials (Hu, Erxleben, Ryder, & McArdle, 2010; Kumar, Tang, & Chen, 2008; Salari & Young, 1998). FTIR is an easy and fast quantitative method which provides reliable results of analysis. Previously, the technique has been applied quantitatively for various food systems to determine solid non-fat content in raw milk (Bassbasi, Platikanov, Tauler, & Oussama, 2014),  $\alpha$ -tocopherol in refined bleached and deodorized palm olein (Che Man, Ammawath, & Mirghani, 2005), fatty acid contents in microencapsulated fish oil supplement (Vongsivut et al., 2012a), sugar and organic acid contents (Bureau et al., 2009). Previously, FTIR has not been reported for the quantification of biodegradable CS/TPP nanoparticles loaded KO, hence keeping in view the above mentioned rationale(s) in this current study we aimed to develop a simple, an inexpensive and rapid method for quantification of KO loaded in CS/TPP nanoparticles.

## II. MATERIALS AND METHODS

### 2.1 MATERIALS

Antarctic krill oil containing ~40 % phospholipid, ~28-30 %  $\Omega$ -3 fatty acids and  $\leq 200$  mg kg<sup>-1</sup> astaxanthin (claimed by manufacturer) was purchased from Hutai Biopharm Inc. Sichuan, China. Partially deacetylated crab shell derived chitosan (CS; degree of deacetylation; 91.5 %;  $M_w$ : 100 kDa) was obtained from Golden-Shell Biochemical Co., Ltd. Hangzhou, China. Tween 80, Glacial acetic acid, Sodium tripolyphosphate (TPP) and rest of all chemicals used in this study were of analytical grade and purchased from Sinopharm Chemical Reagent Co., Ltd., China.

### 2.2 KO-LOADED CS/TPP NANOPARTICLES PREPARATION

KO loaded CS/TPP nanoparticles were prepared following the method described elsewhere with slight modifications (Calvo & Remunan-Lopez, 1997) and (Hosseini, Zandi, Rezaei, & Farahmandghavi, 2013). Briefly, 1.5 % (w/v) CS solution was prepared by agitating CS in 1% v/v aqueous acetic acid solution at ambient temperature for 24 hrs. The solution was centrifuged at 8000 rpm for 20 min and supernatant was filtered using 0.8  $\mu$ m filter paper. Tween 80 (0.5g) was added as a surfactant to the CS solution (40 mL) and the mixture was stirred at 45 °C for 2 hrs till complete homogenization. 0.6 g KO was gradually poured into aqueous CS solution and subsequently the system was homogenized twice using an Ultra-Turrax (T25, Ika-Werke, Staufen, Germany) at a speed of 13,000 rpm for 1 min and 16,500 for 2 min, respectively. Same volume of TPP solution (40 mL) was added drop by drop to the O/W emulsion and agitated for 40 min. The particles formed were collected by centrifugation at 10,000  $\times$ g for 30 min at 20 °C and washed several times with dd H<sub>2</sub>O to remove excess of KO. Wet particles were dispersed in distilled water (25 mL) and suspensions were immediately freeze-dried at -35 °C for 72 hrs to obtain powder samples. Powder samples were stored in dry conditions at 25 °C.

### 2.3 GRAVIMETRIC ANALYSIS

#### 2.3.1 EXTRACTION OF TOTAL OIL

Extraction of total oil was done using the method of Zhang et al. (Klinkesorn, Sophanodora, Chinachoti, Decker, & McClements, 2006) with some modifications. Briefly, 0.5 g particles were agitated with 5 mL water for 15 min. The resulting solution was then extracted with 25 mL hexane/isopropanol (3:1, v/v) and agitation

was executed for 15 min. The solution was centrifuged for another 15 min at 8000×g. The clear organic phase was carefully withdrawn while the aqueous phase was re-extracted with the solvent mixture (Heinzelmann, Franke, Velasco, & Márquez-Ruiz, 2000). After filtration through anhydrous sodium sulfate, the solvent was evaporated in a rotary evaporator (RE-52AA, Shanghai Biochemical Instrument Company, China) at 70 °C. The solvent-free extract was dried at 105 °C until a constant weight reached and the amount of encapsulated oil was determined gravimetrically. The loading capacity was calculated using Eq. (I).

$$LC (\%) = \frac{\text{Total amount of loaded KO}}{\text{Weight of nanoparticles after lyophilization}} \times 100 \quad (\text{I})$$

## 2.4 FOURIER TRANSFORM INFRARED SPECTROSCOPY

Infrared spectra of all samples were obtained using Nicolet iS10, FTIR spectrometer equipped with KBr accessory (Thermo Fisher Scientific Inc., USA). For spectral acquisition, a film of each liquid sample (~2 µL) deposited on a KBr disk. Solid sample of 1 mg was taken in 99 mg KBr to prepare pellet. The mixture was condensed in 13 mm die at a pressure 5 tons for 1 min. The pellets were scanned spectra were obtained using 16 scans at a resolution of 4 cm<sup>-1</sup> over the frequency range of 4000-400 cm<sup>-1</sup>. All the spectra were recorded using Nicolet OMNIC software (Version 8.2)

## 2.5 ATOMIC FORCE MICROSCOPY

Bruker Dimension Icon atomic force microscopy (Bruker AXS, Germany) in ScanAsyst mode was employed to record the image of CS/TPP nanoparticles and KO loaded CS/TPP nanoparticles using silicon tip (TESP, Bruker, nom. Freq. 320 kHz, nom. Spring constant of 42 N/m). A drop of nanoparticle suspension (0.05 mg/mL) deposited on freshly cleaved mica surface and air dried overnight at 25 °C. Deflection and height mode image, both were obtained simultaneously at a fixed scan rate frequency of 0.997 Hz (resolution of 512×512 pixels in 5×5 µm dimensions). All images analysed using Digital NanoScope Analysis software (version 1.40, Bruker Corporation) and presented in zero order two-dimensional flattening.

## 2.6 FTIR CALIBRATIONS

Measured amounts of CS and KO were mixed for standard calibration curve. Lyophilized CS and KO mixture ranging from 0.005 mg to 1.5 mg in oven dried KBr were prepared to formulate uniform 100 g pellets. All the standards spectra were analysed in Essential FTIR software v3.50.059 (Operant LLC) to plot a calibration model.

## 2.7 FTIR SPECTRA PROCESSING AND METHOD DEVELOPMENT

Quantification of KO embedded in nanoparticles was carried determined by FTIR following the method described by Reig et al. 2002 (Reig, Adelantado, & Moya Moreno, 2002) based on Beer-Lambert law and the principle of constant ratio. Essential FTIR software v3.10.016 was used for the computation (Operant LLC). Based on the constant ratio method, the quantity of the standard mixtures or nanoparticles which were mixed or added to KBr had no effect on the ratio between the selected peaks. Nevertheless, KO is in liquid state this procedure did not require special liquid cuvette with the fixed path length. Instead, the common solid holder with KBr disc was utilised and found to be reliable. In this study, the interference between CS/TPP nanoparticles and KO peaks was minimised by selecting the absorption peaks for each material that appeared to be minimally interfered by the other materials. This was performed by comparing the spectra of all the raw materials as shown in Fig. 1. Furthermore, the interference between CS/TPP nanoparticles and KO was minimised by selecting the ratio  $A_{KO}/A_{CS/TPP \text{ nanoparticles}}$  and assigned it to be the “quantitative response” for this method. Selected peaks are shown in Table 1 and Fig. 2.

The predictive values were calculated by the software based on Beer-Lambert law which can be further interpreted in this study based on the following Eq. II.

$$\left( \frac{A_{KO} - A_{KO \text{ baseline}}}{A_{CSNPs} - A_{CSNPs \text{ baseline}}} \right) = \text{Slope} \cdot \frac{KO}{CSNPs} + \text{Constant} \quad (\text{II})$$

Repeatability test, relative standard deviation (RSD), was performed by taking 6 repeated FTIR scans for the standard mixture KO:CS/TPP nanoparticles 1:1. The predicted quantitative response,  $A_{Koil} / A_{CS/TPP \text{ nanoparticles}}$ , was calculated for each scan to determine RSD.

Limit of detection (LOD) and limit of quantification (LOQ) were calculated based on the following Eqs. III and IV, respectively:

$$LOD = 3.3 \frac{\sigma}{S} \quad (\text{III})$$

$$LOQ = 10 \frac{\sigma}{S} \quad (\text{IV})$$

Where:  $\sigma$  and  $S$  are standard deviations of the response and the slope, respectively.

After plotting standard curves,  $R^2$  and RSD values were compared between the selected peaks (Table 1) in order to choose the best calibration curve as a reference for KO quantification from nanoparticles, the best curve was characterized by  $R^2$  closest to 1 and the lowest RSD.

### III. RESULTS AND DISCUSSION

#### 3.1 FOURIER TRANSFORM INFRARED SPECTROSCOPIC ANALYSIS

Fabrication material used in this study and formation of KO loaded in CS/TPP nanoparticles was characterized by FTIR. The major IR absorption bands of CS spectrum were attributed to O–H ( $3451\text{ cm}^{-1}$ ), C–H ( $2876\text{ cm}^{-1}$ ), C–O stretch ( $1647\text{ cm}^{-1}$ ) and N–H stretching vibration of amide II at  $1588\text{ cm}^{-1}$  (Fig. 1A). In the TPP spectrum, two intense absorption bands were found. The peaks in the range of  $1220\text{--}1080\text{ cm}^{-1}$  attributed to P=O stretching and at  $899\text{ cm}^{-1}$  to P–O along with P–O–P (Rodrigues, da Costa, & Grenha, 2012) (Fig. 1B).

With incorporation of TPP in CS the peak of  $3421\text{ cm}^{-1}$  becomes wider indicating that the hydrogen bonding is enhanced. Also, in the TPP spectra the peak at  $1212\text{ cm}^{-1}$  which indicates P=O stretch, appeared in the CS/TPP nanoparticles spectra at  $1218\text{ cm}^{-1}$  as a result of the cross-linking between CS and TPP. Finally, in the spectra of the nanoparticles the peaks for N–H bending vibration of amine I at  $1598\text{ cm}^{-1}$  and the amide II carbonyl stretch at  $1654\text{ cm}^{-1}$  shifted to  $1568\text{ cm}^{-1}$  and  $1630\text{ cm}^{-1}$ , respectively. These results indicate the interaction between amino groups of CS and phosphate groups of TPP. We may conclude that the appearing of these peaks is an indication of nanoparticle formation and inter- as well as intra-molecular actions are enhanced in CS/TPP nanoparticles (Bhumkar & Pokharkar, 2006; De Moura et al., 2009; De Pinho Neves et al., 2014; Xu & Du, 2003) (Fig. 1C).

Further, we confirmed the incorporation of KO in CS/TPP nanoparticles by FTIR via comparing with characteristic peaks in the KO spectra. On the other hand, the increase in CH stretching peak intensity at  $2869\text{--}2974\text{ cm}^{-1}$  reflects the location of KO in the CS matrix. These results were further strengthened as the increase in CH stretching peak intensity was observed with increasing KO content. Therefore, we can consider CH stretching as a strong indicator of KO encapsulation in any matrix (Vongsvivut et al., 2012b; Zhao, Wei, Liu, & Liu, 2014). Thus, emulsion and later electrostatic interaction of CS with TPP, a two-step process successfully encapsulated KO in CS/TPP nanoparticles. The results confirmed the presence of KO with specific peaks at  $3416\text{ cm}^{-1}$  (OH),  $3012\text{ cm}^{-1}$  (=C–H stretching),  $3000\text{--}2800\text{ cm}^{-1}$  (C–H stretching),  $1740\text{ cm}^{-1}$  (C=O stretching band),  $1465\text{ cm}^{-1}$  (–CH<sub>2</sub>– bending),  $1379\text{ cm}^{-1}$  (–CH<sub>3</sub> bending),  $1091\text{ cm}^{-1}$  (CO stretching),  $971\text{ cm}^{-1}$  (C=C stretching band) as shown in (Fig. 1D, E and Fig. 2).

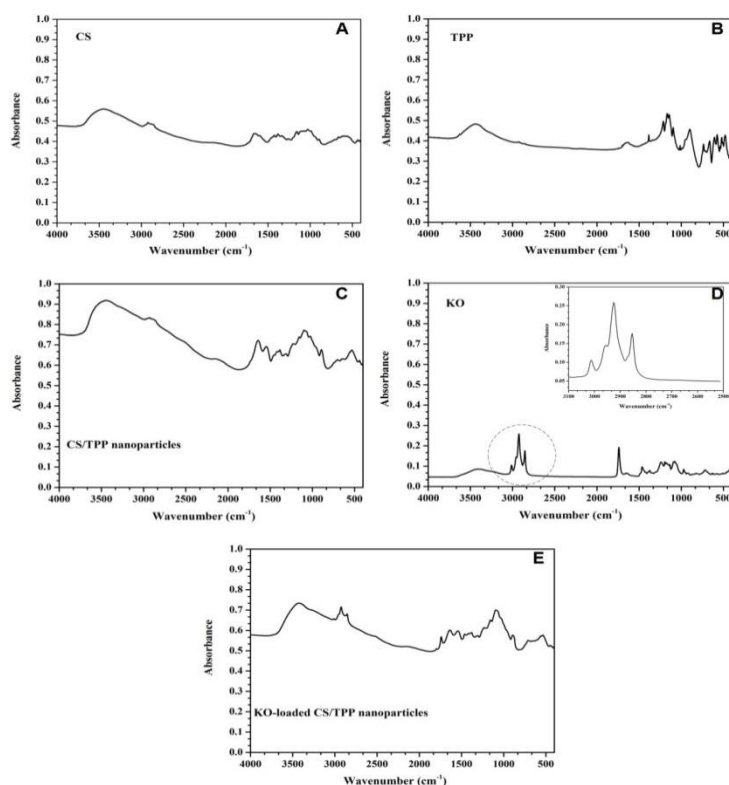
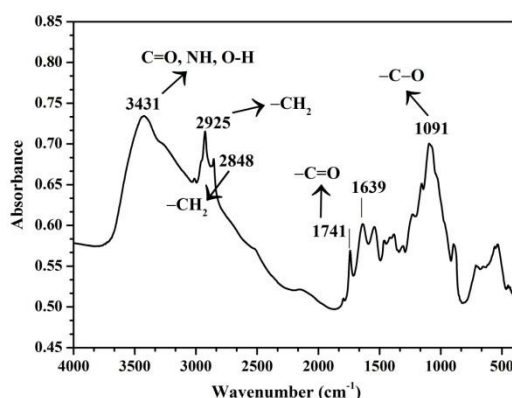


Figure 1: FTIR spectra of the raw materials used in nanoparticles fabrication.



**Figure 2:** Selected peaks from FTIR spectrum of KOloaded CS/TPP nanoparticles at 1:1 ratio.

### 3.2 ATOMIC FORCE MICROSCOPY ANALYSIS

The surface morphology of the particles was observed by atomic force microscopy (AFM) imaging. The AFM images of the CS/TPP nanoparticles demonstrate regular distribution and spherical shape that appear to be well separated and stable over the steps of the preparation process (**Fig. 3A and B**). Next we continue to investigate the KOloaded CS/TPP nanoparticles. AFM imaging has revealed aggregation that due to the presence of remaining KO around the particles (**Fig. 3C and D**).

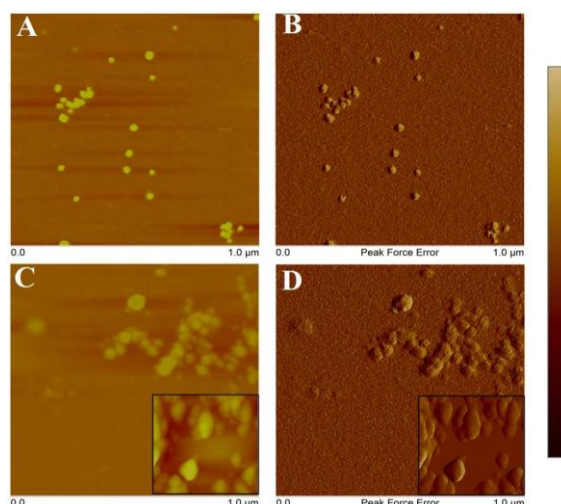


**Figure 3:** (A and B) AFM images showing the surface morphology of CS/TPP nanoparticles; (C and D) KOloaded CS/TPP nanoparticles (C, D). (A, C are height images; B, D are deflection images). The colorscale on the right side is 100 nm.

### 3.3 STANDARD CURVE CONSTRUCTION

Quantification of KO was based on Beer-Lambert law and constant ratio method (Reig et al., 2002). Absorbance peaks were selected with minimal interference from the other components by comparing the spectra of the raw materials (**Fig. 4**). Consequently, peak selection was made mainly by comparing the FTIR spectra of CS/TPP nanoparticle and KO and their mixture as shown in **Fig. 1 and 2**. The two distinct peaks at about 2925  $\text{cm}^{-1}$  and 2848  $\text{cm}^{-1}$  were selected for KO. For CS/TPP nanoparticle, peak at 1741  $\text{cm}^{-1}$  and 1091  $\text{cm}^{-1}$  were chosen. Different mathematical combinations of the peak's heights and the baseline regions were tested in order to obtain the best standard curve (**Table 1 and Fig. 4**).

Based on **Table 1**, the best standard curve was obtained at the absorbance 2925  $\text{cm}^{-1}$  with the baseline correction at 1845 – 1898  $\text{cm}^{-1}$  for KO, and the absorbance 1091  $\text{cm}^{-1}$  with baseline correction at 1845–1898  $\text{cm}^{-1}$  for CS/TPP nanoparticle (**Fig. 4D**). At these range of wavelength, the  $R^2$  and the RSD values are the closest to 1 (0.99) and the lowest (1.075%), respectively.

**Table 1:** Selected peaks from FTIR spectra of the KO and CS/TPP nanoparticles standard mixtures in order to construct the best standard curve LOD and LOQ are represented by % (w/w)KO/CS-TPP nanoparticles.

KO peak (cm <sup>-1</sup> )			CS/TPP nanoparticles peaks (cm <sup>-1</sup> )			R2	RSD (%)	LOD	LOQ	Figure
Region	Peak	Baseline	Region	Peak	Baseline					
2866-2875	2848	2455-2550	1704-1765	1741	1845-1898	0.9431	3.037	3.56	10.80	Fig. 4A
2896-2946	2925	1845-1898	1704-1765	1741	1845-1898	0.9689	2.793	2.70	8.18	Fig. 4B
2866-2875	2848	2455-2550	1086-1099	1091	1845-1898	0.9826	1.531	1.78	5.39	Fig. 4C
2896-2946	2925	1845-1898	1086-1099	1091	1845-1898	0.9959	1.075	1.24	3.77	Fig. 4D

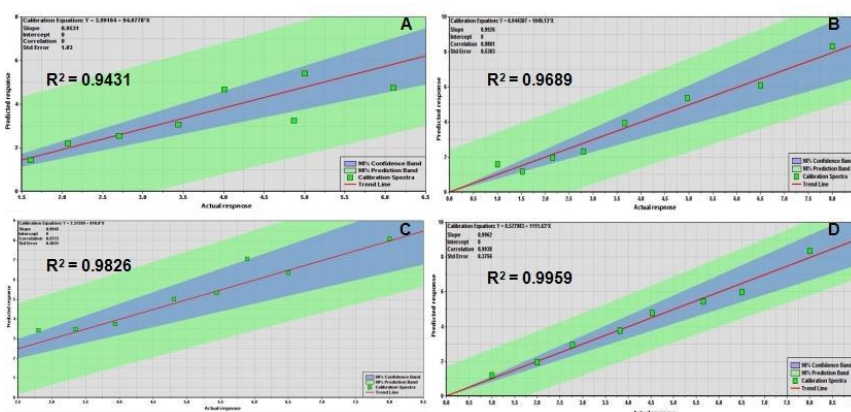


**Figure 4:** Standard curves obtained from FTIR spectra based on Beer- Lambert law. Each curve represents a set of selected peaks explained in Table 1.

### 3.4 QUANTIFICATION OF KO IN KO-LOADED CS/TPP NANOPARTICLES

FTIR spectrum of CS/TPP nanoparticles (Fig. 1) was used to quantify the loading efficiency of KO. Using the abovementioned best standard curve (Fig. 4D), KO loading efficiency was estimated to be  $22.2 \pm 0.26$  % using FTIR method and it was  $23.8 \pm 0.07$  %, when estimated gravimetrically. The study recommends the use of FTIR as quantitative analytical tool for PUFA supplements to avoid sample preparation complexity and time consumption. The most impressive thing is that once the initial calibration curve is set up, the analysis is extremely rapid and simple with no accuracy issues.

## IV. CONCLUSION

Quantification of KO in nanoparticles by means of FTIR is rapid and easy approach to apply. Acquisition of FTIR spectral data directly from the KO loaded CS/TPP nanoparticles, a good linear calibration curve ( $R^2 = 0.9959$ ) was achieved. The FTIR spectroscopic technique is advantageous over gravimetric method due to rapid spectral data collection directly from original KO loaded CS/TPP nanoparticles without any sample pre-treatment. Further, technique is also environmentally friendly and very cost effective since there is no other solvent or chemical, besides the samples, involved in the process of the analysis. The method will help to accelerate and improve the characterisation of KO nanoparticles during development and optimization stage.

## ACKNOWLEDGEMENT

The authors declare no conflict of interest. This work was financially supported by NSFC 31571891 and 31401533; JUSRP 51507 and 11422; 111Project B07029 and PCSIRT0627.

## REFERENCES

- [1]. Acosta, E. (2009). Bioavailability of nanoparticles in nutrient and nutraceutical delivery. *Current Opinion in Colloid & Interface Science*, 14(1), 3–15.
- [2]. Anzanello, M. J., Fogliatto, F. S., Ortiz, R. S., Limberger, R., & Mariotti, K. (2014). Selecting relevant Fourier transform infrared spectroscopy wavenumbers for clustering authentic and counterfeit drug samples. *Science & Justice: Journal of the Forensic Science Society*, 54(5), 363–8.
- [3]. Aziz, S., Gill, J., Dutilleul, P., Neufeld, R., & Kermasha, S. (2014). Microencapsulation of krill oil using complex coacervation. *Journal of Microencapsulation*, 31(8), 774–784.
- [4]. Barrow, C. J., Nolan, C., & Jin, Y. (2007). Stabilization of highly unsaturated fatty acids and delivery into foods. *Lipid Technology*, 19(5), 108–111.
- [5]. Bassbasi, M., Platikanov, S., Tauler, R., & Oussama, A. (2014). FTIR-ATR determination of solid non fat (SNF) in raw milk using PLS and SVM chemometric methods. *Food Chemistry*, 146, 250–4.
- [6]. Bhumkar, D. R., & Pokharkar, V. B. (2006). Studies on effect of pH on cross-linking of chitosan with sodium tripolyphosphate: A technical note. *AAPS PharmSciTech*, 7(2), E138–E143.

- [7]. Blanco, M., Valdés, D., Bayod, M., Fernández-Marí, F., & Llorente, I. (2004). Characterization and analysis of polymorphs by near-infrared spectrometry. *Analytica Chimica Acta*, 502(2), 221–227.
- [8]. Burdge, G. C., & Calder, P. C. (2005). Conversion of alpha-linolenic acid to longer-chain polyunsaturated fatty acids in human adults. *Reproduction, Nutrition, Development*, 45(5), 581–97.
- [9]. Bureau, S., Ruiz, D., Reich, M., Gouble, B., Bertrand, D., Audergon, J.-M., & Renard, C. M. G. C. (2009). Application of ATR-FTIR for a rapid and simultaneous determination of sugars and organic acids in apricot fruit. *Food Chemistry*, 115(3), 1133–1140.
- [10]. Bustos, R., Romo, L., Yáñez, K., Díaz, G., & Romo, C. (2003). Oxidative stability of carotenoid pigments and polyunsaturated fatty acids in microparticulate diets containing krill oil for nutrition of marine fish larvae. *Journal of Food Engineering*, 56(2-3), 289–293.
- [11]. Calvo, P., & Remunan-Lopez, C. (1997). Novel hydrophilic chitosan-polyethylene oxide nanoparticles as protein carriers. *Journal of Applied Polymer Science*, 63(1), 125–132.
- [12]. Che Man, Y. B., Ammawath, W., & Mirghani, M. E. S. (2005). Determining  $\alpha$ -tocopherol in refined bleached and deodorized palm olein by Fourier transform infrared spectroscopy. *Food Chemistry*, 90(1-2), 323–327.
- [13]. Chen, L., Remondetto, G. E., & Subirade, M. (2006). Food protein-based materials as nutraceutical delivery systems. *Trends in Food Science & Technology*, 17(5), 272–283.
- [14]. De Moura, M. R., Aouada, F. A., Avena-Bustillos, R. J., McHugh, T. H., Krochta, J. M., & Mattoso, L. H. C. (2009). Improved barrier and mechanical properties of novel hydroxypropyl methylcellulose edible films with chitosan/tripolyphosphate nanoparticles. *Journal of Food Engineering*, 92(4), 448–453.
- [15]. De Pinho Neves, A. L., Milioli, C. C., Müller, L., Riella, H. G., Kuhnen, N. C., & Stulzer, H. K. (2014). Factorial design as tool in chitosan nanoparticles development by ionic gelation technique. *Colloids and Surfaces A: Physicochemical and Engineering Aspects*, 445, 34–39.
- [16]. Duclairroir, C., Orecchioni, A.-M., Depraetere, P., Osterstock, F., & Nakache, E. (2003). Evaluation of gliadins nanoparticles as drug delivery systems: a study of three different drugs. *International Journal of Pharmaceutics*, 253(1-2), 133–144.
- [17]. Guterres, S. S., Alves, M. P., & Pohlmann, A. R. (2007). Polymeric nanoparticles, nanospheres and nanocapsules, for cutaneous applications. *Drug Target Insights*, 2, 147–57.
- [18]. Heinzelmann, K., Franke, K., Velasco, J., & Márquez-Ruiz, G. (2000). Microencapsulation of fish oil by freeze-drying techniques and influence of process parameters on oxidative stability during storage. *European Food Research and Technology*, 211(4), 234–239.
- [19]. Hosseini, S. F., Zandi, M., Rezaei, M., & Farahmandghavi, F. (2013). Two-step method for encapsulation of oregano essential oil in chitosan nanoparticles: Preparation, characterization and in vitro release study. *Carbohydrate Polymers*, 95(1), 50–56.
- [20]. Hu, Y., Erxleben, A., Ryder, A. G., & McArdle, P. (2010). Quantitative analysis of sulfathiazole polymorphs in ternary mixtures by attenuated total reflectance infrared, near-infrared and Raman spectroscopy. *Journal of Pharmaceutical and Biomedical Analysis*, 53(3), 412–20.
- [21]. Indarti, E., Majid, M. I. A., Hashim, R., & Chong, A. (2005). Direct FAME synthesis for rapid total lipid analysis from fish oil and cod liver oil. *Journal of Food Composition and Analysis*, 18(2-3), 161–170.
- [22]. Jang, K.-I., & Lee, H. G. (2008). Stability of chitosan nanoparticles for L-ascorbic acid during heat treatment in aqueous solution. *Journal of Agricultural and Food Chemistry*, 56(6), 1936–41.
- [23]. Klinkesorn, U., Sophanodora, P., Chinachoti, P., Decker, E. a., & McClements, D. J. (2006). Characterization of spray-dried tuna oil emulsified in two-layered interfacial membranes prepared using electrostatic layer-by-layer deposition. *Food Research International*, 39(4), 449–457.
- [24]. Kolakowska, A., Kolakowski, E., & Szczygielski, M. (1994). Winter season krill (*Euphausia superba* D.) as a source of n-3 polyunsaturated fatty acids. *Food / Nahrung*, 38(2), 128–134.
- [25]. Kondepati, V. R., Keese, M., Michael Heise, H., & Backhaus, J. (2006). Detection of structural disorders in pancreatic tumour DNA with Fourier-transform infrared spectroscopy. *Vibrational Spectroscopy*, 40(1), 33–39.
- [26]. Kumar, S. A., Tang, C.-F., & Chen, S.-M. (2008). Electroanalytical determination of acetaminophen using nano-TiO<sub>2</sub>/polymer coated electrode in the presence of dopamine. *Talanta*, 76(5), 997–1005.
- [27]. Liu, S., Low, N. H., & Nickerson, M. T. (2010). Entrapment of flaxseed oil within gelatin-gum Arabic capsules. *JAOCs, Journal of the American Oil Chemists' Society*, 87(7), 809–815.
- [28]. Malafaya, P. B., Silva, G. a., & Reis, R. L. (2007). Natural-origin polymers as carriers and scaffolds for biomolecules and cell delivery in tissue engineering applications. *Advanced Drug Delivery Reviews*, 59(4-5), 207–233.
- [29]. Ortiz, R. S., Mariotti, K. de C., Fank, B., Limberger, R. P., Anzanello, M. J., & Mayorga, P. (2013). Counterfeit Cialis and Viagra fingerprinting by ATR-FTIR spectroscopy with chemometry: can the same pharmaceutical powder mixture be used to falsify two medicines? *Forensic Science International*, 226(1-3), 282–9.
- [30]. Pietrowski, B. N., Tahergorabi, R., Matak, K. E., Tou, J. C., & Jaczynski, J. (2011). Chemical properties of surimi seafood nutrified with  $\omega$ -3 rich oils. *Food Chemistry*, 129(3), 912–9.
- [31]. Pinto Reis, C., Neufeld, R. J., Ribeiro, A. J., & Veiga, F. (2006). Nanoencapsulation I. Methods for preparation of drug-loaded polymeric nanoparticles. *Nanomedicine: Nanotechnology, Biology, and Medicine*, 2(1), 8–21.
- [32]. Reig, F. B., Adelantado, J. V. G., & Moya Moreno, M. C. M. (2002). FTIR quantitative analysis of calcium carbonate (calcite) and silica (quartz) mixtures using the constant ratio method. Application to geological samples. *Talanta*, 58(4), 811–21.
- [33]. Rodionova, O. Y., Houmøller, L. P., Pomerantsev, A. L., Geladi, P., Burger, J., Dorofeyev, V. L., & Arzamastsev, A. P. (2005). NIR spectrometry for counterfeit drug detection. *Analytica Chimica Acta*, 549(1-2), 151–158.
- [34]. Rodrigues, S., da Costa, A.M.R., & Grenha, A. (2012). Chitosan/carrageenan nanoparticles: effect of cross-linking with tripolyphosphate and charge ratios. *Carbohydrate Polymers*, 89(1), 282-9.
- [35]. Rothenfluh, D. A., Bermudez, H., O'Neil, C. P., & Hubbell, J. A. (2008). Biofunctional polymer nanoparticles for intra-articular targeting and retention in cartilage. *Nature Materials*, 7(3), 248–54.
- [36]. Salari, A., & Young, R. E. (1998). Application of attenuated total reflectance FTIR spectroscopy to the analysis of mixtures of pharmaceutical polymorphs. *International Journal of Pharmaceutics*, 163(1-2), 157–166.
- [37]. Schuchardt, J. P., & Hahn, A. (2013). Bioavailability of long-chain omega-3 fatty acids. *Prostaglandins, Leukotrienes, and Essential Fatty Acids*, 89(1), 1–8.
- [38]. Shu, X., & Zhu, K. (2002). The influence of multivalent phosphate structure on the properties of ionically cross-linked chitosan films for controlled drug release. *European Journal of Pharmaceutics and Biopharmaceutics*, 54(2), 235–243.
- [39]. Ulberth, F., & Henninger, M. (1992). One-step extraction/methylation method for determining the fatty acid composition of processed foods. *Journal of the American Oil Chemists' Society*, 69(2), 174–177.

- [40]. Vongsivut, J., Heraud, P., Zhang, W., Kralovec, J. A., McNaughton, D., & Barrow, C. J. (2012a). Quantitative determination of fatty acid compositions in micro-encapsulated fish-oil supplements using Fourier transform infrared (FTIR) spectroscopy. *Food Chemistry*, 135(2), 603–9.
- [41]. Vongsivut, J., Heraud, P., Zhang, W., Kralovec, J. a., McNaughton, D., & Barrow, C. J. (2012b). Quantitative determination of fatty acid compositions in micro-encapsulated fish-oil supplements using Fourier transform infrared (FTIR) spectroscopy. *Food Chemistry*, 135(2), 603–9.
- [42]. Werner, A., Havinga, R., Kuipers, F., & Verkade, H. J. (2004). Treatment of EFA deficiency with dietary triglycerides or phospholipids in a murine model of extrahepatic cholestasis. *American Journal of Physiology. Gastrointestinal and Liver Physiology*, 286(5), G822–32.
- [43]. Xu, Y., & Du, Y. (2003). Effect of molecular structure of chitosan on protein delivery properties of chitosan nanoparticles. *International Journal of Pharmaceutics*, 250(1), 215–226.
- [44]. Yang, S.-J., Lin, F.-H., Tsai, H.-M., Lin, C.-F., Chin, H.-C., Wong, J.-M., & Shieh, M.-J. (2011). Alginate-folic acid-modified chitosan nanoparticles for photodynamic detection of intestinal neoplasms. *Biomaterials*, 32(8), 2174–2182.
- [45]. Yao, M., Xiao, H., & McClements, D. J. (2014). Delivery of lipophilic bioactives: assembly, disassembly, and reassembly of lipid nanoparticles. *Annual Review of Food Science and Technology*, 5, 53–81.
- [46]. Zhao, J., Wei, S., Liu, F., & Liu, D. (2014). Separation and characterization of acetone-soluble phosphatidylcholine from Antarctic krill (*Euphausia superba*) oil. *European Food Research and Technology*, 238, 1023–1028.

## Over Coming of Errors in Tmr System Utilizing Scanchain Methods

PARAMESHAPPA.G<sup>1</sup>, MADHUKAR.G.N.MALIGERA<sup>2</sup>,  
Dr. D. JAYADEVAPPA<sup>3</sup>

<sup>1,2</sup>Department of Electronics & communication, JSS Academy of Technical Education, Bengaluru, India.

<sup>3</sup>Department of Electronics & instrumentation, JSS Academy of Technical Education, Bengaluru, India.

**ABSTRACT:** in this paper, we depict a Scan-chain-based triple modular redundancy and Scan chain based multiple error recovery technique for triple modular redundancy systems. Scan-chain-based triple modular redundancy identifies and corrects only one fault whereas the SMERTMR technique reuses scan-chain flip-flops invented for testability functions to observe and correct faulty modules within the presence of single or multiple transient faults. In this planned technique, the faults are identified at the output of the modules, but the faults which are latent are identified by monitoring the interior states of the TMR modules. Once the fault is identified, the output of fault free module will be copied into the module which is faulty. If in case any modules are identified as permanent fault then the whole system will enter into the Master/Checker configuration. The last method which is enhanced SMERTMR is implemented with the aim to improve the overall performance of system. Finally all three methods are compared with their performance time.

**Keywords:** scan chain, triple modular redundancy (TMR), scan-chain-based triple modular redundancy (ScTMR), Scan chain based multiple error recovery technique for triple modular redundancy systems (SMERTMR).

### I. INTRODUCTION

In present days the system which has to meet the specified function within the deadline are used in various situations such as nuclear power plants and spacecraft [2], [3]. Along such circumstance these systems are at a very high risk of getting affected by errors. So identification of these errors and rectifying them will be time consuming. Along with this it has to correct the faults within the specified deadline. Hence error identification and correction will be a major challenge to meet with in the system deadline. Therefore in order to achieve the reliability, the systems should be made available with the suitable error tolerant systems. Thus meeting reliability and achieving timing constraints are a bit of contradicting things.

For instance one of the method called roll back recovery, in this the retry mechanism in which the fault or error will be rectified but with the major disadvantage of crossing the deadline period [11]. Redundancy (extra information) is one of the attribute to be made use during the transfer of message. With the help of the extra information the receivers will be in safer side to determine the correct data without any corruption.

In system such as life monitoring systems where the purpose of safety is critical, roll forward methodology like Triple modular redundancy (TMR) is one of the popular and most often used [4], [5] in such applications. The TMR will be holding three modules which are redundant (extra) along with a voter at the outputs of three modules. The main drawback of TMR is its failures, which refers to multiple errors caused in the system or a fault occurring in the voter. For instance error occurring in more than one module, if it is not corrected it will cause to failure of TMR. For applications which use retry methodology, they will be at a risk of consuming time more than the specified deadline time. Hence roll forward methodology is made use widely.

So roll forward methodology can be made used in a technique called ScTMR (Scan chain based TMR). This technique also suffers from major drawbacks. First, when a fault which is latent appears in the system the ScTMR cannot recover from this. The fault is recognized as latent only when the fault does not propagate to the output but will make the states of the modules to be mismatched. Second, ScTMR will not be in a state of recovery if more than one fault appears in the modules. Hence Scan chain based multiple error recovery in TMR (SMERTMR) and enhanced part of SMERTMR has the feature of overcoming the errors or faults affecting more than one module in TMR.

The rest of this paper is organized as follows. Section II - SCTMR technique, Section III - Architecture of SMERTMR, Section IV- Enhanced SMERTMR, Section V - Concludes the paper VI – Simulated Results.

### II. SC TMR TECHNIQUE

The module which is faulty one is identified and corrected in ScTMR with the help of scan chain. In order to test the circuits scan chain is one of the effective method in the way of cost. In this methodology of scan chain a long sequence of flip flops will be made use of in the form of shift register and a multiplexer will be placed in front of these flip flops which will intern switch between mode of normal operation and mode of testing operation.

The major disadvantage of this system is that it cannot rectify more than one fault in the system. For instance if one of module is identified as faulty at the same time if a latent fault appears in other module then it cannot overcome these two faults. Ultimately the system will go in to the mode of unrecoverable state.

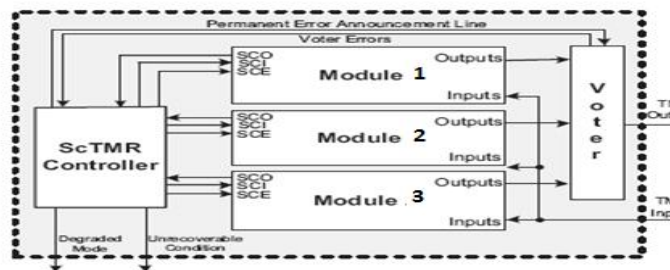


Figure 1 Sc TMR Block Diagram

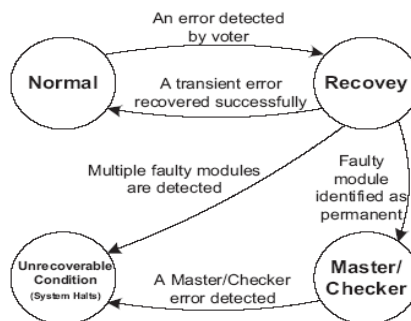


Figure 2 Sc TMR State Diagram

#### A. Sc TMR Voter

The major part in the ScTMR system which identifies the modules, whether they are faulty and also identifies the faults in comparator is voter. The voter is depicted in figure 3 which holds 3 comparators. The working of voter can be explained with an example. For instance if there is a fault in module 1 then the output of the comparators C12 and C13 will be high and C23 will be low. The error signals E12 and E13 will act as input to an AND gate which will produce the select signal to mux, this entire thing will act as output selector. With the help of Table 1 the modules which are faulty are identified and the correct output will be displayed.

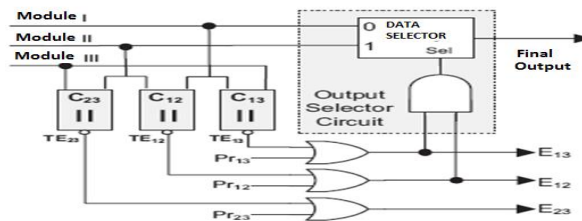


Figure 3 Sc TMR Voter

$E_{12}$	$E_{13}$	$E_{23}$	Faulty module	Output
0	0	0	-	Output I
0	0	1	Comparator_23	Output I
0	1	0	Comparator_13	Output I
0	1	1	Module 3	Output I
1	0	0	Comparator_12	Output I
1	0	1	Module 2	Output I
1	1	0	Module 1	Output II
1	1	1	Unrecoverable	X

**Table 1 Identifying Faulty Module and Selecting Correct Voter Output Using Error Signals**

**B. TRANSIENT AND PERMANENT ERROR RECOVERY MECHANISMS**

If there is a mismatch which will be detected by the voter. It will activate the error signal to alert the controller. Once the error signal is activated the system will be transferred from mode of normal operation to mode of recovery in which the module which was faulty will be recovered with the help of fault free module.

So in the mode of recovery the controller will configure the multiplexer and allows the scan chain to function. Also the SCI signal of module which is faulty will be connected to the SCO of the module which is free from fault. Along with this the SCI of fault free module will be connected to its own Scan chain output (SCO) signal. The entire thing which is described above is depicted in figure 4.

Once the system enters to the mode of recovery the counter will be initiated, if the counter reaches to zero then the system will exit from the recovery mode.

This system will utilize two internal registers called MRFM (Most-Recent Faulty Module) and NCF (Number of Consecutive Faults).

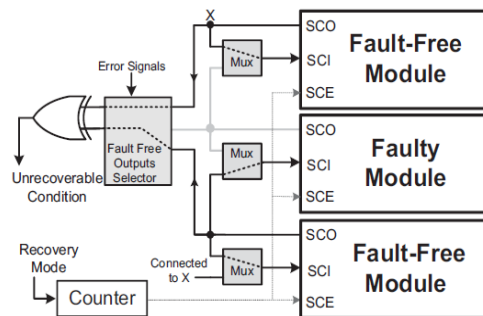


**Figure 4 Sc TMR in recovery mode.**

MRFM stores the module number which was faulty at the last output. If there is the same module which will occur as faulty consecutively then the NCF register will be incremented by one. Along with this if NCF crosses the certain predefined number then that module will be indicated as permanent fault. Or else the fault will be considered as transient.

When the module is designated as permanent fault then the entire system is degraded to Master/Checker configuration. Upon detection of permanent errors the Pr error signal will be activated.

**III. ARCHITECTURE OF SMERTMR**

Once again the figure 1 can be taken as reference for SMERTMR system. The voter will generate the error signal and produces the same to controller where proper mechanism will be held in order to recover the module which was faulty. The whole scan chain along with SCI, SCO, and SCE will be totally controlled by controller.

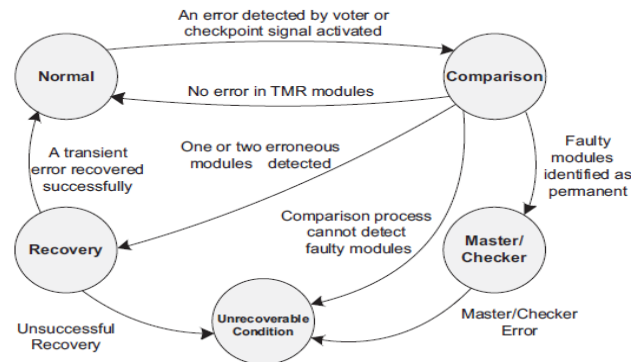


Figure 5 SMERTMR State Diagram

The state diagram is depicted in figure 5. Initially the system will be functioning in the mode of normal operation. If any error is detected by the voter the system will go to the mode of comparison. In this mode the internal states of all the modules in the system will be compared. During this process if there is no mismatch then it will go back to the mode of normal operation or else it will go to the mode of recovery.

Hence when the mode of recovery finishes with success, the system will enter to the mode of normal operation or else if it detects a permanent fault then the system will go to the Master/Checker mode. In this mode if it finds any fault in the master or checker then it will go to the state of unrecoverable condition.

#### A. Comparison Process

The following section will describe how the system will identify the fault in the system.

1) **When there is no fault in any of the modules:** if there are no mismatches between any of the modules, all the three counters will be set to zero

2) **If there is only one faulty module:** Consider that there are 'A' flip flops faulty in the module M and the rest of the modules N and O are fault free. Along such a situation one can find, that counters MN and MO will be incremented to 'A' whereas the counter NO will be of zero. Therefore by getting the values of the counters MN and MO the system will enter in to the mode of recovery and the faults will be corrected. Thus in this case the faulty module is M.

3) **In case of two modules which are faulty:** Assume that there are modules which are faulty such as M and N and the module O is fault free. Also consider that there are A, B set of flip flops faulty in the modules of M and N respectively. Thus there could be either no flip flops which are in similarity or there would be more than one flip flops in similarity of incorrectness.

If there is no similarity of incorrectness between the modules then the value of counters will be having these values. The MO counter will be having the value of A and NO counter will be having the value of B and MN counter will be having the value in-between zero and A+B. Taking in to account of the number of mismatches value in counter the system will detect and correct the faults. Thus in this case the faulty modules are M and N. If there is a common flip flops which are incorrect then the system cannot identify the faults and hence cannot be corrected.

4) **When none of the modules are free from fault:** In such a condition the system can't find out the modules which are faulty. So the system goes to the state of unrecoverable state.

1. If  $\text{counter}_{mn} = \text{counter}_{mo} = \text{counter}_{no} = 0$  then
2. Coming state = normal
3. Else if  $(\text{counter}_{mn} = \text{Counter}_{mo}) \ \& \ (\text{counter}_{no} = 0)$  then
4. Coming state = recovery
5. Faulty module register = M
6. Else if  $(\text{counter}_{no} = A) \ \& \ (\text{counter}_{mo} = B) \ \& \ (\text{counter}_{mn} = A+B)$  then
7. Coming state = recovery
8. Faulty module register = M,N
9. Else
10. Coming state = unrecoverable condition
11. End if

Figure 6 Algorithm

**B. Transient and Permanent Error Recovery Mechanisms**

While the process of comparison is over, where the FLU (Fault Locator Unit) will detect the modules which are faulty and free from fault, next the system goes to the mode of recovery during which it will correct up to two modules which are faulty utilizing the scan chain.

The controller of SMERTMR in mode of recovery is depicted in figure 7. Along with this the scan chains are enabled within the modules and the controller will configure the mux which is presented in the following section.

The SCO and SCI signals are interconnected in modules which are free from fault, whereas in the modules which are faulty the SCI of this module will be interconnected to the SCO of module which is free from fault.

Along the mode of recovery, once a mismatch is identified the equivalent count in the counter will be subtracted by one count, which is the reverse condition in comparison mode where the count will be incremented by one count when it comes across the mismatch. At the end of the mode of recovery if there is zero in all counters then it means that the recovery process is successfully done, if not the system will go to the unrecoverable condition.

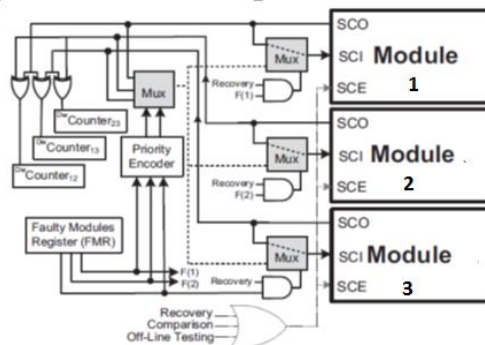


Figure 7 SMERTMR in recovery mode

**IV. ENHANCED SMERTMR**

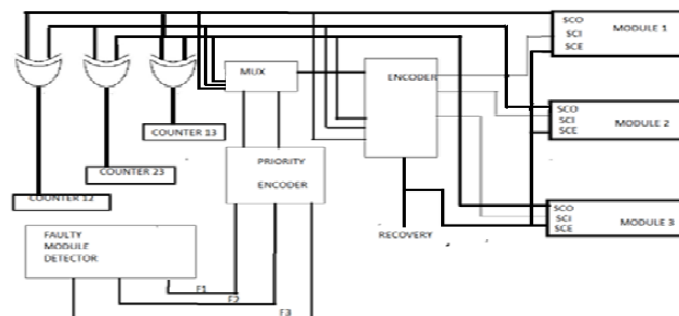


Figure 8 – Enhanced Smertmr

It can be seen from the figure 8 that the MUX, AND gate has been removed from SMERTMR circuit and it is been replaced by a encoder. With the help of this circuit the time for the input to reach the output will be reduced drastically. The comparison table of output time for different technique is been depicted in the table of conclusion part.

**V. CONCLUSION**

A roll forward error recovery methodology named SMERTMR is presented to overcome from multiple errors. During which the system can overcome from more than one faulty modules, which can be transient or latent. The experiments show that SMERTMR can identify and correct up to 100% and 99.7% of multiple faults causing one and two modules respectively. Also it can be shown that the performance overhead of SMERTMR as compared to the SctMR is less. Thus we can conclude that by replacing the multiplexers, and gates by encoder, we can achieve the faster output.

Type	Output Time for the Frequency of 117.889 MHz
ScTMR	20.611 ns
SMERTMR	12.140 ns
Enhanced SMERTMR	3.308ns

Table 2 - Output Performance - comparison table of different methodology

VI. VI. SIMULATED RESULTS



Sc TMR Output



Enhanced SMERTMR Output

REFERENCES

- [1]. SeyedGhassemMiremadi, Senior Member, IEEE,HosseinAsadi, Member, IEEE, and Mahdi Fazeli, Student Member, IEEE “Low-Cost Scan-Chain-Based Technique to RecoverMultiple Errors in TMR Systems”,
- [2]. Bartlett, J. F., Tandem Computers Inc., Cupertino, CA, “A Nonstop Operating System,” Proc. of the 11<sup>th</sup>Hawaii Int’lConf on System Sciences, pp. 103- 1 17, 1978.
- [3]. Losq, J. “A Highly Efficient Redundancy Scheme: Self- Purging Redundancy,” IEEE Trans. Comp. C-25, pp. 569- 578,1976.
- [4]. Mathur, F. P., “Reliability Estimation Procedures and CARE: The Computer Aided Reliability Estimation Program,” Jet Propulsion Laboratoty Quarterly Tech. Review I ,Oct I97 1.
- [5]. Mathur F. P. and P. DeSousa, “Reliability Modeling and Analysis of General Modular Redundant Systems,” IEEETrans. Rel., R- 24, No. 5, pp. 296-299, 1975.
- [6]. Webber, S. and J. Beime, “The Stratus Architecture,” Digest of Papers. Fault-Tolerant Computing: Twenty-First International Symposium, pp. 79-85, 1991.
- [7]. Lala, J. H., L. S. Alger, R. J. Gauthier, M. J. Gauthier, and M. J. Dzwonczyk, “A Fault Tolerant Processor to MeetRigorous Failure,” Proc. of IEEE/AIAA 7<sup>th</sup>Digital AvionicsSystems Conf. pp. 555-562, 1986.
- [8]. Adams, S. J., “Hardware Assisted Recovery from Transient Errors in Redundant Processing Systems,” FTCS 19<sup>th</sup>DigestofPapers, pp. 512-519, 1989.
- [9]. S. D’Angelo, C. Metra, and G. Sechi, “Transient and permanent faultdiagnosis for FPGA-based TMR systems,” in Proc. Int. Symp. DefectFault Tolerance VLSI Syst., 1999, pp. 330–338.
- [10]. J. Yoon and H. Kim, “Time-redundant recovery policy of TMR failuresusing rollback and roll-forward methods,” IEE Proc. - Comput. Digit.Tech., vol. 147, no. 2, pp. 124–132, Mar. 2000.
- [11]. M. Ebrahimi, S. G. Miremadi, and H. Asadi, “ScTMR: A scan chainbasederror recovery technique for TMR systems in safety-criticalapplications,” in Proc. Design Autom. Test Eur. Conf. Exhibit., 2011.
- [12]. The Leon2 Processor User Manual. (2007) [Online].
- [13]. G. Latif-Shabgahi and S. Bennett, “Adaptive majority voter: A novelvoting algorithm for real-time fault-tolerant control systems,” in Proc.25th EUROMICRO Conf., vol. 2. 1999, pp. 113–120.

## Marine Offshore Accidents in Nigeria, Causes and Necessary Preventive Measures

Oyinkepreye L. Bebetidoh<sup>1</sup>, Robert Poku<sup>1</sup>,

<sup>1</sup>Department of Marine and Mechanical Engineering, Niger Delta University, Wilberforce Island, P.M.B 071, Yenagoa, Bayelsa State, Nigeria

**ABSTRACT:** *With the ground-breaking developments in the maritime industry and the implementation of safety-related regulations and the institution of International Safety Codes and Protocols, marine offshore accidents in Nigeria are still a serious concern for global maritime organizations as the rate of offshore accidents has not reduced to the expected level. Ensuring the consistency of offshore accident investigation reports is recognized as a significant goal in order to plainly ascertain the core causes of offshore accidents. This research work though limited due to poor response on the part of the respondents as regards to releasing some data that would have been helpful, the researchers were still able to investigate the core causes of marine offshore accidents in Nigeria's maritime industry. With emphasis on the scope of work essentially, data was collected through the administration of a well-structured questionnaire to selected seafarers connected with the offshore oil and gas industry in Nigeria, which included Captains, engineers, deckhands, oilers and Quartermasters. The data's collected through the administration of a self-constructed questionnaire was analyzed using the concept of the statistical tool, Chi-Square, which was considered appropriate for testing the validity and reliability of each hypothesis established in this research. The aim of this research was to determine the causes of marine offshore accidents in Nigeria, which identified that human, environmental/natural, design, and technical factors comprises the major causes of marine offshore accidents. With the findings gotten, recommendations were made which if implemented by governments and maritime organizations and adhered to by maritime operators will go a long way to reduce marine offshore accidents.*

**Keywords:** *Marine Offshore, Accidents, Preventive measures, and Chi-Square*

### I. INTRODUCTION:

Accidents are basically a shady spot in human history; they are also a source of challenge and inspiration to engineers and scientist in their drive towards crafting methods and measures in the prevention of all nature of accidents in the feature (6). Some marine accidents has had high impact on the society and has also prompted international protocols and conventions with unforeseeable consequences (14). As a result of increased oil prospecting activities in the Niger Delta region on Nigeria, there has been a tremendous increase in marine vessel accidents, leading to personal injuries, loss of lives and tremendous damage to facilities (6). According to (5) marine accidents is on the increase not minding the measures put in place to regulate such from happening. According to (6) accidents are basically unintended happenings. While both researchers agree with this assertion, (10) opined that accidents don't just occur; they are customarily the product of several causative elements of which each one is manageable, in other words accidents are caused. Vessels sunk in waterways, shallow approaches and channels, and wrecks constitute danger to navigation and free movement of ships and crafts (5). Exploration and production of oil and gas in marine offshore environment by their nature are not fundamentally safe and are relatively multifarious and if not handled properly will lead to accident (16). (13) In his earlier research averred that there is an urgent need to set up accident and control mechanism as a result of the "epidemic" nature accidents have become.

Research has shown that key offshore accidents have ensued in several offshore platforms, ships and small craft in Nigeria's offshore region which resulted in damage to the environment, destruction of assets and loss of lives (14) (16). (5) In his earlier research noted that from 2000 through 2009, a total number of five hundred and fifty-two seafarers lost their lives due to vessel collisions and capsizing in Nigerian inland waterways. This number points to an average casualty rate of fifty-five deaths yearly excluding losses to cargos and vessels. These mishaps and accidents are attributed to factors which include environmental, technical, human factors or human

error and organizational errors (16) at sea, platforms and rigs leading to personal injuries, or death (6). (15) States that the error inducing character of the system in shipping lies in the social organization of the personnel onboard, economic pressure, the structure of the industry, and insurance and difficulties in international regulation. This research examines the present role safety plays in the maritime industry and the human factors that may contribute to the causal chain in offshore accidents. According to (12) there is a particular combination of demands characteristic of the maritime industry such as fatigue, stress, work pressure, communication, environmental factors, and long periods of time away from home, which could be potential contributors. Exemplifying that in shipping “there are a number of workplace dangers in combination, something rare in other industries” The 21st century shipping industry faces new challenges. For instance, 25 years ago the average cargo ship would have been manned with a crew of between 40 and 50 (8), but today technological advancement have contributed to a decreased manning, in some cases to just 22 seafarers on a Very Large Crude Carrier (VLCC) (9). There are two sides to the technological advances. Improvements in ship design and navigation aids have reduced the frequency and severity of shipping incidents; in turn, the reduction of failures in technology has revealed the underlying level of influence of human error in accident causation (9). The UK Marine Accident Investigation Branch (MAIB) states that “one factor still dominates the majority of maritime accidents; human error” (11).

The occurrence of a major leak event is a key cause that has the potential of resulting in a major accident (16). Also, Blow-out accidents consist of the major marine offshore accidents, like the Texaco Funiwa-5 blowout in 1980 in which, well over 400,000 barrels of crude spilled into the marine environment of Nigeria (1). A blow-out accident is a common name for uncontrolled release of hydrocarbons (gas, gas condensate and oil) from an oil and gas production well (19).

### 1.1 HUMAN ERROR:

(18) Defines human error as an omission or action from which liability arises, stretching from lack of training to lack of adequate experience and knowledge. (17) Defined human error as an improperly executed action or inaction or an incorrect decision. According to (9) 75-96% of offshore accidents are as a result of human error. In a recent research (7) averred that accidents that happened in lakes, crossings, seas and rivers occurred as a result of human error 65%, and only a scarce number of this is caused by natural factors as shown in figure 1. Drawing from the Costa Concordia accident research, (4) averred that the first error that led to the accident of the cruise liner was made by the Captain of the vessel, by changing the original voyage plan without coming to agreement with that local authorities and the company. This is another case of human error which did not only lead to loss of lives, but also led to permanent damage to the cruise liner and leakage of Marine Diesel Oil to the environment. In their research (3) as shown in Fig. 2 averred that human error, such as sleepiness of marine watch keepers resulting in grounding and collisions is a contributory factor of about 60% of shipping accidents, and a higher percentage for collision alone.

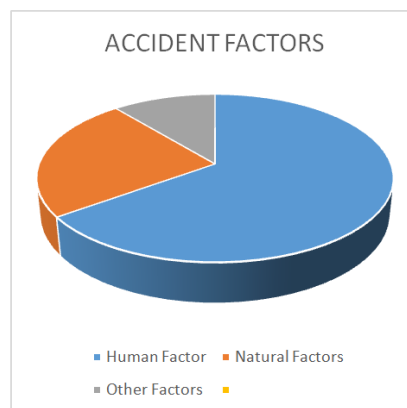


Figure1. Ship Accidents Factors (7)

### 1.2 TECHNICAL/ENVIRONMENTAL ERRORS:

Equipment on onboard vessels/ships are numerous. It should be of note that these equipment's are being operated by humans. According to (10) the sudden malfunction of any of these equipment ranging from propeller to rudder damage leading to accidents cannot be over looked. In their research (7) averred that just 11% of ship accidents are caused by other factor like equipment malfunction.

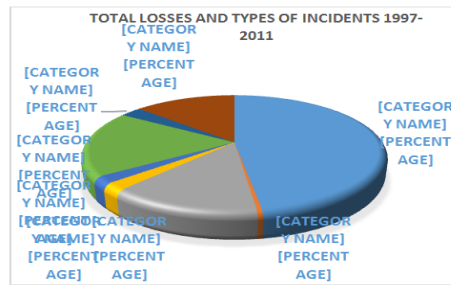


Figure 2. Ship Losses and type of incident (3)

According to (3) while foundering is a huge cause of maritime accidents, these accidents could only be associated with geographical areas, and extreme weather conditions, observed in the Black Sea and North Sea. Grounding and hitting of wrecks are other significant causes of marine offshore accidents (2).

### 1.3 PROBLEM STATEMENT:

The yearly increase in maritime accidents all over the world, with particular reference to Nigeria led to this study. The non-adherence to safety rules and regulations onboard vessels and platforms, the use of unregistered vessels and the non-adherence to international safety protocols at sea has led to several deaths. Year in year out the Nigerian waterways has been bedeviled with accidents leading to fatality (6). The (21) in its October 23<sup>rd</sup>, 2015 edition broke the news of the collision of “two vessels – MT Elixir and MT Tank”. Both vessels collided at midstream leading to fatalities. The (20) in its February 10<sup>th</sup>, 2015 edition titled “Casualties in maritime-related accidents may rise in 2015” averred that in the year 2014 there was a ten percent increase in maritime accidents reported from 2013. The Guardian further reported that in the year 2014 there was also a 23% year-on-year increase in vessel collision.

### 1.4 THE OBJECTIVE OF STUDY:

The research has shown so far that marine offshore accidents do occur year in year out, and when they do, it usually leads to loss of lives and property. Using qualitative and quantitative methods the research is aimed at fulfilling these explicit objectives.

- To determine the causes of marine offshore accidents in Nigeria
- To investigate the level of safety practices adopted onboard offshore platforms, ships and small crafts
- To evaluate the safety checks put in place by regulatory agencies in Nigeria to prevent offshore accidents
- To determine if marine offshore accidents in Nigeria are caused by human error, environmental, management or technical errors.

### 1.5 RESEARCH QUESTIONS:

In achieving the above set objectives of this research, attempt will be made to answer the following research questions;

- What are the causes of marine offshore accidents in Nigeria
- What are the safety measure put in place by regulatory agencies to prevent or reduce incidences
- To what extent can marine offshore accidents be attributed to human error, technical or management
- To what extent can marine offshore accidents be attributed to environmental factors

## II. METHODOLOGY AND DATA:

### 2.1 METHODOLOGY:

The study makes use of both primary and secondary sources of information and data to analyze the issues in contention. Data on marine accidents within the Nigerian coastal and offshore waters were obtained from questionnaires administered to marine vessel operators. The sample size chosen for this research was limited to 100 respondents consisting of rig workers, Captains and Chief mates of marine vessels that operate within Nigeria’s coastal and offshore waters. The marine vessels surveyed include mainly service boats, freight barges, fishing vessels, oil tankers and tug boats. The questionnaires also provided for their responses regarding other human, environmental and vessel characteristics which they consider as related to such incidences. The researchers also used numerous electronic article databases and research articles as secondary.

### 2.2 ADMINISTRATION OF APPARATUS:

A total of a hundred (100) questionnaires were administered to the respondents in both public and private establishments operating within Nigeria’s coastal and inland waterways stretching mainly from Lagos through

Warri to Port Harcourt Ports. These were chosen as a result of the high concentration of marine vessels, oil company activities in these areas.

**2.3 HYPOTHESIS TESTED AND DISCUSSION:**

To offer solutions for the research questions of this study, the following hypothesis was tested

- H0<sub>1</sub>: That human factor constitute the core causes of marine offshore accidents in Nigeria
- H0<sub>2</sub>: that environmental factor constitute the core causes of marine offshore accidents in Nigeria
- H0<sub>3</sub>: that technical factor constitute the core causes of marine offshore accidents in Nigeria
- H0<sub>4</sub>: That stricter enforcement of maritime safety rules and regulations will ameliorate the frequencies of accidents onboard offshore vessels and platforms

**2.4 REPRESENTATION OF DATA:**

Table 1 gives details of data collected and the nature of responses received for the ‘YES’ and ‘NO’ questions. It also shows how the questionnaires were distributed and the number of questionnaires distributed to the different groups of respondents.

The responses to the administered questionnaires as shown in table 2 (70) questionnaires were completed and returned out of the 100 questionnaires administered. Thirty (30) questionnaires or 30%, ( $\frac{30}{100} \times 100 = 30\%$ ) of the total number of respondents did not complete or return the questionnaire. These questionnaires could not be retrieved probably due to lack of willingness to complete and return them on time. The (70) completed questionnaires returned represent 70% ( $\frac{70}{100} \times 100 = 70\%$ ) as shown in table 3.

To further verify the validity of the data obtained from the field study from the table 1, 2 and 3, the use of Chi-Square analysis was then applied.

With the use of Chi-Square Analysis, the four hypotheses above were then tested;

**Table 1: Sample Size Selection**

RESPONDENTS	NUMBER SELECTED
CAPTAINS	10
ENGINEERS	20
DECKHANDS	20
QUARTERMASTER	20
OILERS	20
OTHERS	10
TOTAL	100

The use of the Chi-Square test was considered appropriate for testing the validity and reliability of each hypothesis. The formula used for a “Yes” or “NO” question was:

$$X^2 = \sum \frac{(fo - fe)^2}{fe} \dots\dots\dots (1)$$

Where: fo = Observed frequency of the value;

fe = expected frequency of the value;

X<sup>2</sup> = calculated value;

Σ = summation.

The level of confidence used was 0.05 (5%) and would be adopted for this work.

The degree of freedom was calculated as follows:

Where R = Row, C = Column total

Degree of freedom, V = (R-1) (C - 1)

R = 4, C = 2 (these values are represented in the Chi-Square distribution table, in appendix A)

= (4-1) (2-1)

= (3) (1) = 3;

⇒ Degree of Freedom, V = 3

The five null hypotheses were tested one after the other to ascertain their validity.

Expected value =  $\frac{\text{Row Total} \times \text{Column Total}}{\text{Grand Total}}$

**2.5 HYPOTHESIS 1:**

•  $H_{01}$ : That human factor constitute the core causes of marine offshore accidents in Nigeria  
From table 4, a total of sixty-six (66) respondents responded 'YES' while only four (4) says; 'NO' an indication that 94%, ( $\frac{66}{70} \times 100 = 94\%$ ) support the fact that human factor constitute the core causes of marine offshore accidents while only 6%, ( $\frac{4}{70} \times 100 = 6\%$ ) disagreed.

Response to this question was then analyzed in Table 4, 4a and 4b to obtain  $X^2$ .  
Table 5b shows the computation for the  $X^2$  from the different values of  $f_o, f_e, (f_o - f_e)^2$ , and  $\frac{(f_o - f_e)^2}{f_e}$ . The theoretical value of  $X^2$  obtained at the degree of freedom 3, and at the level of confidence of 0.05 was 7.815. Since the calculated value of  $X^2 = 0.241$  which is less than the theoretical value, it therefore, follows that the null hypothesis as stated is valid.

**2.6 HYPOTHESIS 2:**

•  $H_{02}$ : that environmental factor constitute the core causes of marine offshore accidents in Nigeria  
From the field study, as shown in table 5, a total of fifty-nine (59) respondents responded 'YES' while eleven (11) says; 'NO' an indication that 84%, ( $\frac{59}{70} \times 100 = 84\%$ ) support the fact that environmental factor constitute the core causes of marine offshore accidents while only 16%, ( $\frac{11}{70} \times 100 = 16\%$ ) disagreed.

Response to this question was then analyzed in table 5a and 5b as shown to obtain  $X^2$ . The results from the computation of  $X^2 = 2.084$ . Therefore the second null hypothesis as stated is valid since the computation of  $X^2$  is = 2.084 and is less than the theoretical value of 7.815. The null hypothesis stated earlier is valid.

**2.7 HYPOTHESIS 3**

•  $H_{03}$ : that technical factor constitute the core causes of marine offshore accidents in Nigeria  
From table 6, a total of fifty (50) respondents responded 'YES' while twenty (20) says; 'NO' an indication that 71%, ( $\frac{50}{70} \times 100 = 71\%$ ) support the fact that technical factor constitute the core causes of marine offshore accidents in Nigeria while 29%, ( $\frac{20}{70} \times 100 = 29\%$ ) disagreed.

Response to this question was then analyzed in table 6a and 6b to obtain  $X^2$ . Since the sample result fails to support the null hypothesis because the calculated value of  $X^2$  does not fall within the acceptance region as shown in table 6b, it is subsequently concluded that something else is true, which is the alternative hypothesis  $H_3$ . This statement is specifying that the population parameter is a value other than that specified in the null hypothesis  $H_{03}$ .

**2.8 HYPOTHESIS 4**

•  $H_{04}$ : That stricter enforcement of maritime safety rules and regulations will ameliorate the frequencies of accidents onboard.

From table 7, a total of sixty-seven (67) respondents responded 'YES' while only (3) says; 'NO' an indication that 96%, ( $\frac{67}{70} \times 100 = 96\%$ ) support the fact that stricter enforcement of maritime safety rules and regulations will ameliorate the frequencies of accidents onboard while 4%, ( $\frac{3}{70} \times 100 = 4\%$ ) disagreed. Response to this

question was then analyzed in table 7a and 7b to obtain  $X^2$ .  
The theoretical value of  $X^2$  at the degree of freedom 3 at a level of confidence of 0.05 is 7.815. Since the calculated value of  $X^2$  is 0.133 as shown in table 7b is below the theoretical value and within the acceptance region. It follows therefore that the null hypothesis is valid.

The validity of the four hypotheses above further confirmed the logical empirical analysis of the results obtained from the survey.

**Table 2: Responses and Refusal Rate**

RESPONDENTS	NUMBER	No. OF RESPONSE EXPECTED	ACTUAL RESPONSE	REFUSAL RATE
CAPTAINS	10	10	10	0
ENGINEERS	20	20	17	3
DECKHANDS	20	20	10	10

QUARTERMASTERS	20	20	14	6
OILERS	20	20	13	7
OTHERS	10	10	6	4
TOTAL	100	100	70	30

**Table 3: Responses to Administered Questionnaires**

RESPONDENTS	No OF QUESTIONNAIRES SENT OUT"	No OF QUESTIONNAIRES RETURNED
CAPTAINS	10	10
ENGINEERS	20	17
DECKHANDS	20	10

QUARTERMASTERS	20	14
OILERS	20	13
OTHERS	10	6

Table 4: Observed Values Compiled From the ‘Yes’ & ‘No’ Respondents

	RESPONDENTS		TOTAL
	YES	NO	
CAPTAINS	9	1	10
ENGINEERS	15	2	17
DECKHANDS	10	0	10
QUARTERMASTERS	14	0	14
OILERS	13	0	13
OTHERS	5	1	6

Table 4a: The value of  $\chi^2$  Obtained

“YES” COLUMN	“NO” COLUMN
$\frac{9 \times 66}{70} = 8.486$	$\frac{1 \times 66}{70} = 0.943$
$\frac{15 \times 66}{70} = 14.143$	$\frac{2 \times 66}{70} = 1.886$
$\frac{10 \times 66}{70} = 9.429$	$\frac{0 \times 66}{70} = 0$
$\frac{14 \times 66}{70} = 13.2$	$\frac{0 \times 66}{70} = 0$
$\frac{13 \times 66}{70} = 12.257$	$\frac{0 \times 66}{70} = 0$
$\frac{5 \times 66}{70} = 4.714$	$\frac{1 \times 66}{70} = 0.943$

Table 4b: Computation Of  $\chi^2$

$f_o$	$f_e$	$(f_o - f_e)$	$(f_o - f_e)^2$	$\frac{(f_o - f_e)^2}{f_e}$
9	8.486	0.514	0.264	0.031
15	14.143	0.857	0.734	0.052
10	9.429	0.571	0.326	0.035
14	13.2	0.800	0.640	0.048
13	12.257	0.743	0.552	0.045
5	4.714	0.286	0.082	0.017
1	0.943	0.057	0.003	0.003
2	1.886	0.114	0.012	0.007

0	0.0	0.000	0.000	0.000
0	0.0	0.000	0.000	0.000
0	0.0	0.000	0.000	0.000
1	0.943	0.057	0.003	0.003
				$\chi^2 =$ 0.241

Table 5: Observed Values Compiled From the “Yes” & “No” Respondents

	RESPONDENTS		TOTAL
	YES	NO	
CAPTAINS	10	0	10
ENGINEERS	13	4	17
DECKHANDS	8	2	10
QUARTERMASTERS	11	3	14
OILERS	12	1	13
OTHERS	5	1	6
TOTAL	59	11	70

**Table 5a: The value of  $X^2$  Obtained**

“YES” COLUMN	“NO” COLUMN
$\frac{10 \times 59}{70} = 8.429$	$\frac{0 \times 59}{70} = 0.00$
$\frac{13 \times 59}{70} = 10.957$	$\frac{4 \times 59}{70} = 3.371$
$\frac{8 \times 59}{70} = 6.743$	$\frac{2 \times 59}{70} = 1.686$
$\frac{11 \times 59}{70} = 9.271$	$\frac{3 \times 59}{70} = 2.529$
$\frac{12 \times 59}{70} = 10.114$	$\frac{1 \times 59}{70} = 0.843$
$\frac{5 \times 59}{70} = 4.214$	$\frac{1 \times 59}{70} = 0.843$

**Table 5b: Computation of  $X^2$**

$f_o$	$f_e$	$(f_o - f_e)$	$(f_o - f_e)^2$	$\frac{(f_o - f_e)^2}{f_e}$
10	8.429	1.571	2.468	0.293
13	10.957	2.034	4.174	0.381
8	6.743	1.257	1.580	0.234
11	9.271	1.729	2.989	0.322
12	10.114	1.886	3.557	0.357
5	4.214	0.860	0.739	0.176
0	0.000	0.000	0.000	0.000
4	3.371	0.629	0.396	0.117
2	1.686	0.314	0.099	0.058
3	2.529	0.471	0.222	0.088
1	0.843	0.127	0.025	0.029
1	0.843	0.127	0.025	0.029
				$X^2 =$
				2.084

**Table 6: Observed Values Compiled From the “Yes” & “No” Respondents**

RESPONDENTS	YES	NO	TOTAL
CAPTAINS	8	2	10
ENGINEERS	12	5	17
DECKHANDS	9	1	10

QUARTERMASTERS	10	4	14
OILERS	9	4	13
OTHERS	2	4	6
TOTAL	50	20	70

**Table 6a: The value of  $\chi^2$  Obtained**

"YES" COLUMN		"NO" COLUMN	
I.	$\frac{8 \times 50}{70} = 5.714$	$\frac{2 \times 50}{70} = 1.429$	
II.	$\frac{12 \times 50}{70} = 8.571$	$\frac{5 \times 50}{70} = 3.571$	
III.	$\frac{9 \times 50}{70} = 6.429$	$\frac{1 \times 50}{70} = 0.714$	
IV.	$\frac{10 \times 50}{70} = 7.143$	$\frac{4 \times 50}{70} = 2.857$	
V.	$\frac{9 \times 50}{70} = 6.429$	$\frac{4 \times 50}{70} = 2.857$	
VI.	$\frac{2 \times 50}{70} = 1.429$	$\frac{4 \times 50}{70} = 2.857$	

**Table 6b: Computation Of  $\chi^2$**

$f_o$	$f_e$	$(f_o - f_e)$	$(f_o - f_e)^2$	$\frac{(f_o - f_e)^2}{f_e}$
8	5.714	2.286	5.225	0.915
12	8.571	3.429	11.758	1.372
9	6.429	2.571	6.610	1.028
10	7.143	2.857	8.162	1.143
9	6.429	2.571	6.610	1.028
2	1.429	0.571	0.326	0.228
2	1.429	0.571	0.326	0.228
5	3.571	1.429	2.042	0.572
1	0.714	0.286	0.082	0.115
4	2.857	1.143	1.306	0.457
4	2.857	1.143	1.306	0.457
4	2.857	1.143	1.306	0.457
				$\chi^2 = 8.00$

Table 7: Observed Values Compiled From the “Yes” &amp; “No” Respondents

RESPONDENTS	YES	NO	TOTAL
CAPTAINS	9	1	10
ENGINEERS	17	0	17
DECKHANDS	9	1	10
QUARTERMASTERS	14	0	14
OILERS	13	0	13
OTHERS	5	1	6
TOTAL	67	3	70

**Table 7a: The value of  $X^2$  Obtained**

“YES” COLUMN	“NO” COLUMN
$\frac{9 \times 67}{70} = 8.614$	$\frac{1 \times 67}{70} = 0.957$
$\frac{17 \times 67}{70} = 16.271$	$\frac{0 \times 67}{70} = 0.000$
$\frac{9 \times 67}{70} = 8.614$	$\frac{1 \times 67}{70} = 0.957$
$\frac{14 \times 67}{70} = 13.40$	$\frac{0 \times 67}{70} = 0.000$
$\frac{13 \times 67}{70} = 12.443$	$\frac{0 \times 67}{70} = 0.000$
$\frac{5 \times 67}{70} = 4.786$	$\frac{1 \times 67}{70} = 0.957$

**Table 7b: Computation Of  $X^2$**

$f_o$	$f_e$	$(f_o - f_e)$	$(f_o - f_e)^2$	$\frac{(f_o - f_e)^2}{f_e}$
9	8.614	0.386	0.149	0.017
17	16.271	0.729	0.531	0.033
9	8.614	0.386	0.149	0.017
14	13.40	0.600	0.360	0.027
13	12.443	0.557	0.310	0.024
5	4.786	0.214	0.046	0.009
1	0.957	0.043	0.002	0.002
0	0.000	0.000	0.000	0.000
1	0.957	0.043	0.002	0.002
0	0.000	0.000	0.000	0.000
0	0.000	0.000	0.000	0.000
1	0.957	0.043	0.002	0.002
				$X^2 = 0.133$

**III. RECOMMENDATION**

In view of the findings and conclusions drawn from this research the following recommendations will aid in the prevention of marine offshore accidents in Nigeria and ensure sustained safety during navigation.

- Government should fully establish a body such as the Coast Guard charged with the responsibility of enforcing already existing laws and regulations that has to do with the protection of the Nigeria coastal environment. Such as criminal code of Nigeria.
- Organizations should ensure that staff onboard offshore platform, vessels and crafts adhere to companies’ policies and international protocols on safety at sea.
- The Federal Ministry of Transport of Nigeria should institute a competent Port Safety Control department (PSCD) which will handle issue of safety on board ships in all ports.
- The Nigerian Maritime and Safety Agency (NIMASA) in conjunction with the Ship Owners Association of Nigeria should ensure that seafarers are trained and retrained in International best practices and safety protocols at sea.
- The Nigerian Government should remove wrecks including vessels, sunk, stranded or abandoned, jetsam, all derelicts (including logs) floating or submerged in the tidal waters constituting a great danger to navigation.
- The Nigerian Government should endeavor to dredge the estuaries to ease the smooth passage of marine vessels in order to avoid grounding.

**IV. REFERENCES:**

[1]. Aghalino, S. O., &Eyinla, B. (2009). Oil exploitation and marine pollution: Evidence from the Niger Delta, Nigeria. Journal of Human Ecology, 28(3), 177-182.

[2]. Akten, N. (2006). Shipping accidents: a serious threat for marineenvironment. Journal of Black Sea/Mediterranean Environment, 12(3).

[3]. Butt, N., Johnson, D., Pike, K., Pryce-Roberts, N., &Vigar, N. (2012). 15 Years of Shipping Accidents: A review for WWF.

[4]. Di Lieto, C. A. (2012). Costa Concordia Anatomy of an organizational accident.

[5]. Dogarawa, L. B. (2012) ‘Marine accidents in Northern Nigeria: Causes, prevention and management’. International Journal of Academic Research in Business and Social Sciences, 2(11), 378-389.

- [6]. Donatus E. O. (2013) 'An Analysis of Determinants of Accident Involving Marine Vessels in Nigeria's Waterways'. Management Science and Engineering Journal
- [7]. Faturachman, D., Shariman, M., Octaviani, F., & Novita, T. D. (2013). Failure Mode and Effects Analysis of Diesel Engine for Ship Navigation System Improvement.
- [8]. Grech, M. R., Horberry, T., & Smith, A. (2002, September). Human error in maritime operations: Analyses of accident reports using the Leximancer tool. In Proceedings of the human factors and ergonomics society annual meeting, Vol. 46, No. 19, pp. 1718-1721). SAGE Publications.
- [9]. Hetherington, C., Flin, R., & Mearns, K. (2006). Safety in shipping: The human element. *Journal of safety research*, 37(4), 401-411.
- [10]. Julius O. Anyanwu (2014) 'The Causes and Minimization of Maritime Disasters on Passenger Vessels'. Global Journal of Researches in Engineering: G Industrial Engineering. Federal University of Technology, Nigeria
- [11]. MAIB. (2000) Annual Report, London Department of the Environment Transport and Regions
- [12]. McNamara, R., Collins, A., and Matthews, V., (2000) A Review of Research into Fatigue in Offshore Shipping, Maritime Review. pp. 118-122
- [13]. Norman, L. G. (1962). Road traffic accidents: epidemiology, control, and prevention
- [14]. Okechukwu J.A. (2014) 'Maritime Tanker Accident on Coastal Areas in Nigeria'. Global Journal of Researches in Engineering, G Industrial Engineering.
- [15]. Perrow, C (1999), *Marine Accidents, Normal Accidents: Living with high risk technologies* (pp. 170-231). Princeton, New Jersey: Princeton University Press
- [16]. Pitblado R., Bjerager P., Andreassen E., ørstad E. (2010) "Key aspects of an effective US offshore safety regime". DNV Position Paper
- [17]. Rothblum, A., Wheal, D., Withington, S., Shappell, S. A., Wiegmann, D. A., Boehm, W., & Chaderjian, M. (2002). Improving incident investigation through inclusion of human factors.
- [18]. Sharma, S. B., Yadav, R., & Dorothy (2013), B. C. A STUDY ON HUMAN ERRORS AND CLASSIFICATION OF COMMONLY PREVALENT ERRORS IN SHIPPING OPERATIONAL PRACTICES
- [19]. Thomas G Sætren, (2015) 'Offshore Blow-out Accidents: An Analysis of Causes of Vulnerability Exposing Technological Systems to Accidents'. University of Oslo Universite Louis Pasteur. Assessing and communicating risks
- [20]. The Guardian (2015) Casualties in maritime-related accidents may rise in 2015, [Online] [Available from] <<http://www.ngguardiannews.com/2015/02/casualties-in-maritime-related-accidents-may-rise-in-2015/>> [November 30<sup>th</sup>, 2015]
- [21]. The New (2015) 2 vessels collide on high seas; NIMASA rescues 3 crew members, [Online] [Available from] <<http://thenewsnigeria.com.ng/2015/10/2-vessels-collide-on-the-high-seas-nimasa-rescues-3-crew-members/>> [Oct. 23<sup>rd</sup>, 2015]

## Mapping and Assessment of Soil Loss in Berrechid Plain Using a Gis And the Universal Soil Loss Equation (Usle)

M. Aboulouafa<sup>\*1</sup>, H. Taouil<sup>\*1</sup>, S.Ibn Ahmed<sup>\*1</sup>

*\*1: Laboratoire des Matériaux, d'Electrochimie et d'Environnement.*

*Faculté des Sciences Université IBN Tofail kénitra Morocco*

**ABSTRACT:** Soil and water are basic resources. Their exploitation or development is a matter of survival for many, an escape from poverty for most, and an opportunity to pursue additional power, wealth and selfish interest for some [1]. Soil erosion is a growing problem in particular in the areas of agricultural activity where soil erosion not only leads to decrease agricultural productivity but also reduces the availability of the water. The Universal Soil Loss Equation (USLE) is the most popular empirical model used globally for the prediction and control of erosion. Remote sensing and GIS are powerful tools that can be used in the collection and the combination of data [2]. They are considered our days as essential tools in the interactive systems to aid in the decision [3]. Berrechid plain belongs to the bioclimatic Floor semi-arid with an average annual precipitation of 380 mm, and knows a development of agricultural activities with more and more exaggerated use of chemical fertilizers. An attempt has been made to assess the annual soil loss in Berrechid the plain using the Universal Soil Loss Equation (USLE) in the framework of the SIG. Such information can help considerably to identify the priority areas for the implementation of measures to control erosion. The rate of soil erosion has been determined depending on the topography, on the soil, the texture of the soil, land use and land cover, rainfall erosivity, and the management of the cultures and the practice in the watershed using the Universal Soil Loss Equation, imaging of remote sensing and GIS techniques. The rainfed erosivity, R-factor of the USLE, varies between 40.85 and 57,549 with an average of 49,362 MJ mm/ha/h/year and erodibility of the soil K-factor is 0.02 - 0.26. The slopes in the basin are low and the LS factor has values ranging from 0 - 2.79. The factor of C has been calculated on the basis of NDVI (Normalized Difference Vegetation Index) values derived from Landsat Image-ETM. The value of P was calculated from the cropping patterns in the watershed. The loss of soil estimated annual in the watershed with the help of (USLE) is low to medium (ranging from 0 to 9.42 t/ha/year)

**Keywords:** Universal Soil Loss Equation (USLE); Remote Sensing & GIS; Soil Loss; Berrechid Plain.

### I. INTRODUCTION

Although the climate of Berrechid plain is located in the bioclimatic Floor semi arid with an annual precipitation average of 380 mm, these last are very variable and have a stormy character and know fluctuations over the years.

One of the objectives of this work is to provide a method of mapping of areas at erosion risk, and illustrate the possibility to determine the change of the soil occupation, as well as the spatialization of USLE model, to limit the process of soil degradation in Berrechid plain. The assessment of the soil erosion risk in the study area has a need the mapping and analysis of the many factors involved in the process erosive: The Rainfalls aggressiveness, the slope and the slope length, the soil erodibility, vegetation cover and cropping practices. Each factor has a different behavior from one area to the other of the study area. It has led to a multitude of data to map, store, structure and process in a rational way.

Remote sensing and GIS are powerful tools that can be used in the collection and the combination of data [2]. They are our days as essential tools in the interactive systems to aid in the decision [3].

### II. PRESENTATION OF THE STUDY AREA

The Berrechid plain, for a total surface area adjacent to 1500 km<sup>2</sup>, is located to the south of Casablanca. It has the form of a broad cup, limited to the south and the South-East by the plateau of Settat, to the East and North is

by the Oued Mellah, to the West and North West by the Primary outcrops and on the North by the coastal Chaouia[4]. The morphology of Berrechid plain is regular. Level curves are directed NE-SW on the major part of the plain. Altitudes vary from 350 m in extreme cases related to Settât's plateau and 140m north of the plain related to the transition zone towards Chaouia [5]. From a geological point of view, this plain is composed of sedimentary rocks formed Cretaceous of marly limestone (Cenomanian) with intercalations of clays and marls and sedimentary rocks formed of calcareous sandstone to cemented conglomerates toward the base .The whole is surmounted by a coverage of clayey silts of the recent quaternary. This part of the low Chaouia, receives of the upstream elements of varied erosion from the high Chaouia (Plateau of Settât - Ben Ahmed) from which it is separated by the flexure of Settât [6]. The annual precipitations average in Berrechid plain varies between 280 and 310mm/year. The temperature presents wide variations between the winter and the summer, with 24.9°C as an average of the maxima and 9.6°C as an average of the minima (ABHBC). The Berrechid plain hydrographic network is little developed, although many small wadis drain the watershed of Settât - Ben Ahmed and converging toward the center of the plain. The most important wadis that threaten the city of Berrechid are essentially Mazer, Tamdrost and Lhaimour [7].

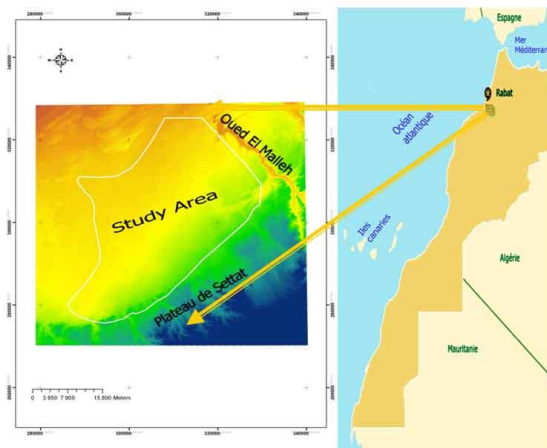


Fig. 1: The study area location [8]

### III. MATERIALS AND METHODS

#### MATERIALS

For this study of the soil erosion in Berrechid plain we used:

- Satellite Images ETM (Sensor Enhanced Thematic Mapper ETM) of the 06/01/2016.
- A MNT (DEM) integrated in the GIS to achieve the maps of the slope length and the angle of the slope.
- The geological map and the soil map of Berrechid groundwater of [5].
- Rainfall data and climate data (ABHCH 2016).

#### METHODS

The methodology is to study first the parameters of the relevant factors influencing the phenomenon (the rain erosivity, the topographic index, NDVI, and the soil erodibility). Then after an Individual codification of the parameters (weight) of the different factors they were crusaders in the GIS according to the universal equation of soil loss [9]. It is a multiplicative function of five factors which control the water erosion: Climate aggressiveness, soil erodibility, tilt and slope length, soil occupation and erosion control practices (**equation 1**):

$$A = R * K * LS * C * P \quad (1)$$

Where A is the annual rate of soil loss in t/ha/year,

- **R** is the factor of the rain erosivity; it corresponds to the annual average of the sums of the products of the kinetic energy of the rain by its intensity in 30 consecutive Min; it is expressed in MJ.mm / ha.H.year,
- **K** is the soil erodibility; it depends on the granularity, of the quantity of organic matter, the permeability and the structure of the Ground; it is expressed in t.ha.h/ha.MJ.MM,
- **LS** is a dimensionless factor depends both on the slope length and the angle of the slope. It varies from 0.1 to 5 in the most common situations of culture and can reach 20 in mountain.
- **C** is a factor without dimension that represents the effect of the plant cover,
- **P**, factor without dimension, is a report which takes account of cultural techniques “control erosion” structures such as plowing in the level curves.

The GIS allows assessing the rate of erosion on all points of the plain and the development of the synthetic map of soil loss according to the methodological flowchart (**Fig. 2**).

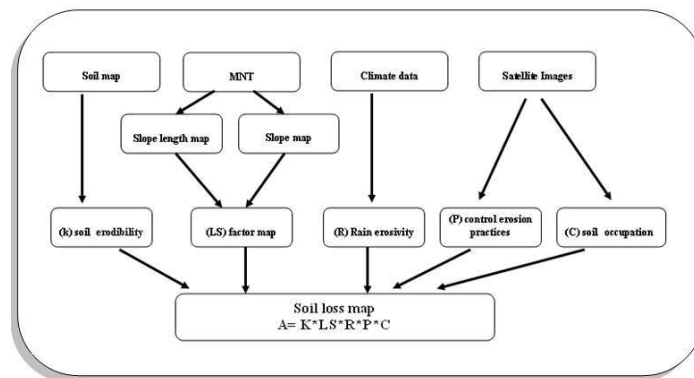


Fig. 2: The methodological flowchart

#### IV. RESULTS AND DISCUSSION

##### RESULTS

The application of the methodology described above has allowed estimating and mapping the potential erosion as well as the present erosion by the combination of the factors influencing on the water erosion.

##### K. SOIL ERODIBILITY FACTOR

The K factor expresses the vulnerability of the soil to be eroded by the rain. This factor depends on the physical and chemical properties of the soil particle size (particle size, aggregation, structural stability, porosity, organic matter content, etc.). The resistance to water erosion is lower for soils relatively thick than for the deep soils [10]. As well, when superficial soils are saturated with water by the rains, a particle displacement occurs toward the bottom of the slope, even if the latter is very low. For the determination of this parameter, we retained the equation of Wischmeier and Smith. The K factor is determined according to the formula of Wischmeier and Smith, which is based on the texture of the soil (M= (% sand and % silt)\*(100-% clay)), the organic matter content (a), of the structure of the ground (B) which is between 1 and 4 and the permeability (C) between 1 and 6, according to the following equation:

$$1000 k = 2.1 * 10^{-4} * (12-a) M^{1.4} + 3.25 (b-2) + 2.5 (c-3) \quad (2)$$

Starting from the soil map of Berrechid plain and based on our knowledge of the field, we classified, and then codified, the different units of soil, which has led to a map of erodibility (Fig.3).

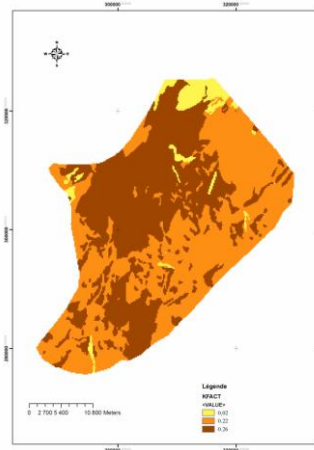


Fig. 3: K. soil erodibility map

##### THE TOPOGRAPHIC FACTOR, LS

This factor represents the combined effect of the length and the angle of the slope. It plays an important role with the stiffness and the length of the slope (from the place where the elements of the soil are detached up to the place where they are deposited [11]).

The topographic factor (LS) was calculated from the tilt of the slopes and their length by the formula of Wischmeier & Smith (**equation 3**):

$$LS = (L / 22.13)^m * (0.065 + 0.045.S + 0.065.S^2) \quad (3)$$

Where **L** is the length of slope in m,

**S** is the inclination of the slope in %,

**M** is a parameter such as  $m = 0.5$  If the slope is  $> 5\%$ ,  $m = 0.4$  If the slope is 3.5 to 4.5%,  $m = 0.3$  If the slope is 1 to 3 per cent and  $m = 0.2$  If the slope is  $< 1\%$ . **m** is a parameter such as  $m = 0.5$  If the slope is  $> 5\%$ ,  $m = 0.4$  if the slope is 3.5 to 4.5%,  $m = 0.3$  If the slope is 1 to 3 per cent and  $m = 0.2$  If the slope is  $< 1\%$ .

From the digital terrain model (MNT), and using GIS we obtained the slope map and the map of the slope length, and using the formula of Equation 3 the GIS compute the LS factor map (**Fig. 4**).

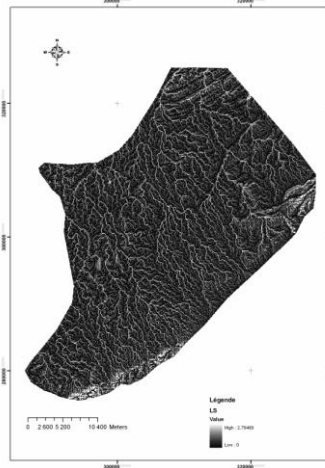


**Fig. 4:** the topographic factor map, LS

#### CLIMATE FACTOR (R)

The rain is the engine component of the erosion. Without precipitation there is no water erosion. However the rain intensity is the main factor in the erosion. The more the intensity is high, more the effect of threshing of the soil is pronounced.

The estimation of the R factor according to the formula of Wischmeier & Smith requires knowledge of the kinetic energies (EC) and the average intensity on 30 minutes ( $I_{30}$ ) of rain drops of each shower. It is given by the empirical formula of Wischmeier & Smith (1978) (**equation 4**):

$$R = k * EC * I_{30} \quad (4)$$

**K** is a coefficient that depends on the system of units of measurement.

The only available data concerning precipitation in the stations that are located in the basin or in its vicinity are monthly averages and annual. Some authors [12—14] have developed alternative formulas that do only imply the annual precipitation to determine the R factor.

HEUSCH [15] has developed for stations of Morocco an empirical formula which allows calculating the factor of the rain erosivity; (**equation 5**):

$$R = 143 \log (p * p_{24}^2 * 10^{-6}) + 89.7 \quad (5)$$

**P** = precipitation Annual Average (mm);

**P24** = Maximum precipitation in 24 hours, return period 20 years (mm).

These data are transformed into matrix map by ordinary kriging in the GIS (**Fig.5**).

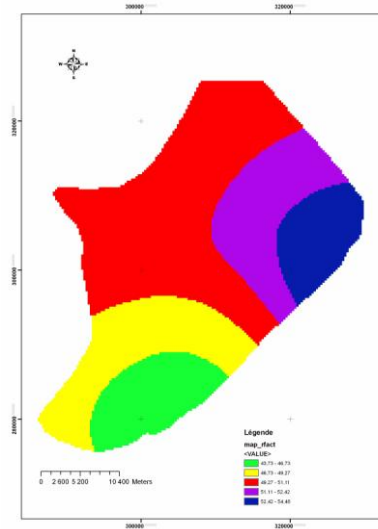


Fig. 5: the Climate factor map, R

**THE GROUND OCCUPANCY FACTOR (C)**

The plant cover is the essential element of the soil protection against erosion. It provides information on the degree of Soil protection. In effect the plant cover allows the reduction of the splash effect on the soil. A soil well covered by vegetation slows the water flow while a bare soil is more exposed to erosion. The values of C vary from 1 for the bare soil to 0.001 for the dense forests and mulched cultures crops abundantly [16].Table 1 gives the values of C of a few crops [17].

Table1: Cultural Index C of a few crops [17].

Type of vegetation	C
Bare land, Bare fallowing	1
Fruit Cultivation	0,9
Winter Wheat	0,7
Grain rotation	0,4
Fodder	0,2
Grain rotation + Fodder	0,1 à 0,01
Improved Pasture	0,01

The C coefficient used in our case it is that calculated by remote sensing: the NDVI (Fig. 6).

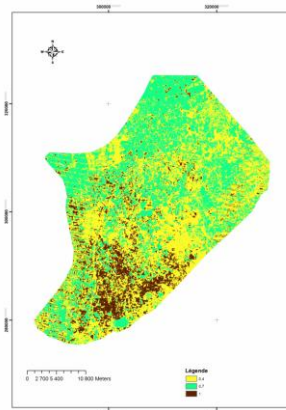


Fig. 6: The ground occupancy factor map “C”.

**THE CONTROL EROSION FACTOR (P)**

The cultures in the level curves, in alternating bands or in terraces, the reforestation in benches, mounding and ridging are the most effective practices for the conservation of soils. The values of P are less than or equal to 1.

The value 1 is assigned to the land on which any of the practices mentioned is used [11] [18]. The values of P vary according to the practice adopted and also according to the slope. In all the plain, there are no control erosion facilities, and farmers do not use farming practices anti-erosion structures. Cultures are especially grain and the plowing is rarely parallel to the level curves. There are a few tests of rehabilitation of forests by reforestation but not in benches. In this context, the P value = 1 has been assigned to the whole area of the plain.

### THE SOIL LOSS MAP

By applying the USLE equation (equation 1), the GIS compute the risk map of soil loss of in Berrechid plain, the soil loss estimated annual in the watershed with using the USLE is low to medium (ranging from 0 to 9.42 t/ha/year) (Fig.7)

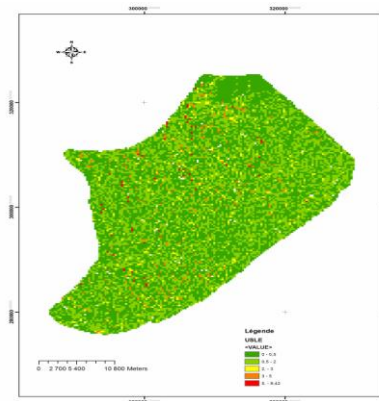


Fig. 7: The Soil loss map of Berrechid plain (USLE).

## V. DISCUSSION

The implementation of the USLE model brings interesting information on the ongoing process in Berrechid plain. The estimate of soil loss given would therefore be representative of the situation on the study area. Soil losses averages vary in function of the occupation of the land. The greater rate of soil loss is located in the regions of bare soil; however the existence of such a loss of soil is not only due to the lack of vegetative cover; in effect, the erosive potential, which is the abstraction of the nature of the soil occupation, has always assigned the greatest value for the bare soil. The type of cover in place is necessary to curb the water erosion; The loss of soil estimated annual in the watershed with the help of (USLE) is low to medium (ranging from 0 to 9.42 t/ha/year), a large percentage of the sector of study presents a low loss of soil this does especially not say that these sectors are well developed because this rate of loss of soil come either from the fact that the slope is low or the fact that the nature of the soil and the aggressiveness of the rains intervenes against erosion.

## VI. CONCLUSION

The results of the application of the universal equation of losses in soil using the geographic information system in the plain of Berrechid showed that the Watershed loses up to 9.42 t/ha/year. These values correspond to a low to average soil erosion. The decisive factors for the erosion in the plain of Berrechid are the rain aggressiveness and to a lesser degree the soil erodibility and vegetation cover. This work results show the interest of the use of the technology of remote sensing and GIS in the assessment of the vulnerability to erosion in Berrechid plain. The method used has helped to identify areas at risk of erosion in the water in Berrechid plain and the erosion risk map developed could constitute a basic document for any proposed development. The method of soil loss (USLE) under GIS provides an important aid to decision makers and planners to simulate scenarios of the evolution of the region and plan interventions to combat erosion. It also allows following the impact of these developments controlling the erosion in the region.

## REFERENCES

- [1]. Wilfredop. david (1988), soil and water conservation planning: policy issues and recommendations
- [2]. DAURIAC F., DESHAYES M., GILLON D., ROGER J.-M., (2001). Suivi de la teneur en eau de la végétation méditerranéenne par télédétection. Application au risque de feu de forêt. Colloque SIRNAT 2001 (Systèmes d'Information pour les Risques Naturels), Sophia Antipolis, 6-7 décembre 2001, 10 p.
- [3]. B.ROY & D.BOUYOUSSOU (1993). 'Méthodes multicritères d'aide à la décision ' Economica PARIS 1993.
- [4]. A. Aït Sliman,(2009). Utilisation des systèmes d'information géographique et du modèle drastique pour l'évaluation de la vulnérabilité des eaux souterraines dans la plaine de Berrechid, Maroc Géographia Technica, no.2, 2009. PP:83.
- [5]. N.ElAssaoui (2015), Modeling of Climate Changes Impact on Groundwater Resources of Berrechid Aquifer
- [6]. R. Hazan and L. Mouillard (1964), Notice hydrogéologique de la plaine de Berrechid .

- [7]. A. El Idrissi (2006). planification urbaine et protection contre les risques urbains cas du plan d'aménagement de Berrechid
- [8]. M.Aboulouafa (2016), Assessment of groundwater vulnerability and sensitivity to pollution in Berrechid plain, using drastic model.
- [9]. Wischmeier W.H. & Smith D.D. (1978). Prediction rainfall erosion losses, a guide to conservation planning Science. U.S. Dept. Agriculture. Agric. Handbook 537, 60 p.
- [10]. RYAN J., (1982). A perspective on soil erosion and conservation in Lebanon. Publication 69, American University of Beirut, 15-38.
- [11]. T.Mostephaoui, (2013). Cartographie des risques d'érosion hydrique par l'application de l'équation universelle de pertes en sol à l'aide d'un Système d'Information Géographique dans le bassin versant d'El Hamel (Boussaâda).
- [12]. Kalman R. (1967). Le facteur climatique de l'érosion dans le bassin de Sebou. *Projet Sebou, Rapp. inédit*, 40 p.
- [13]. Arnoldus H.M.J. (1980). Methodologie used to determine the maximum potential average soil loss due to sheet and rill erosion in Morocco, Bulletin F.A.O., 34.
- [14]. Rango A. & Arnoldus H.M.J. (1987). Aménagement des bassins versants. *Cahiers techniques de la FAO*.
- [15]. Heusch B., Kalman R., Duhamel P.L. & Robert P. (1970). Erosion, transport solide, sédimentation. Ann. Rech. Forest. Maroc. n° sp. Etude sur l'érosion, 10, 390 p.
- [16]. Roose E. (1994). Introduction à la GCES. Bull Sols FAO, 70 : 420p.
- [17]. MASSON J. M. , (1971) : L'érosion des sols par l'eau en climat méditerranéen. Méthode expérimentale pour l'étude des quantités érodées à l'échelle du champ. Thèse – Université des Sciences et Techniques de Languedoc – 213 p.
- [18]. A.SADIKI, (2004). Utilisation d'un SIG pour l'évaluation et la cartographie des risques d'érosion par l'Equation universelle des pertes en sol dans le Rif oriental (Maroc) : cas du bassin versant de l'oued Boussouab.

## A brief review of biomedical sensors and robotics sensors

Yanli Luo<sup>1</sup>, Qiaoying Zhou<sup>2</sup>, Wenbin Luo<sup>3</sup>,

<sup>1</sup>(People's Hospital of Zhangshu City, Zhangshu, Jiangxi 331200, P.R. China)

<sup>2</sup>(Northwest Vista College, San Antonio, TX 78251, USA)

<sup>3</sup>(Engineering Department, St. Mary's University of San Antonio, USA)

**ABSTRACT:** In this paper, we present a brief review of biomedical sensors and robotics sensors. More specifically, we will review the cochlear sensors and retinal sensors in the category of biomedical sensors and ultrasonic Sensors and infrared motion detection sensors in the category of robotic sensors. Our goal is to familiarize readers with the common sensors used in the fields of both biomedical engineering and robotics. In addition, we will provide a list of some suppliers of those common sensors.

**Keyword:** Biomedical sensors, cochlear sensors, retinal sensors, robotics sensors, ultrasonic sensors

### I. BIOMEDICAL SENSORS

With the advance of computer and information technology, computers and computerized systems play an increasing role in our daily life. As a result, medical doctors and professionals routinely use biomedical sensors, computers, and associated software to perform medical diagnosis, examine wounded areas, and monitor critical vital signals. For example, eye doctors use advanced software systems for detection and staging of papilledema and other eye diseases automatically [Echegaray et al 2011]. To make accurate diagnosis of various diseases, medical doctors need to have high quality biomedical signals taken from different human organs. Therefore, biomedical sensors, as the interface between human organism and computer systems, are very important in the modern medical diagnosis systems that are used to acquire medical information. For example, electrocardiogram (ECG) measurement, ultrasonic, and CT scan images are all taken by sophisticated computerized systems with advanced biomedical sensors.

Biomedical sensors serve as a gateway between a biological system and an electronic system. As such, it takes biological signals such as body temperature, blood pressure, heart beat rates, the presence of certain chemical compounds, or chemical activities in the human body as inputs and converts them into electronic signals in digital forms for processing by microcontrollers or powerful computers. Depending on what a biomedical sensor measures, it can be classified into two major categories: physical sensors or chemical sensors. A physical sensor measures physical quantities in the human body such as blood pressure and heart beat rates. A chemical sensor examines chemical components or activities in the body such as chemical concentrations and enzyme-substrate. Some sensors, for example, the ones used to measure the blood pressure in a clinic setting, are noninvasive while others that need to be surgically implanted in the body are invasive in nature.

There are many biomedical sensors available such as those designed for eye, ear, brain, heart, and lung implants. Here two popular ones, cochlear sensors and retinal sensors, will be presented because of their widespread usage. It should be pointed out that many new biomedical sensors are in the development and testing phase and may be available soon in the market. For example, it was reported that ultrasensitive artificial skin [Patel 2010] and electronic skin [McCormick 2012] were under successful development and testing. Some of those synthetic skins can feel the lightest touch (up to less than 1k pascal) and can be used for prosthetics and robots.

### II. COCHLEAR SENSORS

A cochlear sensor is the main component used in a cochlear implant that is arguably the most widely used and successful neural prosthesis. Cochlear implants have given hundreds of thousands of people worldwide partial hearing so that they can live a normal life. It is extremely important for little children to have cochlear implants in the early age so that they can hear and develop normal language skills.

A cochlear implant typically consists of two units: one external unit and one internal unit as shown in Figure 1 [Zeng et al 2008].

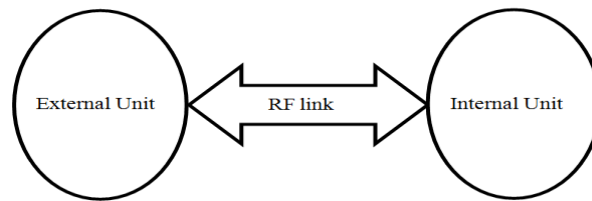


**Figure1.** Illustration of a cochlear implant

The external unit is usually placed behind-the-ear with an ear hook while the internal unit sits under the skin behind the ear. The main function of the external unit is to pick up outside sound, process it, convert it into a digital signal, and send it to the internal unit via a radio frequency (RF) link. The internal unit then converts the received signal into electric currents that will be used by the electrodes to simulate the auditory nerve. The electrical impulses generated by the auditory nerve are passed to the central nervous system for interpretation as sound. It should be mentioned that the parameters of a cochlear implant can be adjusted by computer software for each individual when the external unit is connected to a computer.

### III. RETINAL SENSORS

Similar to the cochlear implant, a retinal implant comprises an external unit and an internal unit as well. The external unit includes a microcontroller with a graphic user interface to adjust the parameters of the current pulses generated by the internal unit such as strength, duration, and frequency [Kelly et al 2011]. The internal unit has a custom Application Specific Integrated Circuit (ASIC) that converts an image into current pulses with aforementioned programmable parameters (strength, duration, and frequency). The external unit and internal unit communicate with each other via near-field inductive coupling as shown in Figure 2.

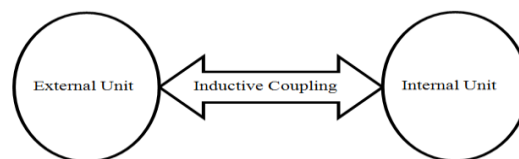


**Figure2.** Illustration of a retinal implant

In another study, researchers showed that both actively biased photoconductive and passive photovoltaic circuits could play an important role in developing high-resolution optoelectronic retinal prostheses [Loudin et al 2011]. For biomedical sensors, low power and security are two important design considerations. Ideally, a biomedical implant should be able to function continuously through a patient's life time without the need of being replaced or changing its battery. As for the security, a biomedical device should be able to withstand malicious manipulation or attacks from outside attackers. This is especially critical when a biomedical device contains programmable units that can be controlled wirelessly. For example, it was demonstrated that a hacker can remotely take control of insulin pumps and kill patients [Ngak 2011].

### IV. ROBOTICS SENSORS

Robots have been widely used in many fields nowadays. For example, The National Aeronautics and Space Administration (NASA) uses robotic cars to search for the evidence of life in the Red Planet Mars. A recent example is the Mars rover Curiosity's landing on the Red Planet using technologies such as radar and dead reckoning [Everett 1995]. The Defense Advanced Research Projects Agency (DARPA) grand challenge promotes the design and implementation of driverless vehicles that can be used to rescue soldiers and deliver supplies in dangerous regions. Google also joined the force to create a new generation of autonomous cars. Sony designed QRIO (QRIO stands for quest for curiosity) robots as personal assistants that can talk, dance, and even conduct an orchestra. In addition, many different kinds of robots were being created to suit special needs in various fields such as environmental monitoring, health, safety, and electronics. It was also known that robots were being used to infiltrate hard-to-reach areas such as nuclear plants after a disaster.

Regardless of what a robot is used for, it must have a very critical component: Sensors. Without sensors, a robot cannot see, feel, and move around accurately to complete its mission. A robot relies on its sensors to interact with outside world and monitor its own inner status and parameters. With its sensors, a robot can sense its environment and adapt its actions on that basis. Sensors provide a robot the possibility of having artificial intelligence. Without sensors, a robot can at most perform some fixed movements, conducting the same repetitive routines again and again.

Hundreds of types of sensors were created over years for robots to perform different tasks. Some of the popular ones include: odometry sensors, tactile sensors, proximity sensors, ultrasonic sensors, motion detection sensors, light sensors, sound sensors, touch sensors, temperature and humidity sensors, force sensors, accelerometers, inclination and tilt sensors, digital compass sensors, vision sensors, WiFi sensors, RFID sensors, current and voltage sensors, inertial motion sensors, stretch and bend sensors, gas sensors, radiation detection sensors, radar sensors, and GPS sensors. In this chapter, two common ones: ultrasonic sensors and infrared motion detection sensors, will be discussed. It should be mentioned that new sensors are in active development. For example, it was reported that ultrasensitive artificial skin [Patel 2010] and electronic skin [McCormick 2012] can feel the lightest touch (up to 3 pascals) and can be used for robots as pressure sensors.

**V. ULTRASONIC SENSORS**

An ultrasonic sensor measures the round-trip time required for a pulse of sound waves in the ultrasonic range (above the normal range of human hearing) to reach to a reflecting object and echo back to the sensor. Assume that  $v$  is the propagation speed of the sound wave and  $t$  is the elapsed time between sending the sound wave and receiving its echo. The distance  $d$  between the ultrasonic sensor and the reflecting object could be calculated as follows.

$$d = v * t / 2 \dots\dots\dots (1)$$

Ultrasonic sensors are also known as transceivers when they both send and receive the sound waves, as shown below.

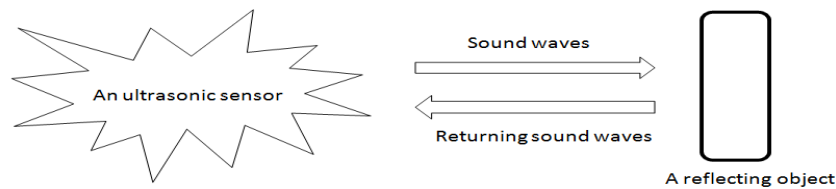


**Figure3.** Illustration of an ultrasonic sensor acting as a transceiver

In some applications such as ranging application, an ultrasonic sensor can also use both a transmitter and a receiver to measure the distance of a remote object from the sensor, as illustrated below.

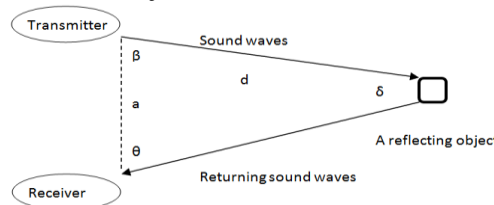


**Figure4.** Illustration of an ultrasonic sensor consisting of a transmitter and receiver

The desired distance  $d$  can be calculated by applying the basic Law of Sines to the triangle whose vertices include the transmitter, the receiver, and the reflecting object, as follows.

$$d = a \frac{\sin \theta}{\sin \delta} = a \frac{\sin \theta}{\sin(\theta + \beta)} \dots\dots\dots (2)$$

It should be mentioned that ultrasonic waves can also be used to detect flaws in a metal structure such as in a pipe [Bond 2012]. Any flaw in the metal structure will reflect part of the guided wave back toward the sensor that pulses ultrasonic waves through the material to be examined.

**VI. INFRARED MOTION DETECTION SENSORS**

An infrared motion detection sensor can be used to sense the movement of various objects such as people, animals, and other moving objects. It usually utilizes a passive infrared (PIR) sensor to measure infrared energy radiated from moving objects in its field of view. When a moving object, such as a person, passes through a given location, the temperature at that point will fluctuate, rising from the room temperature to the body temperature first and then dropping down to the room temperature again. This rapid change in temperature will signal the existence of a moving object.

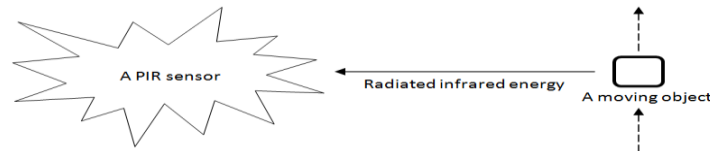


**Figure5.** Illustration of a passive infrared (PIR) sensor

A PIR sensor detects an object's temperature based on the fact that all objects with an absolute temperature above  $0^{\circ}\text{K}$  emit radiant energy in accordance with the following Stephan-Boltzman equation [Buschling 1994]:

$$W = e S T^4 \quad \dots\dots\dots (3)$$

where:

$W$  = emitted energy from an object

$e$  = emissivity

$S$  = Stephan-Boltzman constant ( $5.670373 * 10^{-8} \text{ watts } m^{-2} K^{-4}$ )

$T$  = absolute temperature of the object in degrees  $K$

Emissivity is a measure of an object's ability to either emit or absorb radiant energy [Buschling 1994]. As shown in the above equation, the emissivity  $e$  and the absolute temperature  $T$  of an object determine the amount of its emitted radiation energy. It should be mentioned that researchers also implemented a PIR-based remote thermometer using a PIR based circuit to measure the temperature of a remote object [Tsai and Young 2003].

## VII. CONCLUSION

In this paper, we presented a brief review of biomedical sensors, including cochlear sensors and retinal sensors, and robotics sensors, including ultrasonic sensors and infrared motion detection sensors. It is our hope that through this paper, readers become familiar with common sensors used in the fields of both biomedical engineering and robotics. In the appendix, we provided a list of some suppliers of the aforementioned sensors, from which the interested readers should be able to obtain those common sensors in order to conduct their research.

## REFERENCES

- [1]. S. Echegaray, G. Zamora, H. Yu, W. Luo, P. Soliz, and R. Kardon, Automated Analysis of Optic Nerve Images for Detection and Staging of Papilledema. *Investigative Ophthalmology and Visual Science*, 52(10),2011, 7470-7478.
- [2]. S.K. Kelly, D.B. Shire, J. Chen, P. Doyle, M.D. Gingerich, S.F. Cogan, W.A. Drohan, S. Behan, L. Theogarajan, J.L. Wyatt, and J.F. Rizzo, A hermetic wireless subretinal neurostimulator for vision prostheses. *IEEE Transactions on Biomedical Engineering*, 58(11),2011, 3197-3205.
- [3]. J.D. Loudin, S.F. Cogan, K. Mathieson, A. Sher, and D.V. Palanker, Photodiode Circuits for Retinal Prostheses. *IEEE Transactions on Biomedical Circuits and Systems*, 5(5),2011, 468-480.
- [4]. D. McCormick, Cheap, Pressure-Sensing 'Electronic Skin', *IEEE Spectrum*, 2012, <http://spectrum.ieee.org/tech-talk/at-work/test-and-measurement/cheap-pressuresensing-electronic-skin>
- [5]. C. Ngak, Black hat hacker can remotely attack insulin pumps and kill people, *CBSNEWS*, 2011, [http://www.cbsnews.com/8301-501465\\_162-20088598-501465.html](http://www.cbsnews.com/8301-501465_162-20088598-501465.html)
- [6]. P. Patel, Synthetic Skin Sensitive to the Lightest Touch, *IEEE Spectrum*, 2010, <http://spectrum.ieee.org/biomedical/bionics/synthetic-skin-sensitive-to-the-lightest-touch>
- [7]. F. Zeng, S. Rebscher, W. Harrison, X. Sun, and H. Feng, Cochlear Implants: System Design, Integration, and Evaluation, *IEEE Reviews in Biomedical Engineering*, 1,2008, 115-142.
- [8]. L.J. Bond, Old reactors, new tricks. *IEEE Spectrum*, 49(8), 2012, 30-35.
- [9]. R. Buschling, Understanding and Applying IR Temperature Sensors, *Sensors* 11(10),1994, 32-37.
- [10]. H. R. Everett, *Sensors for mobile robots: theory and application* (Wellesley, MA: A K Peters, 1995).
- [11]. C.F. Tsai and M.S. Young, Pyroelectric infrared sensor-based thermometer for monitoring indoor objects, *Review of Scientific Instruments* 74(12),2003, 5267-5273.
- [12].

## Appendix

### PARTIAL LIST OF SUPPLIERS FOR BIOMEDICAL SENSORS:

Advanced Bionics Corporation (<http://www.advancedbionics.com/>)

Med-El Corporation (<http://www.medel.com/us/>)

Cochlear Corporation (<http://www.cochlear.com/>)

Nurotron Biotechnology Inc. (<http://www.nurotron.com>)

### PARTIAL LIST OF SUPPLIERS FOR ROBOTICS SENSORS:

SICK (<http://www.sick.com>)

Figaro Engineering Inc. (<http://www.figarosensor.com>)

RobotShop (<http://www.robotshop.com>)

Intelligent Agent (<http://www.intelligentagent.no>)

Dexter industries (<http://dexterindustries.com>)

## Bluetooth Based Android Controlled Robot

Rowjatul Zannat Eshita<sup>1</sup>, Tanwy Barua<sup>2</sup>, Arzon Barua<sup>3</sup>, Anik Mahamood Dip<sup>4</sup>

<sup>1</sup>(M. Sc. in IT, University of Dhaka, Bangladesh)

<sup>2</sup>(MTEE, American International University-Bangladesh, Bangladesh)

<sup>3</sup>(B.Sc.in CSE, Ahsanullah University of Science & Technology, Bangladesh)

<sup>4</sup>(B.Sc.in CSE, Ahsanullah University of Science & Technology, Bangladesh)

**ABSTRACT :** The project aims in designing a Robot that can be operated using Android Apps. The controlling of the Robot is done wirelessly through Android smart phone using the Bluetooth module feature present in it. Here in the project the Android smart phone is used as a remote control for operating the Robot. Android is a software stack for mobile devices that includes an operating system, middleware and key applications. Android boasts a healthy array of connectivity options, including Wi-Fi, Bluetooth, and wireless data over a cellular connection (for example, GPRS, EDGE (Enhanced Data rates for GSM Evolution), and 3G). Android provides access to a wide range of useful libraries and tools that can be used to build rich applications. Bluetooth is an open standard specification for a radio frequency (RF)-based, short-range connectivity technology that promises to change the face of computing and wireless communication. It is designed to be an inexpensive, wireless networking system for all classes of portable devices, such as laptops, PDAs (personal digital assistants), and mobile phones. The controlling device of the whole system is a Microcontroller. Bluetooth module, DC motors are interfaced to the Microcontroller. The data received by the Bluetooth module from Android smart phone is fed as input to the controller. The controller acts accordingly on the DC motors of the Robot. The robot in the project can be made to move in all the four directions using the Android phone. The direction of the robot is indicated using LED indicators of the Robot system. In achieving the task the controller is loaded with a program written using Embedded 'C' language.

**Keywords:** Android, Proteus, RF Modules, PIC 16f877a, DC Motor.

### I. INTRODUCTION

**Android controlled robot** project make use of an Android mobile phone for robotic control with the help of Bluetooth technology. This is a simple robotics projects using microcontroller. We have already seen Mobile Controlled Robot using DTMF technology which uses call based method to control robot. Also many wireless-controlled robots use RF modules. The control commands available are more than RF modules. Smartphone controlled robot is superior to all these robots.

This project is a Bluetooth controlled robot. For this the android mobile user has to install an application on her/his mobile. Then user needs to turn on the Bluetooth in the mobile. The wireless communication techniques used to control the robot is Bluetooth technology. User can use various commands like move forward, reverse, stop move left, and move right. These commands are sent from the Android mobile to the Bluetooth receiver. **Android based robot** has a Bluetooth receiver unit which receives the commands and give it to the microcontroller circuit to control the motors. The microcontroller then transmits the signal to the motor driver IC's to operate the motors.

- Android is an Open Source operating system based on the Linux Kernel, and designed primarily for touchscreen mobile devices such as smartphones and tablets.
- It was built to be truly open. For example, an application can call upon any of the phone's core functionality such as making calls, sending text messages, or using the Bluetooth, camera etc. [1].

The Android SDK provides the API libraries and developer tools necessary to build, test, and debug apps for Android

The main objectives of the project are:

1. Operating the Robot wirelessly through mobile phone.
2. Usage of Android touchscreen smart phone in performing the task.
3. Bluetooth wireless transmission.
4. Indicating Robot directions using LED indicators.

### II. BLOCK DIAGRAM & WORKING PRINCIPLE

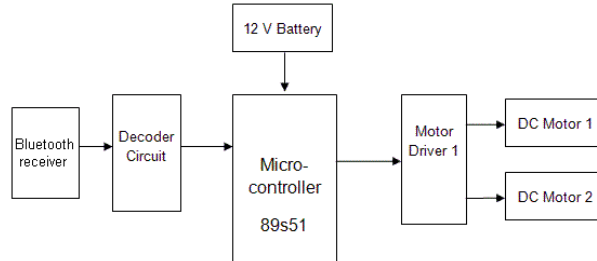


Figure 1: Block Diagram

The android application controlled robot communicates via Bluetooth to the Bluetooth module present on the robot. While pressing each button on the application, corresponding commands are sent via Bluetooth to the robot. The commands that are sent are in the form of ASCII. The PIC on the robot then checks the command received with its previously defined commands and controls the DC motors depending on the command received to cause it to move forward, backward, left, right or to stop. Thus allowing us to create an android controlled robot.

The major building blocks of the project are:

1. Regulated Power Supply.
  2. Microcontroller.
  3. Android smart phone.
  4. Bluetooth module.
  5. DC motors with driver.
  6. Crystal oscillator.
  7. Reset.
  8. LED indicators.
- Software's used:

1. PIC-C compiler for Embedded C programming.
2. PIC kit 2 programmer for dumping code into Micro controller.
3. Proteus for Circuit design.

### III. PIC Microcontroller & DC Motor



Figure 2: Pin configuration of PIC 16F877A

This powerful (200 nanosecond instruction execution) yet easy-to-program (only 35 single word instructions) CMOS FLASH-based 8-bit microcontroller packs Microchip's powerful PIC® architecture into an 40- or 44-pin package and is upwards compatible with the PIC16C5X, PIC12CXXX and PIC16C7X devices. The PIC16F877A features 256 bytes of EEPROM data memory, self-programming, an ICD, 2 Comparators, 8 channels of 10-bit Analog-to-Digital (A/D) converter, 2 capture/compare/PWM functions, the synchronous serial port can be configured as either 3-wire Serial Peripheral Interface (SPI™) or the 2-wire Inter-Integrated Circuit (I²C™) bus and a Universal Asynchronous Receiver Transmitter (USART) [2]. All of these features make it ideal for more advanced level A/D applications in automotive, industrial, appliances and consumer applications.

DC MOTOR:

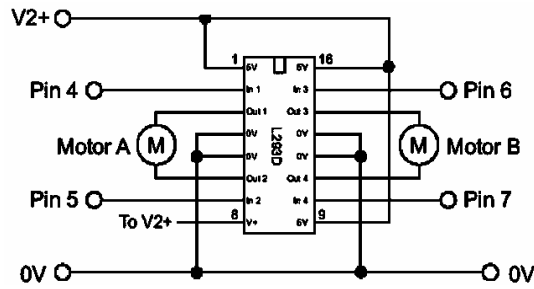


Figure 3: DC Motor

INSTRUCTIONS:

- Both inputs low -Motor Halt.
- First input high & second input low-motor forward.
- First input Low & second input High-motor reverse.
- Both inputs high-Motor Halt.

IV. Lists of AT Command & Register Segment

Command	Response	Parameter
AT	OK	None
AT+RESET	OK	None
AT+VERSION?	+VERSION: <Parameter> OK	Parameter: Version number
AT+ORGL	OK	None
AT+PSWD=<Param>	OK	
AT+PSWD?	+PSWD : <Param> OK	" Param: passkey Default: "1234
AT+UART=<Param1>,<Param2>,<Param3>	OK	Param1-baud rate Usually 9600 Param2-stop bit Param3- parity bit

Register A: UCSRA

RXC	TXC	UDRE	FE	DOR	PE	U2X	MPCM
R	R/W	R	R	R	R	R/W	R/W

Our Value: UCSRA –OXOO

Register B: UCSRB

RXCIE	TXCIE	UDRIE	RXEN	TXEN	UCSZ2	RXB8	TXB8
R/W	R/W	R/W	R/W	R/W	R/W	R	R/W

Our Value: USCRA - 0X18

Register C: USCR

URSEL	UMSEL	UPM1	UPM0	USBS	USCZ1	UCSZ0	UCPOL
R/W	R/W	R/W	R/W	R/W	R/W	R/W	R/W
1	0	0	0	0	1	1	0

Our Value: USCR - 0x86

URSEL	-	-	-	UBRR-11	UBRR-10	UBRR-9	UBRR-8
UBRR-7	UBRR-6	UBRR-5	UBRR4	UBRR-3	UBRR-2	UBRR-1	UBRR-0
0	0	0	0	0	0	0	0
0	0	0	0	0	0	0	0

Our Value: UBRRH, UBRRL - 75

#### IV. ANDROID APP

Below is the screenshot of Android application which is used in this project to control the Robot. This application has 9 keys / commands. We have used 7 commands. Command 7 and 9 are not used and are reserved for future scope. User can even rename these key text as Forward / Reverse using the Set Keys option [3]. User needs to turn on the Bluetooth on his/her mobile and press scan button as shown below. Then connect to the Bluetooth receiver on robot [4]. Once the connection is established then the application will show connected status as shown below.



Figure 4: Android Apps control screen shot

#### V. PROTEUS SIMULATION & HARDWARE

This project consists of a microcontroller, 16 x 2 alphanumeric LCD, two 5V relays, a lamp, DC motor and Bluetooth module. Here at89c51 microcontroller is used. It is an 8 bit microcontroller and it requires supply voltage of 5V DC [5] [6]. Use 7805 power supply circuit to provide 5V DC to the microcontroller. We can use 9V DC battery or 12V, 1A adapter to provide the supply to the circuit. For the above circuit additionally you need to connect reset circuit and crystal circuit to the controller to work properly. In the above circuit LCD is used to indicate the status of electrical loads and also used to display received data from Bluetooth. Here LCD is interfaced to the PORT1 of the microcontroller in 4 bit mode. Bluetooth module TX and RX pins are connected to the RXD and TXD pins of controller [7]. Vcc pin is connected to the 5V and GND pin is connected to ground. Controller communicates with Bluetooth module using serial communication (UART protocol). Use a baud rate of 9600 to communicate with Bluetooth. If you want to change the Bluetooth name and password then you need to use Bluetooth AT commands.

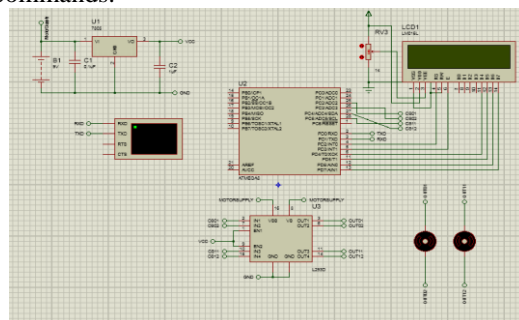


Figure 5: Proteus Simulation



Figure 6: Hardware

## VI. APPLICATIONS & FUTURE SCOPES

### APPLICATIONS:

- Surveillance Device
- Home automation
- Wheelchairs
- Military Applications
- Hostages Rescue

### FUTURE SCOPES:

- In future we plan to implement our project as follows  
It will contain following 3 components:
- A Robot Mounted with camera
- A headset, with a full-color display
- A mission control center

## VII. CONCLUSION

We select all equipment's based on data sheets. It is feasible to implement Bluetooth communication between smartphone and microcontroller. It can be used in various industries for picking various objects where human intervention is not desired. On a large scale, it can be used to develop robots with military applications. It can be used to target enemy without any human being crossing the territory. It provides for more development of applications based on android operating system. Such as, Application based on sensors (accelerometer, gyroscope) etc. The development of apps for Android in Android SDK is easy and free of cost. With tremendous smart phone in markets, it is bound to have many more applications in near future. It is robust, sensitive and fast moving, hence can be applied in rescue operations.

## ACKNOWLEDGEMENTS

We are earnestly grateful to our mentor, Mihir Barua, Manager-Technical Sales (Siemens Bangladesh Limited) for providing us with his special advice and guidance for this project. Finally, we express our heartiest gratefulness to the Almighty and our parents who have courageous throughout our work of the project.

## REFERENCES

- [1]. P. D. Minns, Atmega32 for Arduino Microcontroller System. Author House, 2013
- [2]. M. Banzl, Getting started with PIC 16f877a. "O'Reilly Media, Inc.", 2009
- [3]. Arduino Apps, "Arduinouno." Last visited on 06/09/2014
- [4]. A. M. Gibb, New media art, design, and the Arduino microcontroller: A malleable tool. PhD thesis, Pratt Institute, 2010
- [5]. M. Margolis, Proteus cookbook. "O'Reilly Media, Inc.", 2011
- [6]. D. Mellis, M. Banzl, D. Cuartielles, and T. Igoe, "Arduino with Proteus: An open electronic prototyping platform, " in Proc. CHI, vol. 2007, 2007
- [7]. A. U. ARDUINO UNO, "Front. arduinouno board implement simulation, " 2012